

**CONTINUOUS VERSUS DISCRETE SLIDING MODE CONTROL  
AS APPLIED TO A PNEUMATIC POSITIONING SYSTEM**

**by**

**HARRY N. IORDANOU**

*A thesis submitted to the Department of Mechanical Engineering  
in conformity with the requirements for the degree of  
**Doctor of Philosophy***

*Queen's University,  
Kingston, Ontario  
CANADA K7L 3N6*

**April, 1998**

**copyright © Harry N. Iordanou, 1998**



National Library  
of Canada

Acquisitions and  
Bibliographic Services

395 Wellington Street  
Ottawa ON K1A 0N4  
Canada

Bibliothèque nationale  
du Canada

Acquisitions et  
services bibliographiques

395, rue Wellington  
Ottawa ON K1A 0N4  
Canada

*Your file Votre référence*

*Our file Notre référence*

The author has granted a non-exclusive licence allowing the National Library of Canada to reproduce, loan, distribute or sell copies of this thesis in microform, paper or electronic formats.

The author retains ownership of the copyright in this thesis. Neither the thesis nor substantial extracts from it may be printed or otherwise reproduced without the author's permission.

L'auteur a accordé une licence non exclusive permettant à la Bibliothèque nationale du Canada de reproduire, prêter, distribuer ou vendre des copies de cette thèse sous la forme de microfiche/film, de reproduction sur papier ou sur format électronique.

L'auteur conserve la propriété du droit d'auteur qui protège cette thèse. Ni la thèse ni des extraits substantiels de celle-ci ne doivent être imprimés ou autrement reproduits sans son autorisation.

0-612-27830-1

**Canada**

## ABSTRACT

Harry Nicos Iordanou: *Continuous Versus Discrete Sliding Mode Control as Applied to a Pneumatic Positioning System*. Ph.D.Thesis, Queen's University at Kingston, April 1998.

Presented in this thesis is the development of a practical set of design guidelines to improve the performance of pneumatic positioning systems by appropriate sizing of the valve and the cylinder, and by careful choice of the tuning parameters for Continuous Sliding Mode (CSLM) and Discrete Sliding Mode (DSLM) controllers. CSLM and DSLM were selected because of their robustness in the presence of nonlinearities such as those found in a pneumatic positioning system.

Pneumatic systems exhibit parameter variations along the length of the stroke due to air compressibility. The size ratio (area to stroke) of the cylinder was found to dictate the limitations on the sampling time for adequate performance with a linear controller. A technique to identify the ultimate gain is presented, in order to illustrate how system stability varies with piston position and cylinder size ratio. Finally, the effect of the cylinder size ratio, valve port area and valve configuration on system performance with a linear Proportional-Velocity-Acceleration (PVA) controller is documented.

The first nonlinear controller investigated was CSLM. Techniques for the design of the sliding surface, the selection of the boundary layer thickness and sliding gain, as well as the effect of the equivalent gain, were investigated and a comprehensive design procedure was developed. With CSLM, the sliding surface design can be linked to familiar time domain performance parameters, but its performance is limited to relatively small sampling times. The robustness of CSLM in the context of its ability to maintain specified overshoot and settling time was tested by changing the payload mass.

The second nonlinear controller investigated was DSLM which is intended for discrete implementation and consequently takes explicit account of the sampling time. Techniques for the design of the controller are presented that are based on a compilation of existing methods, but with new features added for sliding surface design and controller tuning. The main contributions are: 1) the design approach for the sliding surface, where a link to time domain performance is established, and 2) the switching elements of DSLM which are selected by means of a classical linear controls approach. Finally, an original set of comprehensive design guidelines for DSLM are documented.

Following a set of experimental tests to validate the system model, a series of additional robustness tests were performed in simulation. These tests were designed to further verify the performance of the linear PVA and the nonlinear CSLM and DSLM controllers in the presence of model errors such as incorrect bore size and incorrect stroke length. In conclusion, DSLM was found to be the more robust of the three controllers for large sampling times. On the other hand, CSLM was competitive with DSLM for small sampling times.

## **ACKNOWLEDGEMENTS**

First, I would like to extend my deep gratitude to my supervisor Dr. Brian Surgenor for his motivation and supervision the past years. Undoubtedly, his constant support and guidance helped bring this thesis to completion.

Appreciation is also extended to Dr. Laeeque Daneshmend for his help and encouragement especially towards the final stages of the thesis.

The financial support provided to me by the Department of Mechanical Engineering and the School of Graduate Studies and Research is greatly appreciated and acknowledged.

Many thanks also to all my friends in Kingston, Canada and in Cyprus for their love and confidence. Special thanks to Gregg Logan, Terry Elles, Rob Hall and Habib Abou-Fayssal for being as good as family.

## **DEDICATION**

This thesis is dedicated to my wife Katerina, for her eternal love, support and understanding and to my parents Nicos and Loulla and my brother Chris for a lifetime of love, trust and confidence.



# CONTENTS

	<u>Page</u>
<b>Abstract</b>	i
<b>Acknowledgements - Dedication</b>	ii
<b>Table of Contents</b>	iii
<b>List of Figures</b>	vii
<b>List of Tables</b>	x
<b>Nomenclature</b>	xi
<b>1.0 Chapter 1 Introduction</b>	1
<i>1.1</i> Background	1
<i>1.2</i> Objectives	4
<i>1.2.1</i> Examination of Pneumatic Positioner Design	4
<i>1.2.2</i> Examination of Nonlinear System Controller Design	4
<i>1.3</i> Overall Objective	5
<i>1.4</i> Thesis Outline	6
<b>2.0 Chapter 2 Pneumatic Systems</b>	7
<i>2.1</i> Introduction to Pneumatic Systems	7
<i>2.1.1</i> Modelling Valves	10
<i>2.1.2</i> Modelling Actuators	14
<i>2.2</i> Linearisation of Pneumatic Model	17
<i>2.2.1</i> Stability Issue	22
<i>2.2.2</i> Natural Frequency and Cylinder Size Ratio	24
<i>2.2.3</i> Natural Frequency and Operating Position	28
<i>2.2.4</i> System Damping and Operating Position	28
<i>2.2.5</i> Asymmetric Cylinder	29
<i>2.3</i> Steady State Considerations	32
<i>2.3.1</i> Symmetric Actuator	33

2.3.2	Asymmetric Actuator	35
2.3.3	Valve Port Areas	39
2.3.4	Other Considerations	39
2.4	Summary	41
<b>3.0</b>	<b>Chapter 3</b>	
	Continuous Sliding Mode Control	43
3.1	Traditional Continuous Sliding Mode Control	44
3.1.1	Alternate Approaches to CSLM	49
3.1.2	Summary of Literature Review	57
3.2	Design of the Sliding Surface	58
3.2.1	Stability of a Continuous System	58
3.2.2	Canonical Form of a Continuous System	58
3.3	Switching Control Law	61
3.4	Controller Parameter Issues	61
3.4.1	The Boundary Layer	63
3.4.2	Sampling Time Considerations	65
3.4.3	Sliding Gain and Transient Response	65
3.4.4	Robustness Test for CSLM	68
3.4.5	Robustness Test for CSLM with Inadequate Sampling Time	72
3.4.6	Equivalent Action and Robustness	74
3.4.7	Sliding Surface Design Parameters	76
3.5	Static Coulomb Friction and Noise Considerations	79
3.6	Summary	82
<b>4.0</b>	<b>Chapter 4</b>	
	Discrete Sliding Mode Control	84
4.1	Traditional Discrete Sliding Mode Control	84
4.2	Design of Sliding Surface	88
4.2.1	Discrete Time Domain	88
4.2.1a	Stability of a Discrete System	89

4.2.1b	Canonical Form of a Discrete System	90
4.2.1c	Pole Placement Method	92
4.2.1d	Pole Placement for a Pure Second Order System	95
4.2.1e	Application to 3 <sup>rd</sup> Order System	96
4.3	Switching Laws for DSLM	98
4.4	Sliding Gain	100
4.4.1	Permissible Range for the Sliding Gain	107
4.4.2	Varying Sliding Gain	109
4.4.3	State Weights and the link to PVA Gains	114
4.5	Simulation Results using the Pole Placement Technique	116
4.5.1	Sampling Time Tolerance on DSLM	118
4.5.2	Effect of the Size of the Sliding Gain	120
4.5.3	Effect of the Size of the Sliding Gain and State Weights	122
4.5.4	Sliding Versus Equivalent Control Actions	124
4.5.5	DSLM Robustness	125
4.5.6	Sliding Surface Design Parameters	127
4.5.7	Static Coulomb Friction Result	130
4.5.8	Effect of Sensor Noise and Filtering on DSLM	132
4.6	Summary	134
<b>5.0</b>	<b>Chapter 5</b> Experimental and Simulation Results	136
5.1	Experimental Setup	136
5.2	Valve Modelling	137
5.3	Actuator Modelling	140
5.3.1	Static Coulomb and Dynamic Coulomb Forces	140
5.3.2	Viscous Friction Coefficient and Effective Mass	143
5.4	Choice of Setpoint Change	147
5.4.1	Closed Loop Experiment and Model Validation	149

5.5	Robustness Results of PVA, CSLM and DSLM with Different Cylinders	151
5.6	Summary	159
<b>6.0</b>	<b>Chapter 6</b> Conclusions and Recommendations	160
6.1	Conclusions	160
6.1.1	Pneumatic Positioning System	160
6.1.2	Continuous Sliding Mode Control	162
6.1.3	Discrete Sliding Mode Control	164
6.1.4	Robustness Tests	166
6.2	Design Recommendations	167
6.3	Recommendations for Future Work	167
	<b>References</b>	168
	<b>Appendix A</b> Technical Specifications	173
	<b>Appendix B</b> Simulation Code - Model Parameters	176
	<b>VITAE</b>	180
	<b>Publications</b>	181

## LIST OF FIGURES

	<u>Page</u>
Figure 2.1:	3-way, 5-port valve and asymmetric cylinder 8
Figure 2.2:	3-way valve configurations 9
Figure 2.3:	Flow coefficient versus Pressure Ratio 12
Figure 2.4:	Typical Friction Versus Speed Models 15
Figure 2.5:	Nominal Operating Position and Pressures 18
Figure 2.6:	Marginal Response with Ultimate Gain for Cylinder of $d_c=6.1$ 26
Figure 2.7:	Marginal Response with Ultimate Gain for Cylinder of $d_c=2.0$ 27
Figure 2.8:	Marginal Response with Ultimate Gain for Cylinder of $d_c=1.2$ 27
Figure 2.9:	Normalised Natural Frequency and Damping versus Operating Position 30
Figure 2.10:	Marginal Response with Ultimate Gain for Asymmetric Cylinder 31
Figure 2.11:	Closed Center valve with PVA on equal cylinder areas and equal valve ports 34
Figure 2.12:	Open Center valve with PVA on unequal cylinder areas and equal valve ports. Note poor responses 37
Figure 2.13:	Closed Center valve with PVA on unequal cylinder areas and equal valve ports. Note improved response as pressure increases 38
Figure 2.14:	Closed Center valve with PVA on unequal cylinder areas and valve port ratio at 0.5. Note further improvement in the responses 40
Figure 3.1:	Sliding Control, from Ideal to Nonideal to Idealized 48

Figure 3.2:	Effect of Size of Boundary Layer with $h=1ms$	64
Figure 3.3:	Effect of Sampling Time on Stability of CSLM	66
Figure 3.4:	Effect of size of $K_f$ on Performance with Small Sampling Time	67
Figure 3.5:	Robustness of CSLM with 3 masses and $h=1ms$	69
Figure 3.6:	Robustness of PVA with 3 masses and $h=1ms$	71
Figure 3.7:	Robustness of CSLM with 3 masses and $h=10ms$	73
Figure 3.8:	Equivalent Gain and Robustness of CSLM	75
Figure 3.9:	Sliding Surface Design for a Set of Settling Times	77
Figure 3.10:	Sliding Surface Design for a Set of Damping Factors	78
Figure 3.11:	Effect of Static Coulomb Friction on Performance of CSLM	80
Figure 3.12:	Effect of Noise and Filtering on CSLM	81
Figure 3.13:	Sliding Surface Design Procedure for CSLM	83
Figure 4.1:	DSL <sub>M</sub> Boundary Layer Action Modifications	110
Figure 4.2:	Effect of Boundary Layer Action in Simulation	113
Figure 4.3:	Effect of Sampling Time	119
Figure 4.4:	Effect of Size of Sliding Gain	121
Figure 4.5:	Effect of State Weights and Sliding Gain	123
Figure 4.6:	Sliding Versus Equivalent Control Action	124
Figure 4.7:	DSL <sub>M</sub> Robustness Result	126
Figure 4.8:	Sliding Surface Settling Time (0.2 sec) and 3 Damping Factors	128
Figure 4.9:	Sliding Surface Settling Time (0.3 sec) and 3 Damping Factors	129
Figure 4.10:	Static Friction Result ( $F_c=0-5-10N$ )	131
Figure 4.11:	Noise and Filtering on DSL <sub>M</sub>	133
Figure 4.12:	DSL <sub>M</sub> Design Procedure	135

Figure 5.1:	Experimental Apparatus	137
Figure 5.2:	Flow vs. Control Input for <i>HR-Textron 4</i>	139
Figure 5.3:	Dynamic and Static Coulomb Forces - Extension and Retraction	142
Figure 5.4:	Viscous Friction Force and Effective Mass Payload	145
Figure 5.5:	Effective Mass Components	146
Figure 5.6:	Robustness Test with DSLM, Experiment	147
Figure 5.7:	4-Step Setpoint-change Scenario with PVA	148
Figure 5.8:	Closed Loop Pneumatic Positioner Response, Simulation and Experiment	150
Figure 5.9:	Robustness Tests with PVA - Simulation	155
Figure 5.10:	Robustness Tests with CSLM - Simulation	157
Figure 5.11:	Robustness Tests with DSLM - Simulation	158

## LIST OF TABLES

	<u>Page</u>
Table 2.1: Ultimate Gain for Cylinders of Different Size Ratios	25
Table 5.1: Flow versus Valve Control Input	139
Table 5.2: Summary of Quantitative Performance Measures for Robustness Tests	155



## NOMENCLATURE

$a_j$	= coefficients of 2 <sup>nd</sup> order transfer function with $j=0,1,2$
$\bar{A}$	= continuous time system matrix
$A_a, A_b$	= areas for chambers $a$ and $b$
$A_s$	= symmetric cylinder chamber area
$A_{vv}$	= instantaneous valve opening area
$A_{vs}, A_{ve}$	= valve supply and exhaust port areas
$A_v$	= maximum valve opening area
$\tilde{A}$	= augmented closed loop system dynamics
$b$	= control uncertainty
$b_j$	= arbitrary constants determined from initial conditions
$b(x)$	= nonlinear state gain matrix
$B$	= continuous time gain matrix
$c_1, c_2, c_3$	= sliding surface coefficients
$C_1, C_2$	= sliding vectors
$C$	= sliding surface matrix
$C_A$	= companion matrix of $A$
$C_d$	= discharge coefficient
$C_m$	= flow coefficient
$C_p$	= constant-pressure specific heat
$C_v$	= constant-volume specific heat
$C_\Phi$	= companion matrix of $\Phi$
$\bar{C}$	= canonical sliding surface matrix
$d_e$	= cylinder size ratio
$\bar{d}$	= disturbance bound
$D$	= disturbance vector
$D_c$	= cylinder diameter
$E$	= total internal energy of the control volume
$f(x)$	= nonlinear state system matrix
$f_j$	= switching elements
$f_v$	= viscous friction coefficient
$f_n$	= nonlinear state system matrix
$\hat{f}$	= estimated dynamics
$F$	= constant external force
$F_{cs}$	= static coulomb force
$F_{cd}$	= dynamic coulomb force
$F_e$	= estimation error
$F_{eq}$	= discrete equivalent gain matrix

$F_f$	= overall friction force
$F_{sw}$	= discrete sliding gain matrix
$g(x)$	= nonlinear gain matrix
$G$	= matrix of desired eigenvalue sector
$h$	= sampling time
$h_{in}$	= total energy per unit mass of fluid into the control volume
$h_{out}$	= total energy per unit mass of fluid out of the control volume
$h_p$	= system opening ratio
$I$	= identity matrix
$k_1$	= flow gain
$k_2$	= flow-pressure coefficient
$k_i$	= varying sliding gain slope factor
$k_j^+, k_j^-$	= switching feedback gains
$K$	= pole placement gain matrix
$K_a$	= acceleration gain
$K_{eq}$	= continuous equivalent control gain matrix
$K_j$	= matrix of switching feedback gains
$K_p$	= proportional gain
$K_s$	= sliding gain
$K_s^u, K_s^l$	= upper and lower sliding gain limits
$K_{sj}$	= varying sliding gain (inside boundary layer)
$K_{sw}$	= continuous sliding gain matrix
$K_u$	= ultimate gain
$K_v$	= velocity gain
$L$	= cylinder stroke length
$\bar{L}$	= function used by <i>Furuta and Pan (1995)</i>
$L_f, L_g$	= Lie Derivatives
$L_s, L_c$	= sliding and convergence condition functions
$m$	= air mass
$M_e$	= effective load inertia or mass
$M_p$	= maximum overshoot
$n$	= number of states, or system order
$N$	= valve opening coefficient
$\mathcal{N}$	= null space
$p$	= rectangular coordinate
$P$	= pressure

$P_d$	= downstream pressure
$P_r$	= pressure ratio
$P_s$	= supply pressure
$P_u$	= upstream pressure
$P_{vc}$	= pressure at vena contracta
$\bar{P}_n$	= norm of discrete state
$q$	= rectangular coordinate
$Q$	= weighting matrix
$Q_h$	= heat flow to the control volume
$r$	= polar coordinate, vector length
$r(k)$	= transformed variables
$r_m$	= modal transformation
$r_p$	= steady state pressure ratio
$\hat{R}$	= weighting matrix
$R_u$	= gas constant
$\mathcal{R}$	= range space
$s$	= sliding function
$S$	= sliding surface
$S_{up}, S_{dw}$	= directional ( <i>up</i> and <i>down</i> ) sensitivities
$t$	= time
$t_f$	= total settling time
$t_r$	= reaching time
$t_s$	= sliding settling time
$T$	= transformation matrix
$T_a, T_b$	= temperatures for chambers <i>a</i> and <i>b</i>
$T_d$	= desired eigenvector matrix
$T_s$	= supply temperature
$T_u$	= upstream temperature
$T_v$	= eigenvector (modal) matrix
$u$	= control signal
$u_m, u_t, u_d, u_w, u_x$	= coefficients for steady state analysis
$u_{eq}$	= equivalent action
$u_{sw}$	= sliding action
$U$	= valve underlap
$\hat{u}_{eq}$	= estimated equivalent action
$v_1, v_2, \dots$	= eigenvectors
$V$	= cylinder volume
$V(x)$	= Lyapunov's function

$V_n$	= Vandermonde matrix
$V_p$	= projector vector
$w_j$	= internal switching states
$W_o$	= controllability matrix (original)
$W_j$	= strictly positive state weight for $j$
$\bar{W}_c$	= controllability matrix (transformed)
$x$	= state variable(s)
$x_e$	= tracking error in state variable(s)
$x_l$	= transformed state as in <i>Zodhy (1995)</i>
$\tilde{x}$	= perturbation in state variable(s)
$\bar{x}$	= canonical form state variable(s)
$y$	= position of cylinder piston
$y_o$	= nominal operating point
$y_v$	= valve spool displacement
$y(t)$	= external states
$z$	= z-transform
$z_F$	= stability variable as in <i>Furuta (1990)</i>
$z_z$	= transformed state as in <i>Woodham and Zinober (1993)</i>

### Greek Symbols

$\alpha$	= real, non-zero root of 3 <sup>rd</sup> order system
$\alpha_1, \alpha_2 \dots$	= coefficients of characteristic equation
$\beta$	= gain margin
$\gamma$	= specific heat ratio
$\delta(k), \delta_j$	= boundary layer for DSLM
$\varepsilon$	= strictly positive constant
$\zeta$	= damping ratio
$\eta$	= strictly positive constant
$\theta$	= polar coordinate, argument
$\lambda_1, \lambda_2 \dots \lambda_n$	= eigenvalues for system of order $n$
$\lambda$	= filter cut-off frequency
$\mu, \chi$	= pneumatic model coefficients
$\nu$	= positive real number
$\xi$	= rate of convergence (to sliding surface)
$\xi_z$	= transformed state as in <i>Woodham and Zinober (1993)</i>
$\rho$	= density
$\tau$	= time constant
$\bar{u}$	= perturbation gain bounds for discrete control
$\phi$	= fixed boundary layer for CSLM

$\psi_j$  = switching weight for state  $j$   
 $\omega_n$  = natural frequency  
 $\Delta j$  = uncertainty on variable  $j$   
 $\Lambda$  = eigenvalue matrix  
 $\Phi, \Gamma$  = discrete time matrices  
 $\Phi_c$  = closed loop dynamics for canonical system  
 $\Phi_h$  = work done by the fluid system  
 $\Phi_z$  = closed loop dynamics for system presented in *Furuta (1990)*  
 $\bar{\Phi}, \bar{\Gamma}$  = discrete time canonical matrices  
 $\Psi_i$  = switching element presented in *Utkin (1977)*

### Superscripts

ss = steady state  
T = transpose  
g = generalised inverse of matrix

### Subscripts

$a$  = cylinder chamber “a”  
 $b$  = cylinder chamber “b”  
 $i$  = initial  
 $in$  = in  
 $max$  = maximum  
 $min$  = minimum  
 $out$  = out  
 $set$  = setpoint  
 $u$  = ultimate

### Functions

$\inf(x)$  = infimum function of vector  $x$   
 $\text{sat}(x)$  = saturation function for scalar  $x$   
 $\text{sign}(x)$  = signum function for scalar  $x$   
 $\sup(x)$  = supremum function of vector  $x$   
 $|x|$  = absolute value for the scalar  $x$   
 $\|x\|$  = norm function of vector  $x$

### Acronyms

CSLM = Continuous Sliding Mode  
DSLm = Discrete Sliding Mode  
MPZ = matched-pole zero  
PVA = Proportional-Velocity-Acceleration  
SLM = Sliding Mode  
ZOH = zero-order hold

# CHAPTER 1

## INTRODUCTION

### 1.1 Background

Pneumatics retain a dominant role in many automated, materials-handling tasks due to their ability to provide a low-cost, safe and compact positioning system that is well suited for light to medium-duty applications. Furthermore, they are fast acting, clean and require little maintenance. They are widely used in industry to perform simple pick-and-place fixed-setpoint tasks. However, pneumatic systems have not been widely used for servo-applications (variable setpoint) because of their poor dynamic response as compared to electric or hydraulic systems. Air compressibility can cause spongy operation and delays in signal transmission, affecting both response time and positioning accuracy. Friction in pneumatic systems is generally much higher than in hydraulic systems since oil in hydraulic systems is both the working fluid and the lubricant. In general, static friction in a pneumatic cylinder combined with valve hysteresis create undesirable setpoint offsets which can cause high control chatter and erratic system behaviour. Furthermore, the dynamic stability of pneumatic systems is known to be dependent on stroke position. It has been observed that pneumatic systems are less stable when operating about the mid-stroke position compared with the end-stroke position (*Burrows, 1972*).

A typical pneumatic system uses an *air compressor* to pressurise air to a desired level. An *air filter* traps air impurities and a *pressure regulator* maintains the air pressure to a constant level. A *control valve* allows flow of air into one chamber of a *cylinder*, while air is allowed to exit from the other chamber to atmosphere. The most critical of the components of a pneumatic system are the valve and the cylinder. Over the years, many improvements have been made on pneumatic component design. For instance, rodless cylinders have been introduced as an alternative to conventional rodded cylinders. One arrangement for a rodless cylinder is to have the in-cylinder piston connected to the load

carrying carriage through a direct physical coupling. A seal across the track prevents air leakage. The lack of a rod means that a rodless cylinder requires half the space of a rodded cylinder and more importantly from a dynamic standpoint, has a symmetric piston area. This is in contrast to a rodded cylinder which, of course has unequal piston areas and consequently a nonlinear force characteristic. However, rodless cylinders can exhibit high friction due to the requirement for stiff sealing. Another rodless cylinder arrangement is one that magnetically couples the carriage to the in-cylinder piston. However, magnetic coupling can also exhibit high friction due to the requirement for a minimal air leak between piston, seal and carriage. To counter the effect of friction in rodded cylinders, low friction seals and bearing materials, along with innovative seal designs, have been introduced.

Given that the “heart” of a pneumatic positioning system is the control valve, it is worthwhile to note that there are three major configurations for proportional actuation:

- *Digital stepping*, where multiple conventional ON/OFF solenoid valves, a digital multiplexer and a switched-output programmable controller is used. The control signal is received by the multiplexer, which in turn activates the appropriate number of solenoid valves whose combined flow output equals that required.
- *Pulse-Width-Modulation*, where the actuator is initially powered in the normal manner through an ON/OFF valve, but as the actuator nears its final position, the valve is pulsed rapidly ON/OFF, feathering the actuator into position.
- *Proportional servovalves*, which resemble their hydraulic counterparts. A spool moves within the valve body and provides a flow of air in proportion to the control signal. New valve designs incorporate a servomotor to move the spool via an eccentric. This approach is not possible with most hydraulic valves due to higher flow forces and spool masses. Hydraulic valves tend to use proportional solenoids to move the spool. The use of a servomotor enables higher valve bandwidths.

It is generally acknowledged that proportional servovalves offer the best opportunity for high performance. However, the cost differential is on the order of a factor of *ten* (\$100 for an ON/OFF solenoid valve versus \$1000 for a proportional servovalve). Servovalves have improved in terms of both their linearity and bandwidth. Proportional pneumatic servovalves were not even commercially available 10 years ago. Furthermore, it is only in recent years that more than one size of valve has become available.

With advancements in pneumatic component design, positioning accuracies in the order of  $\pm 0.025 \text{ mm}$  ( $0.001 \text{ in}$ ) are readily achievable. The overall improvement in the performance of pneumatic systems opens a wider range of possible applications. Apart from the traditional industrial uses, one can now see pneumatic systems being used in:

- *Vehicle gearshifts:* The transmission servo includes a number of components such as pneumatic cylinders, solenoid valves, sensors and on-board computer. The computer monitors instantaneous values such as road speed, engine speed and the selected gear, and controls the gear level and clutch in accordance to the selected program and any changes in the parameters (*Wright, 1996*).
- *Walking Robots:* Walking robots are designed to perform the work of human workers in hazardous areas (such as nuclear disposal sites) and are equipped with legs for greater mobility on uneven terrain and active cushioning. Walking robots with six legs are now available: linear pneumatic actuators lift the legs, swivel pneumatic actuators perform the fine tuning movements required for walking by adjusting vertical and transverse positions. An on-board computer serves as the system's controller (*FESTO, 1995*).



## 1.2 Objectives

The work documented in this thesis, which is motivated by an increasing interest towards the use of high-performance pneumatic systems, has two main features:

### 1.2.1 Examination of Pneumatic Positioner Design

The examination is conducted by means of simulation and experiment. Simulation will be used to examine the performance of the pneumatic system in terms of system design issues such as the size of the valve, the stroke and the bore of the cylinder. For example, a design issue that will be considered is the square root ratio of the cylinder chamber area to the cylinder stroke. It will be shown that the smaller the ratio is, the harder it is to provide smooth setpoint tracking.

Another aspect of the hardware design is the size of the valve. Selecting a valve that is too small for a certain application (*undersizing*) means that maximum actuator speed may not be accomplished which would result in longer settling times. Selecting a valve too large (*oversizing*) does improve speed of response but may result in poor sensitivity which in turn could cause higher steady state errors.

### 1.2.2 Examination of Nonlinear System Controller Design

A pneumatic system is inherently a nonlinear system. Sliding Mode Control (SLM) has been promoted as a particularly *robust* controller as applied to nonlinear systems. In the context of this thesis, the meaning of “robust” refers to the ability of a model-based controller to maintain system performance in the presence of bounded errors in the modelled parameters. This thesis sets out to investigate the robustness of SLM controllers in both the continuous (CSLM) and discrete (DSLM) implementations. To put the performance of the SLM controllers into perspective, a comparison will be made to a well designed linear Proportional-Velocity-Acceleration (PVA) controller.

The objective is to determine which one of the three controllers (PVA, CSLM, DSLM) provides the "best" control in terms of speed of action, elimination of steady state errors and robustness. A good actuator speed is considered to be  $1\text{ m/s}$ . Steady state errors in the order of  $\pm 0.2\text{ mm}$  are judged acceptable. The robustness of the controllers will be examined in terms of deliberate model errors. These model errors include an incorrect mass payload and an incorrect cylinder, either in terms of using a cylinder with a double bore, or with a double stroke. Doubling the stroke or the bore of cylinder without suitable compensation in the controller gains normally degrades the system's response. The question is: how much does the performance of each controller degrade ?

To optimize the design of SLM, a number of tests will be performed to investigate the effect of controller design parameters such as the sampling interval, boundary layer thickness, sliding gain and state weights.

### **1.2.3 Overall Objective**

The overall objective of the research is to improve the performance of pneumatic positioning systems through an appropriate selection of the tuning parameters of CSLM and DSLM. This can be done by careful selection of the pneumatic system components and by customising the controller to the system needs and requirements. By examining the effects of the sliding gain, state weights, etc. a set of gain selection guidelines can be generated for CSLM and DSLM. Furthermore, a simple design for the sliding surface of DSLM which links time-domain performance parameters to the coefficients of the sliding surface needs to be generated. With a comprehensive understanding of pneumatic system behavior and with a good set of gain selection guidelines, pneumatic positioning systems will be better located to challenge electric and/or hydraulic systems.

### **1.3 Thesis Outline**

Chapter 2 presents a literature review on pneumatic systems. Modelling considerations for valves and cylinders, which compose the core of pneumatic system design are presented. Both linear and nonlinear models of a pneumatic system are developed. Fundamental dynamic behavior such as the effect of system nonlinearities on the ultimate gain for a proportional only controller are presented.

Chapters 3 and 4 include a literature review on CSLM and DSLM, respectively. Furthermore, various modifications suggested by researchers over the years are addressed and new modifications that improve the performance of the controllers are presented. The gradual improvement in the performance of the controllers is demonstrated by a set of simulation results.

Chapter 5 presents the model validation procedure for the experimental setup. The model parameters are determined from a set of open and closed loop tests. To further evaluate the robustness of the controllers, a set of tests are conducted to examine the effect of doubling the cylinder bore, and doubling the cylinder stroke, without correcting the design of the controller. The degradation in the performance of the pneumatic system under these tests is an indication of the robustness of the controller.

Chapter 6 summarises the experimental and simulation results presented in earlier chapters. It also provides a set of guidelines for customising and tuning SLM controllers to pneumatic systems. Some guidelines for pneumatic system design are also listed. Finally, recommendations for future work are given.

## CHAPTER 2

### PNEUMATIC SYSTEMS

This chapter describes pneumatic positioning systems, from the dynamic modelling of the individual components to the analysis of steady state conditions. Some important aspects that will be stressed include: linear versus nonlinear models, modelling static and dynamic friction, subsonic versus choked flow, steady versus variable pressures and volumes.

#### 2.1 Introduction to Pneumatic Systems

Pneumatic systems utilize the energy of compressed air. Such systems have been applied traditionally to non-industrial applications such as dental drills and surgical instruments as well as to many industrial applications that do *not* involve a control system such as chipping, reaming, drilling, forming and stamping operations. With advancements in microcomputer and servovalve technology, pneumatic systems are now being considered for industrial applications that do involve a control system, such as for free positioning of a workpiece.

Fig. 2.1 shows a typical pneumatic setup for position control with a directional valve controlling the flow of air from a regulated supply to a rodded cylinder. Fig. 2.1a shows the different components of the valve and the cylinder together with the key nomenclature to be used in this chapter. The control signal to the valve determines the position of the spool, which allows air to flow into either cylinder chamber “a” or “b”. The illustrated valve has 5 ports and allows 3 ways of motion. Thus, it is referred to as a 5-port 3-way, directional valve. Depending on the location of the valve spool, the piston could be extending or retracting (Fig. 2.1b and 2.1c respectively).

When the spool is centered and there is an *overlap* (area of spool peg greater than the valve port), then there is no air flow to either end of the cylinder and its position is “frozen”. This type of valve is called a *closed-center* valve. If there is an *underlap*

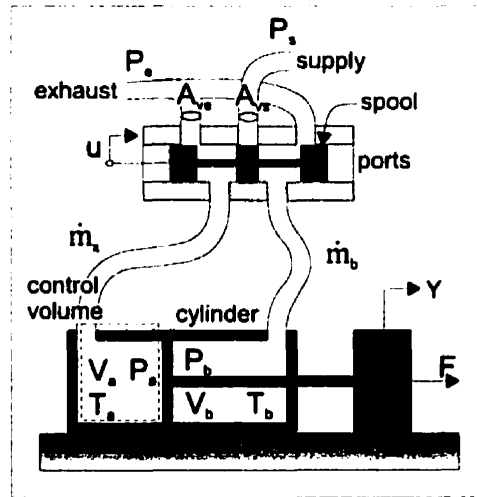


Figure 2.1a: 3-way, 5-port valve and asymmetric cylinder

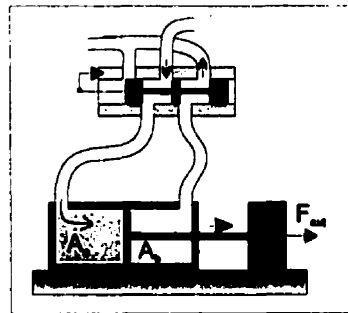


Figure 2.1b: Extending

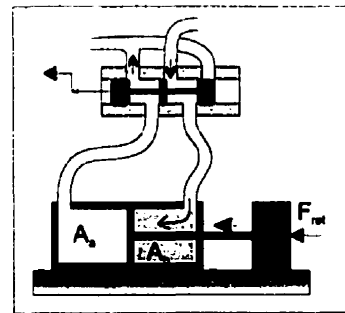


Figure 2.1c: Retracting

Figure 2.1: 3-way, 5-port valve and asymmetric cylinder

(area of spool peg smaller than the valve port), then both chambers exhaust to the atmosphere if the spool is centered. This is called an *open-center* valve. Finally, if the spool is centered while the supply port is greater than the spool peg and the exhaust ports are blocked, then both chambers are charged. This type of valve is called the *pressure-center* valve. These three configurations are shown in Fig. 2.2. The choice of which configuration to use depends on the process requirement when the system is at rest and the valve is centered (*Lansky and Schrader, 1986*).

The open-center valve allows free positioning of the cylinder (ports open to atmosphere), the pressure-center valve holds the cylinder in place by maintaining the

pressure at both ends (ports to supply pressure), and the closed-center valve also holds the cylinder, but at whatever pressure was present at the time when the valve was centered (closed port). The 5-port 3-way valve shown in Fig. 2.1 is an open-center valve. As will be shown later in this chapter, the center configuration greatly affects the dynamic behaviour of the pneumatic system.

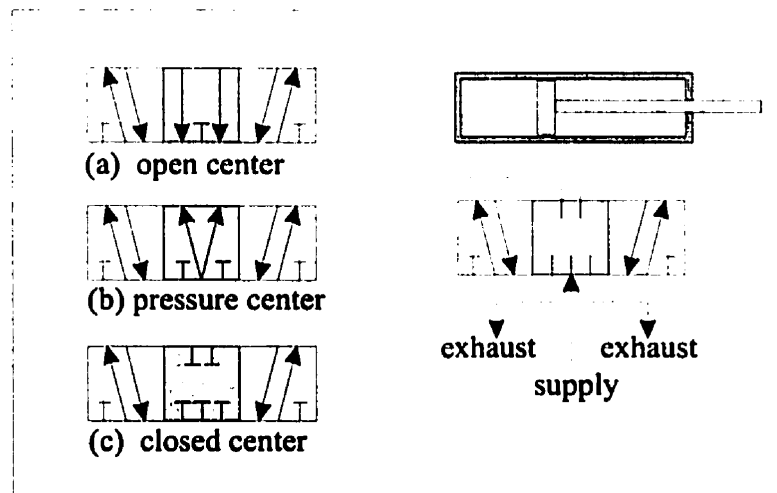


Figure 2.2: 3-way valve configurations

Typically, since the driving medium is pressurised air, a compressor is used to charge a receiver tank with the required air pressure. A relief valve, a pressure operated valve which bypasses compressor air delivery to the atmosphere, is included to limit pressure to a predetermined maximum value. Further downstream, an air filter is introduced which traps air impurities from contaminating the valve and cylinder. The next downstream component is a pressure regulator which further controls the pressure of the stored potential energy and prevents fluctuations caused by the compressor. A filtered and regulated air supply is then ready to enter the directional pneumatic valves.

Proportional servovalves are directional valves that may be variably positioned to provide control of both the amount and the direction of fluid flow. A great deal of research has been done on the modelling of servovalves for pneumatic systems (*Pu and Weston, 1990, Moore et al, 1992, Ye et al, 1992, Uebing et al, 1997*). The basic approach is to consider the valve as a variable orifice restriction. The mass flow rate across a variable orifice can be given as (*McCloy and Martin, 1980*):

where  $C_d$  is called the discharge coefficient and it depends on the geometry of the orifice. It is introduced as a correction factor to take into account the jet contraction and is usually determined experimentally. Values for the discharge coefficient can range from 0.61 to 0.95 depending on the type of valve opening. Typical values for  $C_d$  are reported as (Andersen, 1967):

- The valve that was modelled in simulation and used in experiment is the *HR-Textron* valve. The valve was chosen despite its high cost (\$1700) because it has a machined metallic spool with internal position feedback which makes the valve a rugged system which does not require an air filter, or need special setup. Other valves, such as the *FESTO* valves, although cheaper (\$700) have a plastic spool and are more susceptible to air impurities. Therefore, they require air filtration to the order of a  $\mu\text{m}$ . Furthermore, all components such as fittings, exhaust mufflers and tubing need to be ultrasonically cleaned for the *FESTO* valves, and no teflon tape for fittings is permitted.

10

opening area and is variable in the case of servovalves, as it can be controlled by the adjusting the position of the spool.  $P_u$  is the upstream pressure,  $T_u$  is the upstream absolute temperature and  $C_m$  is the flow coefficient. The value of the flow coefficient depends on whether the flow through the valve orifice is *subsonic* or *choked*. At this point, the pressure ratio needs to be introduced:

$$P_r = P_{vc} / P_u \quad (2.2)$$

where  $P_{vc}$  represents the static pressure at the vena contracta, or the throat of the downstream flow. The pressure at the throat is very difficult to measure but can be assumed equal to the downstream static pressure provided that the downstream chamber is considerably larger than the orifice area (*McCloy and Martin, 1980*). This modifies Eq. 2.2 to:

$$P_r \equiv P_d / P_u \quad (2.3)$$

Fig. 2.3 shows the variation of  $C_m$  with the pressure ratio. It can be seen that if the pressure ratio is greater than a critical value ( $P_r=0.528$ ), the flow is subsonic. If this is the case, then the flow coefficient is:

$$C_m = \sqrt{\left[ \frac{2\gamma}{R_u(\gamma-1)} \left\{ (P_r)^{\gamma/\gamma} - (P_r)^{(\gamma+1)/\gamma} \right\} \right]} \quad (2.4)$$

where  $R_u$  is the gas constant ( $0.287 \text{ kJ/kgK}$ ) and  $\gamma$  is the ratio of the specific heats,  $c_p/c_v$  ( $1.4$  for air). For values of the pressure ratio less than the critical, the flow can be assumed to be choked and the flow coefficient has:

$$C_m = \left( \frac{2}{\gamma+1} \right)^{1/(\gamma-1)} \sqrt{\frac{2\gamma}{R_u(\gamma+1)}} \quad (2.5)$$

In the case where the working fluid is air and the flow is choked,  $C_m$  is  $0.0405$ .

Given the physical setup illustrated in Fig. 2.1b and using Eq. 2.1, the mass flow rates into chamber *a* and out of chamber *b* are:

$$\dot{m}_a = C_{da} C_{ma} A_{va} \frac{P_s}{\sqrt{T_s}} \quad (2.6)$$



and,

$$\dot{m}_b = -C_{db} C_{mb} A_{vb} \frac{P_b}{\sqrt{T_b}} \quad (2.7)$$

In other words, chamber *a* is charging, while chamber *b* is discharging, or exhausting.

Note that  $C_{ma}$  and  $C_{mb}$  are functions of  $P_{ra} = P_a/P_s$  and  $P_{rb} = P_e/P_h$  respectively.

From the energy standpoint, one can say that the rate of energy being stored inside the control volume (as seen in Fig. 2.1a) is equal to the energy inflow minus the energy outflow.

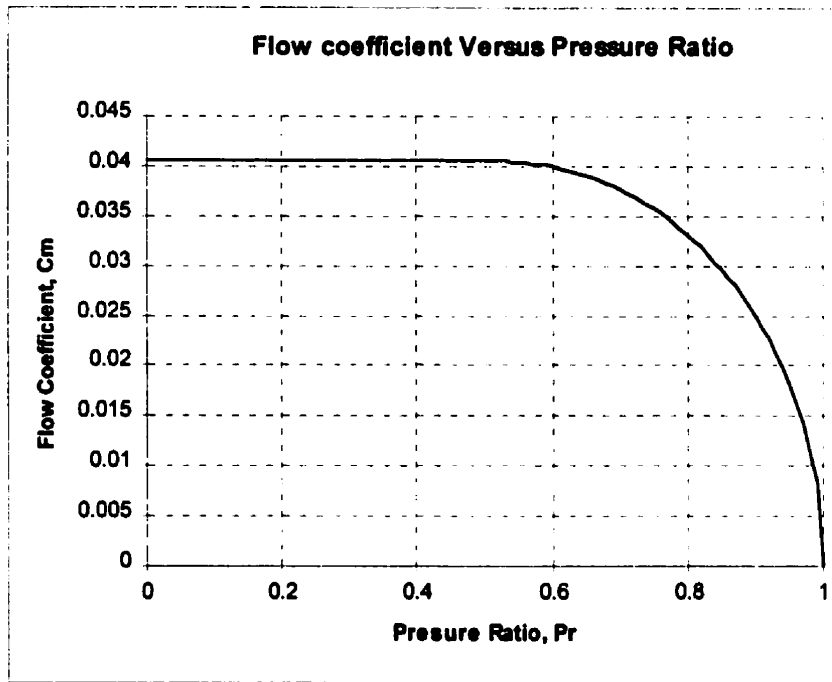


Figure 2.3: Flow coefficient versus Pressure Ratio

This gives:

$$\Sigma \dot{m}_{in} h_{in} - \Sigma \dot{m}_{out} h_{out} + \left\{ \frac{dQ_h}{dt} - \frac{d\Phi_h}{dt} \right\} = \frac{dE}{dt} \quad (2.8)$$

where  $Q_h$  is the heat flow to the control volume,  $\Phi_h$  is the work done by the system,  $h_{in}$  and  $h_{out}$  are the total energies per unit mass of fluid, *in* and *out* of the control

volume. Finally,  $E$  is the total internal energy stored in the control volume. The rate of heat flow to the control volume has:

$$C_p \dot{m}_a T_a - P_a \frac{dV_a}{dt} + \frac{dQ_h}{dt} = \frac{d(C_v \rho_a V_a T_a)}{dt} \quad (2.9)$$

where  $\rho = P/R_u T$  for air behaving as an *ideal gas*. The constant pressure specific heat can be set as  $C_p = \gamma R_u / (\gamma - 1)$ . It is then assumed that there is no heat *to* or *from* the control volume, that is adiabatic conditions with  $dQ_h = 0$ .

In later chapters, the performance of the controllers under investigation will be evaluated in a series of robustness tests. These tests include: increasing or decreasing the payload by a factor of 3 and increasing the volume of the cylinder by up to a factor of 4. The linear gains of these controllers are based on a linearised model of the pneumatic positioner. As will be shown later in this chapter, the dynamic performance of pneumatic actuators (natural frequency and damping) is heavily dependent on the location of the setpoint and on the direction of motion (in the case of asymmetric cylinders). Since there are so many other dynamic effects that dominate the performance of pneumatic actuators, then a further assumption can be made for the energy balance of Eq. 2.9: that the temperature variation in the chambers is *negligible*, i.e.  $\delta T_a = \delta T_b = 0$  (Uebing *et al*, 1997). The mass flows *in* and *out* of the chambers can then be shown as:

$$\dot{m}_a = \frac{l}{R_u T_a} \left( P_a \frac{dV_a}{dt} + \frac{V_a}{\gamma} \frac{dP_a}{dt} \right) \quad (2.10)$$

$$\dot{m}_b = - \frac{l}{R_u T_b} \left( P_b \frac{dV_b}{dt} + \frac{V_b}{\gamma} \frac{dP_b}{dt} \right) \quad (2.11)$$

*Pu et al (1995)* have shown charging and discharging flow equations for a pneumatic servomechanism that are identical to Eq. 2.10 and Eq. 2.11. *McCloy and Martin (1980)* show charging and discharging flow equations only for a symmetric actuator, therefore  $P_a = P_b$ . A further assumption is that  $T_a$  and  $T_b$  are equal to the supply pressure  $T_s$ . Steady state analysis that will be presented later in the chapter will demonstrate how a

scaling factor between steady state chamber pressures and the supply pressure can be determined.

### 2.1.2 Modelling Actuators

Connected to the servovalve is the pneumatic cylinder, of which the piston moves back and forth according to the forces acting on it. A force balance on the piston yields:

$$P_a A_a - P_b A_b = M_e \frac{d^2 y}{dt^2} + F + F_f \quad (2.12)$$

where  $M_e$  is the effective inertial load or mass,  $F$  is a constant external force such as gravity (this could be zero if the cylinder is horizontal) and  $F_f$  which is the friction force. Typical friction versus speed plots are shown in Fig. 2.4. The static coulomb friction force is the friction that opposes motion when the cylinder is at rest and is denoted as  $F_{cs}$ . Once motion is initiated, the static coulomb friction force is replaced by the dynamic friction force. One formulation of the dynamic friction force is:

$$F_f = F_{cd} \operatorname{sgn}\left(\frac{dy}{dt}\right) + f_v \frac{dy}{dt} \quad (2.13)$$

where  $F_{cd}$  is the directional dynamic coulomb friction force and  $f_v$  is the viscous friction coefficient. Typically, piston and rod seals tend to have a greater breakaway (static) friction than running (dynamic) friction - a condition known as *stiction*. The presence of stiction can cause undesirable position tracking performance when the load approaches the setpoint and the controller decreases flow to decelerate the load in preparation for stopping. When the speed drops to a certain point, stiction inhibits further motion which stops the load short of the setpoint. The controller compensates by increasing pressure in the charging chamber and as a result the load most likely jumps ahead of the setpoint. This effect is not as dramatic when it comes to hydraulic systems since the working fluid is also the lubricant, which decreases both friction coefficients. Stiction still occurs, but  $F_{cd} \approx F_{cs}$ .

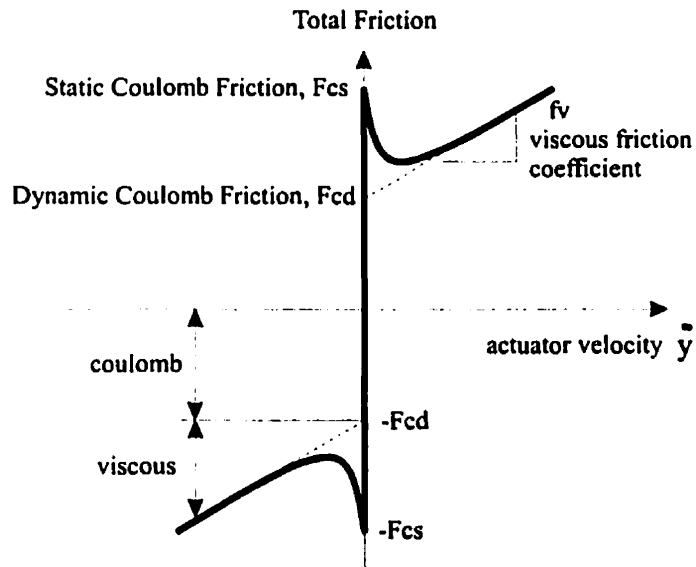


Figure 2.4a: Exponential Friction Model

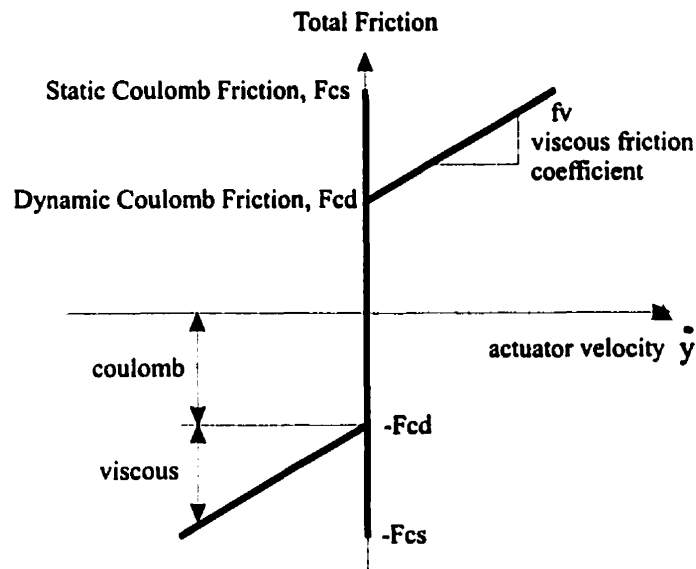


Figure 2.4b: Simplified Friction Model

Figure 2.4: Typical Friction Versus Speed Models

The pneumatic system model is therefore described by Eq. 2.6, 2.7, 2.10, 2.11, 2.12 and 2.13. It is a nonlinear model as governed by: air compressibility effects, choked/subsonic flow conditions and, presence of static friction. A summary of assumptions used in the derivation of the pneumatic system model equations is given below:

- Air behaves as an ideal gas
- No external forces on cylinder (horizontal loading), which implies that  $F$  shown in Eq. 2.12 is *zero*.
- Adiabatic conditions, i.e. no heat flow from, or to the control volume
- Pressure at vena contracta is same as downstream pressure
- Valve spool dynamics (with internal feedback) have a bandwidth of 200 Hz and are much faster than the dynamics of the rest of the pneumatic system, which has a bandwidth in the order of 10 Hz. Therefore, the valve spool dynamics can be neglected. This implies that the valve opening,  $A_{vV}$  can be set directly proportional to the control input to the valve,  $u$ ; hence  $A_{vV}=u$ .

## 2.2 Linearisation of Pneumatic Model

The derivation of the pneumatic model in the previous section highlighted the presence of nonlinearities. An additional set of assumptions can be made to enable model linearisation:

- Supply pressure  $P_s$  and temperature  $T_s$  are constant.
- The piston moves around the center position of the cylinder (linearisation point) and only over small distances.
- Cylinder pressures vary only by a small amount from their steady state values.

Starting with Eq. 2.6 and 2.7, and assuming small variations in pressures and position offsets from the center position, one can write:

$$\delta \dot{m}_a = k_{1a} \delta A_{va} + k_{3a} \delta P_a \quad (2.14)$$

$$\delta \dot{m}_b = k_{1b} \delta A_{vb} + k_{2b} \delta P_b \quad (2.15)$$

Further simplifications are possible since  $k_{1a}=k_{1b}=k_1$  and  $k_{3a}=-k_{2b}=k_2$ . In addition, since most valves are symmetric,  $A_{va} = A_{vb} = A_{vv}$ . Thus the linearised valve model can be written as (McCloy and Martin, 1980):

$$\delta \dot{m}_a = k_1 \delta A_{vv} + k_2 \delta P_a \quad (2.16)$$

$$\delta \dot{m}_b = k_1 \delta A_{vv} - k_2 \delta P_b \quad (2.17)$$

where  $k_1 = (\partial \dot{m} / \partial A_{vv})$  and  $k_2 = (\partial \dot{m} / \partial P)$ .

Combining Eq. 2.16 and 2.17 with Eq. 2.10 and 2.11, and denoting initial conditions with the subscript  $i$ , one can write:

$$\delta \dot{m}_a = \frac{1}{R_u T_s} \left( P_i \frac{d(\delta V_a)}{dt} + \frac{V_i}{\gamma} \frac{d(\delta P_a)}{dt} \right) \quad (2.18)$$

$$\delta \dot{m}_b = -\frac{1}{R_u T_s} \left( P_i \frac{d(\delta V_b)}{dt} + \frac{V_i}{\gamma} \frac{d(\delta P_b)}{dt} \right) \quad (2.19)$$

Assuming a symmetric actuator is in use, i.e.  $A_a=A_b=A_s$ , the chamber control volumes  $V_a$  and  $V_b$  can be given as:

$$V_a = V_i + A_s \delta y \quad (2.20)$$

$$V_b = V_i - A_s \delta y \quad (2.21)$$

with  $y$  measured from the center position of the cylinder and  $V_i$  as the initial volume in each of the cylinder chambers, equal to  $A_s L/2 + V_{min}$ , where  $L$  is the cylinder length and  $V_{min}$  is the volume of air at each end of the cylinder, as Fig. 2.5 shows.

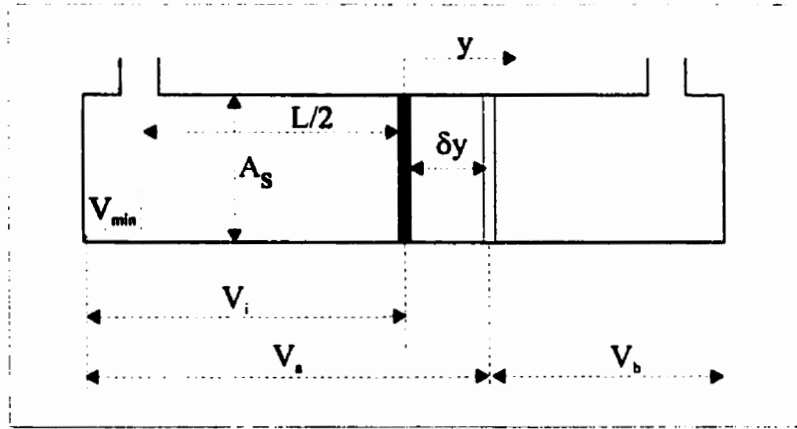


Figure 2.5: Nominal Operating Position and Pressures

Subtracting Eq. 2.19 from 2.18 and using  $V_a - V_b = 2A_s \delta y$  from Eq. 2.20 and 2.21, one has:

$$\delta \dot{m}_a + \delta \dot{m}_b = \frac{l}{R_u T_s} \left( 2 P_i A_s \dot{y} + \frac{V_i}{\gamma} (\dot{P}_a - \dot{P}_b) \right) \quad (2.22)$$

Since a horizontal ( $F=0$  in the absence of other external forces to the system) and symmetric actuator ( $A_a=A_b=A_s$ ) is used, Eq. 2.12 can be simplified to:

$$A_s (\delta P_a - \delta P_b) = M_c \ddot{y} + \delta F_f \quad (2.23)$$

Combining Eq. 2.16, 2.17, 2.22 and substituting into Eq. 2.23 yields:

$$\mu_1 \frac{d^3 \tilde{y}}{dt^3} + \mu_2 \frac{d^2 \tilde{y}}{dt^2} + \mu_3 \frac{d \tilde{y}}{dt} = \chi_1 \tilde{A}_{vv} + \chi_2 \tilde{F}_f + \chi_3 \dot{\tilde{F}}_f \quad (2.24)$$

where  $\tilde{y}$ ,  $\tilde{A}_{vv}$ ,  $\tilde{F}_f$  and  $\dot{\tilde{F}}_f$  are the perturbation variables for position, valve opening, friction and rate of change of friction. The coefficients  $\mu_i$  and  $\chi_i$  are given as:

$$\mu_1 = \frac{M_e V_i}{2\gamma P_i A_s^2}, \quad \mu_2 = \frac{-M_e k_2 R_u T_s}{2P_i A_s^2}, \quad \mu_3 = 1$$

and,

$$\chi_1 = \frac{R_u T_s k_1}{P_i A_s}, \quad \chi_2 = \frac{R_u T_s k_2}{2P_i A_s^2}, \quad \chi_3 = \frac{-V_i}{2\gamma P_i A_s^2}.$$

Note that the linearised pneumatic system model given as Eq. 2.24 is 3<sup>rd</sup> order with respect to position.

The coefficients  $k_1$  and  $k_2$  first appeared in Eq. 2.16 and 2.17. The first coefficient,  $k_1$  is directly proportional to the *flow-gain* coefficient as suggested by *Burrows (1972)*. The second coefficient is called the *flow-pressure* coefficient and it has been shown by *Burrows and Webb (1969)* that the effect of the  $k_2$  term is negligible, which greatly simplifies the coefficients of Eq. 2.24 to:

$$\mu_1 = \frac{M_e V_i}{2\gamma P_i A_s^2}, \quad \mu_2 = 0, \quad \mu_3 = 1$$

and,

$$\chi_1 = \frac{R_u T_s k_1}{P_i A_s}, \quad \chi_2 = 0, \quad \chi_3 = \frac{-V_i}{2\gamma P_i A_s^2}.$$

Dividing all elements of Eq. 2.24 by  $\mu_1$  modifies the linearised pneumatic model to:

$$\ddot{\tilde{y}} + 2\gamma \frac{P_i A_s^2}{M_e V_i} \dot{\tilde{y}} = 2\gamma k_1 \frac{R_u T_s A_s}{M_e V_i} \tilde{A}_{vv} - \frac{1}{M_e} \dot{\tilde{F}}_f \quad (2.25)$$

For further simplification of the above model, one assumes that the static friction can be set to zero ( $F_c=0$ ) which makes  $\dot{\tilde{F}}_f$  equal to  $f_v \frac{d^2 y}{dt^2}$ , as Eq. 2.13 implies. With these simplifications the model shown as Eq. 2.24 can be further simplified to:

$$\ddot{\tilde{y}} + \frac{f_v}{M_e} \ddot{\tilde{y}} + 2\gamma \frac{P_i A_s^2}{M_e V_i} \dot{\tilde{y}} = 2\gamma k_1 \frac{R T_s A_s}{M_e V_i} \tilde{A}_{vv} \quad (2.26)$$



The instantaneous valve opening  $A_{vv}$  can be assumed to be proportional to a normalised control input signal,  $u$  so that  $A_{vv} = A_v u$ , where  $A_v$  is the full valve opening area. The flow coefficient  $k_1$  can then found to be equal to  $C_d C_m \sqrt{P_i / \rho}$ . If the initial pressure in the chamber,  $P_i$  is considered to be at steady state, then there exists a relationship between the chamber pressure and the supply pressure  $P_s$ . For now though, consider that  $P_i = r_p P_s$ , where  $r_p$  is called the steady state pressure ratio. An expression for the steady state pressure ratio will be provided in Section 2.3 of this chapter. With  $k_1$ ,  $r_p$  and  $A_{vv}$  substituted into Eq. 2.26, the linearised pneumatic model becomes:

$$\ddot{y} + \frac{f_v}{M_e} \dot{y} + 2\gamma \frac{P_i A_s^2}{M_e V_i} y = 2\gamma C_d C_m A_v \frac{R_u \sqrt{T_s} A_s P_i}{M_e V_i r_p} u \quad (2.27)$$

Note that the above equation has  $P_i = P_a = P_b$  at initial conditions for a symmetric cylinder and is also the nominal operating pressure. With  $y$  as the nominal operating point, the following is true:

$$2 \frac{P_i}{V_i} = \left( \frac{P_a}{V_a} \right)_i + \left( \frac{P_b}{V_b} \right)_i = \frac{P_a}{A_s (l/2 + y) + V_{min}} + \frac{P_b}{A_s (l/2 - y) + V_{min}} \quad (2.28)$$

which modifies Eq. 2.27 to the following:

$$\begin{aligned} \ddot{y} + \frac{f_v}{M_e} \dot{y} + \frac{\gamma A_s^2 P_i}{M_e} \left[ \frac{l}{A_s (l/2 + y) + V_{min}} + \frac{l}{A_s (l/2 - y) + V_{min}} \right] y \\ = \frac{R_u \gamma C_d C_m A_v \sqrt{T_s} P_i}{M_e r_p} \left[ \frac{l}{A_s (l/2 + y) + V_{min}} + \frac{l}{A_s (l/2 - y) + V_{min}} \right] u \end{aligned} \quad (2.29)$$

Once a linearisation point is chosen (eg.  $y=0$ ), the coefficients of Eq. 2.29 assume constant values. The resulting linearised model can then be used to generate the linear gains for the PVA controller and the equivalent gains for the SLM Controllers.

A PC-MATLAB program was written to simulate the process for which selected parts are listed in Appendix B. The model used was nonlinear to account for nonlinear valve dynamics (choked versus subsonic flow, hysteresis) and nonlinear friction. In the linear model, chamber volumes are considered constant as well as the chamber pressures. In

simulation, the pressures in the cylinders can be found by differentiating the ideal gas law with respect to time. The ideal gas law is given as:

$$P = \frac{mR_u T_c}{V} \quad (2.30)$$

In reality, only parameters  $P$ ,  $m$  and  $V$  are time-variant. Differentiating Eq. 2.30 with respect to time (for chamber  $a$ ), and assuming negligible temperature variations:

$$\dot{P}_a = \frac{R_u T_c \dot{m}_a}{V_a} - \frac{m_a R_u T_c \dot{V}_a}{V_a^2} = \frac{R_u T_c \dot{m}_a}{V_a} - \frac{P_a \dot{V}_a}{V_a} \quad (2.31)$$

The pressures in chambers  $a$  and  $b$ , can be found sequentially by using *Euler's* 1<sup>st</sup> order approach for numerical implementation of the difference equation. The resulting difference equation for any pressure, is given as:

$$P_{k+1} = P_k + \dot{P}_k h \quad (2.32)$$

where  $k$  is the “ $k^{\text{th}}$ ” time step.

The simulation sampling time used was set to  $10ms$ , to match the sampling time available to the experimental setup by the microcomputer in use. This sampling time was adequate considering that the smallest settling time for the smallest mass ( $2.2 \text{ kg}$ ) in open loop was  $250 \text{ ms}$ . Numerical stability issues are addressed in *Uebing et al (1997)*.

### 2.2.1 Stability Issue

One recognises that the linearised model of the pneumatic system can be written as:

$$\ddot{y} + a_2 \dot{y} + a_1 y = a_0 u \quad (2.33)$$

where the coefficients  $a_0$ ,  $a_1$  and  $a_2$  are defined according to Eq. 2.29. The open loop transfer function for the pneumatic model can be found to be:

$$G(s) = \frac{Y(s)}{U(s)} = \frac{a_0}{s^3 + a_2 s^2 + a_1 s} \quad (2.34)$$

If a proportional-only controller with unity feedback is implemented to the pneumatic model of Eq. 2.34, a closed loop transfer function can be obtained as:

$$T(s) = \frac{Y(s)}{Y_{set}(s)} = \frac{a_0 K_p}{s^3 + a_2 s^2 + a_1 s + a_0 K_p} \quad (2.35)$$

where  $K_p$  is the proportional gain. Using the *Routh-Hurwitz's* stability criterion, one can find the following stability requirement:

$$a_1 - \frac{a_0 K_p}{a_2} > 0 \quad (2.36)$$

which provides the upper limit for  $K_p$ :

$$K_p < \frac{f_v A_s r_p}{M_e C_d C_m A_v R_u \sqrt{T_s}} \quad (2.37)$$

*Uebing et al (1997)* report a similar upper limit for  $K_p$ . *Surgenor and Vaughan (1996)* reported the above upper limit for  $K_p$  with the absence of  $r_p$  which relates the steady state chamber pressures to the supply pressure. Further discussion on the derivation of the steady state pressure ratio,  $r_p$  will be given in Section 2.3.

A larger value for  $K_p$  indicates higher stability margins. One can then say that the stability of the system increases if the viscous friction coefficient and the cylinder areas increase, when the effective mass is reduced or the area of the opening decreases, i.e. a smaller valve is used. Note also that Eq. 2.37 indicates that the ultimate  $K_p$  is independent of the position of the piston along the cylinder. This is in disagreement with results presented in *Pu and Weston (1990)* where such a dependency is reported.

The ratio  $\frac{u}{u_n}$  which results from Eq. 2.36 eliminates any possibility for  $V_i$  to appear, which is the element that causes a position dependency. It should be noted though that the overall **dynamic** behaviour of pneumatic systems **does** depend on the position of the cylinder piston, as originally shown by *Burrows (1969)*. Therefore, a numerical stability issue will arise due to the link between the natural frequency of the system and the sampling interval.

Looking at the denominator of the open loop transfer function given in Eq. 2.34, it can be realised that the pneumatic linear model consists of a second order system and an integrator. Linked to the second order system, parameters such as natural frequency,  $\omega_n$  and damping ratio,  $\zeta$  can be identified:

$$\omega_n = \sqrt{\frac{\gamma A_s^2 P_i}{M_e} \left[ \frac{l}{A_s(l/2 + y) + V_{min}} + \frac{l}{A_s(l/2 - y) + V_{min}} \right]} \quad (2.38)$$

and

$$\zeta = \frac{f_v}{2 A_s \sqrt{\gamma P_i M_e} \left[ \frac{l}{A_s(l/2 + y) + V_{min}} + \frac{l}{A_s(l/2 - y) + V_{min}} \right]} \quad (2.39)$$

The above two equations give rise to the following issues:

- The relationship between cylinder size ratio and natural frequency.
- The relationship between operating position and natural frequency.
- The relationship between operating position and damping.

Both aspects (operating position and cylinder size ratio) will influence sampling interval stability. To proceed with further analysis, the size ratio of a symmetric cylinder needs to be defined:

$$d_e = \sqrt{\frac{A_s}{L}} \quad (2.40)$$

### 2.2.2 Natural Frequency and Cylinder Size Ratio

In order to determine the relationship between the natural frequency and the size ratio, a further simplification was performed. If the operating point is assumed to be at the center of the cylinder, i.e.  $y = 0$  in Eq. 2.38, then the minimum chamber volume  $V_{min}$  can be assumed to be negligible compared to the chamber volumes  $V_a$  and  $V_b$ . This assumption simplifies Eq. 2.38 to:

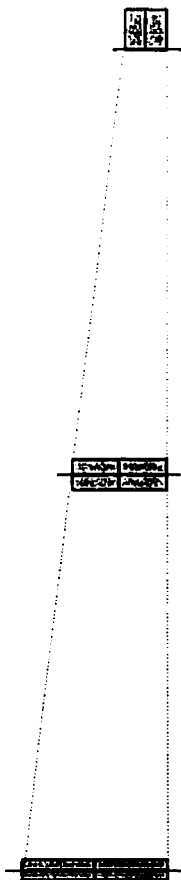
$$\omega_n = 2 d_e \sqrt{\frac{\gamma P_i}{M_e}} \quad (2.41)$$

Table 2.1 shows the ultimate gains predicted by the model (as given in Eq. 2.37) for a series of cylinders with size ratios ranging from 1.2 to 6.1. Size ratios of 1.2 and 6.1 roughly correspond to *stroke / cylinder diameter* ratios of 1.0 and 10.0 respectively. These *stroke / cylinder diameter* ratios correspond to typical low and upper bounds of commercially available pneumatic cylinders.

The “benchmark” cylinder has a stroke of 120 mm and a diameter of 25 mm. It can be seen as the bold entry in the middle of the table. The remaining cylinders have an overall chamber volume equal to the volume of the benchmark cylinder. The stroke, or length of the cylinders was changed by intervals of 10 mm from an initial stroke of 40 mm to a final stroke of 200 mm, while simultaneously adjusting the chamber area so that the overall volume is kept the same (which allows for the use of the same valve). The size ratio,  $d_e$  can be seen as the last column entry.

Upon inspection of Table 2.1, one can see a discrepancy between predicted values for the ultimate gain,  $K_u$  and the one obtained by nonlinear simulation with a proportional only controller (that is the value of  $K_p$  that generated marginal stability in the system’s response). It can be seen though that there exists an approximate ratio of 2 between the linear and the nonlinear ultimate gains. This can be explained if one realises that the linear model makes the assumption that only choked flow occurs throughout the duration of the test, i.e.  $C_m = 0.0405$ , whereas in nonlinear simulation,  $C_m$  can assume

**Table 2.1: Ultimate Gain for cylinders of different Size Ratios**

	Length, (L) mm	Area, (A <sub>c</sub> ) mm <sup>2</sup>	Diameter, (D <sub>c</sub> ) mm	K <sub>p</sub> , <i>nonlinear simulation</i>	K <sub>u</sub> , <i>linear model prediction</i>	Size ratio, (d <sub>t</sub> ) <i>sqrt(A/L)</i>
	40	1472.60	43.3	27.0	14.4	6.1
	50	1178.08	38.7	22.0	11.4	4.9
	60	981.73	35.4	17.5	9.4	4.0
	70	841.49	32.7	16.2	7.9	3.5
	80	736.30	30.6	14.0	6.8	3.0
	90	654.49	28.9	11.5	6.0	2.7
	100	589.04	27.4	9.5	5.3	2.4
	110	535.49	26.1	8.9	4.7	2.2
	120	490.87	25.0	8.0	4.3	2.0
	130	453.11	24.0	7.4	3.9	1.9
	140	420.74	23.1	6.9	3.5	1.7
	150	392.69	22.4	6.4	3.3	1.6
	160	368.15	21.7	5.8	3.0	1.5
	170	346.49	21.0	5.2	2.8	1.4
	180	327.24	20.4	4.9	2.6	1.3
	190	310.02	19.9	4.6	2.4	1.3
	200	294.52	19.4	4.3	2.2	1.2

both choked and subsonic values, for which an average would be about half of the choked value, i.e. 0.0202. Therefore, the ultimate gain obtained by nonlinear simulation would be approximately double the value of the gain predicted by the linear model.

Fig. 2.6, 2.7 and 2.8 show the simulated response of the pneumatic cylinders with size ratios of 6.1, 2.0 and 1.2, respectively for a setpoint scenario where the piston is sequentially moved between center- and quarter-length positions. When comparing the responses shown in Fig. 2.6 and 2.7, one can see that the natural frequency of the cylinder that has a stroke of 40 mm and a diameter of 43.3 mm (i.e.  $d_e = 6.1$ ) is indeed

about 3 times greater than the frequency reached by a cylinder that has a stroke of  $120\text{ mm}$  and a diameter of  $25.0\text{ mm}$  (i.e.  $d_e = 2.0$ ). Similarly, if the responses shown in Fig. 2.7 and 2.8 are compared, then it can be seen that the natural frequency of the cylinder that has a stroke of  $120\text{ mm}$  and a diameter of  $25.0\text{ mm}$  (i.e.  $d_e = 2.0$ ) is indeed about 1.6 times greater than the frequency achieved by a cylinder that has a stroke of  $200\text{ mm}$  and a diameter of  $19.4\text{ mm}$  (i.e.  $d_e = 1.2$ ).

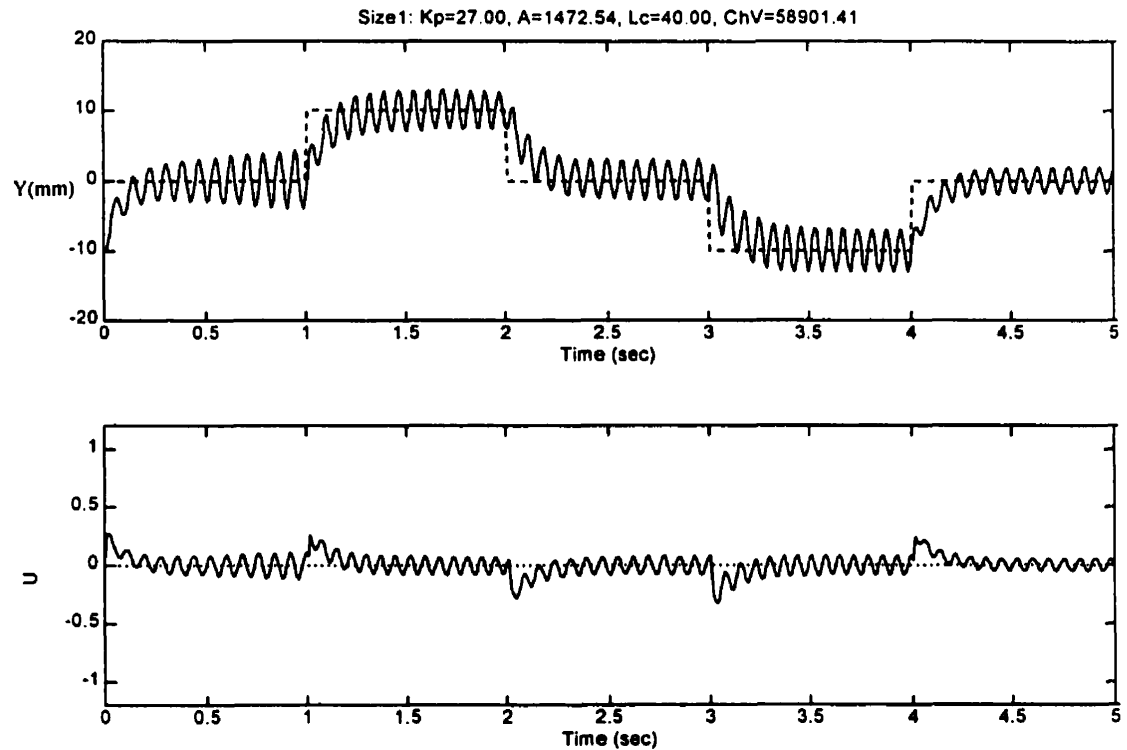


Figure 2.6: Marginal Response with Ultimate Gain for Cylinder of  $d_e=6.1$

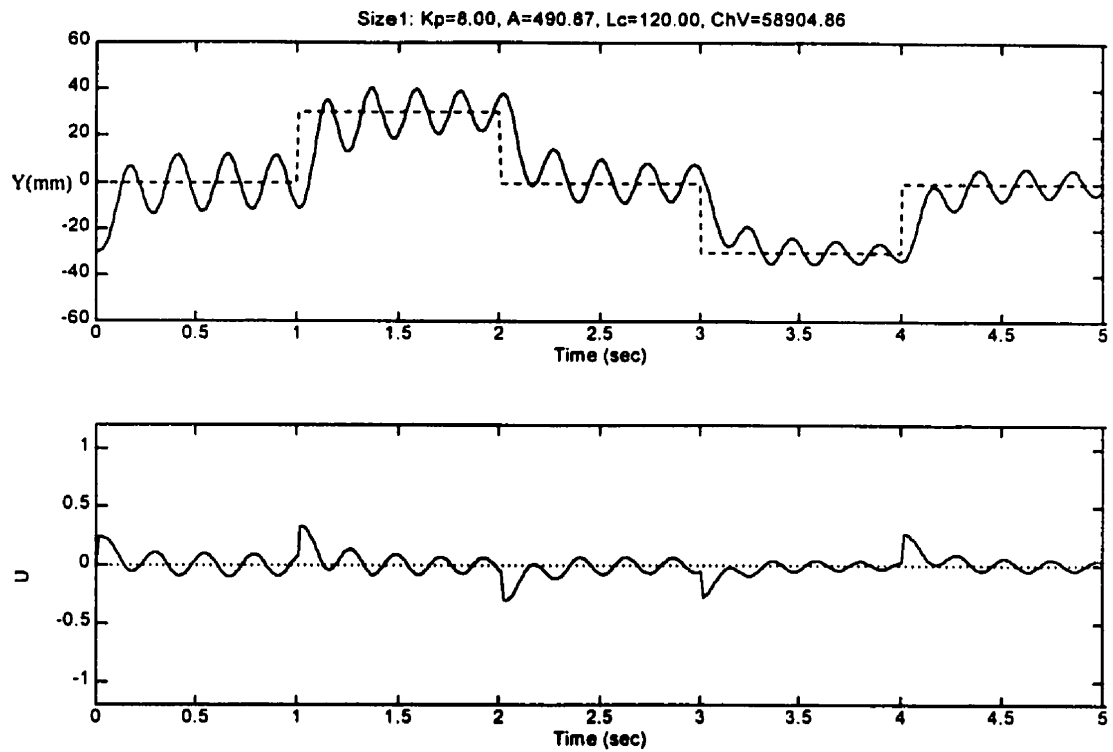


Figure 2.7: Marginal Response with Ultimate Gain for Cylinder of  $d_c=2.0$

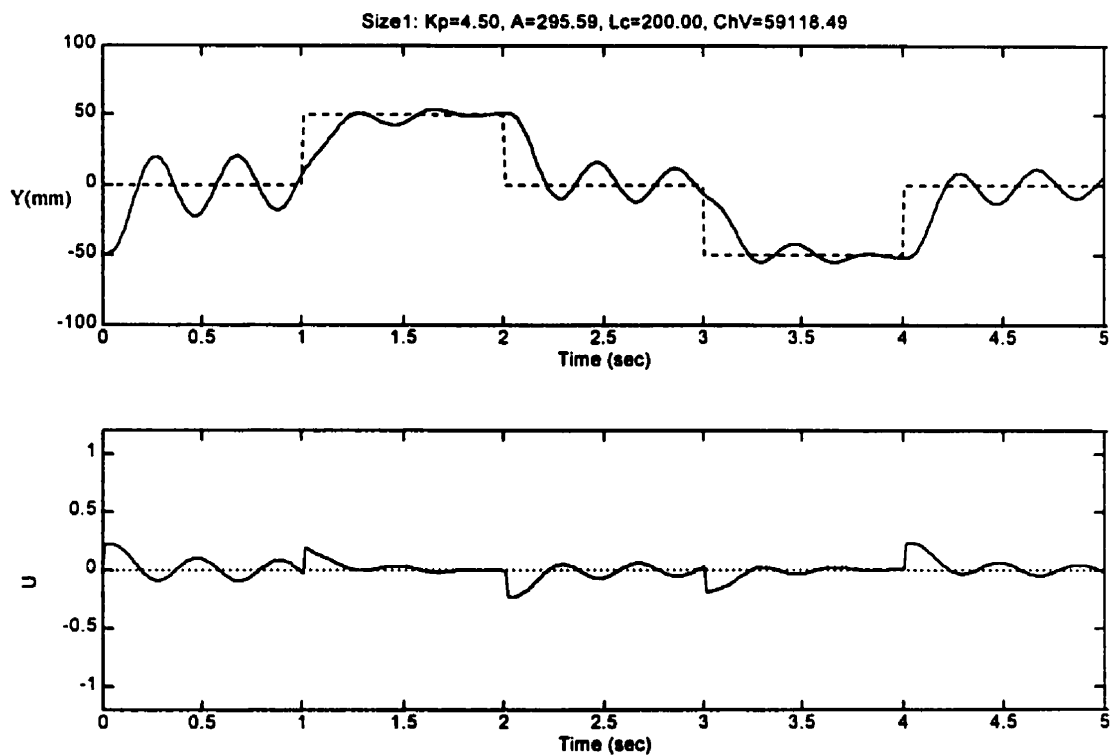


Figure 2.8: Marginal Response with Ultimate Gain for Cylinder of  $d_c=1.2$



In the case of the system shown in Fig. 2.6, the frequency is about *15 Hz*. Thus, for adequate control when applied to a cylinder with this size ratio, one would require a *150 Hz* sampling interval for control purposes. This corresponds to a sampling time of *6.67 ms*. Therefore, the larger the size ratio of the cylinder at hand, the faster the microprocessor used for control has to be.

### 2.2.3 Natural Frequency and Operating Position

If the linearisation point is moved from the center of the cylinder, to the quarter-length position (i.e. at  $y=\pm L/4$ ), then the natural frequency of the pneumatic system, according to Eq. 2.38 (at center) changes from Eq. 2.41 to:

$$\omega_n = 2.3 d_c \sqrt{\frac{\gamma P_i}{M_c}} \quad (2.42)$$

Fig. 2.9a shows how the natural frequency changes along the length of a cylinder. For a symmetric or rodless actuator where the cylinder chambers have the same area, there is a symmetry about the center of the cylinder. It can be shown that at the center of a rodless cylinder, the natural frequency has its lowest value. The normalised frequency,

$\frac{\omega_n}{\omega_n|_{y=0}}$  is shown on the y-axis. At the center ( $y=0$ ) the ratio is *1.00*. At quarter length, the ratio becomes *1.15* (Eq. 2.42 / Eq. 2.41) and at the stroke ends the frequency ratio reaches a value of *2.5*.

### 2.2.4 System Damping and Operating Position

Looking at Eq. 2.39, one can see that there is also a relationship between the operating position and the damping of the pneumatic system. If  $V_{min}$  is neglected in Eq. 2.39, then, if the operating point is at the center of the cylinder, the damping can be given as:

$$\zeta = \left(\frac{1}{4}\right) \frac{f_v}{d_c \sqrt{\gamma P_i M_c}} \quad (2.43)$$

If one assumes that the operating point is halfway between the center and the end of the cylinder, i.e. at  $y=\pm L/4$ , then:

$$\zeta = \left( \sqrt{3}/8 \right) \frac{f_v}{d_c \sqrt{\gamma P_i M_c}} \quad (2.44)$$

Assuming that for a particular pneumatic system the damping coefficient at the center of the cylinder is  $0.50$ , then at the quarter lengths, the damping drops to  $0.42$ . Fig. 2.9b shows how the damping coefficient ratio changes along the length of the cylinder. For a symmetric actuator, there is again symmetry about the center of the cylinder, where it has its maximum. The ratio of damping coefficients,  $\frac{\zeta}{\zeta|_{y=0}}$  is shown on the vertical axis. At the center, i.e.  $y=0$  the ratio is  $1.00$ . At the quarter length, the ratio becomes  $0.86$  and at the stroke ends the ratio of damping coefficients becomes  $0.40$ .

### 2.2.5 Asymmetric Cylinder

The above analysis was performed for a symmetric cylinder ( $A_a = A_b$ ). If an asymmetric cylinder is used instead, a nonlinear model simulation predicts the behavior seen in Fig. 2.10. The simulated asymmetric cylinder has a stroke of  $120 \text{ mm}$  (similar to the cylinder used earlier), a bore diameter of  $25 \text{ mm}$  and a rod (piston) diameter of  $10 \text{ mm}$ . The presence of the rod decreases the area of chamber  $b$ , roughly from  $490 \text{ mm}^2$  to  $410 \text{ mm}^2$ . Fig. 2.10 shows the response of this asymmetric cylinder when subjected to proportional-only control with a gain of  $6.5$ . It can be seen that when the piston is in extension, marginal stability is reached. When the piston is in retraction, the response is still damped. It becomes marginally stable only when the gain is increased to  $8.0$ . An ultimate gain of  $8.0$  was also the gain determined for the symmetric cylinder with  $120 \text{ mm}$  stroke and  $25 \text{ mm}$  bore diameter, shown in Fig. 2.7.

It can then be said that in an asymmetric cylinder the *direction* of motion also affects the natural frequency and the damping of the system. Therefore, asymmetry affects the dynamic response of the system, as well as its ultimate gain. Eq. 2.37 can still be used to predict the ultimate gain for a linear model by setting  $A_s$  equal to the smaller of the chamber areas. This is so because a smaller chamber area decreases the ultimate gain in extension.

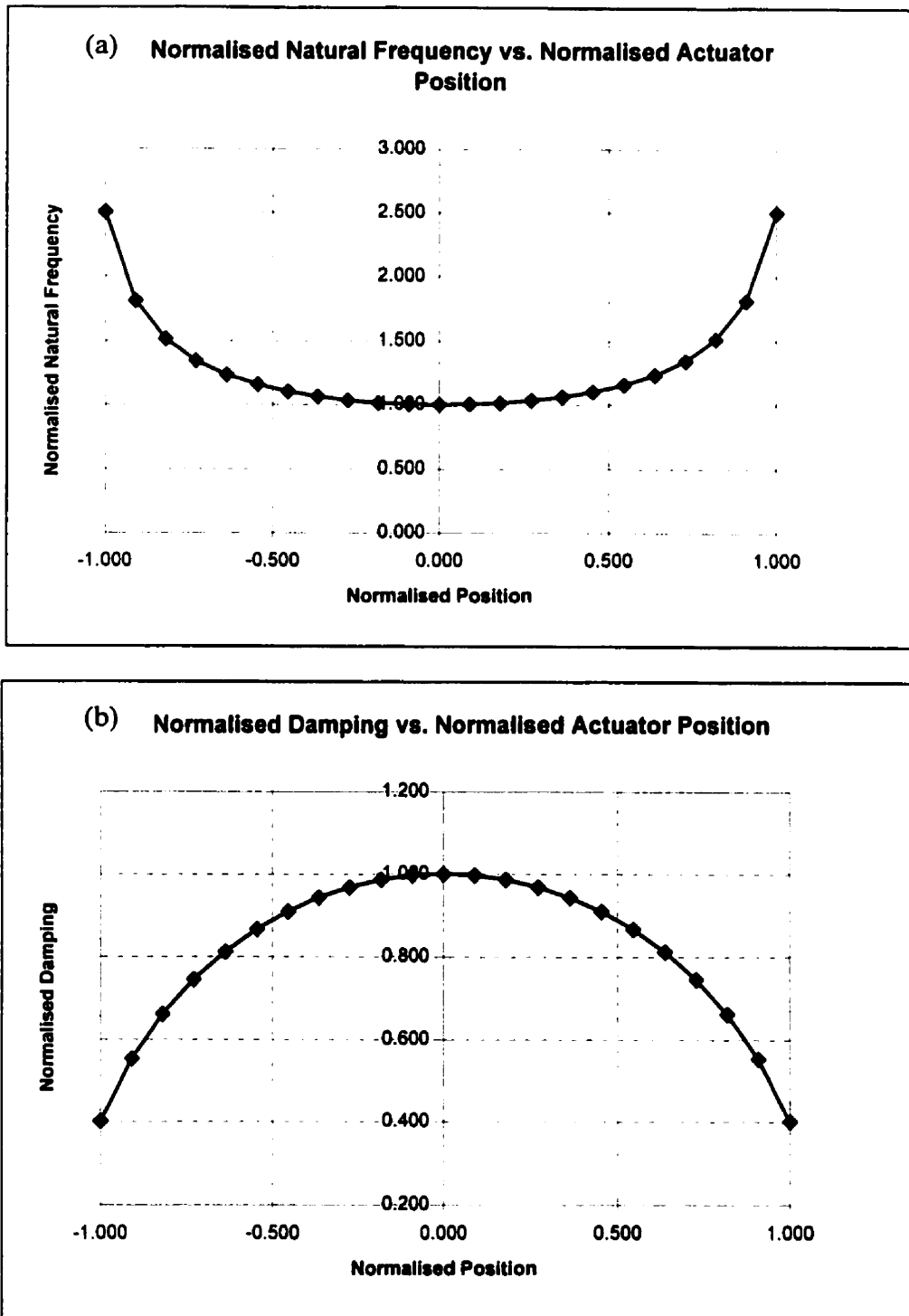


Figure 2.9: Normalised Natural Frequency and Damping versus Normalised Operating Position

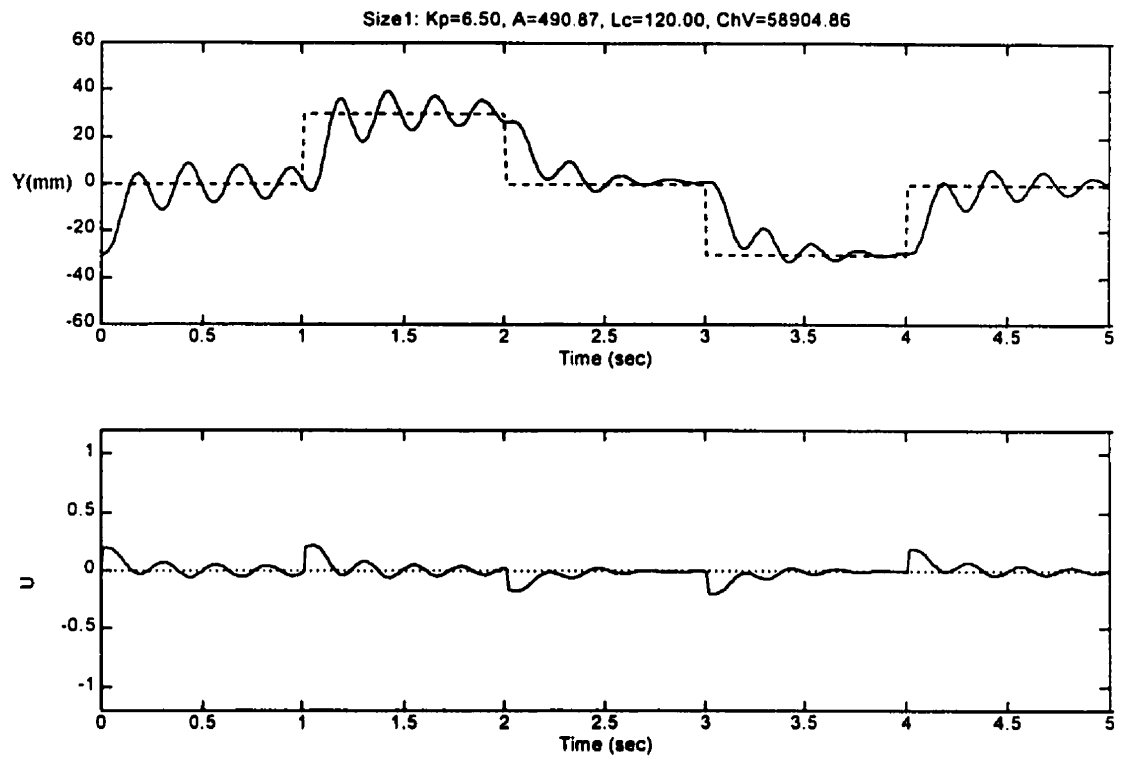


Figure 2.10: Marginal Response with Ultimate Gain for Asymmetric Cylinder

### 2.3 Steady State Considerations

An important consideration in the performance of pneumatic systems is the ratio of the chamber pressures  $P_a$  and  $P_b$  to the supply pressure  $P_s$  at steady state. Note that  $P_i$  as used earlier was in fact equal to the steady state operating pressure. For closed center valves and if the entry port flow is subsonic,  $P_a$  can be given as (Pu and Weston, 1990):

$$P_a^{ss} = P_s r_p = P_s \left[ \frac{2}{1 + \sqrt{1 + \frac{4}{N^2}}} \right]^{\frac{\gamma}{\gamma-1}} \quad (2.45)$$

where  $P_a^{ss}$  denotes a nominal steady state pressure. The ratio of the steady state pressure to the supply pressure corresponds to  $r_p$ , as was first seen in Eq. 2.27.

Note that *subsonic* flow is the **usual** condition for the entry port, whereas for the case of the exit port, the flow is normally *choked*.  $N$ , the valve opening coefficient can be given as:

$$N = h_p C_k \quad (2.46)$$

where  $h_p$  is defined as the system opening ratio, given by:

$$h_p = u_m u_t u_d u_w u_x \quad (2.47)$$

where  $u_m = \frac{A_a}{A_b}$ ,  $u_t = \frac{T_a}{\sqrt{T_b T_s}}$ ,  $u_d = \frac{C_{da}}{C_{db}}$ ,  $u_w = \frac{A_{va}}{A_{vb}}$ ,  $u_x = \left| \frac{U + y_v}{U - y_v} \right|$  and  $U$  denotes the valve spool underlap.  $C_k$  is given by:

$$C_k = \sqrt{\frac{2}{\gamma-1} \left( \frac{\gamma+1}{2} \right)^{\frac{\gamma}{\gamma-1}}} \quad (2.48)$$

Note that for air, where  $\gamma$  is 1.4,  $C_k$  is equal to 3.864.

Usually  $u_t$  and  $u_w$  are equal to unity and ideally  $u_d$  is equal to 1.00. For a small underlap in  $U$  and with  $y_v$  as the displacement of the valve spool from the center position, i.e.  $y_v \gg U$ , then  $u_x$  becomes 1.0. This simplifies Eq. 2.46 to  $N = u_m C_k$ .

For equal cylinder areas ( $u_m=1$ ), the steady state pressures are equal ( $P_a^{ss}=P_b^{ss}$ ), whereas for unequal cylinder areas ( $u_m\neq 1$ )  $P_b^{ss}=P_a^{ss}A_a/A_b$  with  $P_a^{ss}$  given by Eq. 2.45.

To illustrate the effect of some of the parameters of the system, a set of simulation results will be presented (Fig. 2.11 to 2.14). In all cases the initial pressures are  $100\text{ kPa}$  and the cylinder is repeatedly moved from its end position ( $y = -50\text{ mm}$ ) to its center position ( $y = 0\text{ mm}$ ) and vice versa. Each figure gives the cylinder position, the control signal, the absolute cylinder pressures and the differential pressure. The controller used was a typical Proportional-Velocity-Acceleration (PVA). The structure of a traditional PVA controller has:

$$u = K_p (x_{set} - x) - K_v \dot{x} - K_a \ddot{x} \quad (2.49)$$

with  $x$  as the controlled state (position) and  $x_{set}$  as the position setpoint.  $K_p$ ,  $K_v$  and  $K_a$  are the proportional, velocity and acceleration gains respectively. For application to pneumatic systems, it is generally acknowledged that both velocity and acceleration are essential to ensure adequate performance (Burrows, 1972). An alternative linear controller for pneumatic systems is the proportional-differential pressure controller ( $P\Delta P$ ) which can be used for symmetric actuators (Abou-Fayssal, 1997) but was not used due to asymmetry problems.

### 2.3.1 Symmetric Actuator

If the actuator is symmetric ( $u_m = 1$ ) then  $N=3.864$  and according to Eq. 2.12 the ratio of  $P_a^{ss}/P_s$  is equal to  $0.805$ ; Fig. 2.11 illustrates this case. Both  $P_a$  and  $P_b$  start at their initial pressure of  $100\text{ kPa}$  and gradually build up to their steady state values. It can be seen that the steady state pressure  $P_a^{ss}$  does reach  $523\text{ kPa}$  or  $80.5\%$  of the supply pressure  $P_s$  ( $650\text{ kPa}$ ) and  $P_b^{ss}$  is equal to  $P_a^{ss}$ .

Note that as the pressures  $P_a$  and  $P_b$  increase, the quality of the response improves (less overshoot on position). As the pressures increase, the air becomes more

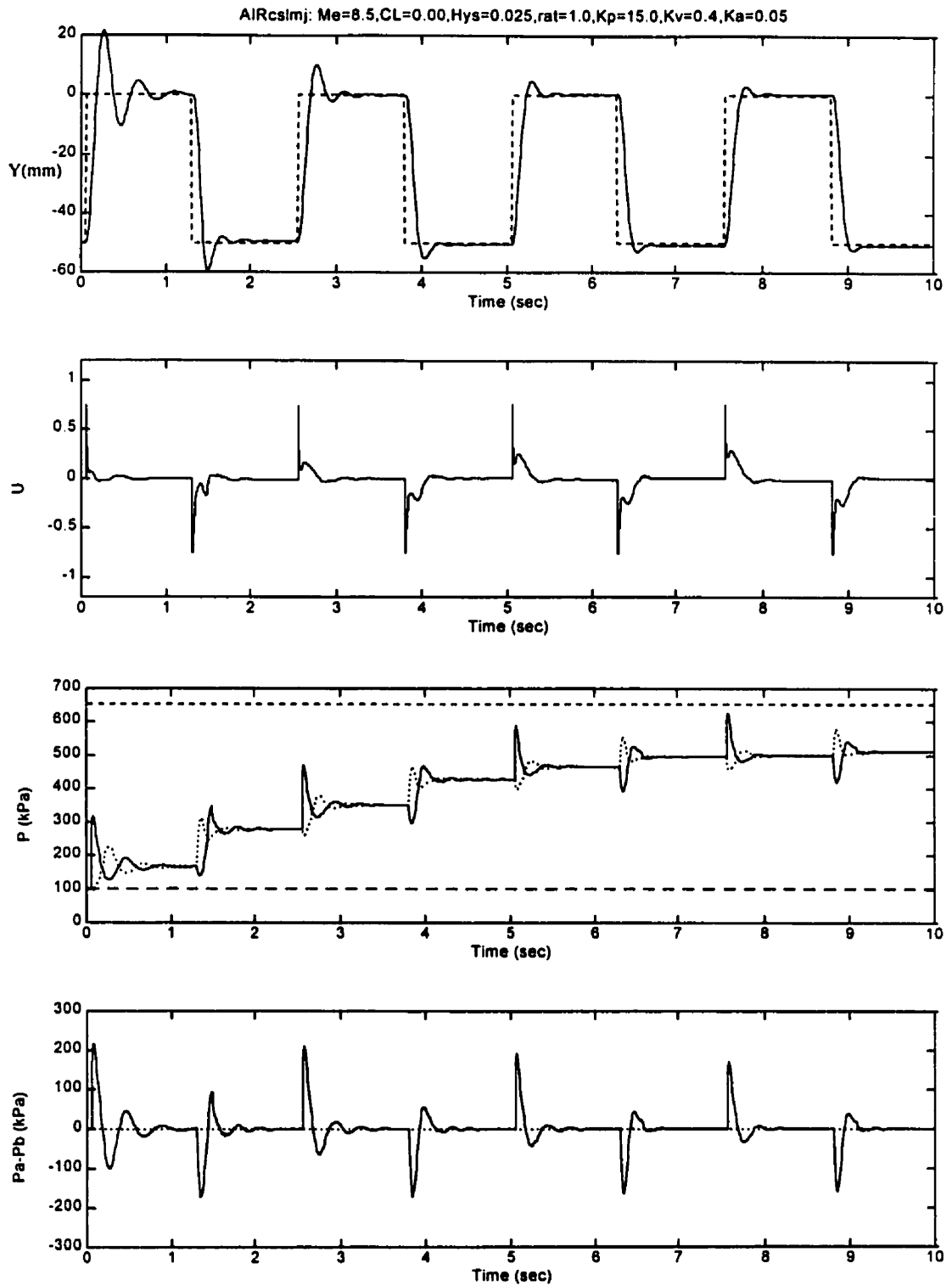


Figure 2.11: Closed Center valve with *PVA* on equal cylinder areas and equal valve ports

compressed and since its density rises, it starts to behave more as an incompressible (linear) fluid.

### 2.3.2 Asymmetric Actuator

Actuators are more commonly asymmetric due to the presence of the cylinder rod that creates non-equal cylinder areas, most commonly with ratios of  $A_b:A_a$  as 1:2 and 1:3. For these, the extending pressure ratios ( $P_a^{ss} / P_s$ ) are equal to 49.9% and 29.1% respectively. The extension of the piston requires that the driving (extending) pressure be applied to the cylinder chamber with the larger area, while for retracting, the opposite is done. The decrease of the pressure ratio in the extension of the piston is a disadvantage.

Fig. 2.12 and 2.13 show the effect of the center configuration being either open (exhaust) or closed (blocked) with an asymmetric cylinder ( $A_b / A_a = 0.84$ ). According to Eq. 2.45, the pressure ratio  $P_a^{ss} / P_s$  is equal to 0.74. In Fig. 2.12, the steady state cylinder pressures remain at their initial values (100 kPa), whereas in Fig. 2.13, the pressures built up to the values dictated by Eq. 2.45 for unequal cylinder areas ( $h_p = 1.167$ ) and with  $N = 4.509$  ( $P_a^{ss} = 483 \text{ kPa}$  and  $P_b^{ss} = 575 \text{ kPa}$ ). It can be seen that in Fig. 2.13 that the responses are smoother than the ones shown in Fig. 2.12 due to the higher operating pressures. Thus, a closed center valve will produce better responses. Another observation is that in Fig. 2.12, steady state error appears in the position response. This cannot be eliminated by simply increasing the proportional gain. It is an effect that results from an open center valve configuration combined with an asymmetric cylinder. Since the cylinder is asymmetric, then at steady state a differential pressure in the cylinders is required to equalise the resulting forces. This is not possible, since the valve is open center and both chambers exhaust to atmosphere. Therefore, a steady state error appears.



When comparing Fig. 2.13 (unequal areas) with Fig. 2.11 (equal areas) one observes little difference in the positioning performance. The only manifestation of the unequal areas in Fig. 2.13 is the nonzero pressure difference ( $P_a - P_b$ ) in the steady state in order to ensure the force balance  $P_a A_a = P_b A_b$ . Therefore, no great advantage can be seen between symmetric and asymmetric actuators in terms of performance. Furthermore, the construction of symmetric actuators requires either a magnetic coupling between the in-cylinder mass and the carriage, or a physical coupling which would require better seals to prevent air leakage. In both cases, frictional effects are increased which tend to degrade the positioning performance of symmetric actuators.

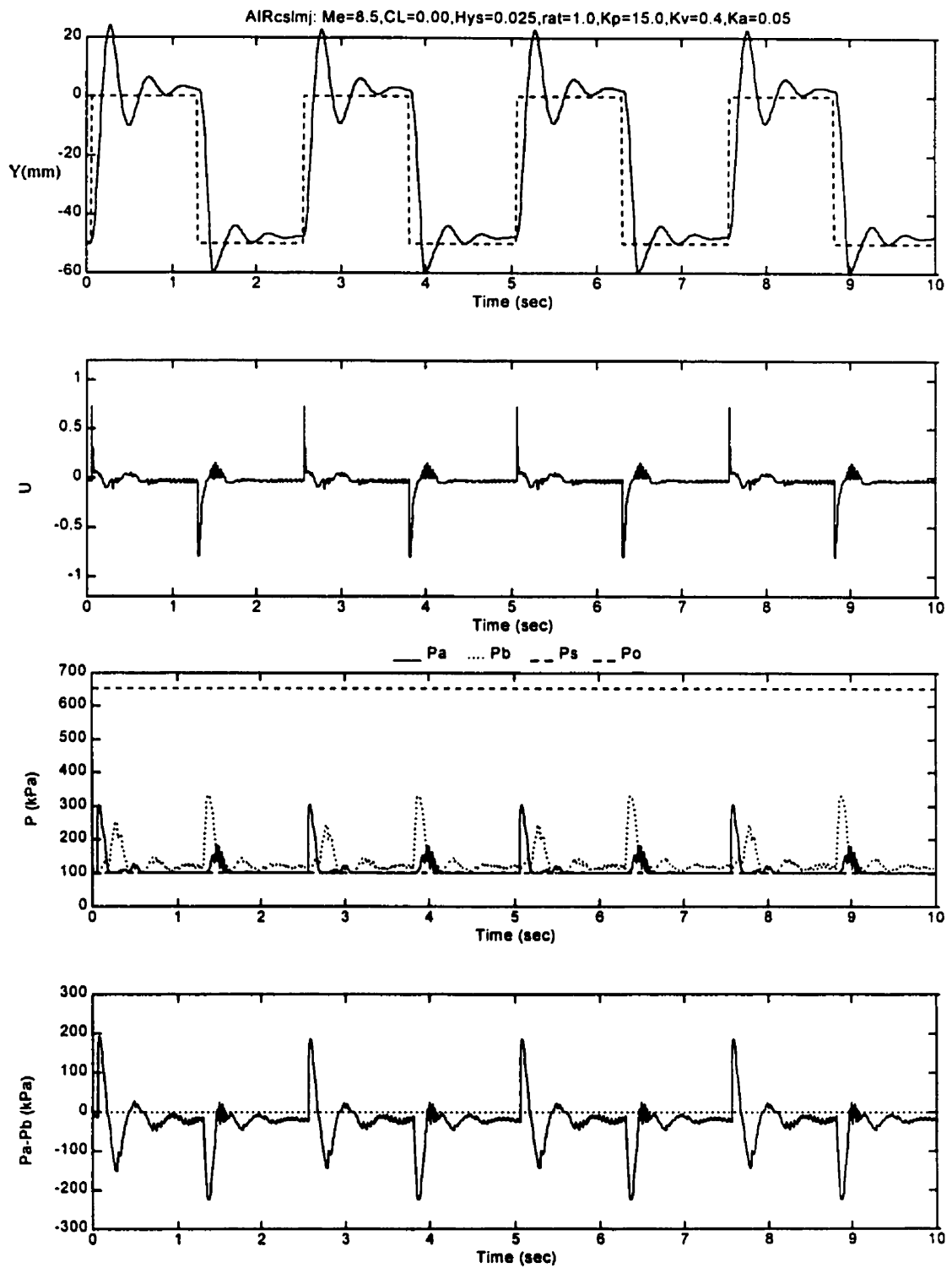


Figure 2.12: Open Center valve with *PVA* on unequal cylinder areas and equal valve ports. Note poor responses

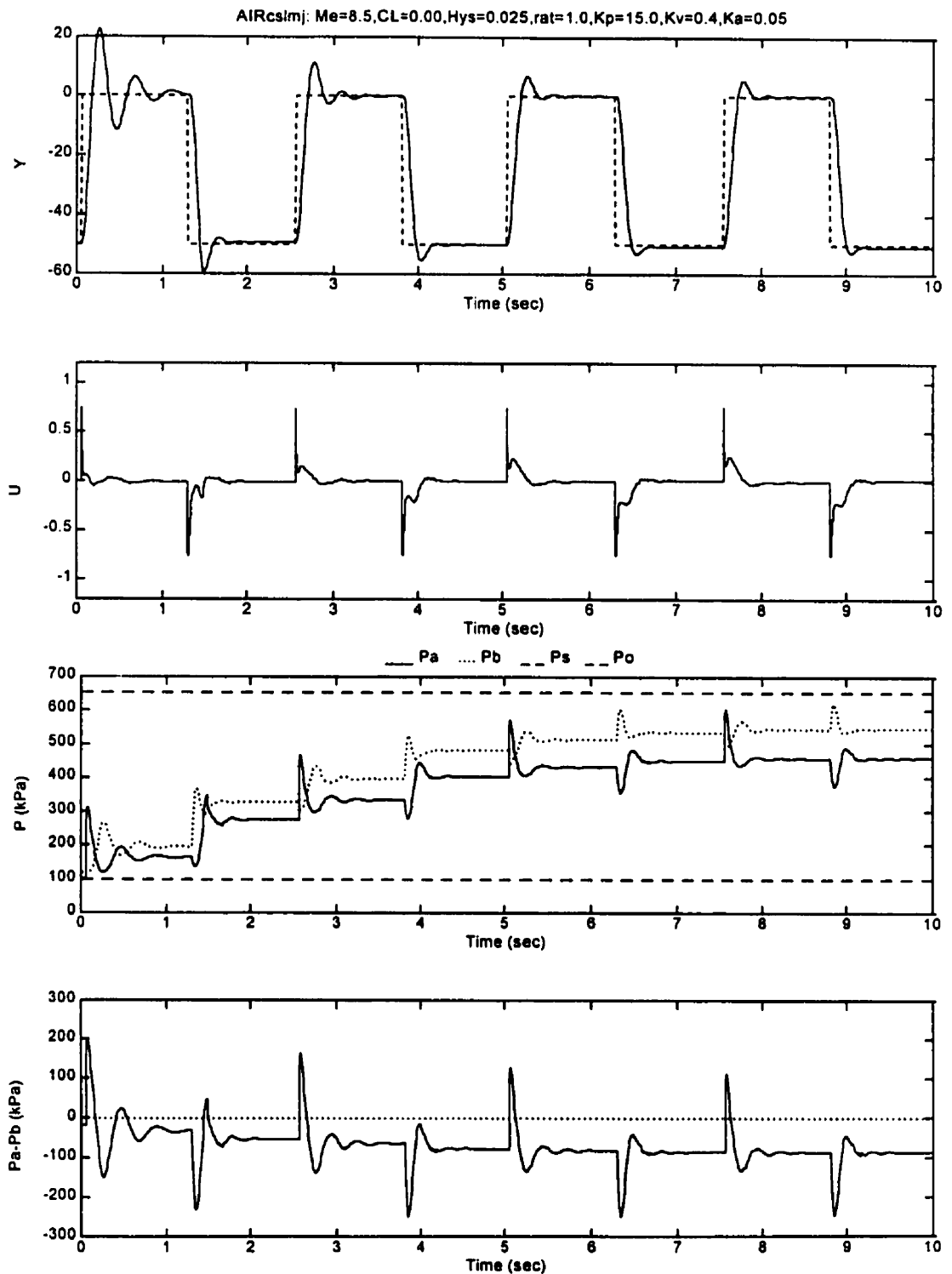


Figure 2.13: Closed Center valve with *PVA* on unequal cylinder areas and equal valve ports. Note improved response as pressure increases

### 2.3.3 Valve Port Areas

It was shown earlier that the system opening ratio,  $h_p$  is a function of the cylinder area ratio ( $u_m$ ) and other parameters, one of which is the valve port area ratio ( $u_w$ ). In a non-symmetric cylinder,  $u_m < 1.0$ , which decreases the cylinder operating pressures as dictated by  $P_a^{ss}$  and  $P_b^{ss}$ . This increases compressibility effects and creates a more “spongy” response. To counteract this effect,  $u_w$  can be made greater than 1.0 and the operating pressures are increased again. Specifically, the supply port area  $A_{vs}$  could be made greater than the exhaust port area  $A_{ve}$ .

Fig. 2.14 shows the *PVA* responses when the ratio of the outlet to the inlet valve port areas is changed from unity (as was the case in Fig. 2.13) to 0.5. The steady state pressures are seen to increase and the system performance improves slightly over that of Fig. 2.13. Therefore, a conclusion is that a ratio of valve port areas less than unity does improve the performance of a pneumatic system. One should realise though, that the improvement is not significant and the use of a more *robust* controller would improve linearity and overall performance without exhaust-metering.

### 2.3.4 Other Considerations

A formal steady state analysis should be performed to select suitable pneumatic system components. Guidelines exist in literature (for example: *Hitchcox, 1996*) and most manufacturers of pneumatic systems provide sufficient information in their catalogues to enable a designer to select a suitable valve and a suitable cylinder to perform a desired task. The valve and the cylinder are the most critical pneumatic system components. Typically the valve is sized for the minimum flow that provides maximum actuator speed. However, oversizing can cause stability and accuracy problems, whereas undersizing can result in slow responses. The cylinder should be sized for the maximum bore that is practical, while keeping in mind that too large a bore increases the volume of air that acts as a compliance chamber. In terms of stability, one should be aware of the cylinder’s size ratio and the possibility of dynamic instability,

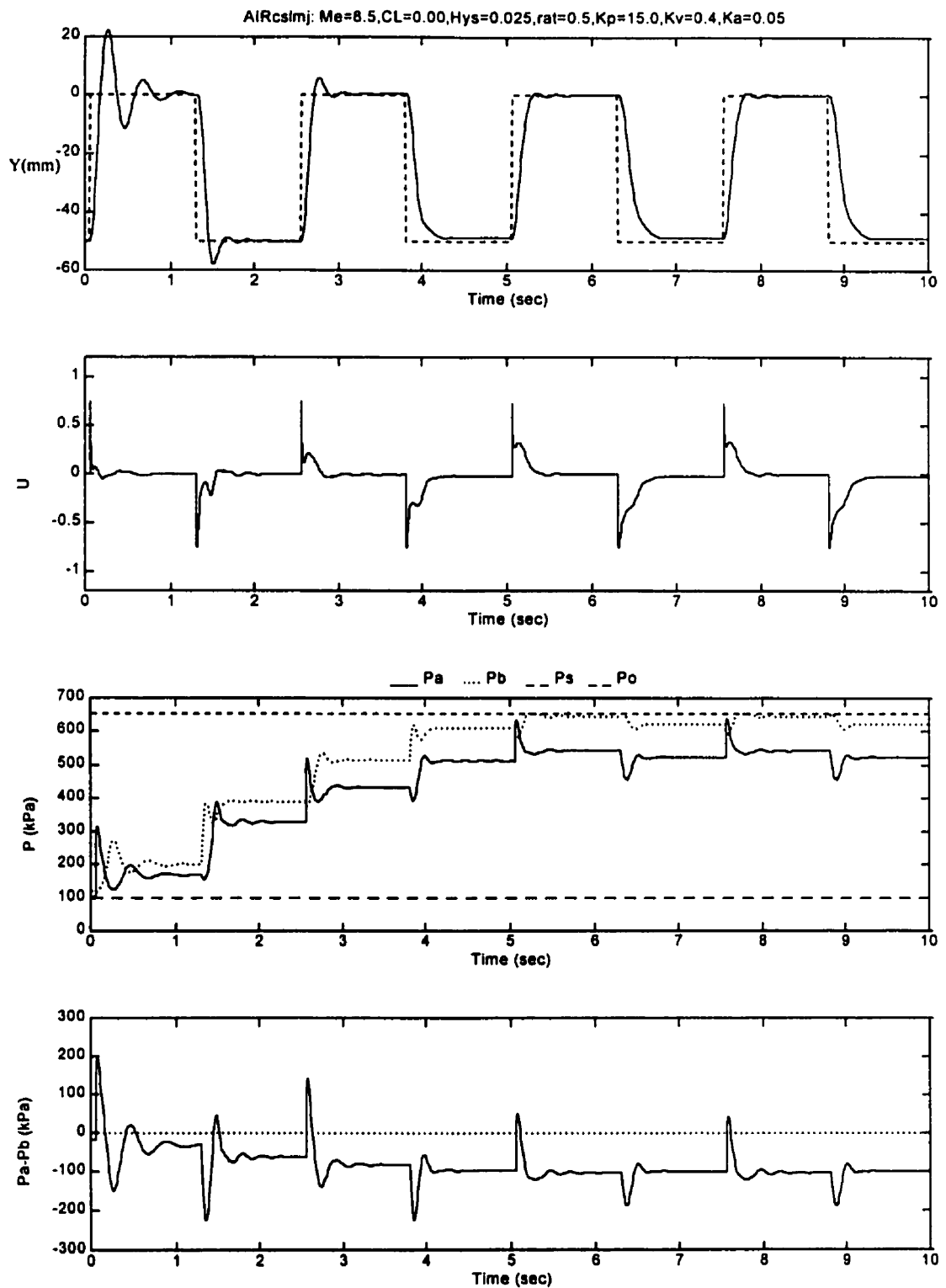


Figure 2.14: Closed Center valve with *PVA* on unequal cylinder areas and valve port ratio at 0.5. Note further improvement in the responses

which might arise at certain locations along the stroke of the cylinder where a localised high natural frequency and a small sampling interval combine.

As far as the operating pressure goes, the highest pressure source available should be used to reduce the effect of air compressibility. However, one should not exceed the pressure rating of any of the components. The air should be clean, dry and with most valves non-lubricated. System filtration should be at least  $25\ \mu m$  or better with a coalescing filter to minimise oil-vapor content. The servovalves should be located as close to the actuators as possible to avoid lags. Typically, every foot of tubing can delay response by  $1\ msec$ . Finally, rigid tubing should be used, unless impossible. Flexible tubing, though cheaper and easier to install, can add compliance to the system.

## **2.4 Summary**

Despite their nonlinear nature, pneumatic servomechanisms can be simplified and linearised about suitable operating points. Once the controller gains are generated from the linearised model and tuned for a desired performance, the pneumatic servomechanism can be tested in simulation. In simulation, the nonlinear state space equations can be used to determine the “true” (nonlinear) performance of the servomechanism. The ultimate gain for a rodless, or symmetric actuator can be determined upon consideration of the linearised model and *Routh-Hurwitz* stability criteria. It was also shown how to determine the ultimate gain for an asymmetric cylinder where the dynamic performance differs when in extension or retraction.

Furthermore, pneumatic system exhibit localised dynamics, which could be a cause for control instability. If, for example one works with a cylinder that has a high size ratio, then the natural frequency is higher than one that would result when a cylinder with a moderate size ratio is used. If the sampling time is not adjusted to account for the increased natural frequency, then the performance of the system degrades and instability could occur.

Finally, in the design of the pneumatic servomechanism, one should also consider the effects of the valve center configuration. Typically, for most position control tasks, the servovalve is a closed center valve. Open center valves are used when free positioning of the end-effector is required. In most cases the valve port area ratio is unity, but when exhaust-metering is required, the ratio can be chosen less than unity. A number of physical measurements of the servovalve and the actuator have been shown to affect the steady state pressures. Typically, higher operating pressures improve performance by decreasing the effects of air compressibility. The only consideration is the maximum operating pressure that the pneumatic equipment can withstand. Finally, low friction cylinders or valves that are insensitive to lubrication should be used to avoid stiction effects.

The presence of so many nonlinearities in pneumatic servosystems calls for a controller that is able to maintain a high level of performance despite:

- Position of the setpoint,
- Direction of motion,
- ♦ Friction and,
- Noise.

Furthermore, the controller should also be able to provide reasonable performance despite:

- Improper selection of pneumatic components and,
- Payload variations.

Hence, the interest in Sliding Mode Controllers which is of course the focus of this thesis.

## CHAPTER 3

### CONTINUOUS SLIDING MODE CONTROL

Under normal operating conditions, conventional linear controllers, such as Proportional-Integral-Derivative offer satisfactory transient response and good disturbance rejection for linear systems. But in reality, there are transient and steady state disturbances, system nonlinearities, imperfect plant models and varying model parameters. Therefore, the performance of linear controllers can degrade as their tuning relies on perfect conditions (perfect model & constant plant parameters). With the addition of plant uncertainties, disturbances etc., they provide unpredictable responses and possible instability. For this reason, there is ongoing interest in the development of more advanced and robust drive controllers.

There are two main categories of controllers, namely linear and nonlinear. Of the two, the more general are the nonlinear controllers since they can be successfully applied to linear systems whereas a linear controller might be insufficient for control of a nonlinear system. From there, the two most important subcategories of nonlinear are *Robust* control and *Adaptive* control. The *Adaptive* control option using gain scheduling, model reference or self-tuning can provide system parameter tracking and good disturbance rejection on stochastic noise but the performance degrades under deterministic disturbances with rising risk of instability. The other option is *Robust* control, an approach of which is the *Sliding Mode Methodology*. Its structure is composed of a linear feedback law and a switching law which deals with the model's uncertainties. Sliding Mode Control can then be defined as a *Variable Structure* controller whereby the gains are switched as the state of the system approaches reference states defined in terms of a switching hyperplane (Zohdy et al, 1995).

Utkin (1977) presented a survey of variable structure systems with sliding modes. In typical linear state regulator design, the feedback gain matrix is determined either from eigenvalue placement, or by quadratic minimisation. In variable structure



systems, the control can change its structure and the design problem is the selection of the structure parameters and the definition of the switching logic. These structures need not be asymptotically stable, but their combination defines an asymptotically stable system. New system properties evolve with these new structures and the desired trajectory is composed from parts of the trajectories of these structures. It is possible to define a trajectory which is not inherent in any of the structures. The motion on this trajectory is called the *sliding motion* and the behavior while on sliding motion depends only on the parameters of the trajectory, i.e. the coefficients of the sliding surface. This invariance with respect to plant parameters and disturbances is of extreme importance.

### 3.1 Traditional Continuous Sliding Mode Control

The Sliding Mode Control (SLM) technique is based on the fact that it is easier to control  $n^{th}$  order differential equations, be they uncertain or nonlinear, than it is to control a general  $n^{th}$  order differential equation (Slotine and Li, 1991). There are two critical design areas for traditional sliding mode control, the design of the sliding surface (*which is a stable integral manifold of the closed loop system*) and the control synthesis in the reduced order space. The sliding surface is considered as a subset of the system space and the procedure for the design of the controller starts with the representation of the system in a “convenient” form. A sliding manifold is then chosen and finally the control action is designed so that the system reaches the manifold in finite time and then “slides” along it.

"Perfect" performance can in principle be achieved in the presence of arbitrary parameter inaccuracies at the price of extremely high control activity. To achieve this, consider the following single-input dynamic system:

$$\dot{x}^{(n)} = f(x) + b(x)u \quad (3.1)$$

where  $x^{(n)}$  is the scalar output ( $n^{th}$  order derivative),  $x$  is the state vector,  $b(x)$  is the control gain,  $u$  is the finite control input and  $n$  is the number of states.

The function  $f(x)$  is generally nonlinear and not exactly known, as well as the control gain  $b(x)$ . Both are bounded by known functions of  $x$ . The control problem is to get the instantaneous state vector to track a specific or desired (setpoint) time-varying state vector  $x_{set}$ , where  $x_{set} = [x_{set} \ \dot{x}_{set} \ \cdots x_{set}^{n-1}]$ , in the presence of model errors of  $f(x)$  and  $b(x)$ .

Consider  $s(x;t)$  as the time-varying sliding function in State-Space  $\mathcal{H}^n$ :

$$s(x;t) = (d/dt + \lambda)^{n-1} x \quad (3.2)$$

where  $s(x;t)$  is the weighted sum of errors in position, velocity etc.,  $\lambda$  is a positive constant and  $x$  is the tracking error state. Eq. 3.2 implies that the tracking error tends exponentially to zero with a time constant  $n-1/\lambda$  (from the sequence of  $n-1$  filters of time constants equal to  $1/\lambda$ ) and provides a general design for the sliding surface (Slotine and Li, 1991). For a 2-state system, the result for  $s(x;t)$  is a first order system:

$$s(x;t) = \dot{x} + \lambda x = Cx \quad (3.3)$$

with the sliding surface matrix  $C$  defined as:

$$C = [1/\tau \quad 1] \quad (3.4)$$

recognizing that the sliding function  $s(x;t) = Cx = 0$  defines a "sliding surface" in the phase plane of  $x$ . For simplicity,  $s(x;t)$  will be written as  $s$ . The time constant of the required trajectory,  $\tau$  is in the time domain of  $x$  and can be shown to be equal to the reciprocal of  $\lambda$ .

In order to keep the scalar quantity  $s$  at zero, the tracking  $n$ -dimensional  $x_{set}$  is replaced by a 1<sup>st</sup>-order stabilising problem in  $s$ . The objective is to keep  $s$  at zero and therefore the control law has to satisfy the following necessary condition:

$$\dot{V}(x) \leq 0 \quad (3.5)$$

Eq. 3.5 which is the sliding condition derived from *Lyapunov's stability equation*. *Lyapunov's stability theorem* is well documented in Slotine and Li (1991).  $V(x)$  is said to be a *Lyapunov function* for a system if it is positive definite, it has continuous

partial derivatives and its time derivative along any state trajectory of the system is negative semi-definite. *Lyapunov's* local stability theorem states that if there exists a scalar function  $V(x)$  with continuous first partial derivatives such that  $V(x)$  is positive semi-definite and  $\dot{V}(x)$  is negative semi-definite then the equilibrium point is stable. For this particular case, *Lyapunov* function is defined by the following equation (*Furuta, 1990*):

$$V(x) = \frac{1}{2}s^2 \quad (3.6)$$

In particular, when on the surface  $S$ , the system trajectories remain on the surface, or simply when they satisfy Eq. 3.5, they make the  $S$ -surface an invariant set, or a domain of attraction of the equilibrium point.

The first derivative of the *Lyapunov* function can be shown to be:

$$\dot{V}(x) = \frac{1}{2} \frac{d}{dt} s^2 \quad (3.7)$$

For stability, the following sufficient condition has to be met:

$$\dot{V}(x) = s\dot{s} \leq -\eta|s| \quad (3.8)$$

where  $\eta$  is a strictly positive constant.

CSLM drives  $s$  to zero as time progresses by forcing  $s\dot{s} < 0$  at all times, despite all parametric uncertainty and input disturbances as long as they satisfy a *norm*-bounded condition which will be shown later in the chapter. This bounded condition deals automatically with parameter uncertainties and implies that the approach condition  $s$  to zero holds at all times.

Fig. 3.1a shows the phase plane  $\dot{x}$  vs.  $x$ , when  $n=2$  and for the ideal case of instantaneous control switchings. This would be the case if an analog controller was used. In the case where a digital computer is used for control, the control input is activated at discrete intervals and a time lag is introduced. Due to this lag, there is

*chattering* in the  $s$ -function, which then causes chattering in the control signal. This is shown in Fig. 3.1b as nonideal sliding control.

The general control law for CSLM is given as:

$$u = u_{eq} - K_s \text{sign}(s) \quad (3.9)$$

where  $u_{eq}$  is the equivalent control action,  $K_s$  the sliding gain and  $\text{sign}(s)$  is the signum function which is discontinuous. The equivalent control action to give optimal control can be evaluated as:

$$u_{eq} = -K_{eq}x \quad (3.10)$$

where  $K_{eq}$  is the linear, or equivalent gain to give  $dx/dt=0$  assuming a perfectly known model. Assume that the system to be controlled has a linear state space representation:

$$\frac{dx}{dt} = Ax + Bu \quad (3.11)$$

To ensure *Lyapunov's* stability,  $\dot{s}=0$  which implies that Eq. 3.11 has to be equal to zero (since  $s=Cx$  and  $C$  is a non zero matrix). Solving for  $u$  and combining with Eq. 3.3-3.9-3.10, Eq. 3.12 is obtained:

$$u = -[(CB)^{-1}CA]x - K_s \text{sign}(s) \quad (3.12)$$

To avoid the chattering shown in Fig. 3.1b, i.e. to smooth out the control discontinuity, a boundary layer  $\phi$ , neighbouring the switching surface can be introduced (*Slotine and Li, 1991*). This boundary layer is shown in Fig. 3.1c. Introducing this parameter into the discontinuous term of Eq. 3.12 yields the following equation:

$$u = -[(CB)^{-1}CA]x - K_s \text{sat}(s) \quad (3.13)$$

where the *saturation* function  $\text{sat}(s)$  is equal to  $\text{sign}(s/\phi)$  when  $|s|>\phi$  and  $s/\phi$  when  $|s|<\phi$ . The effect of the boundary layer will be seen later in Fig. 3.2. A discussion on the issues raised by the figure will be provided in Section 3.4.1. When the system is operating outside the boundary layer (i.e.  $|s|>\phi$ ), then Eq. 3.13 provides a (switched) sliding action and attracts the system towards the boundary layer and effectively towards the sliding surface. When the system enters the boundary layer (i.e.  $|s|<\phi$ ), then the same equation provides a (continuous) proportional action, which causes the

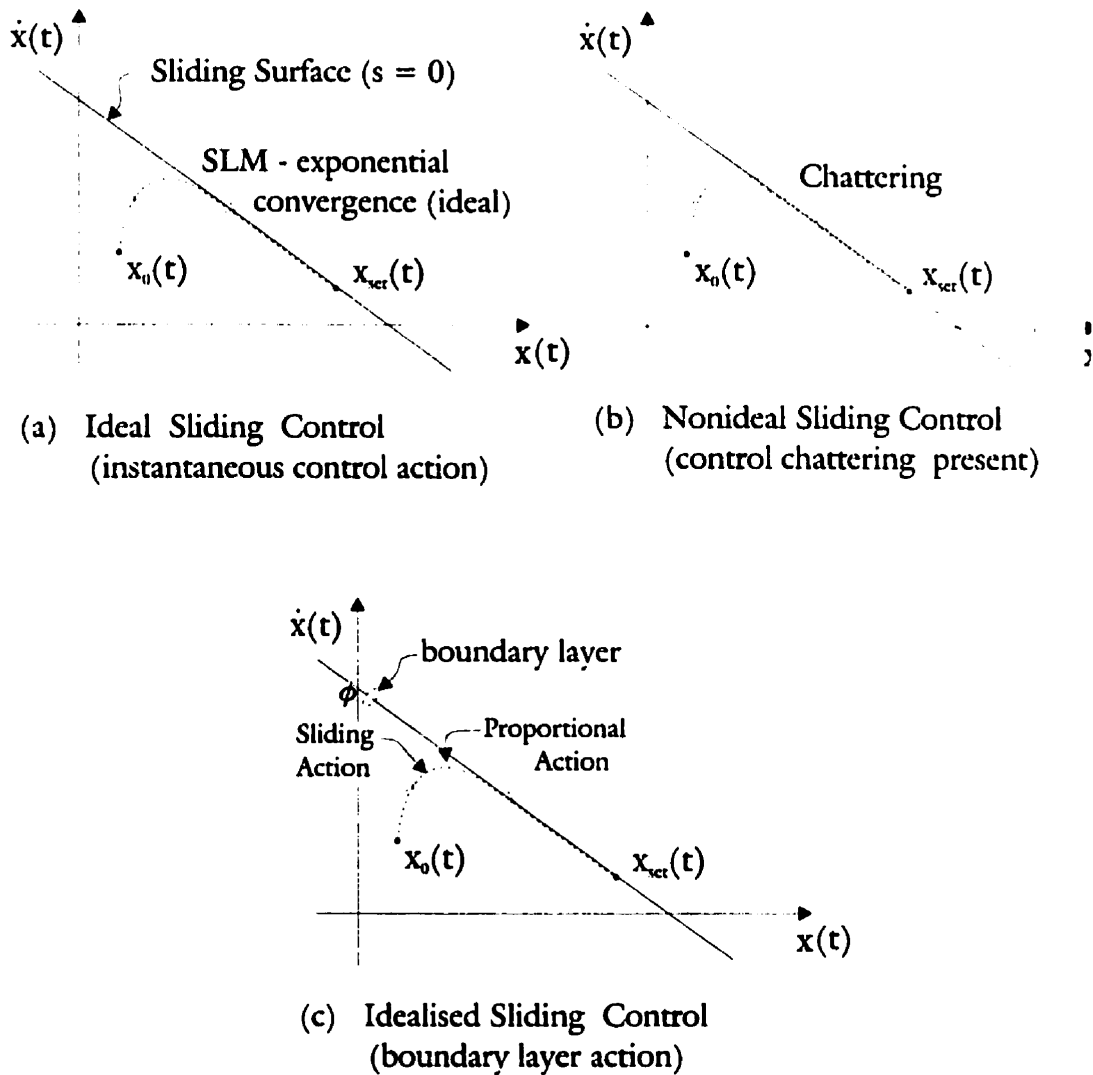


Figure 3.1: Sliding Control, from Ideal to Nonideal to Idealized

system's trajectory to slide along the sliding surface of Eq. 3.3, for which the time response is a 1<sup>st</sup> order dynamic with no overshoot (for the case where  $n=2$ ). The sliding action and the boundary layer proportional action regions can also be seen in Fig. 3.1c. The chattering, in the presence of an appropriately selected boundary layer thickness, can be eliminated in both theory and practise.

### 3.1.1 Alternate Approaches to CSLM

A number of different approaches and versions of the control law given as Eq. 3.12 have been developed and improved over the years. A number of papers were reviewed in order to examine the effect of tuning parameters of Sliding Mode.

*Furuta (1990)* dealt with a SISO system with CSLM. The sliding surface was first designed ( $s=Cx=0$ ) and then the control action needed to transfer the state to the sliding surface was selected. Starting with the state-space equation of the system with the variables in their perturbation form and by using *Lyapunov* function  $V(x) = \frac{1}{2}s^2$  and the requirement for stability ( $dV(x)/dt < 0$ ), *Furuta* derives the following sliding action conditions:

$$\begin{aligned} s(x) CB x_j < 0 &\Rightarrow K_s < 0 \\ s(x) CB x_j > 0 &\Rightarrow K_s > 0 \\ s(x) CB x_j = 0 &\Rightarrow K_s = 0 \end{aligned} \quad (3.14)$$

for  $j=1 \dots n$ . The resultant control law is different from the one presented in Eq. 3.13 :

$$u = (K_{eq} + K_{sw}) x \quad (3.15)$$

where  $K_{eq}$  is as given in Eq. 3.12 and  $K_{sw}$  is given as  $-K_s \text{sign}(s[x(1) \ x(2)])$ . The above control law is for a 2-state system. At steady state the control voltage goes to zero to maintain the required setpoint. Also, note that from the  $K_{sw} x$  expression it can be seen that the feedback control law is of 1<sup>st</sup> order and that boundary layer action is not introduced to eliminate chattering.

*Luo et al. (1995)* investigated the control of uncertain coupled systems using a novel control scheme based on the sliding mode principle. The controller, under *appropriate* assumptions guaranteed the asymptotic stability of the overall system. The first step of the control design was to define a sliding vector  $s \in R^n$  as:

$$s = \dot{x} + c_1 x \quad (3.16)$$

where  $x$  and  $\dot{x}$  are the system states, and  $c_1$  is a scalar (tuning) parameter chosen to guarantee the closed-loop stability of the subsystem. A sliding motion is said to be generated in the subsystem if state variables  $x$  and  $\dot{x}$  reach the sliding surface  $S$  at the

time instant  $t_r$  and then remain in  $S$  for all  $t \geq t_r$ . The equivalent control law,  $u_{eq}$  can be found by setting  $\dot{s}=0$ , which when substituted in the state space equation provides the closed-loop dynamics of the subsystem in sliding mode. The example given was a second order subsystem. The explicit solutions for the subsystem in sliding mode ( $t \geq t_r$ ) are given as:

$$x = x(t_r) e^{-c_1(t-t_r)} \quad \text{and} \quad \dot{x} = \dot{x}(t_r) e^{-c_1(t-t_r)} \quad (3.17)$$

Looking at the above solutions, one can see that  $c_1 > 0$  for stability (or, exponential error decay) and that states  $x$  and  $\dot{x}$  are bounded for all  $t \geq 0$  and converge to zero exponentially as  $t \rightarrow \infty$ . The other observation is that as a tuning parameter,  $c_1$  will increase the speed of response as it increases.

*Jian (1995)* investigated the issue of a variable sliding line, or surface. A  $1^{st}$  order sliding surface is designed for a  $2^{nd}$  system with  $s = c_1 x_1 + x_2$  and  $x_2$  as the first derivative of  $x_1$  and  $c_1$  as the single tuning parameter for this simple case. The larger the value of  $c_1$ , the faster the approach to the sliding surface. But upper limits for  $c_1$  do exist since the presence of large errors in  $x_1$  and  $x_2$  would cause controller saturation, thus jeopardizing the robustness of the controller. The author then provides a limiting equation for the size of  $c_1$  which depends on the controller gain, the size of the sliding gain,  $K_s$  and the expected maximum error in the states. Furthermore, the author implements state weights,  $w_j$  and a proportional action within the boundary layer. The switching control law is given as:

$$u = \begin{cases} K_s & \text{if } K_s < \sum_{j=1}^{n-1} w_j |x_j| \text{sign}(s) \\ \sum_{j=1}^{n-1} w_j |x_j| \text{sign}(s) & \text{if } |K_s| \leq \left| \sum_{j=1}^{n-1} w_j |x_j| \text{sign}(s) \right| \\ -K_s & \text{if } -K_s > \sum_{j=1}^{n-1} w_j |x_j| \text{sign}(s) \end{cases} \quad (3.18)$$

The general principle of state weights and a varying sliding gain have also been used and presented in (*Jordanou and Surgenor, 1995, 1997a*) in the control of an inverted

pendulum using DSLM. The switching laws are different from the ones presented in *Jian*.

*Fortell (1995)* shows how a normal (or canonical) form that corresponds to affine state space systems can be generated. This generalized normal form is then used in the context of sliding mode control. The investigation is for a general, nonlinear system model where the normal form is obtained from the *Lie* derivatives  $L_f$  and  $L_g$ , in the direction  $f(x)$  and  $g(x)$  of  $\dot{x} = f(x) + g(x)u$  respectively. The author then defines an auxiliary output to the general system, the sliding function  $s(x) = \sum_{j=1}^{n-1} c_j x_j + x_n$ . Note that  $c_n$  for  $x_n$  is set to unity which normalizes the sliding surface. By imposing the discontinuous (switching) surface dynamics, and setting  $s(x)=0$ , the system has:

$$\begin{aligned} \dot{x}_1 &= x_2 \\ &\vdots \\ \dot{x}_{n-1} &= x_n = -c_1 x_1 - c_2 x_2 - \dots - c_{n-1} x_{n-1} \end{aligned} \quad (3.19)$$

The author then concludes that a *suitable* choice of  $c_i$  can generate an asymptotically stable motion towards  $x_1=x_2=\dots=x_n=0$ , but does not explain how these coefficients are obtained.

*Sira-Ramirez (1993)* presents a thorough overview of some of the developments in sliding mode theory. Special consideration is given to dynamic sliding mode controllers whereby the sliding surface not only depends on the system states but also on the system inputs. The sliding function,  $s$  is presented as the sum of the input and the output states. In the article, the control input is shown as the output of a low-pass filter (with a cut-off frequency  $\lambda$ ) which has a discontinuous structure (with an amplitude  $v/\lambda$ ). The amplitude of the switching action,  $v/\lambda$  is better known as the sliding gain,  $K_s$ . The cut-off frequency  $\lambda$  relates to the exponential rate of approach of the controlled state to the desired value. The quantity  $v$  is defined as an arbitrary



positive real number arising from  $ds/dt = -\nu \text{sign}(s)$  and can be used to measure the reaching time  $t_r$  of the condition  $s=0$ . It is shown as  $\nu = \lambda u_u$  where  $u_u$  represents the maximum input signal. This also provides a design approach to  $K_S$ . For a fixed  $u_u$ , the relationship establishes an important tradeoff: the smaller the reaching time  $t_r$ , the higher  $\nu$  as the following equation indicates:

$$t_r = \frac{|s(0)|}{\lambda u_u} \quad (3.20)$$

For a small reaching time one would require a higher cut-off frequency  $\lambda$  of the low-pass filter. This though, may give rise to a larger number of harmonic oscillations and when combined with external noise, could affect the control input.

Noise in a measured variable can also present problems, especially if the higher states (e.g. velocity) are obtained through differentiation of a measured state (e.g. position). Filtering the signals decreases the noise, but introduces signal transmission delay which can then deteriorate the overall system response. State estimators can therefore be used to “predict” the states. *Misawa (1995)* uses the discrete sliding mode controller structure as proposed by *Furuta (1990)* with the addition of state estimators. An additional condition ensures that the estimation error for each state tends asymptotically to zero.

*Woodham and Zinober (1993)* presented a sliding surface design originating from placement of the closed-loop eigenvalues in a specified sector in the left hand plane of the continuous-time root-locus domain. An orthogonal transformation matrix  $T$  (where  $T^T=T^{-1}$ ) is used which modifies the original  $B$  matrix of a general linear state space model, to one in canonical form,  $T B$ . Note that this transformation does not change  $A$  to its canonical form. The original states  $x(t)$  are transformed into  $z_z(t)$ , where  $z_z(t)=T x(t)$ . If one only considers the reduced order system, which is outside the range of the control action (i.e., for a *SISO*  $n \times n$  system with system matrices  $TAT^{-1}$  and  $T B$ , which has the control input appear in the  $n^{th}$  row, the reduced order system is  $(n-1) \times (n-1)$ ), then the reduced order dynamics are:

$$\begin{bmatrix} \dot{z}_z \\ \dot{\xi}_z \end{bmatrix} = \begin{bmatrix} A_{11} & A_{12} \\ A_{21} & A_{22} \end{bmatrix} \begin{bmatrix} z_z \\ \xi_z \end{bmatrix} + \begin{bmatrix} 0 \\ B_2 \end{bmatrix} u \quad (3.21)$$

The sliding function for the new coordinate system has  $s=C_1 z_z + C_2 x$  where  $C_1$  and  $C_2$  are sliding vectors. This reduces the equivalent dynamics to:

$$\dot{z}_z = [A_{11} - A_{12}G]z_z \quad (3.22)$$

where  $G=C_2^{-1}C_1$ . Matrix  $G$  can be obtained for a required eigenvalue sector where the real intercept and the angle of sector line need to be specified. With these values of the real intercept and the angle of sector line, a hermitian, positive-definite matrix is obtained using the *Riccati* equation with weighting matrices  $Q$  and  $R$  as positive symmetric. Since the dynamics under sliding are also independent of control input, the above equation provides, through the selection of  $G$  the dynamics of the system under pure sliding as  $C=[G \ I] \ T$ , which for a *SISO* system reduces to  $C=[G \ 1] \ T$ . The question is whether the above procedure can be extended to the design of a discrete time sliding surface.

*Habibi* (1995) applies a variable structure controller to a multi-link hydraulic industrial robot. The implemented controller can offer robust control against bounded parametric variations, friction and other uncertainties. A sliding surface with integral action is selected. The sliding function which is defined as the distance of the states from the switching hyperplane is given as:

$$s(x, t) = (d/dt + \lambda)^n \int \tilde{x} dt \quad (3.23)$$

The hydraulic robot is considered to be a third order system (as is the pneumatic system for this thesis). For a 3<sup>rd</sup> order system the sliding function becomes:

$$s(x, t) = \ddot{\tilde{x}} + 3\lambda \dot{\tilde{x}} + 3\lambda^2 \tilde{x} + \lambda^3 \int \tilde{x} dt \quad (3.24)$$

The author then sets the coefficients of  $\ddot{\tilde{x}}, \dot{\tilde{x}}, \int \tilde{x} dt$  equal to the acceleration, velocity and position gains of a PVA controller, if one was to be designed for this particular system. However, it is not possible to achieve triple coincident eigenvalues as

demanding by Eq. 3.24 due to model inaccuracies. Therefore, it is assumed that the sliding function, for best performance should be defined as:

$$s(x, t) = \ddot{\tilde{x}} + K_a \dot{\tilde{x}} + K_v \tilde{x} + K_p \int \tilde{x} dt \quad (3.25)$$

The control law used in the paper was the same as in *Slotine and Li (1991)*.

*Paul et al (1994)* present an implementation of a modified sliding mode controller to a pneumatic system. Servocontrol in pneumatic systems is of great interest to designers since pneumatics have a great economic advantage over electric and/or hydraulic systems. But the use of servovalves for pneumatic systems increases the cost considerably. The authors replace the servovalve by 2 ON-OFF solenoid valves in order to cut down the cost. They also claim that 2 control inputs increase the flexibility of the controller. The cylinder dynamics are assumed  $2^{nd}$  order and static friction is neglected. A symmetric cylinder is used. When combined with valve dynamics (since flowrates to the chambers are the inputs), the overall system becomes  $3^{rd}$  order with 2 inputs, one for each valve. Typically, a  $2^{nd}$  order sliding surface would need to be designed. Instead, *Paul et al* implement a  $1^{st}$  order sliding surface:

$$s(x; t) = [c_1 \quad 1] x \quad (3.26)$$

The reduced order sliding surface requires complicated reachability and sliding mode existence conditions. The eigenvalues of the higher order range space that guarantee reachability become intricate. The complexity is increased further if a broader range of cylinders is used, especially if small stroke cylinders are used for which wide parameter variations take place for a small displacement of the piston. The structure of the control law is presented as:

$$u(x) = \begin{cases} u^+(x) & \text{if } sx_1 > 0 \\ u^-(x) & \text{if } sx_1 < 0 \end{cases} \quad (3.27)$$

so that  $s \frac{ds}{dt} < 0$ .

During charging, ( $sx_1 > 0$ ), the chamber pressures  $P_a$  and  $P_b$  are considered as functions of the supply and initial chamber pressures, as well as the time constants for

chamber charging and discharging. These depend on the chamber volumes, hence they are position dependent. For a sliding mode to exist with  $sx_1 > 0$ , a high differential pressure is essential. The stroke of the cylinder used, combined with a high value of  $c_1$  resulted in a required differential pressure of  $3.5 \text{ bar}$ . For fast reachability, the switching line slope,  $c_1$  should be as large as possible. An assumption is then made, that for a supply of  $10.5 \text{ bar}$  the required differential pressure of  $3.5 \text{ bar}$  is developed instantaneously.

During discharging ( $sx_1 < 0$ ), both solenoid valves are kept OFF. The chamber pressures  $P_a$  and  $P_b$ , which are functions of both the position and speed of the piston, are presented as decreasing and increasing functions respectively. This implies that the piston slows down and reverses direction even with both valves OFF. To avoid limit cycles (near zero position error or in noisy environments) due to noninstantaneous pressure development, the sliding mode controller is switched to Pulse Width Modulation. The use of a reduced order Sliding Mode is therefore misleading. In the experiment, the piston is required to move a payload across a distance of  $120 \text{ mm}$ . A  $0.006 \text{ sec}$  sampling time was used; the resulting settling time was close to  $1.80 \text{ sec}$  and the steady state error was close to  $1 \text{ mm}$ , a result which is not particularly impressive.

Zohdy et al (1995) present a new output feedback variable structure controller design using dynamic output feedback control. The original state space model as:

$$\begin{aligned}\dot{x}(t) &= Ax(t) + Bu(t) \\ y(t) &= x(t)\end{aligned}\tag{3.28}$$

is then modified with the output feedback control approach to:

$$\begin{aligned}\dot{x}_1(t) &= G_{22}x_1(t) + G_{21}y(t) \\ u(t) &= G_{12}x_1(t) + G_{11}y(t)\end{aligned}\tag{3.29}$$

where  $G_{11}$ ,  $G_{12}$  are observable (as  $A$ ,  $I$  of Eq. 3.28) and  $G_{21}$ ,  $G_{22}$  are controllable (as  $A$ ,  $B$  of Eq. 3.28). With  $\tilde{x}(t) = [x(t) \ x_1(t)]^T$  and  $\tilde{y}(t) = [y(t) \ x_1(t)]^T$ , a new matrix  $\tilde{A}_c$  defines the augmented system closed loop dynamics as:

$$\dot{\tilde{x}}(t) = \tilde{A}_c \tilde{x}(t) = \begin{bmatrix} A + BG_{11}C & BG_{12} \\ G_{21} & G_{22} \end{bmatrix} \tilde{x}(t) \quad (3.30)$$

The eigenvalues of  $\tilde{A}_c$  can be arbitrarily selected by proper choice of the feedback matrix  $G$ . The authors then present a procedure for determining  $G$  with  $T$  as a transformation matrix obtained from:

$$TA - QT = R \quad (3.31)$$

where  $R$  and  $Q$  can be arbitrarily selected with the restriction that  $Q$  is a negative definite matrix and that  $Q$  and  $R$  compose a controllable pair. With  $T$  determined from equation 3.31, elements  $G_{11}$  and  $G_{12}$  of matrix  $G$  can be obtained as:

$$[G_{11} \quad G_{12}] = K \begin{bmatrix} I \\ T \end{bmatrix}^{-1} \quad (3.32)$$

with  $K$  denoting the desired closed loop matrix obtained from pole placement. Elements  $G_{21}$  and  $G_{22}$  can then be obtained from:

$$\begin{aligned} Q &= G_{22} - TBG_{12} \\ R &= T(G_{21} - TBG_{11}) \end{aligned} \quad (3.33)$$

The sliding surface is then defined as:

$$s(x, t) = C \tilde{y}(t) = 0 \quad (3.34)$$

$C$  is obtained from the desired dynamics of the switching hyperplane. The control law is composed of the equivalent control part,  $u_{eq}$  which is active in the vicinity of the sliding surface, and a corrective control part,  $u_{sw}$  which directs the system states towards the surface. The corrective control law, or switching control law has:

$$u_{sw} = f_j \text{sign}(s(x; t)) \quad (3.35)$$

where  $f_j$  denotes a column of switching coefficients for the appropriate states. The paper provides simulation results for aircraft control using the augmented system with dynamic output feedback. The design of the switching hyperplane is similar to the one presented in *Woodham and Zinober (1993)* since it originates from a continuous time closed loop system representation, as Eq. 3.30 shows.

### **3.1.2 Summary of Literature Review**

In conclusion, the literature review indicates that there exist a number of CSLM implementation techniques, each with its own strengths and weaknesses. A key issue in CSLM is the design of the sliding surface and the construction of the switching control law. The sliding surface can be designed once a closed loop system representation is generated. *Woodham and Zinober (1993)*, *Zohdy et al (1995)* have considered the closed loop system under pure sliding and commented on the generation of the sliding surface from eigenvalue selection. Most commonly though, the question of how the coefficients of the sliding surface are selected is left unanswered.

All implementations of CSLM use relatively very small sampling times. For example, *Paul et al (1994)* worked with a sampling time of *0.002 sec* for control of a pneumatic system with a required settling time of *1.8 sec*. *Jian (1995)* used a sampling time of *0.001 sec* for control of an electric positioning system with a required settling time of *0.5 sec*. *Zohdy et al (1995)* do not state the sampling time or comment on its effects.

### 3.2 Design of the Sliding Surface

The design of the sliding surface is of primary importance to the performance of a sliding mode controller. In this section, a general technique will be shown for the determination of a canonical matrix system that helps in the design of the sliding surface of a continuous sliding mode controller (*Jordanou and Surgenor, 1997b*).

#### 3.2.1 Stability of a Continuous System

The question of stability of the system  $\dot{x} = Ax$  is important. The matrix  $A$  in this case represents the closed-loop dynamics. It can be derived if one considers that the sliding function has reached the value of zero; from then and on, the system is under pure sliding. Generally, this system has solution  $x(t) = e^{At}x_0$  and is said to be asymptotically stable if the effect of any initial perturbation  $x_0$  from equilibrium dies away as  $t \rightarrow \infty$ . It can be shown that necessary and sufficient conditions for asymptotic stability is that all eigenvalues of  $A$  have *negative* real parts.

The system can also be shown to be asymptotically stable if a positive definite quadratic form  $V(x) = x^T R x$  (equivalent to *Lyapunov* function) can be found such that  $dV(x)/dt$  is negative definite. In other words, for stability:

$$\frac{dV(x)}{dt} = \dot{x}^T R x + x^T R \dot{x} < 0 \quad (3.36)$$

which reduces to:

$$\frac{dV(x)}{dt} = x^T Q x < 0 \quad (3.37)$$

where  $Q = A^T R + R A$  and is a negative-semidefinite, symmetric matrix such as  $-I$ .

The procedure provides sufficient conditions for the design of the switching laws for CSLM.

#### 3.2.2 Canonical Form of a Continuous System

An important part of the sliding surface design is the characterization of the original system in its canonical form. A general  $n \times n$  matrix  $A$  can be represented as  $Ax = \lambda x$ ,

where  $x$  is called the *eigenvector* (usually normalized) and  $\lambda$  its associated *eigenvalue*. The non-trivial solution for  $Ax=\lambda x$  is obtained by considering its characteristic polynomial  $\det(\lambda I-A)=0$  which has:

$$\lambda^n + \alpha_{n-1}\lambda^{n-1} + \dots + \alpha_0 = 0 \quad (3.38)$$

for which there exist  $n$  distinct roots  $\lambda_1, \lambda_2 \dots \lambda_n$ .

If one considers the transformation  $x=T_v r_m$ , where  $T_v$  is the matrix of eigenvectors (usually called the *modal* matrix) and substitutes in  $Ax=\lambda x$ , then:

$$\dot{r}_m = T_v^{-1} A T_v x = \Lambda r_m \quad (3.39)$$

where  $\Lambda$  is a diagonal matrix with the eigenvalues of  $A$  in the diagonal. Therefore

$r_{mj} = a_j e^{\lambda_j t} \forall j=1,2,\dots,n$  and:

$$x(t) = T_v [a_1 e^{\lambda_1 t} \ a_2 e^{\lambda_2 t} \dots a_n e^{\lambda_n t}]^T \quad (3.40)$$

where  $a_j$  are arbitrary constants determined from initial conditions.

A companion matrix to  $A$  is denoted as  $C_A$  and it has the same characteristic equation, or polynomial as shown above and has a canonical form (Barnett, 1990) as:

$$C_A = \begin{bmatrix} 0 & 1 & 0 & \dots & 0 \\ 0 & 0 & 1 & \dots & 0 \\ \vdots & \vdots & \vdots & \ddots & \vdots \\ -\alpha_0 & -\alpha_1 & \dots & \dots & -\alpha_{n-1} \end{bmatrix} \quad (3.41)$$

$C_A$  is obtained by considering the *Vandermonde* matrix  $V_n$  that has the general form:

$$V_n = \begin{bmatrix} 1 & 1 & \dots & 1 \\ \lambda_1 & \lambda_2 & \dots & \lambda_n \\ \lambda_1^2 & \lambda_2^2 & \dots & \lambda_n^2 \\ \vdots & \vdots & \ddots & \vdots \\ \lambda_1^{n-1} & \lambda_2^{n-1} & \dots & \lambda_n^{n-1} \end{bmatrix} \quad (3.42)$$

where  $\lambda_j$ 's represent the eigenvalues of  $A$ . Assuming  $V_n$  is non-singular (i.e. all  $\lambda_j$ 's are distinct), then  $C_A$  can be found as:

$$C_A = (T_v V_n^{-1})^{-1} A (T_v V_n^{-1}) \quad (3.43)$$



The canonical form of the system is now determined. The reason for obtaining this form is to then replace the original variable  $x$  with a transformed variable  $\bar{x}$ , where  $x = T\bar{x}$ . Note that  $x$  relates to  $A$ , and  $\bar{x}$  relates to  $C_A$ , or the companion matrix of  $A$ . The eigenstructures of  $x$  and  $\bar{x}$  are therefore identical and a sliding surface design with the  $\bar{x}$ -variable can be linked directly to the  $x$ -variable through the matrix  $T$  that serves to transform the system to its canonical form.

The derivation of the transformation matrix  $T$  poses as the final part of the sliding surface design. It can be found if the controllability matrix of the system is considered. A system is said to be controllable if the rank of the system is equal to the rank of the controllability matrix  $W_o$  which, for a continuous system is an augmented matrix defined as:

$$W_o = [B \quad AB \quad \dots \quad A^{n-1}B] \quad (3.44)$$

If new coordinates  $\bar{x}$  are introduced by a nonsingular transformation matrix  $T$ , then for the new coordinates the controllability matrix becomes:

$$\bar{W}_c = [\bar{B} \quad \bar{A}\bar{B} \quad \dots \quad \bar{A}^{n-1}\bar{B}] \quad (3.45)$$

The transformed matrices  $\bar{A}$  and  $\bar{B}$  can be shown as  $\bar{A} = TAT^{-1}$  and  $\bar{B} = TB$ . The derivation will be presented in Chapter 4 for their discrete time equivalents  $\Phi$ ,  $\Gamma$  and  $\bar{\Phi}$ ,  $\bar{\Gamma}$ . If these matrices are substituted into Eq. 3.45, then:

$$\bar{W}_c = [TB \quad TAT^{-1}TB \quad \dots \quad TA^{n-1}T^{-1}TB] = TW_o \quad (3.46)$$

One then concludes that the matrix  $T$  can be found by considering the controllability matrices of the original and the transformed system, such that:

$$T = \bar{W}_c W_o^{-1} \quad (3.47)$$

### 3.3 Switching Control Law

The sliding function  $s$  has been shown as a weighted function of the system states:

$$s(t) = Cx = [c_1 \ c_2 \cdots c_n]_x x \quad (3.48)$$

with vector  $x$  denoting the state errors. If one works with the transformed variable  $\bar{x}$ , where  $x = T\bar{x}$ , the above is modified to:

$$s(t) = \bar{C}\bar{x} = \bar{C}T^{-1}x = [c_1 \ c_2 \cdots c_n]_{\bar{x}} T^{-1}x \quad (3.49)$$

Typically the sliding surface is normalized to  $c_n$ , since it does not affect the system's eigenstructure. The switchings of the sliding function were given by Eq. 3.13:

$$u_{sw} = \begin{cases} K_s \frac{s}{\phi} & \text{if } |s| < \phi \\ K_s \operatorname{sign}\left(\frac{s}{\phi}\right) & \text{if } |s| \geq \phi \end{cases} \quad (3.50)$$

For a 3<sup>rd</sup> order system, normalisation of the sliding surface coefficients leads to  $c_3=1$ . The coefficients  $c_1$  and  $c_2$  can be then selected to match performance parameters of a desired 2<sup>nd</sup> order system as shown in *Surgenor and Vaughan (1996)*.

### 3.4 Controller Parameter Issues

The following section will demonstrate some CSLM tuning and stability issues. The CSLM controller was implemented in simulation to control the position of the piston of an asymmetric pneumatic cylinder controlled by a proportional servovalve, similar to the one described in Chapter 2, technical specifications for which are listed in Appendix A. The input to the system (or, the controller output) drive a proportional servovalve. Unless specified otherwise, the benchmark conditions used in the simulations are as follows:

- The sliding surface is designed for a damping factor  $\zeta$  of 1.0 and a settling time  $t_s$  of 0.2 sec.
- The nominal payload mass  $M_e$  is 8.5 kg. Robustness tests were implemented with payloads of 23.0 and 2.2 kg.
- The sampling time  $h$  is 0.001 sec.

- The boundary layer  $\phi$  is 4.5.
- The sliding gain  $K_S$  is 1.0 (normalised).
- The equivalent gain action,  $u_{eq}$  is active.

The last point refers to the fact that some authors (*Jian, 1995, Gamble and Vaughan, 1994, Tang and Walker, 1994*) tend to ignore this term in the sliding control law of Eq. 3.9. *Surgenor and Vaughan (1996)* comment that the equivalent gain can be ignored when a sufficiently large sliding gain that compensates for uncertainties is used and when stability limits are not approached in the application at hand. Even though the sliding action of the overall CSLM control law is independent of the system model, the equivalent control law is designed based on matrices  $A$  and  $B$  of Eq. 3.11; therefore an error in  $A$  and/or  $B$  would induce an incorrect equivalent control law. The fact that the sliding surface (and consequently the sliding action of CSLM) is independent of the system in use will be shown in Chapter 4.

A further consideration for the tuning of CSLM is the boundary layer which is used to minimize chattering effects; a tradeoff exists between steady state positioning accuracy (resulting from a large boundary layer thickness) and chatter (resulting from a small boundary layer thickness).

Important issues that will be addressed in simulation are:

- The effect of the boundary layer on the control signal (chatter) and system response (Fig. 3.2)
- The effect of the sampling time on the system response (Fig. 3.3)
- The effect of the sliding gain on the system response (Fig. 3.4)
- The robustness (*different payloads*) of CSLM vs. PVA with  $h=1\text{ ms}$  (Fig. 3.5 and 3.6)
- The robustness (*different payloads*) of CSLM with  $h=10\text{ ms}$  (Fig. 3.7)
- The effect of  $K_{eq}$  on the robustness of CSLM with  $h=10\text{ ms}$  (Fig. 3.8)

- The effect of the settling time design parameter (Fig. 3.9)
- The effect of the damping factor design parameter (Fig. 3.10)
- The effect of static friction on the system response (Fig. 3.11)
- The effect of noise and filtering on the system response (Fig. 3.12)

The design procedure of the sliding surface and other aspects of CSLM will be shown in Fig. 3.13.

#### 3.4.1 The Boundary Layer

Fig. 3.2 illustrates the effect of the boundary layer thickness,  $\phi$ . The effect of chatter due to non-instantaneous switchings (shown in Fig. 3.1b) when  $\phi=0$  is shown as a dashed line. The position response is linear, but again the control signal exhibits high chatter, as expected. The resulting steady state error was determined to be  $0.3\text{ mm}$ . This large error is caused by the saturated switchings of the controller. The performance of CSLM improves considerably when a boundary layer is implemented, as was demonstrated in Fig. 3.1c. The position response with  $\phi=1.5$  can be seen as a solid line in Fig. 3.2. The response is clearly linear and the control signal is smooth. In addition, the resulting steady state error was determined to be  $0.05\text{ mm}$ , which is a great improvement. If one increases the size of the boundary layer considerably, the controller performance degrades since the proportional action inside the boundary layer can introduce a steady state error. This can be seen in Fig. 3.2 as the dotted line response which corresponds to  $\phi=10.0$ . Though the transient response shows little deviation from the one obtained with a boundary layer of  $1.5$ , the steady state error increases considerably to  $0.5\text{ mm}$ .

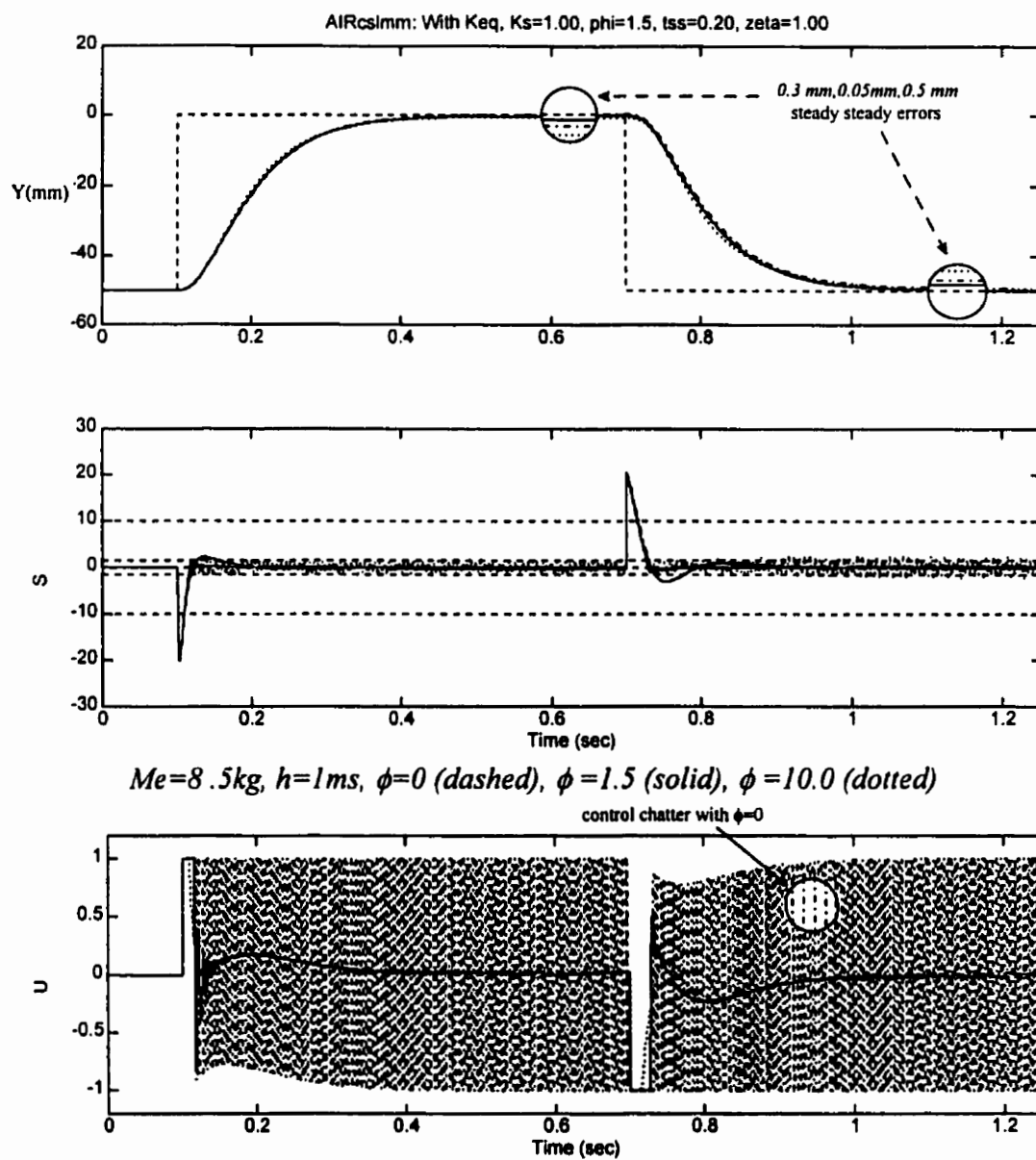


Figure 3.2: Effect of Size of the Boundary Layer with  $h=1ms$

### 3.4.2 Sampling Time Considerations

Fig. 3.3 shows the effect of the sampling time,  $h$ . A boundary layer of  $15.0$  and a sliding gain of  $1.0$  were used. The solid line response corresponds to a sampling time of  $1\text{ ms}$ . It is the smoothest response because of the fast switchings about the surface. If the sampling time is increased ten-fold to  $10\text{ ms}$  (dotted lines), the performance of the system is still considered acceptable. The reason why the performance is still acceptable is due to the large boundary layer ( $\phi=15.0$ ) which “relaxes” the switching action. High chatter appears with  $h=10\text{ ms}$  and a  $\phi=1.5$ .

If the sampling time is further increased to  $50\text{ ms}$  (dashed lines), CSLM becomes unstable. Increasing the boundary layer could restore stability, but the controller would no longer be considered a sliding mode controller since switchings would be explicitly eliminated. Empirically, one needs to use a sampling time at least 20 times smaller than the open loop time constant of the system. For example, if the open loop time constant for a particular pneumatic system is  $0.1\text{ sec}$ , the sampling time should be in the order of  $0.005\text{ sec}$ . Sampling time limits for CSLM have been reported by Pieper (1992) but are not applied in this thesis.

### 3.4.3 Sliding Gain and Transient Response

Fig. 3.4 shows the effect of the sliding gain  $K_S$ . Three responses are shown in the figure. The solid response corresponds to a sliding gain of  $1.0$ . This is a normalized value for the sliding gain which indicates the maximum value permissible for the gain. It corresponds to a valve input of  $5\text{ volts}$  which indicates maximum flow through the valve. The simulated valve has a maximum flow of  $1.88\text{ l/sec}$  ( $4\text{ scfm}$ ). The dotted response corresponds to a sliding gain of  $0.5$  and the dashed response corresponds to a sliding gain of  $2.0$ . A  $\phi=4.5$  is used to eliminate chatter effects that would result with  $K_S=0.5$ . If one compares the three responses, the first realization is that the overall settling time is unaffected. This should be no surprise, since the dominant part of the overall settling time is the sliding settling time which is linked to the sliding surface.

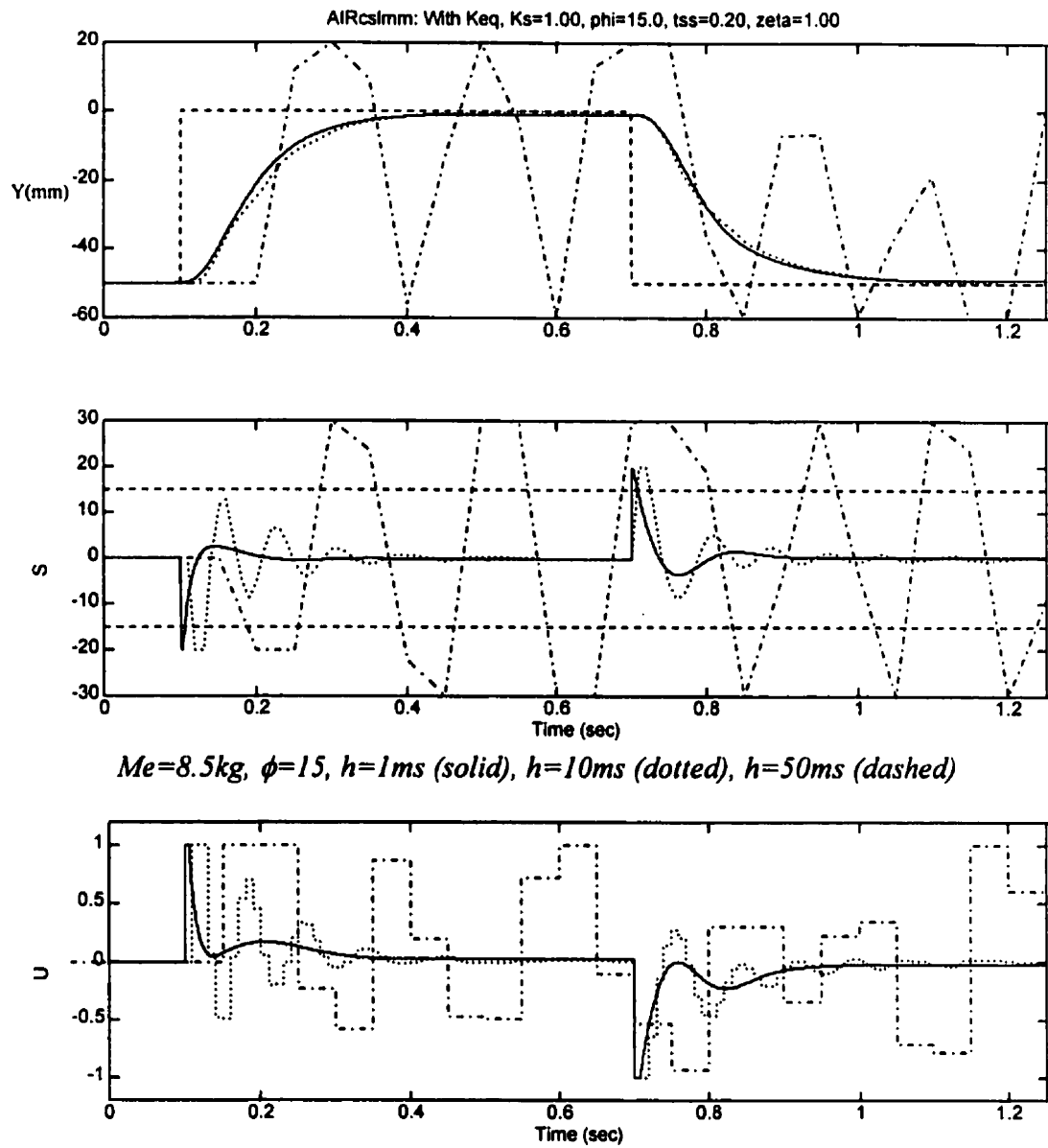


Figure 3.3: Effect of Sampling Time on Stability of CSLM

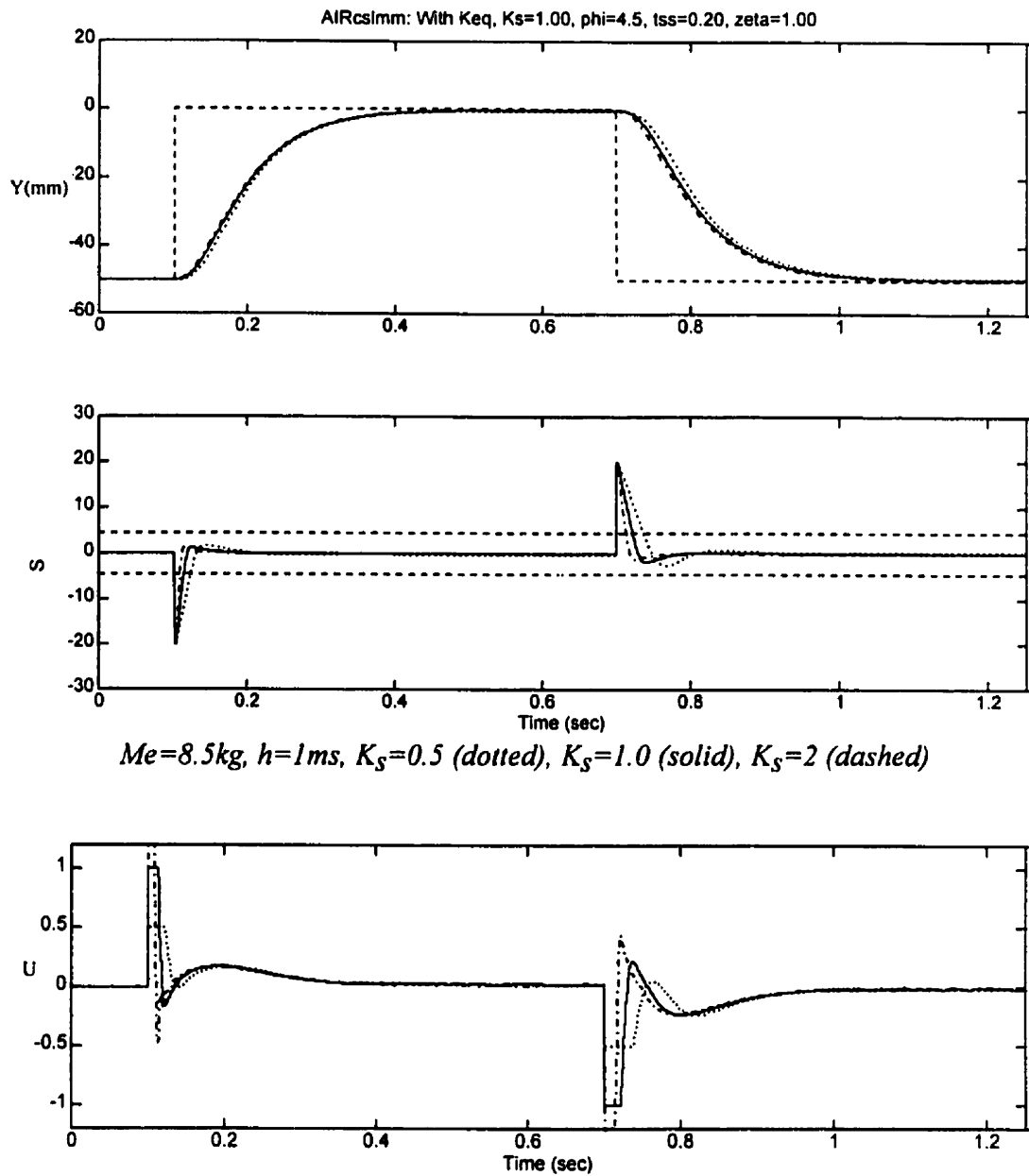


Figure 3.4: Effect of Size of  $K_S$  on Performance with Small Sampling Time



The sliding gain, as will be seen in Chapter 4 can be linked to the reaching time (the time to reach the sliding surface) which can only slightly affect the transient response of the system. This can also be seen in the responses. The dashed line response of the highest sliding gain ( $K_S=2.0$ ) rises faster than the other two responses; the slower of the three, the dotted response corresponds to the lowest sliding gain ( $K_S=0.5$ ).

The effect of  $K_S$  is best highlighted by the sliding function plot which shows that the system is outside the boundary layer the longest when the lowest gain is used, which results in a slowest response.

The nonlinearity in the system (position and direction dependence) can be seen in the dissimilar control input response. Note that the figure shows the normalized control input; in actual fact,  $\pm 1$  v in the plot corresponds to  $\pm 5$  v input to the valve. The input stays saturated for a longer time when the motion is from the center to the end ( $y=0$  to  $y=-50mm$ ), rather than from the end to the center, mainly due to the larger chamber volume that needs to be filled when one moves from the center to the end.

#### 3.4.4 Robustness Test for CSLM

A test for the robustness of CSLM is to design the controller for a certain payload and apply the controller to different payloads. Fig. 3.5 shows the effect of the payload mass,  $M_e$ . The correct mass for which the controller should be designed is  $8.5\text{ kg}$ . The system response with the correct mass is seen in Fig. 3.5 as a solid line.

The controller was then used unaltered to control a payload of  $23.0\text{ kg}$  (dotted line) and a payload of  $2.2\text{ kg}$  (dashed line). One can observe a slightly slower transient response in the case of the larger mass and a slightly faster transient response in the case of the smaller payload mass. This is intuitive. The control signal shows that additional control effort is required to bring the larger mass to the sliding surface. Conversely, “less” control effort is required in the case of the smaller payload mass.

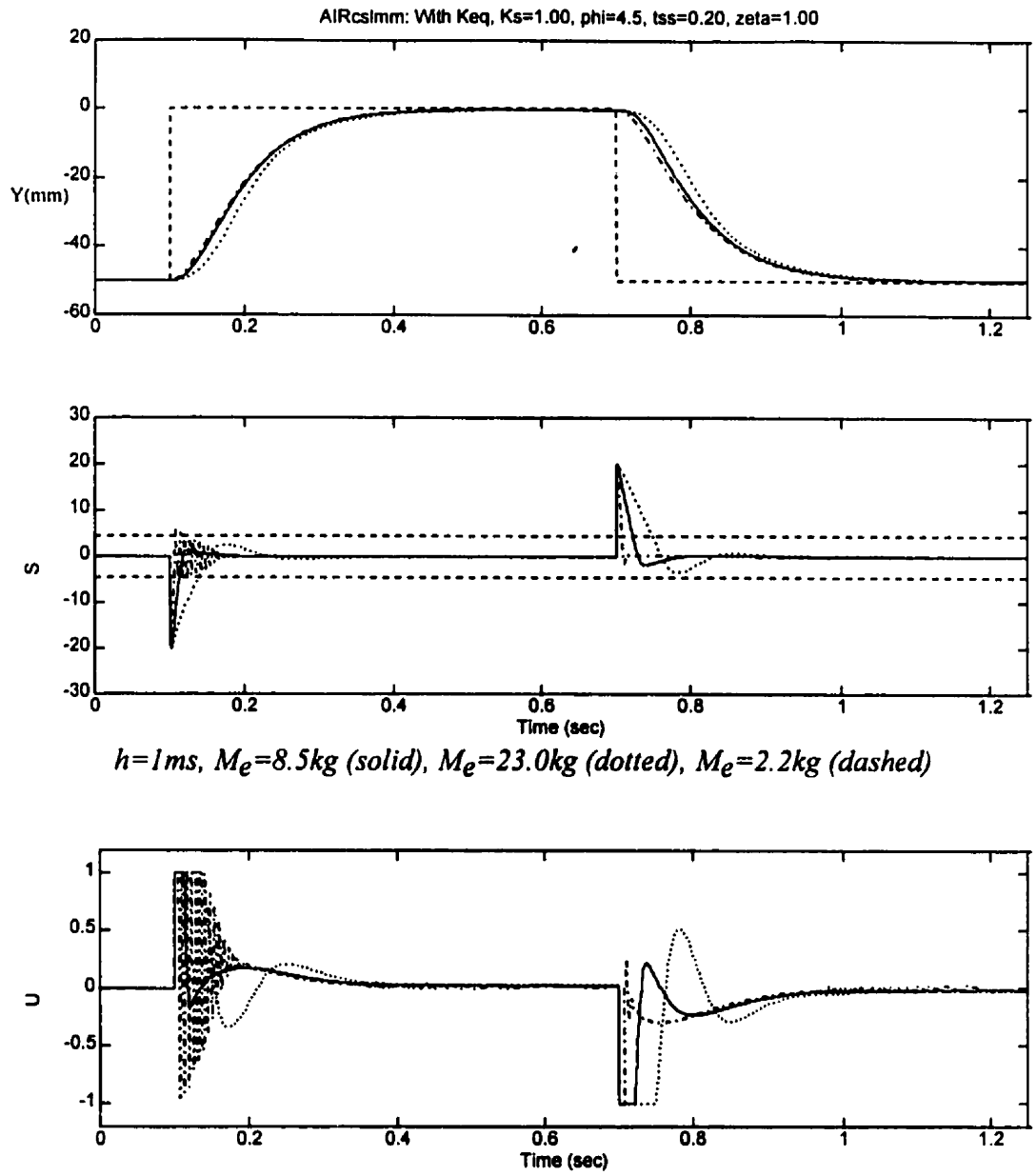


Figure 3.5: Robustness of CSLM with 3 masses and  $h=1ms$

The chatter in the control signal in the case of the smaller payload has to do with the fact the smaller payload responds faster to the input.

In summary, CSLM is robust but only if the sampling time is sufficiently small. The controller robustness deteriorates if an inadequate sampling time is used. In the case of the pneumatic system under study and the available hardware, the limiting sampling time was *10ms*. The responses for the same robustness test with  $h=10ms$  will be shown in the next section.

Fig. 3.6 shows the same robustness test presented in Fig. 3.5 but instead of a CSLM controller, a conventional PVA controller is used. The solid lines correspond to the correct controller design with a payload of *8.5 kg*, the dashed and dotted lines correspond to the incorrect system payloads of *2.2 kg* and *23.0 kg*, respectively. The gains that were used ( $K_p=12.5$ ,  $K_v=0.49$ ,  $K_a=0.06$ ) were calculated for the settling time and damping requirements using pole-placement (*Surgenor and Vaughan, 1996*). One observes that PVA not only has poor robustness, but even in the correct system response (solid lines) it indicates a nonlinear behaviour: an underdamped response when the positioner moves to the center of the stroke, and a damped response when it moves towards the ends of the stroke. Therefore, the nonlinear nature of the pneumatic positioner of which the performance is position dependent is still evident.

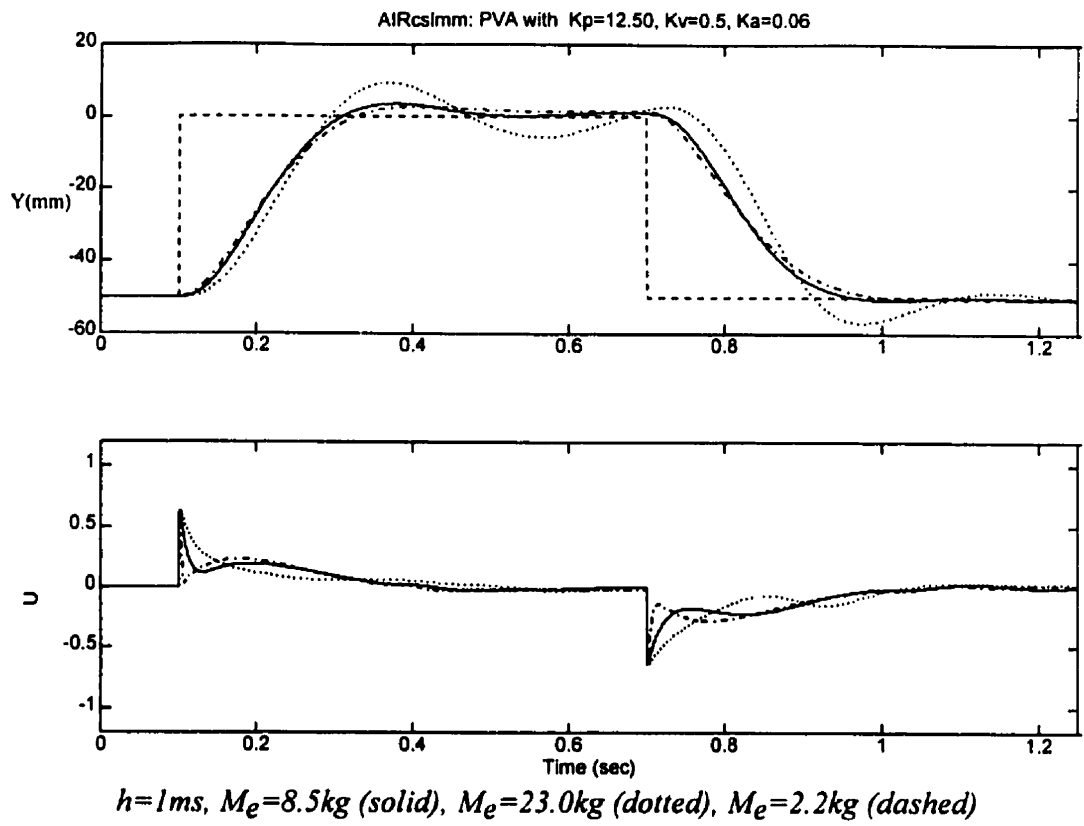


Figure 3.6: Robustness of PVA with 3 masses and  $h=1ms$

### 3.4.5 Robustness Test for CSLM with Inadequate Sampling Time

Fig. 3.7 provides an identical robustness test to the one presented in Fig. 3.5, but with a sampling time that was increased from  $1\text{ ms}$  to  $10\text{ ms}$ . For  $h=10\text{ms}$ ,  $K_S=1$ ,  $\phi=4.5$  and  $M_e=8.5\text{kg}$ , CSLM results in sustained oscillations and poor setpoint tracking which is caused by excessive control chatter, unlike the case when  $h=1\text{ms}$  (Fig. 3.4). Therefore, the boundary layer needs to be increased, from  $4.5$  as used in Fig. 3.4 and Fig. 3.5, to  $15.0$ . The tradeoff for the smooth control signal with a larger boundary layer is a higher steady state error. When using a large sampling time ( $h=10\text{ms}$ ), it was also important to decrease the size of  $K_S$ , from  $1.0$  to  $0.8$  to avoid controller saturation which can cause poor response and possible instability. The solid line responses of Fig. 3.7 illustrates a slight oscillation about the sliding surface, caused by the combination of the large sampling time and the large boundary layer.

The controller was then applied to a payload of  $2.2\text{ kg}$  (dotted line) and a payload of  $23.0\text{ kg}$  (dashed line). The response of the larger payload deteriorates but remains stable. But the smaller mass, due to its small inertia reacts faster than the  $8.5\text{ kg}$ , and overshoots the sliding surface at each switching. This causes oscillations and large steady state errors on the order of  $20\text{ mm}$ . One way of correcting this would be to decrease the size of the switching action ( $K_S$ ) and increase the boundary layer. Unfortunately, with this combination of corrective actions, the large mass response becomes marginally stable. This leads to the conclusion that CSLM has poor robustness in the presence of a large sampling time.

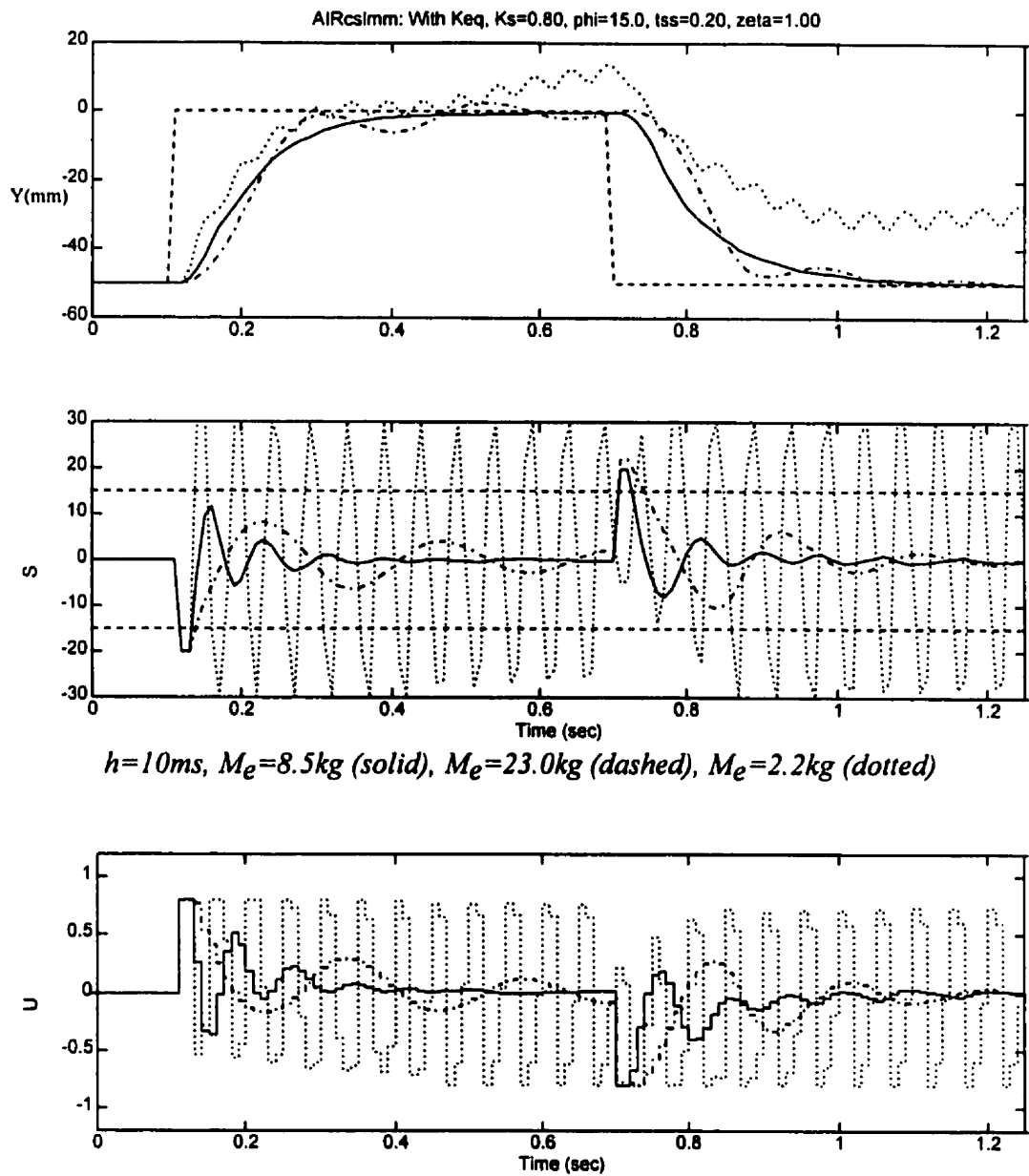


Figure 3.7: Robustness of CSLM with 3 masses and  $h=10\text{ms}$

### 3.4.6 Equivalent Action and Robustness

Fig. 3.8 shows the effect of the equivalent control action. It has been shown that the control law for CSLM is composed of two parts, the equivalent action and the sliding action. The dominant action is the sliding action which directs the system to the sliding surface and to the equilibrium point, or the final setpoint. The equivalent action is a linear feedback law that helps the sliding action in keeping the system on the sliding surface. The solid line response represents the behavior of the 8.5 kg payload when the equivalent gain is used.

If the equivalent action is removed, the performance of the controller degrades (dotted line). First of all, the response is slower due to the decreased control action. Secondly, one can notice that both the sliding function and the control signal begin to “blow up” when the positioner is at the end of the stroke ( $y = -50\text{mm}$ ). This indicates instability. The role of the equivalent action is to keep the system on the sliding surface, therefore its absence will have a negative effect, especially since the sampling time is large (10 ms). When a small sampling time (1 ms) is used, there is no visible change in the performance of the system, mainly because the sliding action is able (on its own) to drive the system to the surface and keep it on the surface by faster switchings.

The larger inertia of a 23.0 kg payload mass eliminates the increasing amplitude of the control signal oscillations, even with no equivalent action (dashed line).

In conclusion, the equivalent action has a positive effect in the overall system behavior. The degree of performance degradation when one neglects the equivalent action depends on the sampling time.

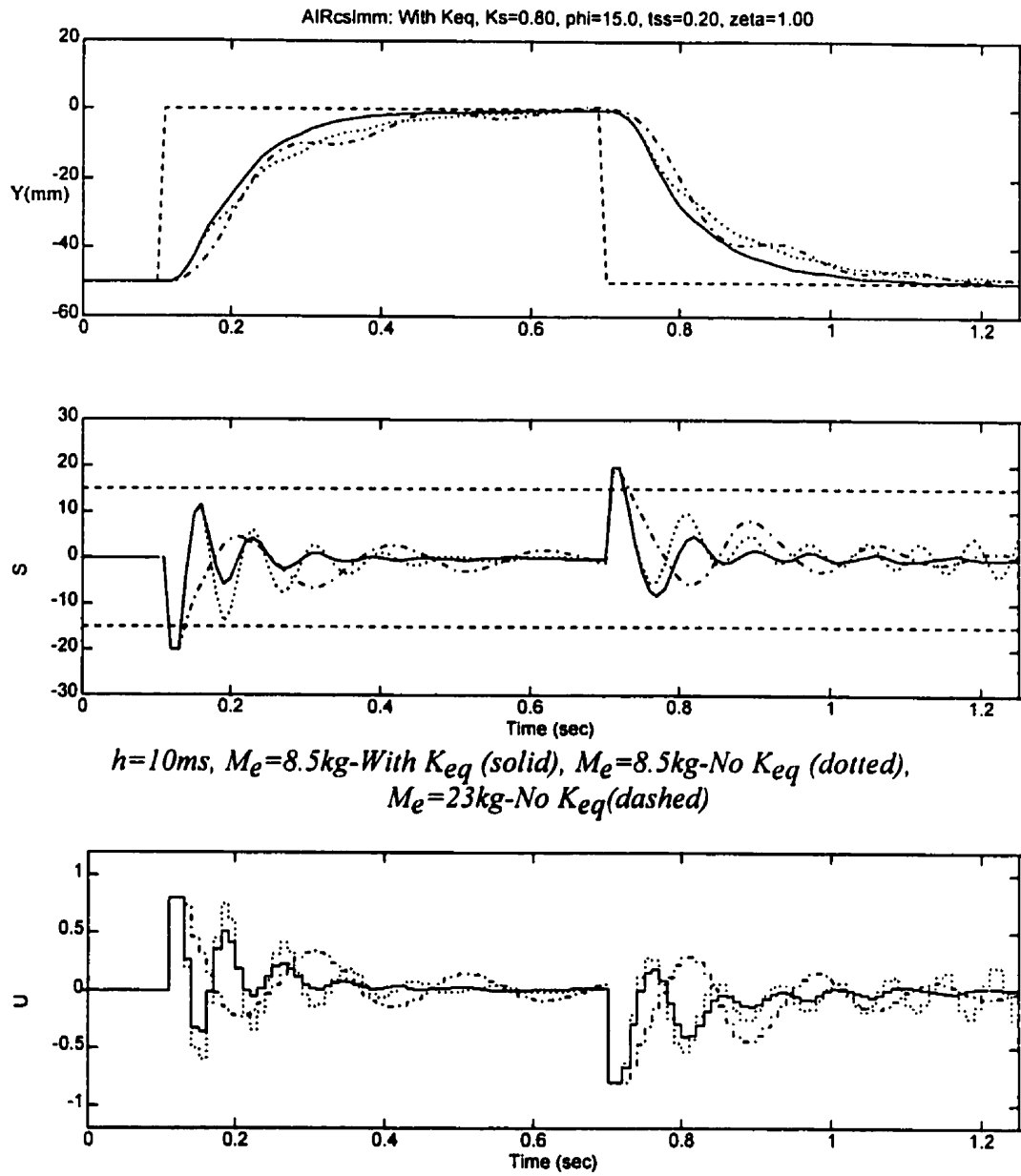


Figure 3.8: Equivalent Gain and Robustness of CSLM



### 3.4.7 Sliding Surface Design Parameters

The sliding surface design for CSLM as applied to a 3<sup>rd</sup> order pneumatic system is simplified to a 2<sup>nd</sup> order sliding surface for which one can select the desired sliding settling time and surface damping factor. The overall settling time is the sum of the sliding settling time and the reaching time. Of the two, the dominant component is the sliding settling time. Fig. 3.9 shows the response of the pneumatic system when the sliding settling time was set to *0.2 sec*, *0.3 sec* and *0.4 sec*. The responses are shown as solid, dotted and dashed lines respectively. For these, the desired damping factor was set to *1.0* (critically damped response).

Fig. 3.10 shows the responses for three designed damping factors of *1.0*, *0.70* and *0.50* and are shown as solid, dotted and dashed lines respectively. For all cases the sliding settling time was required to be *0.20 sec*. The responses clearly indicate that all responses have a settling time comparable to *0.2 sec* while overshoots of about 5% and 16% are seen for the cases where the damping factors were set at *0.70* and *0.50* respectively. The observed overshoots are in agreement with the expected overshoots derived from the classic expression for the percent overshoot for a 2<sup>nd</sup> order system as a function of the damping factor (*Palm, 1986*):

$$M_p = 100 e^{-\pi\zeta/\sqrt{1-\zeta^2}} \% \quad (3.51)$$

Fig. 3.9 and 3.10 clearly illustrate how the shape of the response can be manipulated by the design of the sliding surface. If the sampling time is increased ten-fold to *10 ms*, the shape of the response cannot be manipulated as easily by the designer.

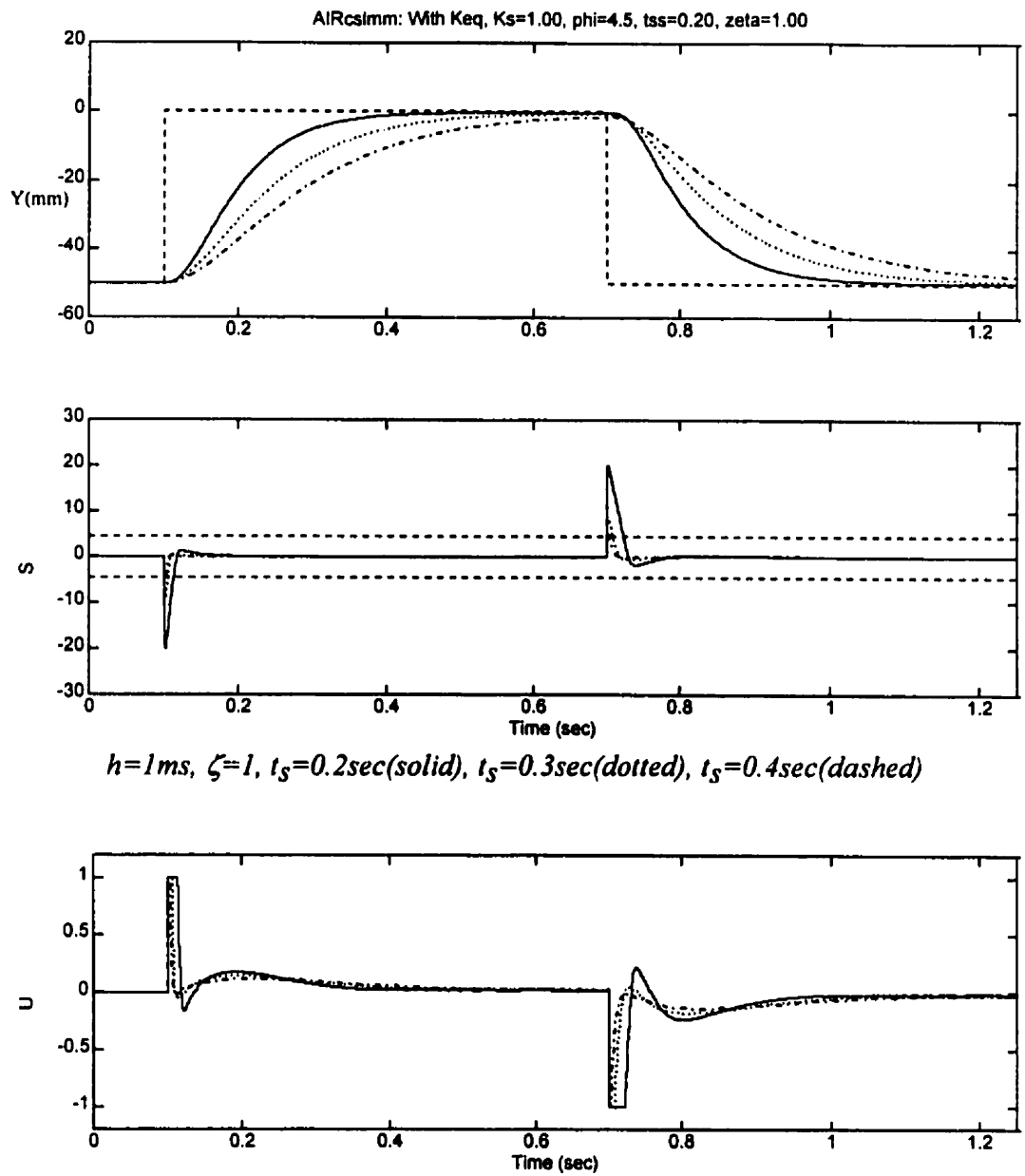


Figure 3.9: Sliding Surface Design for a set of Settling times

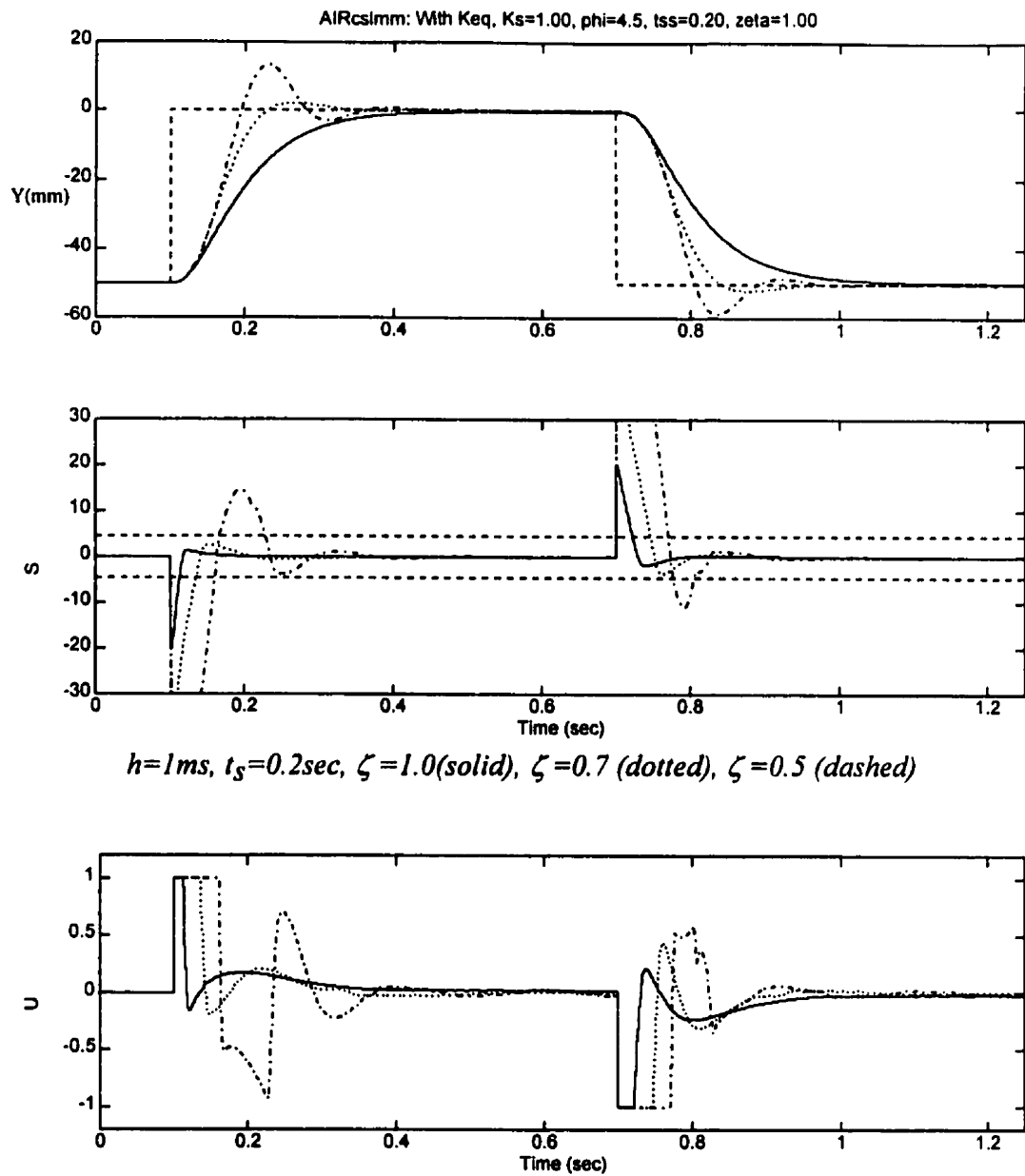


Figure 3.10: Sliding Surface Design for a set of Damping Factors

### 3.5 Static Coulomb Friction and Noise Considerations

Static friction in pneumatic systems is a significant performance inhibitor. Fig. 3.11 shows considerable performance deterioration of the system with increasing static friction. The solid line represents the response of the system with no static coulomb friction. The dotted and the dashed lines show the response of the system with a static coulomb friction of  $5\text{ N}$  and  $10\text{ N}$ , respectively. A static friction test was performed on the experimental setup to determine reasonable values for the static coulomb friction. An average static coulomb force was determined at  $F_{CS}=10\text{ N}$  (see Appendix B for *MARTONAIR* cylinder).

Sensor noise can also be a problem in practise. A realistic level for noise in the measured position was determined by examining the datafiles obtained from experimental tests. It was determined that a  $\pm 0.5\%$  sensor noise was evident in the recorded position when the control signal was constant. For visualisation reasons, the noise level used in simulation was  $\pm 1.0\%$ . A settling time of  $0.3\text{ sec}$  was chosen that better shows the lag that is introduced by the filter. Fig. 3.12 shows the response of the system with no noise in dashed lines.

In simulation, the “clean” actuator position is obtained by a nonlinear simulation. A  $1.0\%$  white noise signal is then added to the “clean” actuator position signal and this becomes the “sensed” position to be fed into the control law. The noise is  $1\%$  of full scale and was obtained from an open loop test. The controller’s response with  $1.0\%$  noise is shown as a solid line in Fig. 3.12. The noise can be better realised if one observes the velocity plot. With the  $1.0\%$  position noise, velocity noise is amplified. Acceleration noise is amplified even further (recall that in experiment, velocity and acceleration are obtained by single and double differentiation of position).

The use of a filter can decrease the effects of sensor noise, but at a cost. A lag can be seen in the dotted response of the system in Fig. 3.12 This is due to the presence of a

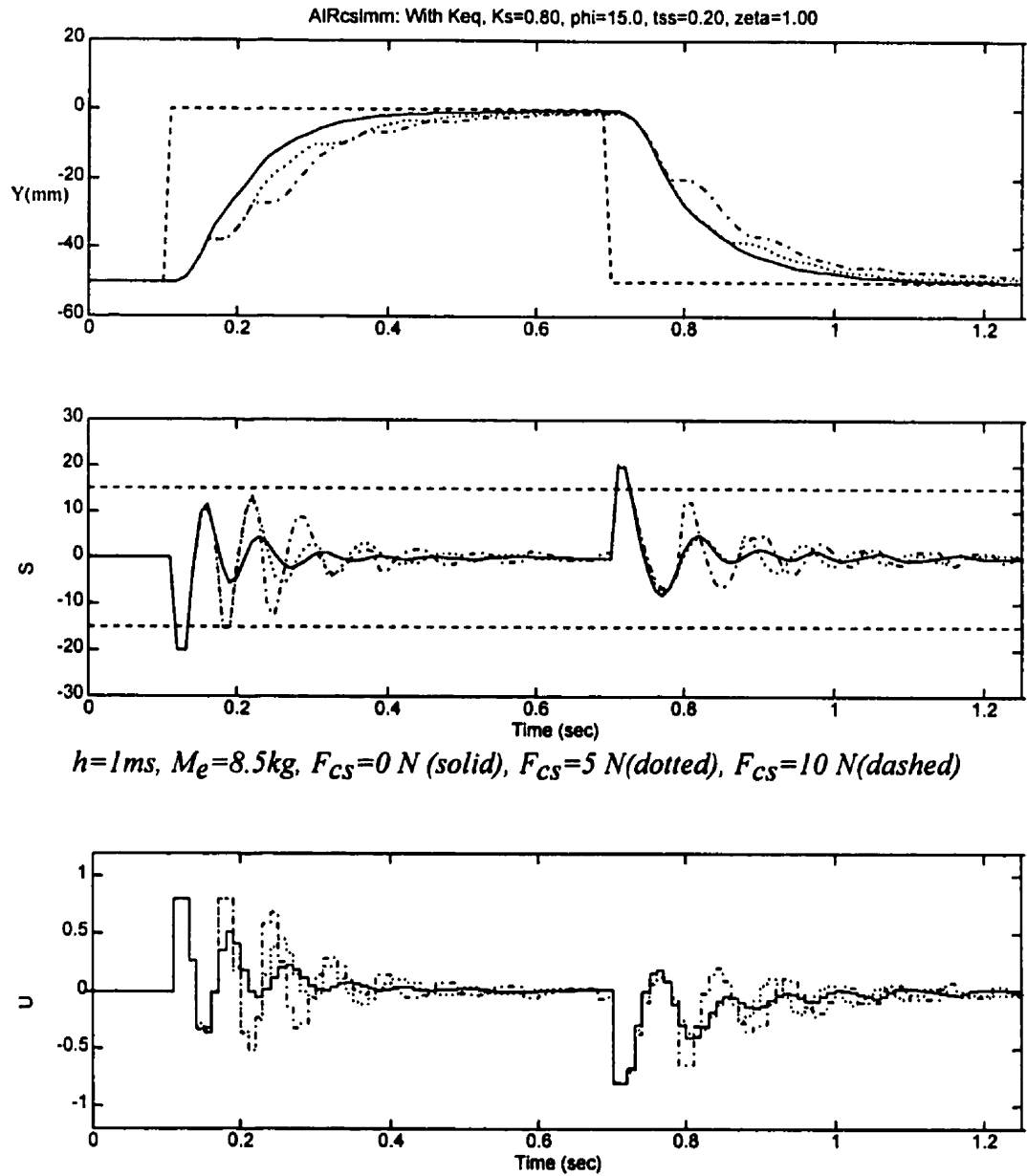


Figure 3.11: Effect of Static Coulomb Friction on performance of CSLM

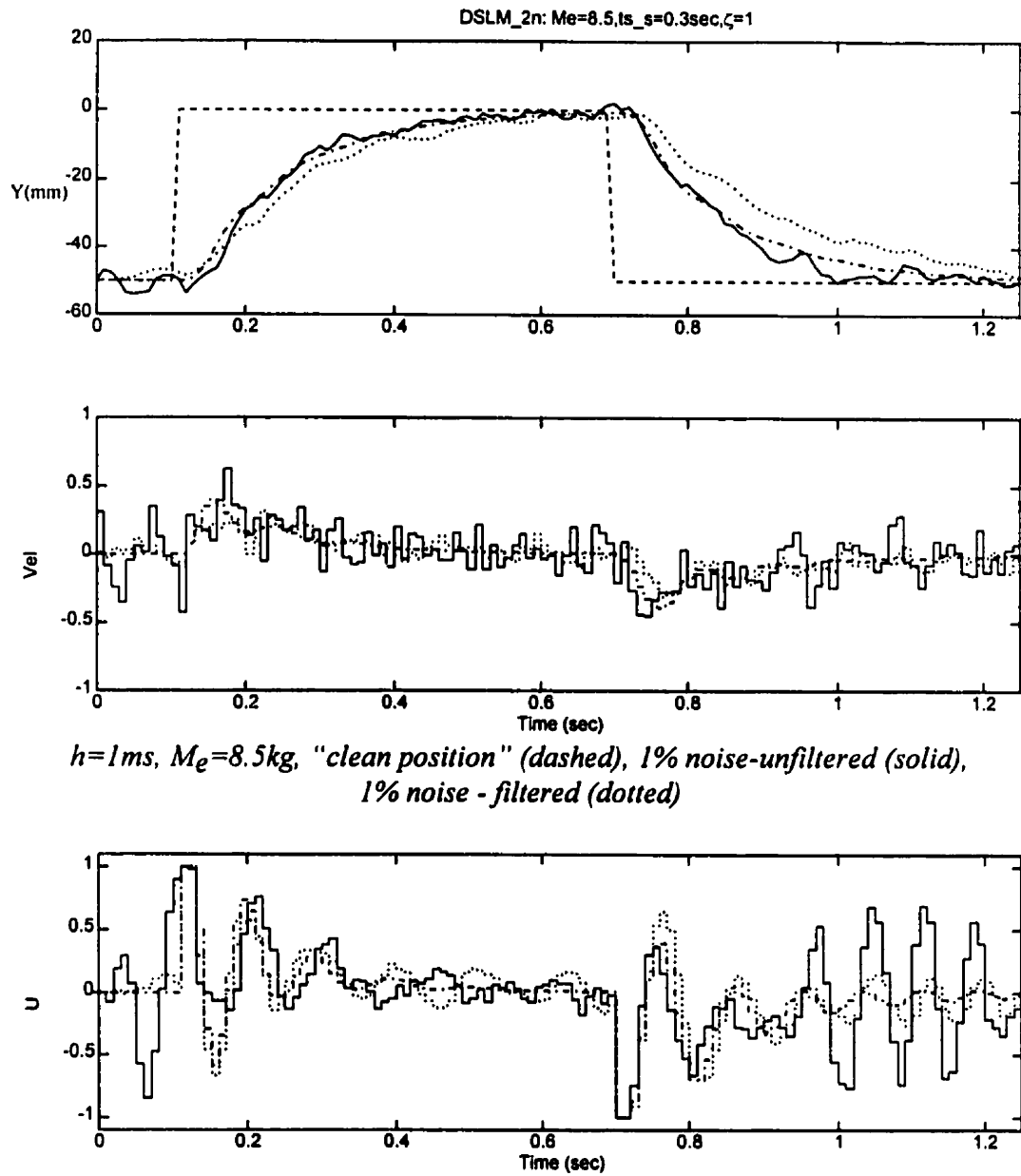


Figure 3.12: Effect of Noise and Filtering on performance of CSLM

2<sup>nd</sup> order Butterworth filter being used with a cut-off frequency of 15 Hz. The response is smooth again, but with a visible lag.

### 3.6 Summary

The design procedure for the sliding surface of CSLM is summarized in Fig. 3.13. The continuous system column shows how the transformation matrix  $T$  is obtained from the controllability matrices of the original state space model and the canonical system state space model. The continuous sliding surface column shows the procedure for the two methods for the design of the sliding surface, the pole placement technique as outlined in the chapter and the filter method which had been shown in *Iordanou and Surgenor (1996)*.

The chapter presented some basic issues for the CSLM controller by means of simulation of pneumatic positioning system. These issues include the effect of the tuning parameters of CSLM, namely:

- The sliding gain, and
- The boundary layer thickness,

as well as the design parameters for the sliding surface, namely:

- The sliding settling time, and
- The damping factor,

and finally the effect of:

- The sampling time.

In summary, CSLM is a highly robust controller under the following conditions:

- The sampling time is sufficiently small, so that the continuous structure of the controller is not negated by large discrete sampling times and yet large enough to be achievable with a modest control computer.
- The sliding gain is sufficiently large without exceeding stability limits, so that model errors do not compromise robustness and yet small enough to be achievable in practise.
- The boundary layer is sufficiently large so that chatter is eliminated and yet sufficiently small so that positioning accuracy is not compromised.

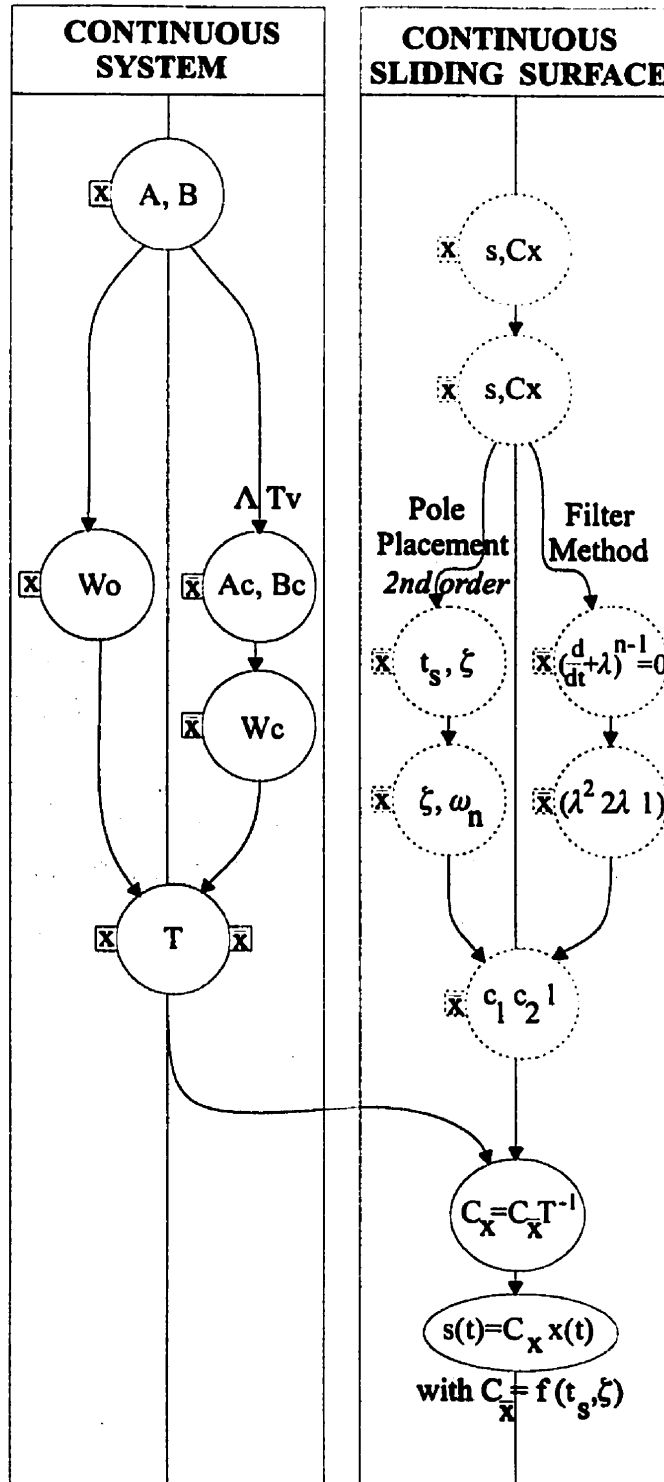


Figure 3.13: Sliding Surface Design Procedures for CSLM



## CHAPTER 4

### DISCRETE SLIDING MODE CONTROL

CSLM with its inevitable implementation on a digital computer ignores by definition the effect of the sampling time. More precisely, the implementation of CSLM assumes that the sampling time is small enough such that its effect can be ignored. In the case of Discrete Sliding Mode Control (DSLM), the stability conditions that generate the switching laws are derived from a difference function as opposed to a derivative function. In other words, the DSLM switching laws take explicit account of the sampling time.

#### 4.1 Traditional Discrete Sliding Mode Control

To help introduce some of the parameters and terms to be used in this chapter, consider a single-input discrete system:

$$x(k+1) = \Phi x(k) + \Gamma u(k) \quad (4.1)$$

with  $\Phi$  and  $\Gamma$  obtained from the state space matrices  $A$  and  $B$  of the continuous domain. A full-state feedback DSLM is designed whereby the discrete sliding function  $s(k)$  can be given as:

$$s(k) = C x(k) \quad (4.2)$$

where  $C$  denotes the discrete sliding surface matrix.

During pure sliding it can be assumed that the value of the sliding function remains the same, i.e.,  $s(k) = s(k+1) = s(k+2) \dots$ . If one sets  $s(k+1) = s(k)$ , then by inspection of Eq. 4.2 one can see that  $C x(k+1) = C x(k)$ . This final equation is used to derive the closed loop dynamics of the system under pure sliding. A full description of the procedure will be provided later in this chapter.

One of the first comprehensive approaches to DSLM was presented by *Furuta (1990)*. A general approach to the selection of the sliding surface  $C$  was presented, which should be selected so that the following system is stable:

$$x(k+1)=[\Phi-\Gamma(C\Gamma)^{-1}C(\Phi-I)]x(k) \quad (4.3)$$

$$s(k)=Cx(k)=0$$

The above equation gives the plant's response once the sliding surface is reached and can be used as the foundation for the design of the sliding surface. The system can be rewritten as :

$$\begin{bmatrix} \Phi - z_F I & \Gamma \\ C & 0 \end{bmatrix} \begin{bmatrix} x(k) \\ u(k) \end{bmatrix} = 0 \quad (4.4)$$

where  $x(k+1)=z_F x(k)$ . The only requirement for stability is that  $|z_F|<1$ .

A more recent paper by *Furuta and Yaodong* (1995) described a new approach to designing the boundary layer directly within the state space, as opposed to around the sliding mode, or sliding surface. The approach can be applied to both continuous-time and discrete-time systems. For the general discrete system shown in Eq. 4.1,  $\bar{P}_n$  or  $\bar{P}$  -norm of the discrete state, the function  $\bar{L}$  and the discrete-time boundary layer, or sliding sector  $\bar{S}$  are defined as:

$$\begin{aligned} \bar{P}_n &= \|x(k)\|_Q = \sqrt{x(k)^T Q x(k)}, \quad x(k) \in R^n \\ \bar{L} &= \|x(k)\|_Q^2 = x(k)^T Q x(k), \quad \forall x(k) \in R^n, x \neq 0 \\ \bar{S} &= \{x | x(k)^T (\Phi^T Q \Phi - Q)x(k) \leq -x(k)^T R x(k), \quad x(k) \in R^n\} \end{aligned} \quad (4.5)$$

where  $Q$  and  $R$  are positive definite symmetric and positive semi-definite symmetric matrices, respectively. For the boundary layer  $\delta(k)$ , we have  $s^2(k) \leq \delta^2(k)$ . A transformation is then defined,  $x(k) = T\bar{x}(k)$  so that the original system is brought to canonical form. The coefficients of the characteristic polynomial of the last row of the canonical system,  $\alpha_0, \alpha_1, \alpha_2 \dots \alpha_n$  compose the transformed sliding surface which can be transformed back to the original state space variable  $x(k)$  by using the transformation matrix  $T$ . The boundary layer  $\delta(k)$  is also defined in terms of the variable  $z(k)$  and is transformed back to the variable  $x(k)$  using  $T$ . However, the

method does not explain how different setpoint profiles can be selected, since  $Q$  and  $R$  are said to be chosen arbitrarily.

*Paden and Tomizuka (1995)* considered a simple nonlinear system with a discrete time state feedback control law. A scalar sliding function  $s(k) = C^T x(k)$  where  $C^T = [c_1 \ c_2 \ \dots \ c_{n-1} \ 1]$  is composed which defines a target manifold for the closed loop dynamics, i.e. sliding surface.  $C^T$  is normalized so that  $c_n = 1$ . Starting from a Lyapunov's function of the system, a sliding manifold is defined and is then used to develop sampling rate thresholds for the discrete controller. The paper concludes that the selection of the gains for a discrete sliding mode controller not only depends on the performance requirements (i.e. reaching time and asymptotic rate of decay on the manifold), but also depends on the discrete sampling time used. A recommendation for systems with higher uncertainties, is to use smaller sampling times.

*Iordanou et al (1995)* presented a procedure for the design of the sliding surface of a DSLM controller for an  $n^{th}$  order system as a combination of a transformation matrix  $T$  with a cascaded series of  $n-1$  first-order filters, thus composing a sliding surface of  $n-1^{th}$  order. The filter bandwidth,  $\lambda$  becomes the sliding surface design parameter. The coefficients of the  $n^{th}$ -state of the canonical system can be linked to closed loop system dynamics. The filter bandwidth is chosen according to the desired decay speed of the system on the surface. In other words, the higher the bandwidth, the faster the decay on the surface. The upper limit for the bandwidth is determined by the available system sampling rate. *Iordanou and Surgenor (1996)* implemented additional features. These features included state weights and a varying sliding gain.

*Pieper (1992)* investigated the issue of optimising the sliding surface coefficients using a minimisation technique similar to the linear quadratic control structure. The work shows stability limits on the sampling time when a *pseudo*-DSLM is implemented to a general  $n^{th}$  order system. From there, two techniques are presented for the design of the  $2^{nd}$  order system sliding surface. The first method is

based on selection of eigenstructures and the second is based on linear quadratic optimisation. The more popular of the two methods is the one that is based on eigenstructure selection. For a general discrete system as shown in Eq. 4.1, the closed loop dynamics can be shaped so that:

$$x(k+1) = ([I - V_p] \Phi + V_p) x(k) \quad (4.6)$$

where  $V_p$  is a projector defined as:

$$V_p = \Gamma [C \Gamma]^{-1} C \quad (4.7)$$

The component  $(I - V_p) \Phi$  of Eq. 4.6 maps  $\Phi$  into the null space of the sliding surface matrix  $C$ , and  $V_p$  maps the state into the range of  $\Gamma$ . A new variable  $T_d$  is defined as the eigenvector matrix of  $I - V_p$ . The desired closed loop eigenvector  $T_d$  is then chosen by eigenvalue assignment by considering Eq. 4.6 and 4.7. The diagonal matrix of eigenvalues  $\lambda$  and the eigenvector matrix  $T_d$  satisfy:

$$\Phi T_d - T_d \lambda = V_p [\Phi - I] T_d \quad (4.8)$$

The left hand side can be chosen arbitrarily, but it should be of full rank. The left generalised inverse of  $\Gamma$  is defined as  $\Gamma^\#$  and is chosen so that  $\Gamma^\# \Gamma = I$  and  $\Gamma^\# T_d = 0$ . The sliding surface matrix  $C$  is then found by solving for:

$$C = [C \Gamma] \Gamma^\# \quad (4.9)$$

The simplest design for the sliding surface with this method would be if the scaling factor  $C \Gamma$  in Eq. 4.9 is assumed to be the identity matrix  $I$  which then makes  $C = \Gamma^\#$ .

## 4.2 Design of the Sliding Surface

The design of the sliding surface is of primary importance to the performance of a sliding mode controller. It defines the nature of the required response, or graphically, the shape of the desired sliding surface. If one considers a 2<sup>nd</sup> order system, the sliding surface is a 1<sup>st</sup> order surface (or a sliding line) since the sliding regime is a dimension less than the system itself. For a third order system, a second order sliding surface is defined.

In this section, an original technique will be developed for the design of the sliding surface of a discrete sliding mode controller where its coefficients are given as functions of desired closed loop performance of the system under pure sliding. The sliding surface is based on a dominant set of desired closed loop poles and can match the more conventional sliding surface design characteristic where the sliding surface has one order less than the system (*Jordanou and Surgenor, 1997b*).

### 4.2.1 Discrete Time Domain

A single-input, single-output (SISO) discrete control system has:

$$x(k+1) = \Phi x(k) + \Gamma u(k) \quad (4.10)$$

with  $\Phi = e^{Ah}$  and  $\Gamma = \int_0^h e^{At} B dt$  where  $h$  represents the sampling time and  $A, B$  are the continuous-time domain state matrices. The matrix exponential can be written as  $e^{Ah} = I + Ah + A^2 h^2 / 2! + A^3 h^3 / 3! + \dots$ . The identities  $I + Ah + A^2 h^2 / 2!$  and  $hB + ABh^2 / 2!$  can be considered as good approximations for the matrix exponential  $\Phi$  and convolution integral  $\Gamma$ , respectively if a small sampling time is used. For example, consider the following continuous time matrix  $A$ , which yields a discrete time matrix  $\Phi$  as obtained using the above matrix exponential equation as:

$$A = \begin{bmatrix} 0 & 1 & 0 \\ 0 & -8 & 0.057 \\ 0 & -26430 & 1 \end{bmatrix} \xrightarrow{c2d.m} \Phi = \begin{bmatrix} 1 & 0.0094 & 2.7 * 10^{-7} \\ 0 & 0.849 & 0.00054 \\ 0 & -246.486 & 0.929 \end{bmatrix}$$

The approximation  $I+Ah+A^2h^2/2!$  and the next term  $(A^3h^3/3!)$  are calculated as:

$$I + Ah + \frac{(Ah)^2}{2!} = \begin{bmatrix} 0 & 0.0096 & 2.8 * 10^{-7} \\ 0 & 0.845 & 0.055 \\ 0 & -252.56 & 0.924 \end{bmatrix} \text{ and } \frac{(Ah)^3}{3!} = \begin{bmatrix} 0 & -0.0001 & 7.9 * 10^{-9} \\ 0 & 0.004 & -0.00001 \\ 0 & -6.38 & 0.002 \end{bmatrix}$$

Clearly, the last term  $(A^3h^3/3!)$  is within  $\pm 2\%$  of  $\Phi$ , therefore  $I+Ah+A^2h^2/2!$  can be given as a good approximation for the matrix exponential. A similar result can be shown for the expansion of the convolution integral,  $\Gamma$ . The discrete sliding function  $s(k)$  can be given as:

$$s(k) = Cx(k) \quad (4.11)$$

where  $C$  denotes the discrete sliding surface matrix.

#### 4.2.1a Stability of a Discrete System

The first consideration for stability of a discrete system is the permissible size of the roots of its characteristic equation. If the system is discrete, it has  $x(k+1) = \Phi x(k)$  where  $x(k) = [x_1(k) \ x_2(k) \ \dots x_n(k)]$  for  $k=0,1,2,\dots$ . Its solution can be written as  $x(k) = \Phi^k x(0)$ . This is obtained by  $x(k+1) = \Phi^{k+1} x(0) = \Phi \Phi^k x(0) = \Phi x(k)$ . For stability of a discrete system, the eigenvalues of  $\Phi$  have a modulus of *less than 1.0*, since  $\Phi^k \rightarrow 0$  as  $t \rightarrow \infty$ . Geometrically, all roots lie inside the unit circle in the complex plane.

The solution for  $x(k+1) = \Phi x(k)$  can then be calculated. If one considers the transformation  $x(k) = T_v r(k)$  then:

$$r(k+1) = \Lambda r(k) \quad (4.12)$$

where  $\Lambda$  is the diagonal eigenvalue matrix of  $\Phi$  and  $T_v$  is the matrix of eigenvectors.

Therefore,  $r_j(k) = b_j \lambda_j^k \ \forall \ i=1,2,\dots,n$  and:

$$x(k) = T_v [b_1 \lambda_1^k \ b_2 \lambda_2^k \ \dots b_n \lambda_n^k]^T \quad (4.13)$$

where  $b_j$  are arbitrary constants determined from initial conditions.

The system can also be shown to be asymptotically stable if a positive-definite quadratic form  $V = x^T R x$  (equivalent to the *Lyapunov* function) can be found such that

the difference (rather than the derivative as in continuous time domain) is negative-definite. Just as before,  $R$  has to be a positive-definite matrix. In other words, for stability:

$$V(k+1) - V(k) = -x^T(k)Qx(k) < 0 \quad (4.14)$$

where in this case  $-Q = \Phi^T R \Phi - R$ . For stability,  $Q$  is positive-semidefinite, real-symmetric matrix and  $\Phi^k \rightarrow 0$  as  $t \rightarrow \infty$ . The procedure provides sufficient conditions for the design of the switching laws for DSLM.

#### 4.2.1b Canonical Form of a Discrete System

For a controllable system, there exists a unique transformation  $T$  for  $x(k) = T \bar{x}(k)$  which transforms the original discrete system, to  $\bar{x}(k+1) = \bar{\Phi} \bar{x}(k) + \bar{\Gamma} u(k)$  which is in pure canonical form (*Jordanou and Surgenor (1997b), Furuta (1990), Pieper (1992)*).

The procedure for generating the canonical form of the original discrete system is similar to the procedure outlined in Chapter 3. The companion matrix  $C_\Phi$  of the original system matrix  $\Phi$  can be found if one considers the Vandermonde matrix  $V_n$ , composed of the eigenvalues  $\lambda_1, \lambda_2 \dots \lambda_n$  as:

$$V_n = \begin{bmatrix} 1 & 1 & 1 & \dots & 1 \\ \lambda_1 & \lambda_2 & \lambda_3 & \dots & \lambda_n \\ \lambda_1^2 & \lambda_2^2 & \lambda_3^2 & \dots & \lambda_n^2 \\ \vdots & \vdots & \vdots & \vdots & \vdots \\ \lambda_1^{n-1} & \lambda_2^{n-1} & \lambda_3^{n-1} & \dots & \lambda_n^{n-1} \end{bmatrix} \quad (4.15)$$

$T_v$  is the matrix of eigenvectors  $v_1, v_2 \dots v_n$  as:

$$T_v = [v_1 | v_2 | \dots | v_n] \quad (4.16)$$

The companion matrix  $C_\Phi$ , or  $\bar{\Phi}$  can then be shown as:

$$C_\Phi = \bar{\Phi} = (T_v V_n^{-1})^{-1} \Phi (T_v V_n^{-1}) \quad (4.17)$$

The discrete system in canonical form can then be shown as:

$$\bar{\Phi} = T^{-1} \Phi T = \begin{bmatrix} 0 & 1 & 0 & \dots & 0 \\ 0 & 0 & 1 & \dots & 0 \\ \vdots & \vdots & \vdots & \ddots & \vdots \\ 0 & 0 & 0 & \vdots & 1 \\ -\alpha_0 & -\alpha_1 & -\alpha_2 & \dots & -\alpha_{n-1} \end{bmatrix}, \quad \bar{\Gamma} = T^{-1} \Gamma = [0 \quad 0 \quad \dots \quad 0 \quad 1] \quad (4.18)$$

For stability, during pure sliding of the transformed discrete system, the following condition should be satisfied:

$$\bar{\Phi}^T R \bar{\Phi} - R = -Q < 0 \quad (4.19)$$

The following section presents the procedure for the determination of a suitable transformation matrix  $T$ . The controllability matrix of the system is therefore considered. A system is said to be controllable if the rank of the system is equal to the rank of the controllability matrix  $W_0$  which, for a discrete system, is an augmented matrix defined as:

$$W_0 = [\Gamma \quad \Phi\Gamma \quad \dots \quad \Phi^{n-1}\Gamma] \quad (4.20)$$

If new coordinates (from  $x(k)$  to  $\bar{x}(k)$ ) are introduced by a nonsingular transformation matrix  $T$ , then for the new coordinates the controllability matrix becomes:

$$\bar{W}_c = [\bar{\Gamma} \quad \bar{\Phi}\bar{\Gamma} \quad \dots \quad \bar{\Phi}^{n-1}\bar{\Gamma}] \quad (4.21)$$

The transformed matrices  $\bar{\Phi}$  and  $\bar{\Gamma}$  were shown in Eq. 4.18 as  $\bar{\Phi} = T^{-1}\Phi T$  and  $\bar{\Gamma} = T^{-1}\Gamma$ . If these matrices are substituted in Eq. 4.21, then:

$$\bar{W}_c = [T^{-1}\Gamma \quad T^{-1}\Phi T T^{-1}\Gamma \quad \dots \quad T^{-1}\Phi^{n-1} T T^{-1}\Gamma] = T^{-1} W_0 \quad (4.22)$$

This concludes that matrix  $T$  that transforms a system to its canonical form can be found by considering the controllability matrices of the original and the transformed system, such as:

$$T = W_0 \bar{W}_c^{-1} \quad (4.23)$$

*Furuta and Pan (1995)* showed that if  $R$  of Eq. 4.19 is set equal to  $(TTT)^{-1}$ , then the following is true:



$$s(k) = \bar{C} \bar{x}(k) = [\alpha_0 \quad \alpha_1 \dots \alpha_{n-1}] \bar{x}(k) \quad (4.24)$$

which gives another design procedure for the discrete sliding surface described by  $C$ , ( $s(k)=Cx(k)$ ) since:

$$C = \bar{C} T^{-1} \quad (4.25)$$

Another technique for  $\bar{C}$  can be given if the modified  $\bar{x}$ -dynamics are required to behave as a set of coupled  $l^{\text{th}}$ -order filters of the form  $(d/dt + \lambda)^{n-l}$  where  $\lambda$ , the filter *bandwidth* represents the rate of decay of the sliding function  $s(k) = \bar{C} \bar{x}(k)$  on the surface (*Jordanou and Surgenor, 1997b*). It can be chosen according to the desired decay speed of the system on the surface. Transformed to the original states, one gets  $s(k) = \bar{C} T^{-1} x(k)$  with the final sliding surface matrix  $C$  defined as  $\bar{C} T^{-1}$ . The main advantage of this procedure is the simplicity of its implementation. The disadvantage is that it limits the flexibility of the sliding surface design.

#### 4.2.1c Pole Placement Method

A novel technique considers the transformed system with  $\bar{x}$ -states from  $x(k)=T \bar{x}(k)$  as:

$$\begin{aligned} \bar{x}(k+1) &= \bar{\Phi} \bar{x}(k) + \bar{\Gamma} u(k) \\ s(k) &= \bar{C} \bar{x}(k) \end{aligned} \quad (4.26)$$

where  $\bar{\Phi}$  and  $\bar{\Gamma}$  are the open loop system matrices in canonical form and the overall system has the same dynamic behavior with the original system with the  $x$ -states. The sliding function  $s(k)$  is a function of the new state vector  $\bar{x}(k)$ .

During pure sliding it is assumed that the value of the sliding function remains the same, i.e.  $s(k)=s(k+1)=s(k+2)\dots$  If one sets  $s(k+1)=s(k)$ , then  $\bar{C} \bar{x}(k+1)=\bar{C} \bar{x}(k)$ . Replacing  $\bar{x}(k+1)$  by Eq. 4.26 and solving for the control signal, one can obtain the *equivalent control action*,  $u_{eq}$  (same context as  $u_{eq}$  for continuous SLM as in Eq. 3.9) which is responsible for maintaining the value of the sliding function *constant* once

the surface is reached; in other words, it keeps the system on the sliding surface at all subsequent times. The equivalent control action can be shown as:

$$u_{eq}(k) = -(\bar{C} \bar{\Gamma})^{-1} \bar{C}(\bar{\Phi} - I) \bar{x}(k) \quad (4.27)$$

If the equivalent control action is replaced in the state equation, one can obtain a state equation for the closed loop system dynamics during pure sliding:

$$\bar{x}(k+1) = [\bar{\Phi} - \bar{\Gamma}(\bar{C} \bar{\Gamma})^{-1} \bar{C}(\bar{\Phi} - I)] \bar{x}(k) \quad (4.28)$$

where  $\Phi_c = [\bar{\Phi} - \bar{\Gamma}(\bar{C} \bar{\Gamma})^{-1} \bar{C}(\bar{\Phi} - I)]$  and simplifies Eq. 4.28 to  $\bar{x}(k+1) = \Phi_c \bar{x}(k)$ .

A few observations can be made for the system under pure sliding. First, no additional control action is required. Since the dynamic response under sliding is unaffected by  $\bar{\Gamma}$ , or the range space of  $\bar{\Gamma}$ ,  $\mathcal{R}(\bar{\Gamma})$ , then ideal sliding occurs only in the null space of  $\bar{C}$ ,  $\mathcal{N}(\bar{C})$ , under the assumption that  $\mathcal{R}(\bar{\Gamma})$  and  $\mathcal{N}(\bar{C})$  are purely complementary subspaces. Therefore, the motion of the system is only dependent on  $\bar{C}$ . The control signal only drives the system to the sliding subspace and maintains it there. Second, convergence of the state vector is ensured by a suitable choice of the feedback matrix  $\Phi_c$ , which in turn constitutes  $\bar{C}$  as the only tuning parameter for the system dynamics under sliding. Some procedures for determining the sliding surface have already been presented.

The closed loop dynamics have been shown to be a direct function of the state canonical state matrices and the sliding surface matrix (Eq. 4.3 and 4.28). The characteristic equation for the discrete system under sliding can be found if one considers the solutions of the following:

$$\det(zI - \Phi_c) = 0 \quad (4.29)$$

where  $z$  denotes the argument of the  $z$ -transform in discrete domain. The solution for a general characteristic equation  $z^n + \alpha_1 z^{n-1} + \dots + \alpha_{n-1} = 0$  gives a set of solutions for  $z$ . An absolute condition for stability of this discrete system would be that all roots have a modulus less than unity, a condition which corresponds to all roots be negative for

stability of a continuous system. If the coefficients  $\alpha_i$  can be selected, then pole-placement on the z-domain is achievable.

The general solution of an  $n^{th}$  order system can be very involved. The following section describes the pole placement design approach for a 3<sup>rd</sup> order system. Specifically, a continuous state space model of a pneumatic positioner is used with the state matrices defined as:

$$A = \begin{bmatrix} 0 & 1 & 0 \\ 0 & -8 & 5.7 \cdot 10^{-3} \\ 0 & -26430 & 1 \end{bmatrix}, B = \begin{bmatrix} 0 \\ 0 \\ 42666 \end{bmatrix} \Rightarrow \Phi = \begin{bmatrix} 1 & 0.01 & 0 \\ 0 & 0.92 & 5.7 \cdot 10^{-3} \\ 0 & -246.5 & 1 \end{bmatrix}, \Gamma = \begin{bmatrix} 0 \\ 0 \\ 426.6 \end{bmatrix} \quad (4.30)$$

The discretised matrices  $\Phi$  and  $\Gamma$  were obtained assuming a sampling time of  $0.01 \text{ sec}$  (Jordanou and Surgenor, 1997b).

The canonical form for the discrete system is then obtained using the procedure described earlier and is found to be:

$$\bar{\Phi} = \begin{bmatrix} 0 & 1 & 0 \\ 0 & 0 & 1 \\ 0.9 & -2.8 & 2.9 \end{bmatrix}, \bar{\Gamma} = \begin{bmatrix} 0 \\ 0 \\ 1 \end{bmatrix} \quad (4.31)$$

A general sliding surface for an  $n^{th}$  order system has  $[c_1 \ c_2 \ c_3 \ \dots \ c_n]$ . It is quite common to normalize the sliding surface matrix to  $c_n$ , since the solution of the characteristic equation is unaffected. Therefore, the sliding surface for the 3<sup>rd</sup> order pneumatic system has:

$$\bar{C} = [c_1 \ c_2 \ 1] \quad (4.32)$$

The closed loop dynamics during sliding were given earlier (Eq. 4.28) as  $\bar{x}(k+1) = \Phi_c \bar{x}(k)$  with  $\Phi_c$  as a function of the canonical state matrices  $\bar{\Phi}$  and  $\bar{\Gamma}$  and the sliding surface matrix  $\bar{C}$ . For the system at hand,  $\Phi_c$  reduces to:

$$\Phi_c = \begin{bmatrix} 0 & 1 & 0 \\ 0 & 0 & 1 \\ c_1 & c_2 - c_1 & 1 - c_2 \end{bmatrix} \quad (4.33)$$

This is an important result since it demonstrates that the closed loop behavior of the system during sliding is only **subject** to the sliding surface and **not** the system itself. It can also be seen that  $\Phi_c$  for a general  $n^{th}$  order system simplifies to canonical form with the sliding surface coefficients composing the last row.

The characteristic equation for the system under sliding (Eq. 4.33) can then be shown as:

$$z^3 + (c_2 - 1)z^2 + (c_1 - c_2)z - c_1 = 0 \quad (4.34)$$

If underdamping is required in the closed loop response of the system, the solution should have a pair of complex roots. In this context, the general solution to any 3<sup>rd</sup> order system can be given as:

$$(z - p - iq)(z - p + iq)(z - \alpha) = 0 \quad (4.35)$$

with the restriction that all roots have a modulus less than *unity* for stability. Note that  $p, q$  and  $\alpha$  are real, non-zero numbers. If the complex pair of roots are the dominant roots of the system, then the closed loop system behavior can be approximated as a 2<sup>nd</sup> order system. This can be done by setting  $\alpha = 1$ . If Eq. 4.34 is divided by  $z - 1$ , then the resulting 2<sup>nd</sup> order polynomial defines the dynamic performance of the 3<sup>rd</sup> order system as a 2<sup>nd</sup> order sliding surface or trajectory.

#### 4.2.1d Pole Placement for a Pure Second Order System

A continuous second order transfer function  $G(s)$  has a pair of complex roots  $s_{1,2}$ :

$$G(s) = \frac{\omega_n^2}{s^2 + 2\zeta\omega_n s + \omega_n^2} \quad \text{with } s_{1,2} = -\zeta\omega_n \pm i\omega_n\sqrt{1 - \zeta^2} \quad (4.36)$$

where  $s$  denotes the Laplace transform in the continuous domain and should not be mistaken with the sliding function variable used in other sections of this chapter. In

the discrete domain, where the z-transform  $z=e^{sh}$  and with  $h$  as the sampling time, the solutions for  $s_{1,2}$  correspond to:

$$z_{1,2} = e^{-\zeta\omega_n h} \angle \pm \omega_n h \sqrt{1 - \zeta^2} \quad (4.37)$$

which can be equated to polar  $z_{1,2}=r\angle\pm\theta$ , with  $r = e^{-\zeta\omega_n h}$  and  $\theta = \omega_n h \sqrt{1 - \zeta^2}$ . By taking the ratio of  $r$  to  $\theta$  and rearranging, the damping factor  $\zeta$  can be shown as:

$$\zeta = \frac{-\ln(r)}{\sqrt{\ln^2(r) + \theta^2}} \quad (4.38)$$

If one considers the time constant of the poles,  $\tau = 1/\zeta\omega_n$ , and assumes that the  $\pm 2\%$  settling time is  $4\tau$ , then the settling time for the 2<sup>nd</sup> order system can be shown to be:

$$t_s = \frac{-4h}{\ln(r)} \quad (4.39)$$

If Eqs.4.38 and 4.39 are rearranged for  $r$  and  $\theta$ , one can get:

$$r = e^{\frac{-4h}{t_s}} \quad \text{and} \quad \theta = \frac{4h}{\zeta t_s} \sqrt{1 - \zeta^2} \quad (4.40)$$

#### 4.2.1e Application to 3<sup>rd</sup> Order System

Eq. 4.35 is the general solution to Eq. 4.34 and can be expanded as:

$$z^3 + z^2(-2p-\alpha) + z(2p\alpha+p^2+q^2) + (-p^2\alpha - q^2\alpha) = 0 \quad (4.41)$$

Eq. 4.34 is the characteristic equation for the system under pure sliding. Its dynamics are a function of the normalised (with  $c_3=1$ ) sliding surface coefficients  $c_1$  and  $c_2$ . When the terms of Eq. 4.34 are compared to the terms of Eq. 4.41, then the following can be derived:

$$\begin{aligned} c_1 &= p^2+q^2 \\ c_2 &= -2p \end{aligned} \quad (4.42)$$

The dominant 2<sup>nd</sup> order polar roots  $z_{1,2}=p\pm iq$  can be shown in terms of the polar coordinates as  $p=r\cos\theta$  and  $q=r\sin\theta$ . Given  $r$  and  $\theta$  in terms of the desired settling time and damping (Eq. 4.40) and then substituting into Eq. 4.42, it can be shown that

the sliding surface coefficients of  $\bar{C} = [c_1 \ c_2 \ 1]$  for a desired closed loop performance under sliding are:

$$\begin{aligned} c_1 &= e^{\frac{-\eta h}{t_s}} \\ c_2 &= -2e^{\frac{-\eta h}{t_s}} \cos\left(\frac{4h}{\zeta t_s} \sqrt{1-\zeta^2}\right) \end{aligned} \quad (4.43)$$

Once the sliding surface has been defined with the use of a canonical system transformation as  $C = \bar{C}T^{-1}$ , it can be substituted back into the original state space model.

### 4.3 Switching Laws for DSLM

The DSLM control law given as Eq. 4.27 is incomplete, as strictly speaking the control law for a sliding mode controller is composed of a linear part ( $F_{eq} x(k)$ ) and a nonlinear part ( $F_{sw} x(k)$ ). Or in other words the design of the sliding surface for  $F_{eq}$  does not solely determine the performance. The complete DSLM control law is:

$$u(k) = F_{eq} x(k) + F_{sw} x(k) \quad (4.44)$$

The relative size of the two parts can determine the nature of the response of the controller when used with systems with varying degrees of uncertainty. The linear control part, or equivalent control law, is generated from a linear model of the system and the sliding surface design. It acts to prevent the system from escaping from the surface, once on it. It has been shown that the equivalent control law  $F_{eq}$  is the control part responsible to keep  $s(k+1)=s(k)$ . This condition is necessary but not sufficient to ensure system convergence.

The nonlinear control law, or sliding control law, directs the system states towards the sliding surface. The size of the switching gain depends on the desired rate of approach to the sliding surface and the magnitude of model inaccuracies and disturbances, as will be shown.

Consider the discrete Lyapunov's function  $V(k) = \frac{1}{2} s^2(k)$  with  $s(k) = Cx(k)$ . A necessary condition for convergence, or stability is that  $V(k+1) < V(k)$ . In other words,  $s^2(k+1) < s^2(k)$  which can be simplified to  $|s(k+1)| < |s(k)|$ . The sliding function difference can be defined as  $\Delta s(k+1) = s(k+1) - s(k)$  where  $s(k+1) = Cx(k+1)$ . It can then be shown that the convergence condition can be rewritten as:

$$s(k)\Delta s(k+1) < -\frac{1}{2} \Delta s^2(k+1) \quad (4.45)$$

The sliding function difference  $\Delta s(k+1)$  can also be given in terms of  $\Phi, \Gamma, C$  if one substitutes the discrete state space equation and sliding function shown as Eq. 4.10 and 4.11 into  $s(k+1) = Cx(k+1)$ :

$$\Delta s(k+1) = C(\Gamma u(k) + (\Phi - I)x(k)) \quad (4.46)$$

If  $F_{eq}$ , shown as Eq. 4.27 is substituted in Eq. 4.44 and rearranged, then the sliding function difference can be shown as:

$$\Delta s(k+1) = C\Gamma F_{sw}x(k) \quad (4.47)$$

where  $F_{sw}$  is a  $l \times n$  matrix with elements  $f_j$  such that  $|f_j^-| = |f_j^+| = K_s$ . The stability condition can then be written as:

$$s(k)C\Gamma F_{sw}x(k) < -\frac{1}{2}(C\Gamma)^2(F_{sw}x(k))^2 \quad (4.48)$$

if one realizes that  $C\Gamma$  and  $F_{sw}x(k)$  are scalars. In fact:

$$F_{sw}x(k) = \sum_{j=1}^n f_j x_j(k) \quad (4.49)$$

The final switching conditions have been shown per state to be:

$$\begin{aligned} \text{if } C\Gamma s(k)x_j(k) < -\delta_j & \Rightarrow f_j = K_s \\ \text{if } |C\Gamma s(k)x_j(k)| \leq |\delta_j| & \Rightarrow f_j = 0 \\ \text{if } C\Gamma s(k)x_j(k) > \delta_j & \Rightarrow f_j = -K_s \end{aligned} \quad (4.50)$$

where  $\delta_j(k)$  can be found as:

$$\delta_j(k) = \frac{1}{2} K_s (C\Gamma)^2 |x_j(k)| \left| \sum_{j=1}^n x_j(k) \right| \quad (4.51)$$

The overall settling time  $t_r$  is composed of 2 parts, the reaching time shown earlier as  $t_r$  and the sliding settling time,  $t_s$ . With the realization that the dominant component of the overall settling time is the sliding settling time, one can then design the DSLM according to  $t_s$ .



#### 4.4 Sliding Gain

*Slotine's* original work on Sliding Mode Control focused on the continuous implementation (*Slotine, 1991*). The procedure that is shown below presents some of the basic issues surrounding the sliding gain and can be extended to discrete systems.

By definition, the stability of a CSLM controller, or the condition for sliding convergence is given by (*Slotine, 1991*):

$$s\dot{s} < 0 \quad (4.52)$$

which can be also written as:

$$s\dot{s} \leq -\eta|s| \quad (4.53)$$

where  $\eta$  is a strictly positive constant that can be related to  $t_r$ , the so-called reaching time or the time the system requires to reach the sliding surface:

$$t_r = \frac{s(0)}{\eta} \quad (4.54)$$

For a general nonlinear system with  $x^{(n)} = f_n + u$ , where  $f_n$  and  $u$  denote plant dynamics and control input respectively, the amount of uncertainty or estimation error  $F_e$  is bounded by:

$$|\hat{f} - f_n| \leq F_e \quad (4.55)$$

where  $\hat{f}$  denotes the estimated plant dynamics.

A typical structure for the control law of CSLM (Eq. 3.9) has,

$$u = u_{eq} - K_s \text{sign}(s) \quad (4.56)$$

For a second order system ( $n=2$ ) the sliding surface can be defined by a series of coupled first-order filters as:

$$s = \left(\frac{d}{dt} + \lambda\right)^{n-1} \tilde{x} = \dot{\tilde{x}} + \lambda \tilde{x} \quad (4.57)$$

and the first derivative of the sliding function becomes:

$$\dot{s} = \ddot{\tilde{x}} - \ddot{x}_{set} + \lambda \dot{\tilde{x}} \quad (4.58)$$

The condition for sliding convergence shown in Eq. 4.40 then becomes:

$$s\dot{s} = (f_n - \hat{f})s - K_s |s| \quad (4.59)$$

which, when rearranged, provides the first sizing guideline for the sliding gain as:

$$K_s \geq F_e + \eta \quad (4.60)$$

Based on the above, the size of the sliding gain should be increased in the presence of large system uncertainties and/or a fast reaching time requirement. If there is uncertainty on the control gain of the nonlinear system  $x^{(n)} = f + bu$ , where the uncertainty  $b$  is bounded by  $b_{min} < b < b_{max}$ , then the gain margin  $\beta$  is defined as:

$$\beta = \sqrt{\frac{b_{max}}{b_{min}}} \quad (4.61)$$

Eq. 4.60 with the addition of the gain uncertainty changes to:

$$K_s \geq \beta(F_e + \eta) + (\beta - 1)|\hat{u}_{eq}| \quad (4.62)$$

In summary, in the case of CSLM, there is only one condition for sliding convergence or stability. The main conclusion is that the required size of the sliding gain increases with larger parametric uncertainty. The overall uncertainty originates from  $F_e$ , the estimation error in the nonlinear model and  $\beta$ , a measure of the gain margin. Furthermore, if a small reaching time is required, the size of  $K_s$  should be increased.

*Furuta (1990)* investigated the stability limits of the sliding gain for both CSLM and DSLM controllers. In discrete time, the state space has  $x(k+1) = \Phi x(k) + \Gamma u(k)$  and the sliding function has  $s(k) = Cx(k)$ . The control law has already been shown as  $u(k) = (F_{eq} + F_{sw})x(k)$  with the  $F_{eq}$  defined as  $F_{eq} = -(C\Gamma)^{-1}C(\Phi - I)$  (see Eq. 4.27).

In *Furuta's* DSLM, the sliding convergence is assured by enforcing the condition  $V(k+1) < V(k)$ , where  $V(k)$  defines the *Lyapunov's* function  $V(k) = \frac{1}{2}s^2(k)$ . The convergence condition can be shown as:

$$s(k)\Delta s_{k+1} < -\frac{1}{2}(\Delta s_{k+1})^2 \quad (4.63)$$

where  $\Delta s(k+1) = s(k+1) - s(k)$ . From Eq. 4.35 and with  $F_{sw} = [f_1 \ f_2 \ \dots \ f_n]$ , where  $|f_j^+| = |f_j^-| = K_s$ , the amplitude of  $K_s$  can be shown to be bounded by:

$$0 < K_s < \left| \frac{2}{C\Gamma \sum_{j=1}^n |t_{1j}|} \right| \quad (4.64)$$

where  $Ct_j=0 \ \forall j=2\dots n$  and  $Ct_1=1$ .

If some uncertainty exists, i.e.  $\Delta\Phi = \hat{\Phi} - \Phi$ , then  $\Delta\Phi = \Gamma D$ , where  $D=[d_1 \ d_2 \ \dots \ d_n]$  and  $d_j$  bounded by  $|d_j| < |\bar{d}|$ . The permissible range for the sliding gain, earlier defined by Eq. 4.34, is now changed to allow for the uncertainties  $|\bar{d}|$ :

$$\bar{d} < K_s < \left| \frac{2}{C\Gamma \sum_{j=1}^n |t_{1j}|} \right| - \bar{d} \quad (4.65)$$

In summary, *Furuta* generates a range for values of the sliding gain that ensure stability and convergence. The range for DSLM, much as in the case of CSLM depends on the parametric uncertainties and also on the sliding surface design, which indirectly links to the time domain performance requirements such as the settling time.

*Pieper and Surgenor (1992)* present a switching function that is equivalent in form to the one presented in *Furuta (1990)*. The authors considered both the *pseudo*-DSLM (discrete implementation of CSLM) and *true*-DSLM (discrete model and controller) and derived bounds for the sliding gain for both implementations. Bounds for the sliding gain are similar to the ones by *Furuta* where the bounds on the perturbation gain for discrete control are given as:

$$\bar{v} < K_s < \left| \frac{2}{C\Gamma} \right| - \bar{v} \quad (4.66)$$

Note also that *Pieper (1992)* considers, without loss of generality that Eq. 4.65 can

use  $\sum_{j=1}^n |t_{1j}| = 1$  for  $t_1 = [0 \ \dots \ 0 \ 1]^T$ .

In the case of the largest possible plant perturbation, the upper bound for the switching gain is reported as:

$$K_s = \left| \frac{I}{C\Gamma} \right| \quad (4.67)$$

In the case where a dynamic, as opposed to a static sliding gain is used, the maximal robust dynamic optimal switching gain is reported as:

$$K_s = \frac{|s(k)|}{4\|x(k)\|_1} \quad (4.68)$$

where  $\|x(k)\|_1 = \sum_{j=1}^n |x_j(k)|$ . In summary, *Pieper* generates upper bounds for a static and a dynamic sliding gain where plant uncertainties and time response requirements define the bounds.

*Hwang* (1992) investigated the permissible size of the sliding gain for a DSLM controller. The switching laws are similar to the ones used by *Furuta* (1990), but the sliding gain is a dynamic gain. The stability limits for the varying sliding gain as suggested by *Hwang* are reported as:

$$0 < K_s(k) < \frac{2|s(k)|}{\sum_{j=1}^n |x_j(k)|} \quad (4.69)$$

The gain  $K_s(k)$  is active if the following condition is satisfied:

$$|s(k)x_j(k)| > \frac{1}{2}|x_j(k)| \sum_{j=1}^n K_s(k)|x_{jj}(k)| \quad (4.70)$$

*Sarpturk et al* (1987) considered the stability limits for DSLM controllers. The sliding motion condition  $\Delta s(k+1)s(k) < 0$  is necessary, but is considered non-sufficient for the existence of sliding motion. The condition, shown earlier as  $|s(k+1)| < |s(k)|$ , which results in Eq. 4.45 is alternatively broken down in 2 parts and is presented as:

$$\{s(k+1)-s(k)\} \text{sign}(s(k)) < 0 \quad (4.71)$$

which is called the *sliding* condition necessary to assure quasi-sliding motion, and:

$$\{s(k+1)+s(k)\} \text{sign}(s(k)) \geq 0 \quad (4.72)$$

which is called the *convergence* condition necessary to prevent a divergent motion from occurring. The two conditions define upper and lower bounds for the control input, which is tightly linked to the sliding gain  $K_S$ . Hence, the upper and lower bounds for the sliding gain. The implemented sliding action has  $u(k)=u^+(k)$  for  $s(k)>0$  and  $u(k)=u^-(k)$  for  $s(k)<0$  and is similar to the traditional sliding action law as  $u(k)=K_S \text{sign}(s(k))$  dictates. Note though that  $u^+(k)$  and  $u^-(k)$  denote the upper and lower bounds for  $K_S$  respectively.

For sliding, a new function is defined for the input to the system:

$$L_S = C[I-\Phi] x(k) - C\Gamma u(k) \quad (4.73)$$

Using Eq. 4.71 and 4.73 a set of upper and lower bounds for the sliding gain are defined for sliding towards the sliding surface as:

$$\sup (C\Gamma u^+(k)) < \inf (L_S^+), \text{ where } L_S^+ \text{ is evaluated for } s(k) > 0 \quad (4.74)$$

and

$$\inf (C\Gamma u^-(k)) > \sup (L_S^-), \text{ where } L_S^- \text{ is evaluated for } s(k) < 0 \quad (4.75)$$

Definitions for the *infimum*<sup>1</sup> (*inf*) and *supremum*<sup>2</sup> (*sup*) functions are given below.

For convergence, a new function is defined for the input to the system:

$$L_C = -C[I+\Phi] x(k) - C\Gamma u(k) \quad (4.76)$$

Using Eq. 4.72 and 4.76 a set of upper and lower bounds for the sliding gain are defined for convergence on the sliding surface as:

---

<sup>1</sup> *inf*( $X$ )

Let  $A$  be an ordered set and  $X$  a subset of  $A$ . An element  $b$  is called a lower bound for the set  $X$  if every element in  $X$  is greater than or equal to  $b$ . If such a lower bound exists, the set  $X$  is called bounded below. Let  $A$  be an ordered set, and  $X$  a subset of  $A$ . An element  $b$  in  $A$  is called a greatest lower bound (or *infimum*) for  $X$  if  $b$  is a lower bound for  $X$  and there is no other lower bound  $b'$  for  $X$  that is greater than  $b$ . We write  $b = \inf(X)$ . By its definition, if a greatest lower bound exists, it is *unique*.

<sup>2</sup> *sup*( $X$ )

Let  $A$  be an ordered set and  $X$  a subset of  $A$ . An element  $b$  is called an upper bound for the set  $X$  if every element in  $X$  is less than or equal to  $b$ . If such an upper bound exists, the set  $X$  is called bounded above. Let  $A$  be an ordered set, and  $X$  a subset of  $A$ . An element  $b$  in  $A$  is called a least upper bound (or *supremum*) for  $X$  if  $b$  is an upper bound for  $X$  and there is no other upper bound  $b'$  for  $X$  that is less than  $b$ . We write  $b = \sup(X)$ . By its definition, if a least upper bound exists, it is *unique*.

$$\inf (C\Gamma u^+(k)) > \sup (L_c^+), \text{ where } L_c^+ \text{ is evaluated for } s(k) > 0 \quad (4.77)$$

and

$$\sup (C\Gamma u^-(k)) < \inf (L_s^+), \text{ where } L_s^- \text{ is evaluated for } s(k) < 0 \quad (4.78)$$

The above control structure is not useful for real time computations and *Sarpturk et al* considered a feedback control law of the form  $u(k) = -K(x,s) x(k)$  where the feedback control matrix contains the switching feedback gains as:

$$K_j(x,s) = \begin{cases} k_j^+; & s(k)x_j(k) > 0 \\ k_j^-; & s(k)x_j(k) < 0 \end{cases} \quad (4.79)$$

with the upper and lower bounds  $k_j^+$  and  $k_j^-$  computed by Eq. 4.71 and 4.72 and the feedback gains  $K_j(x,s)$  as computed using the hierarchy of controls methods of *Utkin (1977)*. The difference between the upper and lower bounds for the switching gains depend on the size of the disturbances and the sampling time. For small sampling periods, the bounds are driven apart and approach the bounds presented for CSLM, as the sampling period approaches zero. For large sampling periods, the lower and upper bounds move closer to each other. For a critical sampling period, no interval can be found between the upper and the lower bound for the gains which indicates marginal numerical stability. In conclusion, the lower bounds for the sliding gain are functions of the parameter variations and input disturbance bounds. The upper bounds appear to be mainly functions of the sampling period.

*Utkin (1977)* presents the control law in sliding mode as:

$$u = -\sum_{i=1}^{n-l} \psi_i x_i - \eta \text{sign}(s) \quad (4.80)$$

$$\psi_i = \begin{cases} \alpha_i & \text{if } x_i s > 0 \\ \beta_i & \text{if } x_i s < 0 \end{cases}$$

with  $\alpha_i$  and  $\beta_i$  as constant coefficients and  $\eta$  as a small positive constant. For a sliding plane to exist, a set of inequalities for  $\alpha_i$  and  $\beta_i$  need to be satisfied. These inequalities include the coefficients of the sliding surface. For a 3<sup>rd</sup> order system in phase canonic form, the sliding function is defined as:

$$s = c_1 x_1 + c_2 x_2 + x_3 \quad (4.81)$$

with the strictly positive sliding surface coefficients  $c_1$  and  $c_2$  given as  $c_1 = c_2^2$ . More importantly the switching elements  $\alpha_i, \beta_i$  are given as  $\alpha_i > -c_1 c_2$  and  $\beta_i < -c_1 c_2$  which constrains the choice of the parameters of the sliding surface and also restricts the variety of sliding modes. Furthermore, the choice of these switching elements is still open for investigation since the only restriction is that they do not violate the condition for existence of the sliding plane.

#### 4.4.1 Permissible Range for the Sliding Gain

The condition for sliding convergence was shown in Section 4.3 as  $|s(k+1)| < |s(k)|$ . It can be rewritten in terms of the rate of convergence,  $\xi$  as:

$$s(k+1) = \xi s(k) \quad (4.82)$$

where  $|\xi| < 1$  for convergence of the sliding function towards the sliding surface. The rate of convergence can be related to the reaching time  $t_r$ . Consider the exponential decay in continuous time:

$$y(t) = y_0 e^{-\frac{t}{\tau}} \quad (4.83)$$

where  $y_0$  denotes the initial condition for state  $y$  and  $\tau$  as the decay time constant. In discrete time notation, the decay can be written as:

$$y(k) = y_0 e^{-\frac{kh}{\tau}} \quad (4.84)$$

where  $h$  denotes the sampling time. If one considers the state change per single sampling time, then:

$$y(k+1) = y(k) e^{-\frac{h}{\tau}} \quad (4.85)$$

At four times the time constant, it is assumed that the steady state is reached. This time denotes the settling time, or in this case the reaching time and can be found by combining Eq. 4.82 and 4.84 so that:

$$\xi = e^{-\frac{4h}{\tau}} \quad (4.86)$$

The sliding function difference  $\Delta s(k+1)$  can be also written in terms of the rate of convergence as:

$$\begin{aligned} \Delta s(k+1) &= s(k+1) - s(k) \\ &= \xi s(k) - s(k) \\ &= s(k) (\xi - 1) \end{aligned} \quad (4.87)$$

For sliding convergence it was shown that  $\Delta s^2(k+1) < -2\Delta s(k+1)s(k)$  which when combined with Eq. 4.47 and substituted in Eq. 4.87 provides the following condition:

$$(f_1 x_1 + f_2 x_2 + \dots + f_n x_n)^2 < \frac{-2s^2(k)}{(CF)^2} \{\xi - 1\} \quad (4.88)$$



with  $f_1, f_2, \dots, f_n$  as the switching gains ( $\pm K_s$ ) for states  $x_1, x_2, \dots, x_n$  respectively. A new variable,  $\psi$  is defined as:

$$\psi_j = W_j \text{sign}(f_j) \quad (4.89)$$

where  $W_j$  denotes the state weight for state  $j$  and is a strictly positive constant. We can assume for now that the size of each of the state weights is the same, therefore  $W_j=1 \forall j=1..n$ . The switching gains can then be shown as:

$$f_j = \psi_j K_s \quad (4.90)$$

where  $K_s$  is now a strictly-positive, static gain since its direction, or sign is subject to  $\psi_j$ .

If Eq. 4.90 is substituted in Eq. 4.88, the convergence condition is modified to:

$$\left( K_s (\psi_1 x_1 + \psi_2 x_2 + \dots \psi_n x_n) \right)^2 < \frac{-2s^2(k)}{(C\Gamma)^2} \{ \xi - 1 \} \quad (4.91)$$

which when rearranged can be written as:

$$\left( \sum_{i=1}^n \psi_i x_i \right)^2 < \frac{2s^2(k)}{(C\Gamma)^2 K_s^2} \{ 1 - \xi \} \quad (4.92)$$

The right hand side of Eq. 4.92 is always positive, since  $\{1-\xi\}$  is positive. Therefore, the condition can be written in terms of the sliding gain as:

$$K_s < \frac{\inf(|s(k)|) \sqrt{2(1-\xi)}}{C\Gamma \sup \left( \left| \sum_{j=1}^n \psi_j x_j \right| \right)} \quad (4.93)$$

which defines the upper bound of the sliding gain for convergence stability.

For position control systems and assuming that initially the system is at steady state,

i.e.  $x_j=0 \forall j \neq 1$ , the  $\sum_{j=1}^n \psi_j x_j$  quantity that appears in Eq. 4.93 can be simplified to:

$$\sum_{j=1}^n \psi_j x_j = \psi_1 x_1(0) \quad (4.94)$$

At the instant the setpoint changes, the value of the sliding function is  $s(0)=c_1x_1(0)$ . Combining Eq. 4.93 and 4.94 gives the upper bound for  $K_S$  for a position control system as:

$$K_s^u = \frac{c_1 \sqrt{2(1-\xi)}}{CF} \quad (4.95)$$

#### 4.4.2 Varying Sliding Gain

Once the size of the sliding gain is selected and the switching laws are set to activate the sliding action in the region outside the inherent boundary layer of the DSLM controller, a few improvements can be made.

*Iordanou and Surgenor (1997a)* demonstrated that instead of implementing a zero-action within the boundary layer, it is more beneficial to maintain the on-off switching of the sliding action but with a magnitude that decreases upon approach to the surface.

Fig. 4.1a shows the original switching behavior for state  $x_j(k)$ . The switching action is *positive* or *zero* or *negative* depending on the relative size of the inherent DSLM boundary layer  $\delta_j$  and the state  $CFs(k)x_j(k)$  of Eq. 4.50 and 4.51. When this switching regime is implemented, the controller exhibits high controller action and sensitivity to the assigned value of  $K_S$ . To alleviate this high controller action, a varying sliding gain was incorporated in the sliding laws and is active only within the boundary layer. This varying sliding gain decreases the magnitude of the sliding action on approach to the sliding surface and can therefore prevent overshoot. The varying sliding gain inside the boundary layer has been shown to improve speed of response and decrease chattering. It also prevents a cyclic control signal which results in those cases where sensor noise causes DSLM to continuously switch between  $\pm$  values of  $K_S$ . Introducing a varying  $K_S$  within the DSLM's inherent boundary  $\delta_j(k)$  eliminates this effect.

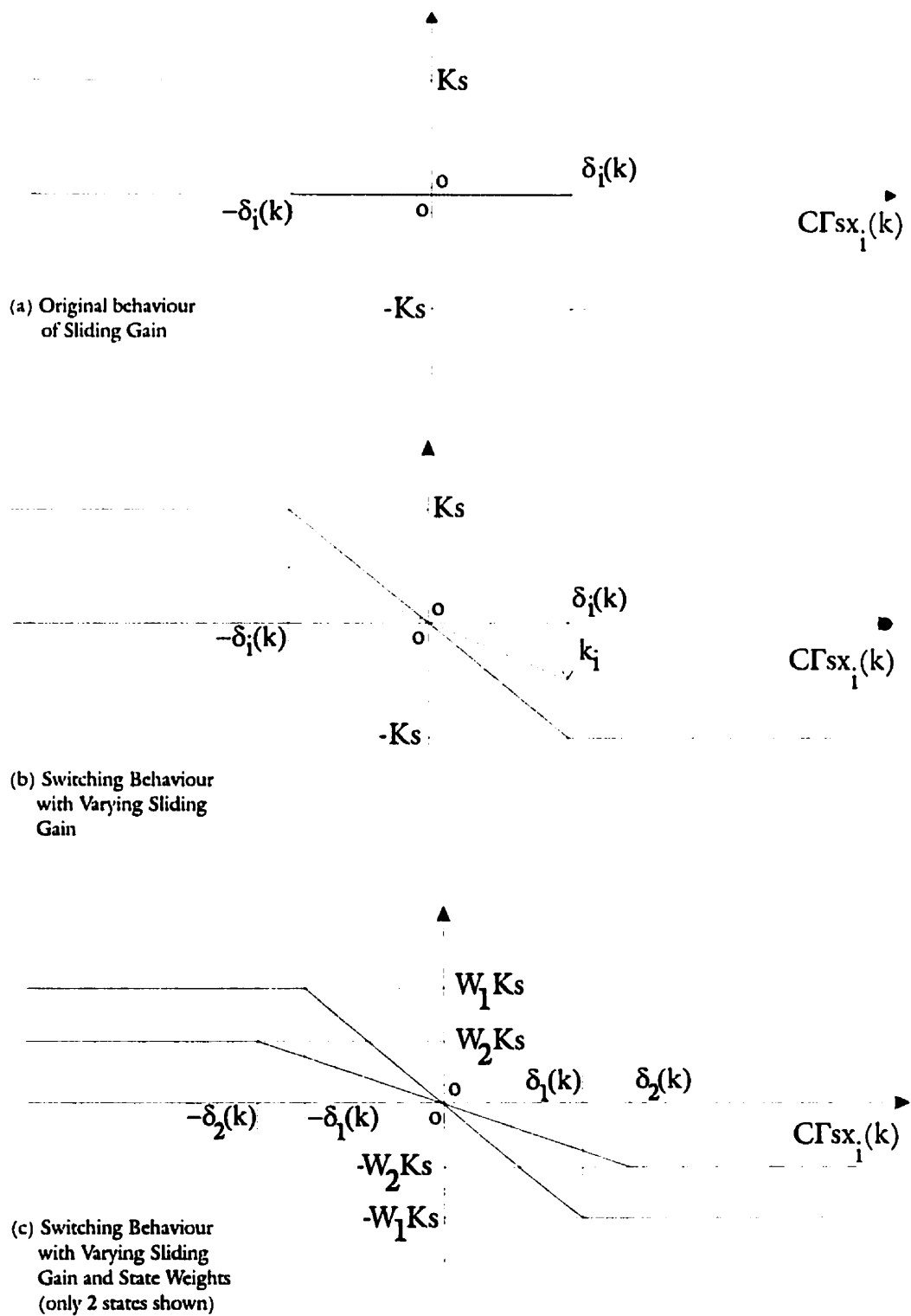


Figure 4.1: DSLM Boundary Layer Action Modifications

Fig. 4.1b shows the modified switching behavior for state  $x_j(k)$  where the zero action within the switching boundary is replaced by a proportional action, i.e., the size of the sliding gain is linearly proportional to  $C\Gamma s(k)x_j(k)$ . The magnitude of the slope of the line enclosed within  $\pm\delta_j$  is:

$$\text{slope} = \frac{K_s}{\delta_j} \quad (4.96)$$

The size of the switching action within the boundary layer can then linked to the magnitude of  $|s(k)x_j(k)|$ :

$$Ks_j^* = \frac{K_s}{\delta_j} |s(k)x_j(k)| \quad (4.97)$$

To allow  $Ks_j$  to attain positive or negative values as dictated by the sign of  $s(k)x_j(k)$ , the following modification can be made:

$$Ks_j = \frac{-K_s}{\delta_j} s(k)x_j(k) \text{sign}(s(k)x_j(k)) \quad (4.98)$$

If  $\delta_j$  is substituted into Eq. 4.98, then:

$$Ks_j = \frac{-K_s s(k)x_j(k)}{\frac{1}{2} C\Gamma K_s |x_j(k)| \sum_{j=1}^n |x_{jj}(k)|} \text{sign}(s(k)x_j(k)) \quad (4.99)$$

which can be rewritten as:

$$Ks_j = \frac{-K_s s(k)x_j(k) \text{sign}(s(k)) \text{sign}(x_j(k))}{\frac{1}{2} C\Gamma K_s |x_j(k)| \sum_{j=1}^n |x_{jj}(k)|} \quad (4.100)$$

With  $s(k) \text{sign}(s(k)) = |s(k)|$ , Eq. 4.100 can be simplified, and the size of the sliding gain within the boundary layer can be shown to be:

$$Ks_j = \frac{-2 |s(k)|}{C\Gamma \sum_{j=1}^n |x_{jj}(k)| + \varepsilon} \quad (4.101)$$

$Ks_j$  denotes the sliding gain within the boundary layer and  $\varepsilon$  represents a small *positive* constant which prevents numerical instability caused by *division by zero* when at rest or when the operation point is on the sliding surface. Note also that the structure of Eq. 4.101 is similar to the structure of Eq. 4.68 as proposed by Pieper (1992).

One should recognise that the implementation of a varying  $K_s$  can be performed by gradually increasing the slope of the sliding gain within the boundary  $\delta_j(k)$ . A slope of zero would imply the use of zero action within the boundary layer, just as shown in Fig. 4.1a. A maximum permissible slope would give a sliding gain as shown in Eq. 4.101. Between the zero- and maximum- sliding gain slope, a scaling factor on the size of the varying gain can be introduced, shown as a dotted line in Fig. 4.1b. Eq. 4.101 changes to:

$$Ks_j = k_j \frac{-2|s(k)|}{C\Gamma \sum_{j=1}^n |x_{jj}(k)| + \varepsilon} \quad (4.102)$$

where  $k_j$  denotes the varying sliding gain slope factor with a possible range of  $0 < k_j \leq 1$ .

The switching laws of Eq. 4.47 remain the same but  $K_s$  inside the boundary layer is given by Eq. 4.102. If one sets  $k_j = 1.0$ , then the switching laws become:

$$\begin{aligned} \text{if } C\Gamma s(k)x_j(k) < -\delta_j & \Rightarrow f_j = K_s \\ \text{if } |C\Gamma s(k)x_j(k)| \leq |\delta_j| & \Rightarrow f_j = \frac{-2|s(k)|}{C\Gamma \sum_{j=1}^n |x_{jj}(k)| + \varepsilon} \\ \text{if } C\Gamma s(k)x_j(k) > \delta_j & \Rightarrow f_j = -K_s \end{aligned} \quad (4.103)$$

Fig. 4.2 shows the simulated response of the pneumatic positioner with the DSLM switching laws as outlined in Eq. 4.50 and Eq. 4.103 as a dotted and dashed line respectively. The solid line response corresponds to the last modification of the switching laws for DSLM, which will be presented in the next section. The simulation model used is the same as the one presented in Chapter 2 for which the parameters are summarised in Appendix B. The setpoint change matches the one presented in Chapter 3. Comparing the original to the varying sliding gain response, one can see a considerable performance improvement due to the elimination of backlash in the control action which can cause sustained oscillations in the response. With the varying sliding gain inside the boundary layer, the action is made “continuous”. Therefore, the position setpoint tracking improves considerably.

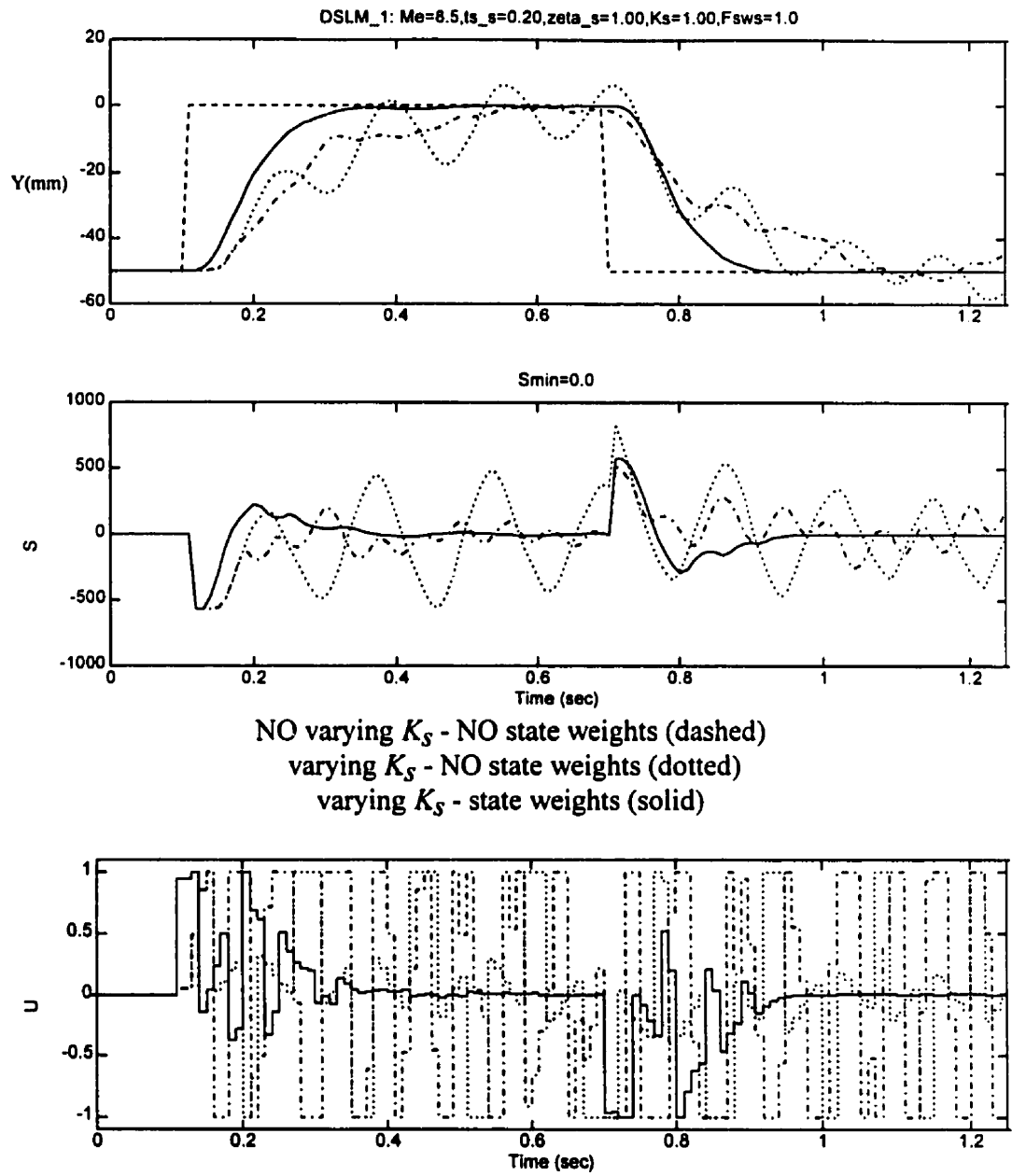


Figure 4.2: Effect of Boundary Layer Action in Simulation

#### 4.4.3 State Weights and the link to PVA gains

To further optimize the responses, *control weights* were assigned to the individual states. The switchings per state can be seen in Fig. 4.1c.

The switching laws of Eq. 4.103 are modified to:

$$\begin{aligned} \text{if } C\Gamma s(k)x_j(k) < -\delta_j & \Rightarrow f_j = W_j K_s \\ \text{if } |C\Gamma s(k)x_j(k)| \leq |\delta_j| & \Rightarrow f_j = W_j \frac{-2|s(k)|}{C\Gamma \sum_{j=1}^n |x_{jj}(k)| + \varepsilon} \\ \text{if } C\Gamma s(k)x_j(k) > \delta_j & \Rightarrow f_j = -W_j K_s \end{aligned} \quad (4.104)$$

with  $W_j$  is the *control weight* on state  $j$ .

In the work presented in *Iordanou and Surgenor (1997a)* the system under control was a four state cart-pendulum arrangement. The control task was to control the position of the cart and the angle of the pendulum, in both the hanging (vertically downwards) and the inverted (vertically upwards) configuration. The state weights for this system were selected under the premise that the main controlled variables were states 1 and 3, i.e. position of cart and pendulum angle. These states are called the primary states. The weights for states 2 and 4, i.e. cart velocity and pendulum angular velocity, which are obtained by direct differentiation of the sensor outputs and are subject to differentiation noise, are called the secondary states.

In the work presented in *Iordanou and Surgenor (1997b)* the state weights implemented on the pneumatic positioner matched the gains of a traditional PVA controller that was used on the same system.

The structure of a traditional PVA controller has been shown as:

$$u = K_p(x_{set} - x) - K_v\dot{x} - K_a\ddot{x} \quad (4.105)$$

with  $x$  as the controlled state (position) and  $x_{set}$  as the position setpoint.  $K_p$ ,  $K_v$  and  $K_a$  are the proportional, velocity and acceleration gains respectively. For application to pneumatic systems, it is generally acknowledged that both velocity and

acceleration are essential to ensure adequate performance (*Burrows, 1972*). The gains can be chosen so that the system can have a general predesigned performance with a specified settling time and overshoot. Typical gains for the PVA controller used for the system were  $K_p=17.0$ ,  $K_v=0.107$  and  $K_a=0.08$ .

This suggested that the choice of the weights can simply be an assignment of gains of a traditional linear controller of a PVA. These gains are selected for a *stable* performance of PVA and result to a critically damped response with a settling time similar to the one for which the sliding surface of DSLM was designed.

Since the DSLM control law has:

$$u(k) = F_{eq}x(k) + F_{sw}x(k) \quad (4.106)$$

with the nonlinear sliding action as  $F_{sw} = [f_1 \ f_2 \ \dots \ f_n]$  for  $|f_j| = |\dot{f}_j| = K_s$ . If one compares the control structure of the DSLM controller to the control structure of the PVA controller as shown in Eq. 4.105, then a relationship can be established between the size of the switching elements (per state) to the linear PVA gains. Normally, the primary element of the equivalent control vector, namely  $f_{eq1}$  is equal to zero. The reason is that the function of the equivalent control law is to prevent the system from escaping the sliding surface once on it, therefore it acts only on the higher states, namely velocity and acceleration if the controlled state is position. The general structure of the nonlinear switching action can be written as:

$$F_{sw} = [W_1 f_1 \ W_2 f_2 \ \dots \ W_n f_n] \quad (4.107)$$

with switching elements  $f_j$  as  $\pm K_s$ .

The relationship between the DSLM state weights (gains) and the PVA gains can then be presented as:

$$K_j = W_j K_s \quad (4.108)$$



with  $K_j$  as the PVA or linear state controller gains. For the system at hand, where the primary or controlled state is position and with velocity and acceleration composing the higher states, Eq. 4.108 can be written as:

$$W_1 \equiv K_p/K_s, \quad W_2 \equiv K_v/K_s, \quad W_3 \equiv K_a/K_s \quad (4.109)$$

The response of the pneumatic positioner with the addition of state weights was shown in Fig. 4.2 as a solid line (*Jordanou and Surgenor, 1997b*). Compared to the original (dotted line) and the varying sliding gain (dashed line) implementations, the performance of the controller with addition of state weights shows a very good setpoint tracking, little oscillations, good sliding function convergence and decreased control action. The setpoint requirements for a sliding settling time of *0.2 sec* and a damping factor of *1.0* are met. Furthermore, the pneumatic positioner response is linear despite the position and direction dependency which was demonstrated in Chapter 2.

#### 4.5 Simulation Results using the Pole Placement Technique

The following section will demonstrate some DSLM tuning and stability issues. The DSLM controller was implemented in simulation to control the position of the piston of an asymmetric pneumatic cylinder, similar to the one described in Chapter 2, technical specifications for which are listed in Appendix B. Unless specified otherwise, the benchmark conditions used in the simulations presented are as follows:

- The sliding surface is designed for a damping factor  $\zeta$  of *1.0* and a settling time  $t_s$  of *0.2 sec*.
- The nominal payload mass  $M_e$  is *8.5 kg*. Robustness tests were implemented with payloads of *23.0* and *2.2 kg*.
- The sampling time  $h$  is *0.01 sec*.
- The sliding gain  $K_s$  is *1.0 (normalised)*.
- The equivalent gain action,  $u_{eq}$  is active.
- The state weights are  $W_1=17 (K_p)$ ,  $W_2=0.107 (K_v)$  and  $W_3=0.08 (K_a)$ .

Important issues that will be addressed are:

- The effect of the sampling time on the system response (Fig. 4.3)
- The effect of the sliding gain on the system response (Fig. 4.4)
- The effect of the sliding gain and state weights (Fig. 4.5)
- The effect of  $u_{eq}$  (Fig. 4.6)
- The robustness (*different payloads*) of DSLM with  $h=10ms$  (Fig. 4.7)
- The effect of the sliding surface design parameters (Fig. 4.8 and Fig. 4.9)
- The effect of static friction on the system response (Fig. 4.10)
- The effect of noise and filtering on the system response (Fig. 4.11)

The design procedure of the sliding surface and other aspects of DSLM is shown in Fig. 4.12.

#### 4.5.1 Sampling Time Tolerance of DSLM

As already stated, the main advantage of DSLM over CSLM is the ability of DSLM to provide stable responses despite greatly increased sampling times. The greater robustness of DSLM with respect to sampling times is due to the fact that the switching action is derived from a discrete Lyapunov's function.

Fig. 4.3 illustrates the effect of the sampling time,  $h$ . The response of the controller with  $1\text{ ms}$ ,  $10\text{ ms}$  and  $50\text{ ms}$  sampling times is shown as a dotted, solid and dashed line, respectively. Note that the responses with  $1$  and  $10\text{ ms}$  appear very similar and satisfy the sliding surface performance requirements. Recall that the canonical system state space matrices are different for each time step (Eq. 4.43), which provide a different set of sliding surface coefficients and transformation matrices for each time step. Furthermore, the state weights have been shown as a function of the PVA gains and the sliding gain,  $K_s$  (Eq. 4.109). The sliding gain has been shown to have an upper bound linked to the rate of convergence  $\xi$  (Eq. 4.95), which in turns is a function of the sampling time (Eq. 4.86). Therefore, the state weights need to be adjusted for each sampling time.

As a test for the suitability of DSLM in the presence of large sampling times is the implementation with a sampling time of  $50\text{ ms}$  (dashed line). Despite the large steady state error, which appears when the positioner is required to move towards the end of the stroke, the response with  $h=50\text{ms}$  is stable throughout the whole test. Arguably, the positioner meets the setpoint requirements.

The ability of DSLM over CSLM to provide stable responses despite greatly increased sampling times, can be seen if one compares Fig. 4.3 (for DSLM) with the corresponding Fig. 3.3 (for CSLM). In Fig. 3.3, CSLM fails dramatically to maintain performance stability at  $50\text{ ms}$ . Though not shown, the linear PVA controller also fails under the  $50\text{ ms}$  stability test. DSLM, on the other hand, not only ensures stability but the response can be considered satisfactory.

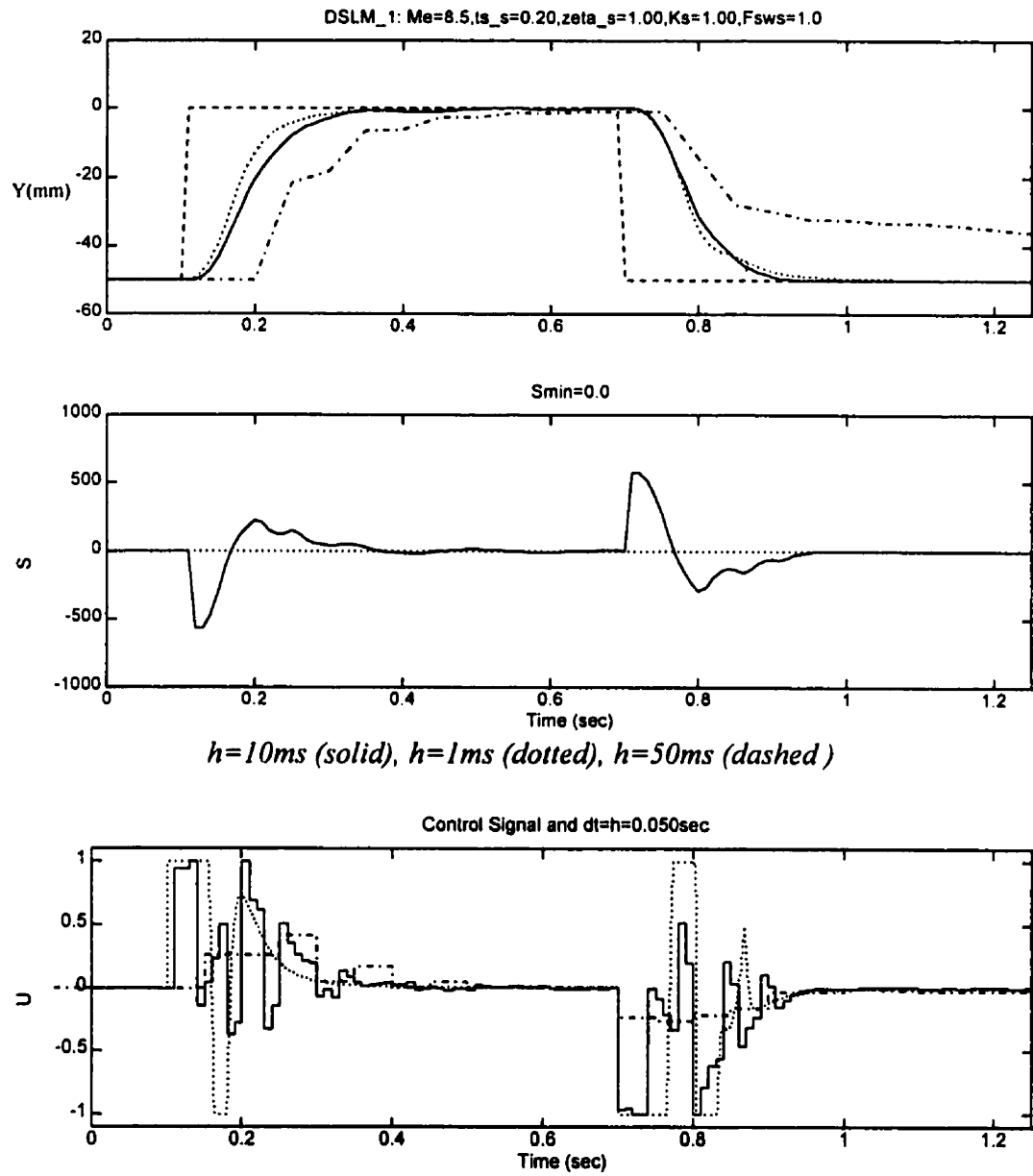


Figure 4.3: Effect of Sampling Time

#### 4.5.2 Effect of the Size of the Sliding Gain

The dominant part of the control law of DSLM is the switching action. Therefore, one would expect that the size of the sliding gain would greatly affect the performance of the system. Eq. 4.95 shows that the permissible maximum size for the sliding gain is inversely proportional to the size of the valve in use. A properly selected valve is one for which the size is selected to match the desired speed of response requirements; in other words, a settling time requirement. For a properly selected valve, one can use the size of its permissible input as the size of the sliding gain. If all is normalised, then the suitable size of the sliding gain is *1.0*.

Fig. 4.4 shows the effect of the size of the sliding gain  $K_S$  on the response of pneumatic positioner. The solid, dotted and dashed lines correspond to sliding gains of *1.0*, *0.5* and *0.25*, respectively. Since a *2.0 scfm* valve is used in simulation, these gains correspond to valve sizes of *2.0*, *1.0* and *0.5 scfm*, respectively. The *2 scfm* valve was selected to provide this speed of response. Clearly, the solid line response is the one that best matches the performance requirement. The performance of the system with sliding gains of *0.5* and *0.25* degrade slightly, but this is to be expected because of the inherent link between valve size and sliding gain. A smaller sliding gain would, in fact suggest a smaller valve. A smaller valve would cause a slower response, if the settling time requirement is too demanding.

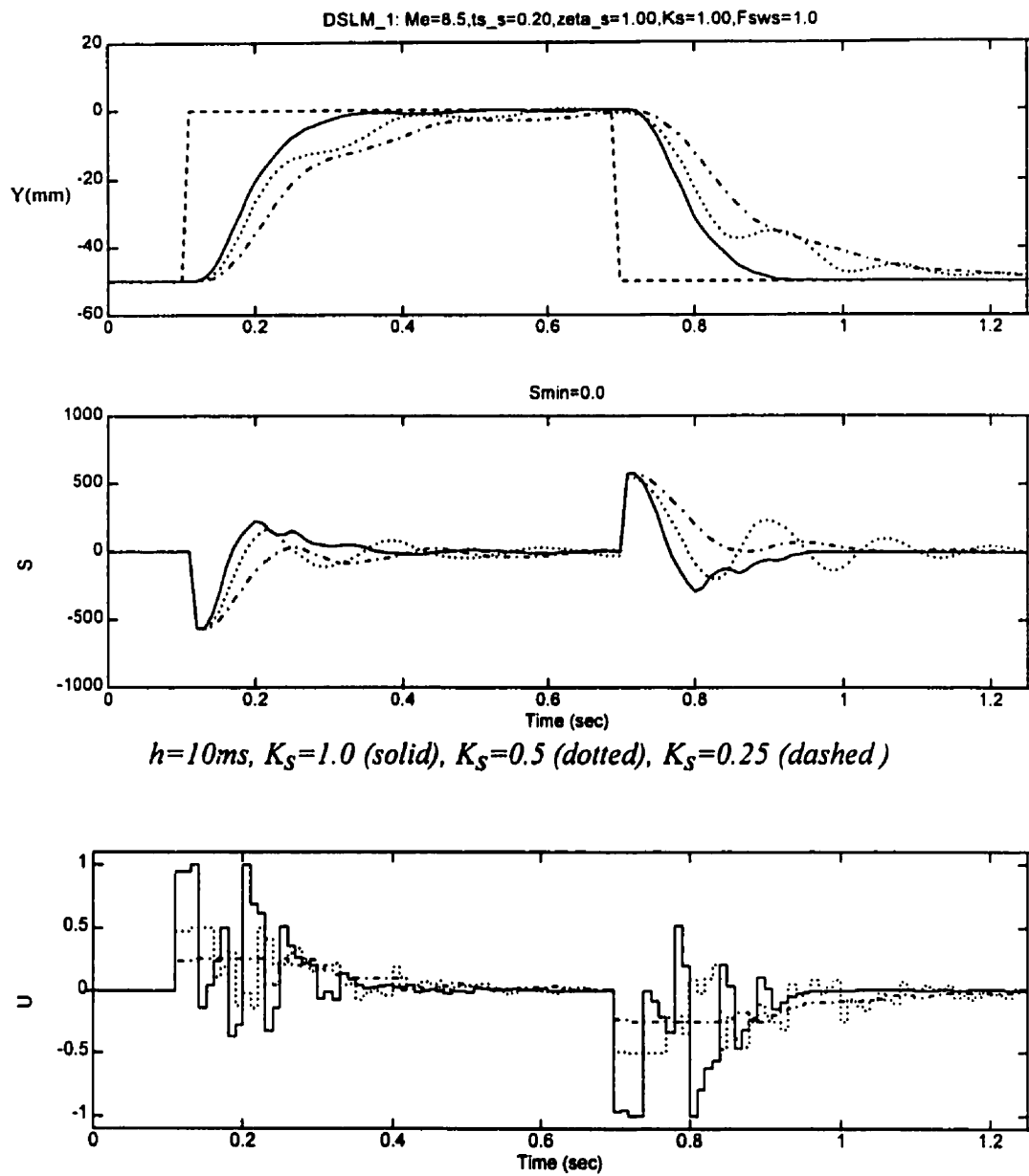


Figure 4.4: Effect of Size of Sliding Gain

### 4.5.3 Effect of the Size of the Sliding Gain and State Weights

The responses presented in Fig. 4.4 were generated with activated state weights. Fig. 4.5 shows the simulated pneumatic system response for 3 cases and demonstrates the effect of the state weights and the sliding gain.

The solid line response presents the case where state weights are inactive ( $W_1 = W_2 = W_3 = 1.0$ ). The switching laws were given in Eq. 4.101 and graphically, the controller's switching regime was shown in Fig. 4.1b. The significance of this response is that it illustrates that even with the aid of the varying sliding gain, the performance of DSLM is limited and does not meet the requirements set by the designed sliding surface unless state weights are used.

The dotted line response presents the case where the state weights are active and  $K_S=1.0$ . The use of state weights considerably improves the performance of the controller. The state weights are given values that correspond to gains of a suitable PVA, as shown in Eq. 4.103 and 4.110. For  $K_S=1$  (corresponds to the fully open valve) and using Eq. 4.107, the state weights are  $W_1=17.0$ ,  $K_V=0.107$  and  $K_A=0.08$ .

The dashed line response presents the case where the state weights are active but  $K_S=0.5$ . The state weights used are the same as appeared previously at  $K_S=1.0$ .

Fig. 4.5 demonstrates that the use of state weights and a varying sliding gain do not guarantee good performance unless a sliding gain that corresponds to the maximum opening possible for a suitable valve is used in conjunction. A suitable valve is one that provides the necessary air flow to match actuator speed requirements of a pneumatic cylinder.

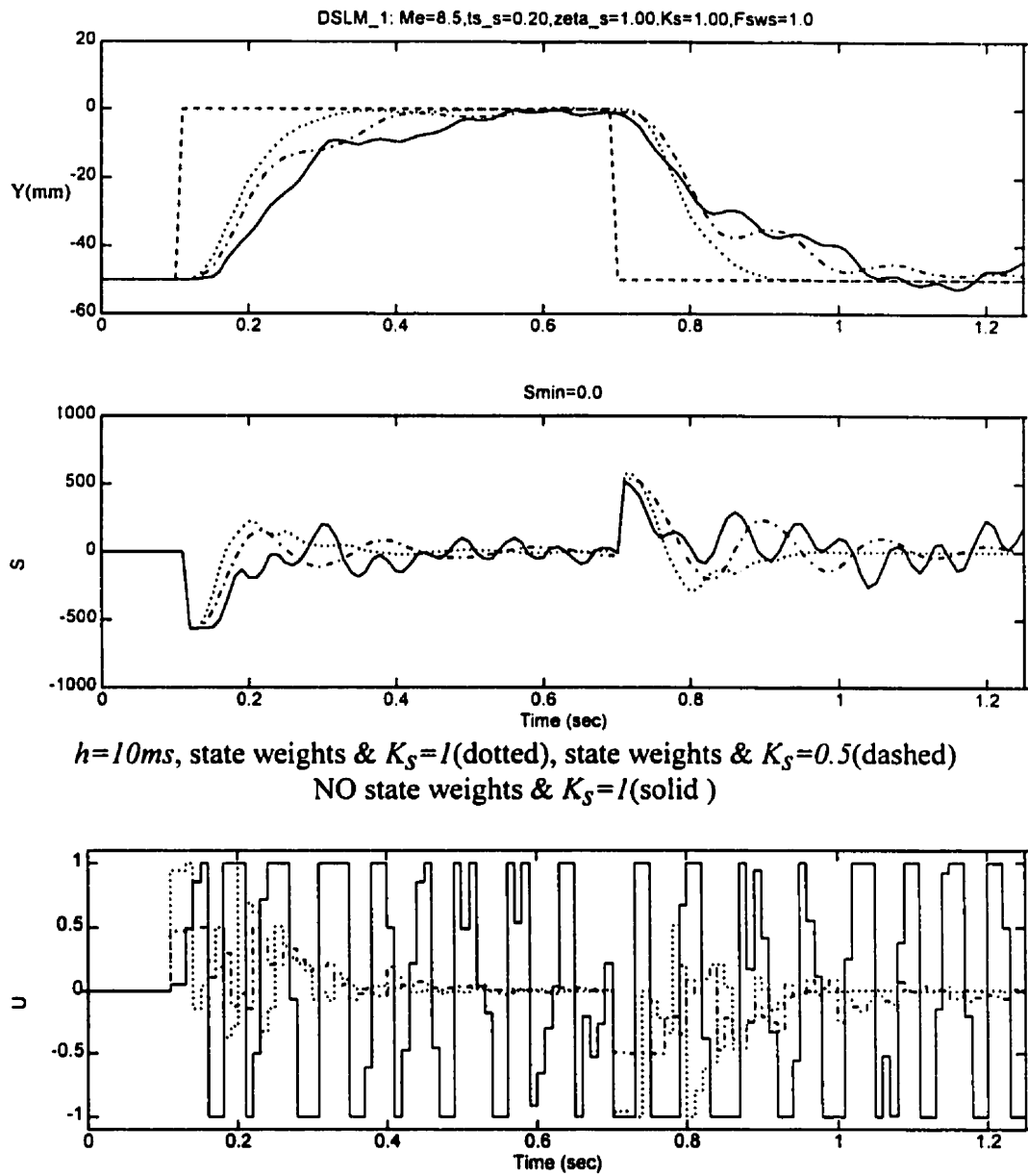


Figure 4.5: Effect of State Weights and Sliding Gain



#### 4.5.4 Sliding Versus Equivalent Control Actions

Fig. 4.6a shows the equivalent (dotted line) and sliding action (dashed line) contribution to the overall control law as was seen in Fig. 4.2. One first observes the smooth profile of the equivalent control action. It is a linear control action with velocity and acceleration components that are active once the system escapes the sliding surface. This is the reason why there is no equivalent action at the instant when the setpoint changes. To better observe this effect, Fig. 4.6b zooms into the first 0.3 sec of the overall test shown in Fig. 4.6a. At 0.10 sec, the position setpoint changes. At the next instant, i.e. at 0.11 sec, the switching action (dashed line) is energised. The pneumatic system requires a couple more time steps before it gets sufficiently charged, to initiate motion. This is due to the delay associated with air compressibility (charging the cylinder) and payload inertia. Once velocity and/or acceleration are detected (at 0.13 sec) and the system starts to move away from the sliding surface and the equivalent action (dotted line) is energised.

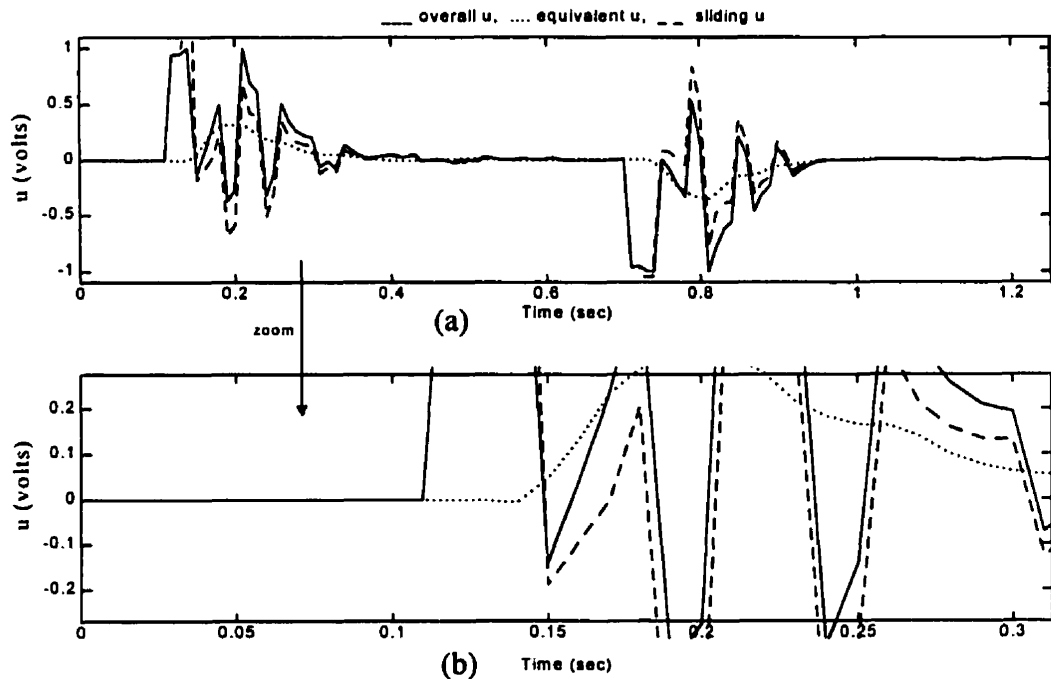


Figure 4.6: Sliding Versus Equivalent Control Action

#### 4.5.5 DSLM Robustness

Fig. 4.7 shows the simulated responses of the pneumatic positioner for a set of three payloads. The DSLM controller was designed for a payload of  $8.5\text{ kg}$  (*nominal* payload) which is shown as the dotted line, and for payloads of  $2.2\text{ kg}$  (*low* payload) and  $23.0\text{ kg}$  (*high* payload) which are shown as dashed and dotted lines, respectively. Despite the large model mismatch in both the low and high payload cases, the responses roughly meet the response requirements set for the nominal payload.

If one compares Fig. 4.7 for DSLM and Fig. 3.7 for CSLM, the robustness advantage of DSLM over CSLM for higher sampling times is in evidence. CSLM exhibited increased sensitivity and reaches marginal stability at the low payload robustness test, which can be explained if one realises that the low payload system has a smaller open loop time constant. CSLM therefore fails because of an insufficient sampling time. DSLM on the other hand, can still maintain stability with greater sampling times which is the reason why the responses of Fig. 4.7 are stable and fit the set of requirements.

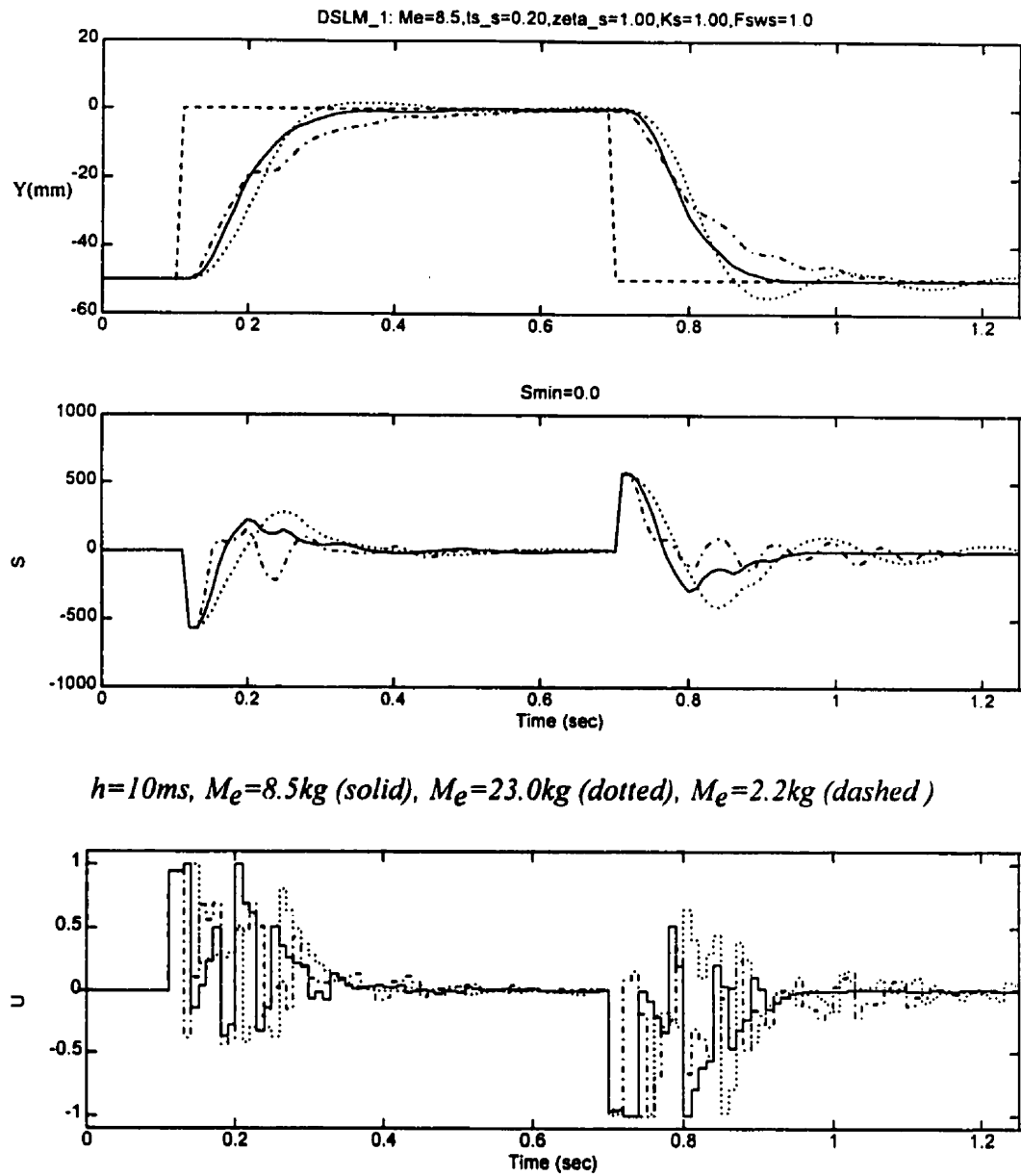


Figure 4.7: DSLM Robustness Test

#### 4.5.6 Sliding Surface Design Parameters

Fig. 4.8 shows the simulated response of the pneumatic positioner with the sliding surface designed for a settling time,  $t_s$  of  $0.2 \text{ sec}$  and for a set of three damping factors,  $\zeta$  of  $1.0$  (solid line),  $0.7$  (dotted line) and  $0.5$  (dashed line).

Fig. 4.9 shows the simulated response of the pneumatic positioner with the sliding surface designed for a settling time,  $t_s$  of  $0.3 \text{ sec}$  and for a set of three damping factors,  $\zeta$  of  $1.0$  (solid line),  $0.7$  (dotted line) and  $0.5$  (dashed line).

Despite the large sampling time of  $0.01 \text{ sec}$ , the controller is able to meet the design requirements in both Fig. 4.8 and 4.9. The roots of the 3<sup>rd</sup> order system under pure sliding had been selected using the pole-placement method and were designed for a dominant 2<sup>nd</sup> order response. The 3<sup>rd</sup> root was chosen as a fast 1<sup>st</sup> order dynamic with a time constant 10 times faster than the time constant of the 2<sup>nd</sup> order system.

It can be seen that despite the large sampling time, the requirements for settling time and damping have been fulfilled by the controller. Figures 3.9 and 3.10 show the respective responses using CSLM but the sampling time used was  $0.001 \text{ sec}$ . CSLM was unable to fully meet settling time and damping requirements with a sampling time of  $0.01 \text{ sec}$ .

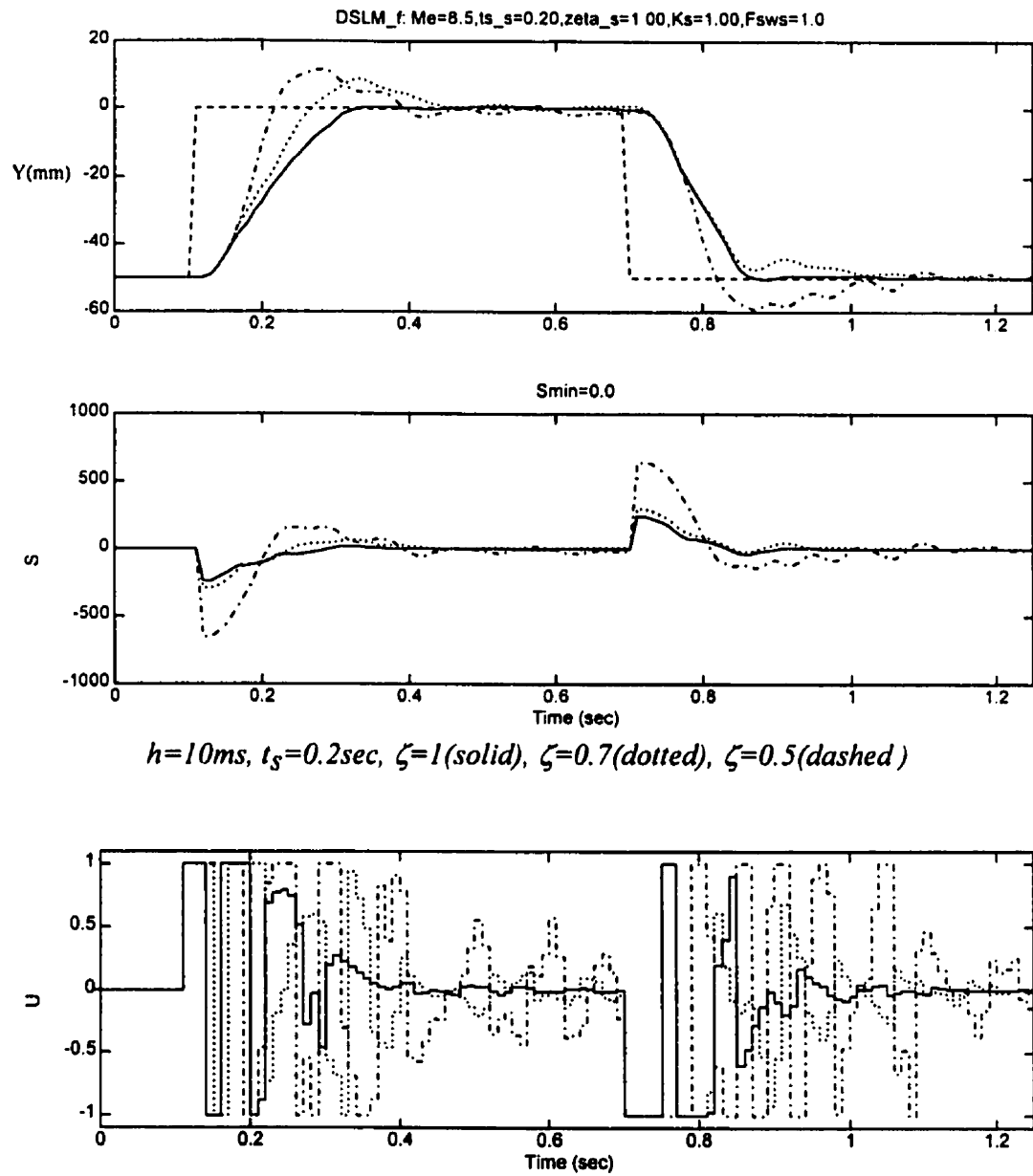


Figure 4.8: Sliding Surface Settling Time (0.2sec) and 3 Damping Factors

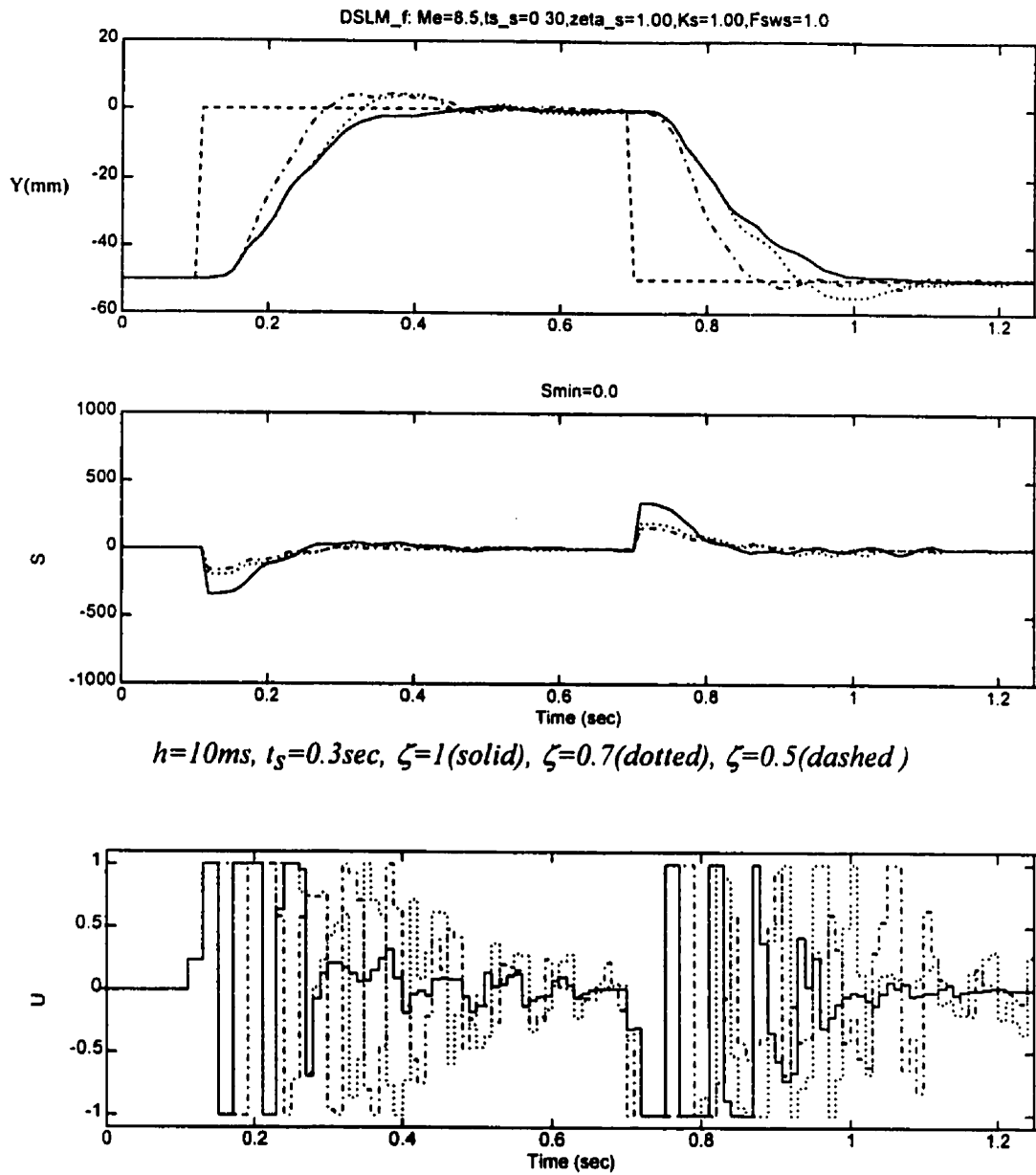


Figure 4.9: Sliding Surface Settling Time (0.3sec) and 3 Damping Factors

#### 4.5.7 Static Coulomb Friction Result

A static friction test was performed on the experimental setup. It was determined that the setup exhibited directional static coulomb friction coefficients. In simulation, the higher of the 2 directional static friction coefficients was used. The maximum static coulomb friction coefficient was determined to have  $F_{CS}=14N$ . An average static coulomb coefficient was determined to have  $F_{CS}=10N$ .

Fig. 4.10 demonstrates a gradual performance deterioration with increased static coulomb friction. The solid line represent the response of the system with no static coulomb friction,  $F_{CS}=0N$ . The dotted and dashed lines give the response of the system with  $F_{CS}=5N$  and  $F_{CS}=10N$ , respectively. The higher the static friction, the greater the likelihood of stiction which in closed-loop causes increased activity in the control action. The stick-slip phenomenon can be seen by the erratic position response.

One observes that, when Fig. 4.10 for DSLM is compared with the corresponding Fig. 3.11 for CSLM, that DSLM can handle static friction better than CSLM.

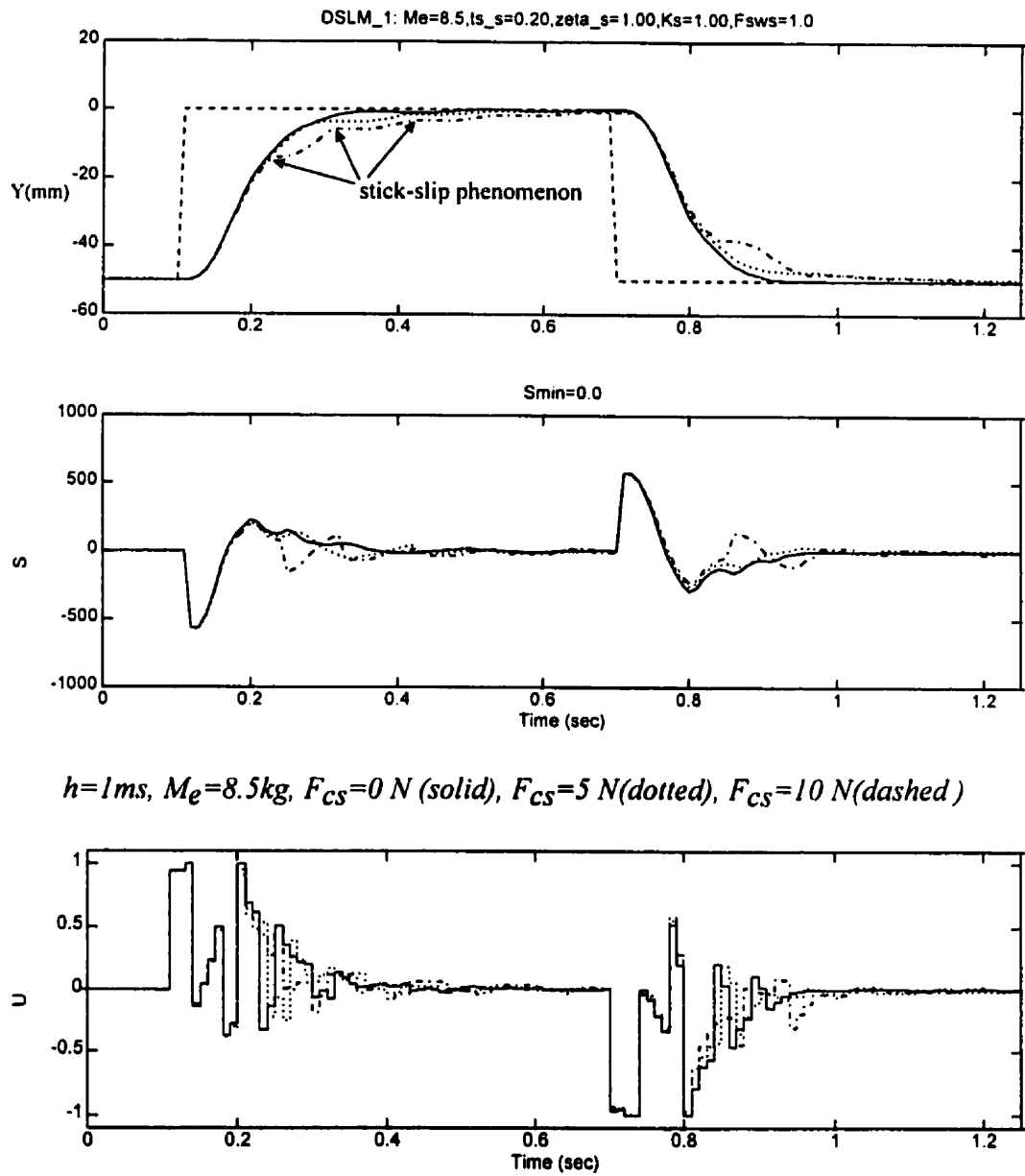


Figure 4.10: Static Friction Result ( $F_c=0\text{-}5\text{-}10\text{ N}$ )



#### **4.5.8 Effect of Sensor Noise and Filtering on DSLM**

Noise in the position, the sensed variable in the actual apparatus was determined by examining the datafiles obtained from open-loop experimental tests on the setup. It was determined that a  $\pm 0.5\%$  sensor noise was present in the recorded position when the control signal was kept constant. The  $\pm 0.5\%$  noise was of full scale with constant variance. In order to provide a conservative result, it was decided to use a value of  $\pm 1.0\%$  for the noise level in simulation. Fig. 4.11 shows in dashed lines the response of the system with no noise.

In order to show the effect of noise in simulation, the position as obtained by the nonlinear state space model was “corrupted” with a  $\pm 1.0\%$  white noise signal. The controller’s response is shown as a solid line and can be seen to degrade relative to the clean dashed line responses. The effect of noise can be better appreciated if one observes the velocity plot (recall that velocity is obtained by differentiation of the position signal). With the  $\pm 1.0\%$  position noise, velocity noise is amplified more than  $\pm 1.0\%$ . Acceleration noise is amplified even further. The use of a filter can decrease the effects of sensor noise, but not without a negative side effect. A lag can be seen in the dotted response of Fig. 4.11. This is due to a 2<sup>nd</sup> order Butterworth filter being added to filter the simulated noise with a cut-off frequency of  $15\text{ Hz}$ . The response is smooth again (compare solid and dashed lines), but with a  $0.1\text{ sec}$  lag.

If Fig. 4.11 for DSLM is compared with Fig. 3.12 for CSLM, one can see that both perform equally well when it comes to noise rejection.

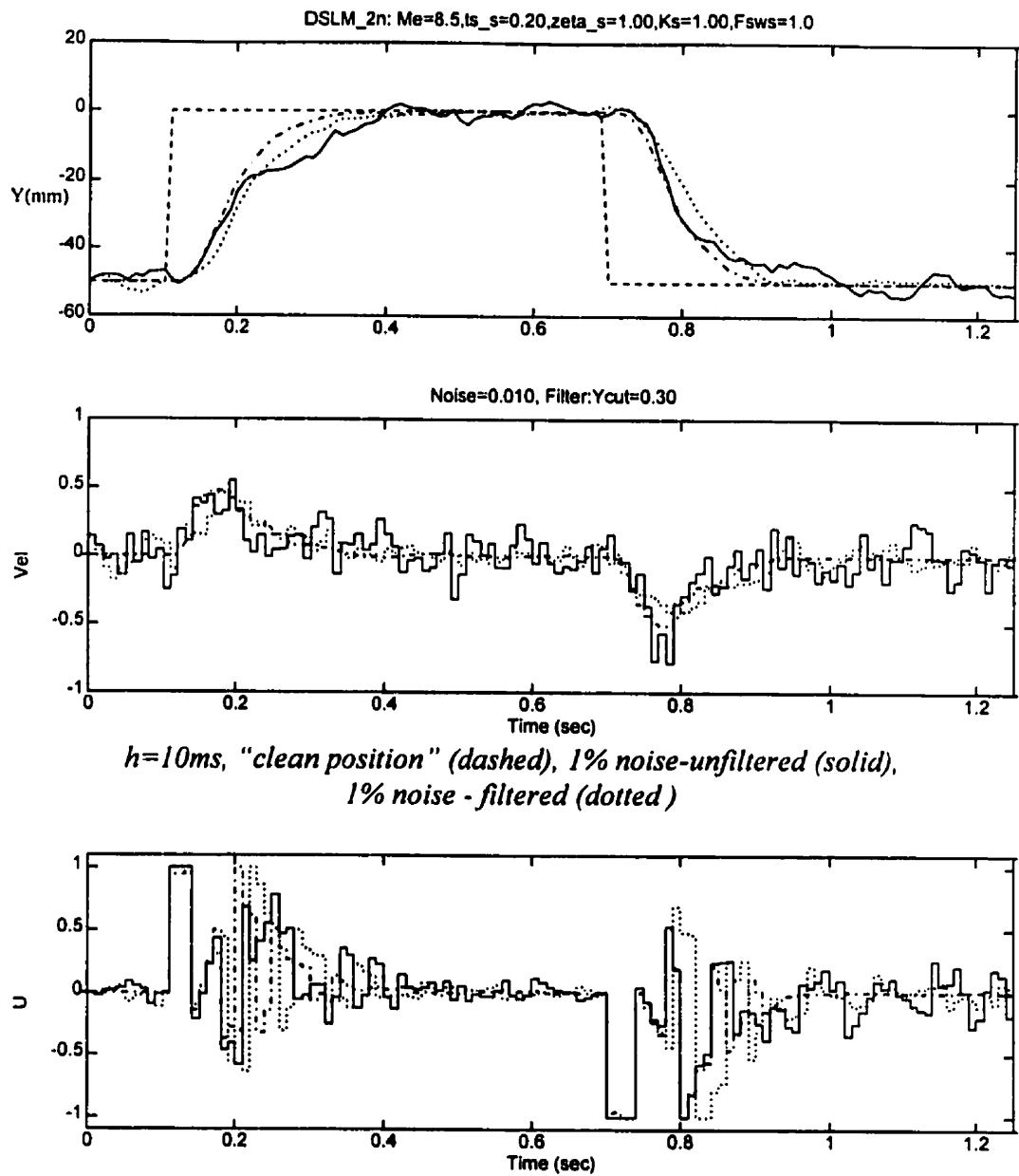


Figure 4.11: Noise and Filtering on DSLM

## 4.6 Summary

A number of papers on the subject of DSLM were reviewed and discussed in this chapter. The authors showed how a traditional DSLM is implemented. Some authors provided techniques for improving the existing algorithm with added features such as state estimators, varying sliding gain, state weights, filters, etc. Just as in CSLM, the design of the DSLM controller was broken in two main parts, the switching control laws and the design of the sliding surface. Some existing techniques for determination of the sliding surface were presented. These techniques were tested in simulation and evaluated. A novel pole-placement technique for designing the sliding surface of a general  $n^{th}$  order system, which then focused on a typical  $3^{rd}$  order pneumatic system, was shown. The technique enables the designer to select sliding surface coefficients which would result in more traditional time performance parameters such as settling time and maximum overshoot (or damping). Furthermore, a varying sliding gain and state weights were implemented to improve the performance of DSLM. These state weights have been linked to gains of a linear PVA controller.

Fig. 4.12 illustrates the general design guidelines for a DSLM controller. The procedure for generating the canonical system matrices and the transformation matrix for the discrete system is shown in the left column of the figure. The right column of the figure shows the procedure for the design of the sliding surface of the canonical discrete system. The two columns combined can generate the sliding surface matrix,  $C$  which is used in both the switching and the equivalent control action of DSLM.

The simulation responses with the pole placement technique for sliding surface design show good trajectory tracking and design flexibility. DSLM can be seen as a robust controller that is able to maintain stability and good performance even at higher sampling times. DSLM also exhibits good behavior in the presence of high static friction and sensor noise. Its main advantage over CSLM is its robustness at higher sampling times.

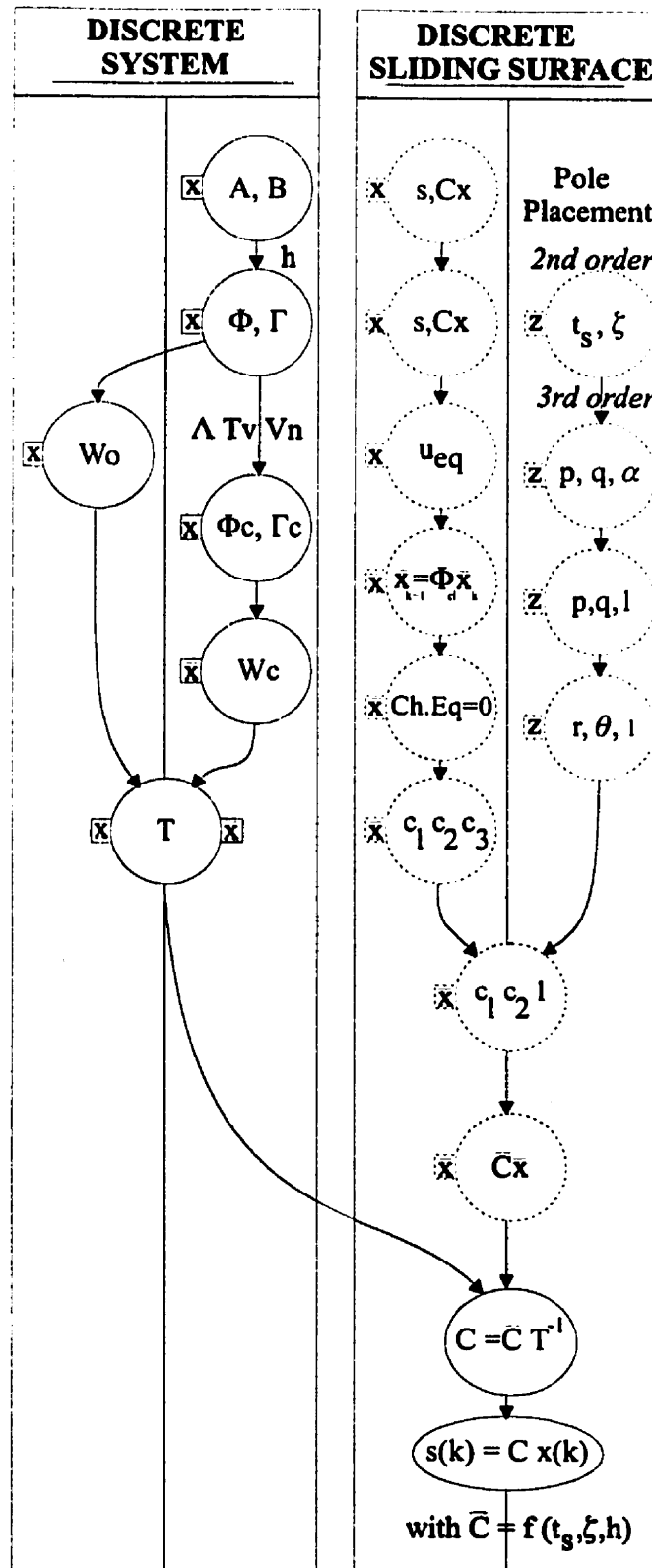


Figure 4.12: DSLM Design Procedure

## CHAPTER 5

### EXPERIMENTAL AND SIMULATION RESULTS

The chapter will present open loop results for the pneumatic system, which will then be used to validate model parameters in simulation. These model parameters include the static coulomb, dynamic coulomb and viscous forces and coefficients. The effective payload masses will also be determined.

The experimental setpoint profile is first selected. A typical *center-left-center-right-center* setpoint change is examined, from which the most demanding 2-step change window was selected. Next, a series of tests are performed to confirm the robustness of 3 controllers: the PVA, the CSLM and the DSLM. These tests evaluate the controllers under different scenarios: double bore - same stroke and double stroke - same bore. Finally, how the results relate to issues presented in Chapters 2, 3 and 4 will be highlighted.

#### 5.1 Experimental Setup

A schematic diagram of the experimental setup is shown in Fig. 5.1. The cylinder is connected to a payload which is free to move on a horizontal track and also moves a continuous belt. The amount of inertial load and "dead" load driven horizontally can be varied. The belt is elastic but pre-tensioned to provide a near rigid coupling to the inertia load. The position of the belt, and consequently that of the cylinder, is measured by a rotary potentiometer. The cylinder air pressures and supply pressures are also measured. An 80-386 microcomputer is used for control and data acquisition and is able to generate a sampling interval of *10 ms*. A *LABMASTER* data acquisition board has an accuracy of  $\pm 0.05\%$ . When combined with the accuracy of the rotary potentiometer, the position can be measured to within  $\pm 0.1 \text{ mm}$ . The velocity is obtained by differentiation of the position signal and subsequently filtered digitally with a second order Butterworth filter. The acceleration is obtained by differentiation of the velocity signal.

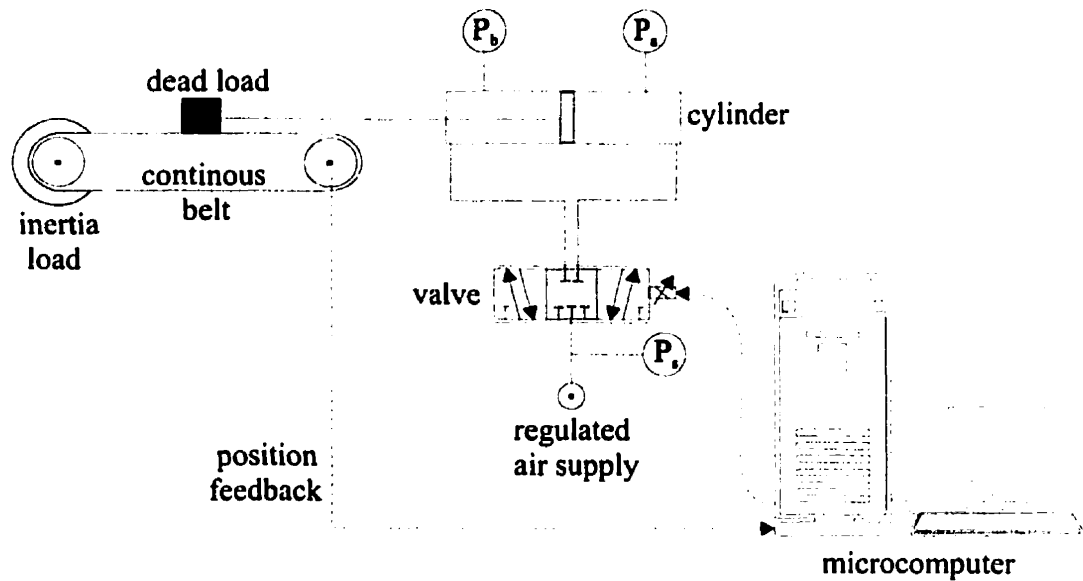


Figure 5.1 Experimental Apparatus

## 5.2 Valve Modeling

The valve used is a linear *HR-Textron* servovalve (part #27A10F-3D01) and is capable of supplying  $1.88 \text{ l/sec}$  ( $4 \text{ scfm}$ ) of air at a supply pressure of  $689.5 \text{ kPa}$  ( $100 \text{ psi}$ ). The valve is positioned by an electric servomotor via a mechanical eccentric and generates flows that are linearly proportional to the valve input. It is the same valve presented in simulation in Chapters 2, 3 and 4. Although designed as a hydraulic, the *HR-Textron* servovalve can be used for pneumatic systems. Internal leakage for pneumatic use is negligible. Another advantage of this valve is that there are no air quality restrictions. Therefore, the air supply does not have to be oil free or filtered. A slight overlap provides a small but measurable deadband on the order of  $\pm 2.5\%$  or  $\pm 0.1v$ . The fact that there is an overlap formulates a closed-center configuration and gives rise to certain dynamic characteristics described in Chapter 2. Technical specifications for the valve can be found in Appendix A.

Typically, the relationship between flow through an orifice and the orifice area is nonlinear. In most valves, there is a linear relationship between valve opening and

valve spool position. The control input to the valve is, in most cases, an electrical signal which activates the valve spool. If a linear relationship between the output flow and the control input to the valve spool is desired, one can either modify the valve opening area or modify the control input by use of an internal positioning circuit. The latter is the case for the *HR-Textron* valves. The control signal to the valve is fed through valve electronics, which linearize the relationship between output flow and the control signal.

In order to confirm the linearity of the *HR-Textron*, a test was performed. The control input to the valve was increased at discrete intervals while the flow was being monitored by use of flowmeters. A total of three flowmeters were used. Each had a different range and therefore a different sensitivity. The large-range flowmeter can read flows up to 3.77 l/sec (8 scfm), the mid-range can read up to 1.57 l/sec (200 scfh or 3.33 scfm) and the small-range flowmeter can read up to 0.39 l/sec (50 scfh or 0.833 scfm). All three flowmeters were required since for medium flows ( $< 0.47$  l/sec or  $< 1$  scfm), the peg of the large-range flowmeter was not responsive, and for small flows ( $< 0.23$  l/sec or  $< 0.5$  scfm) the peg of the mid-range flowmeter was not responsive. Table 5.1 gives the valve input and the resulting flows using the three flowmeters. The supply pressure was 620 kPa (90 psi).

Figure 5.1 shows the flow (scfm) through the valve as a function of the control input (volts). The large-dotted lines correspond to the large-range flowmeter (8 scfm), the solid lines correspond to the mid-range flowmeter (3.33 scfm), and the small-dotted lines correspond to the small-range flowmeter (0.833 scfm). A linear relationship between flow and control input can be seen and the valve supplies the specified rated flow of 4 scfm at the maximum input of  $\pm 5$  v.

HR-Textron input (v)	Q with 3.76 l/sec (8 scfm) units: l/min	Q with 3.76 l/sec (8 scfm) units: scfm	Q with 0.39 l/sec (50 scfh) units: l/min	Q with 0.39 l/sec (50 scfh) units: scfm	Q with 1.57 l/sec (200 scfh) units: l/min	Q with 1.57 l/sec (200 scfh) units: scfm
-5.00	-1.79	-3.80				
-4.50	-1.60	-3.38				
-4.00	-1.42	-3.00				
-3.50	-1.23	-2.61			-1.18	-2.50
-3.00	-1.06	-2.24			-1.02	-2.17
-2.50	-0.94	-2.00			-0.87	-1.83
-2.00	-0.76	-1.60			-0.71	-1.50
-1.50	-0.59	-1.25			-0.55	-1.17
-1.00					-0.47	-1.00
-0.50			-0.14	-0.30		
0.00	0.00	0.00	0.00	0.00	0.00	0.00
0.50			0.22	0.47		
1.00	0.52	1.10			0.50	1.05
1.50	0.67	1.42			0.63	1.33
2.00	0.85	1.80			0.79	1.67
2.50	0.99	2.10			0.94	2.00
3.00	1.13	2.40			1.10	2.33
3.50	1.32	2.80			1.26	2.67
4.00	1.50	3.17				
4.50	1.68	3.55				
5.00	1.84	3.90				

Table 5.1 Flow versus Valve Control Input

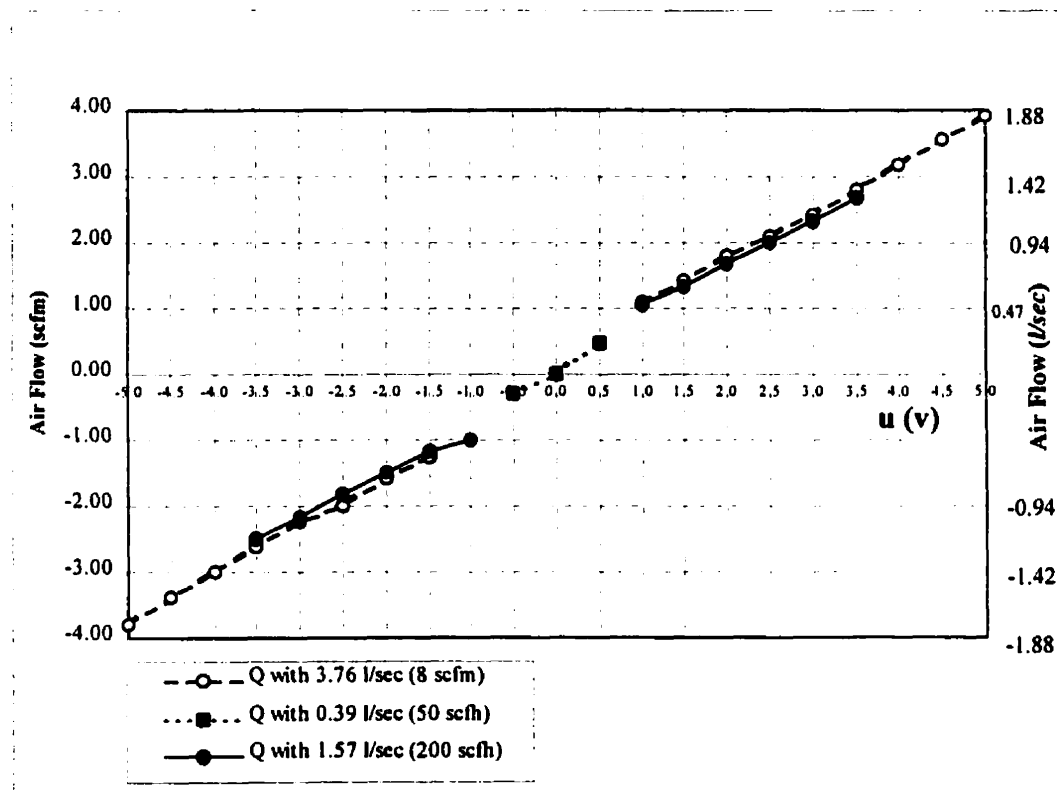


Figure 5.2: Flow vs. Control Input for *HR-Textron 4*



### 5.3 Actuator Modeling

An asymmetric, or rodless cylinder is used in the experimental setup. It is a *BIMBA* cylinder ( part # 095-DX ) which has a stroke of 127 mm (5 in), a bore of 26.9 mm (1-1/16 ") and a piston diameter of 7.9 mm (0.312"). The actuator is a low friction cylinder with a specified breakaway pressure of 34.5 kPa (5 psi) at no load. The breakaway pressure is the minimum pressure required to initiate motion in a frictional cylinder.

More technical specifications on the *BIMBA* cylinder (part # 095-DX) can be found in Appendix A. In later sections of the chapter, the issue of robustness will be investigated. The performance of a set of different cylinders will be compared to the *BIMBA* cylinder (part # 095-DX). The performance of *BIMBA* (part # 095-DX) becomes the benchmark and the cylinder is called the *nominal* cylinder.

#### 5.3.1 Static Coulomb and Dynamic Coulomb Forces

Fig. 2.4 showed typical friction versus speed plots, with the bottom subfigure being the simplified friction model. To completely model friction, one needs to identify three components, two of which are coulomb friction components, namely static coulomb friction,  $F_{cs}$  and dynamic coulomb force,  $F_{cd}$ . Now  $F_{cs}$  can be thought of as the breakaway force, whereas  $F_{cd}$  is the running friction with constant amplitude and a sign that depends on the direction of motion. The third friction component stems the viscous friction coefficient,  $f_v$ , which increases linearly with speed.

In order to estimate the values for the  $F_{cs}$  and  $F_{cd}$  a technique first documented for pneumatic systems by *Abou-Faissal (1997)* is used. The procedure consists of applying a positive ramp control signal until the breakaway force is reached and the piston starts moving. The pressure in the cylinder chambers is measured at that instant and is then used to determine the net force that acts on the piston. That force equals the static friction. Once motion is detected, the ramp is reversed and consequently the velocity starts dropping. When the piston reaches a relatively low

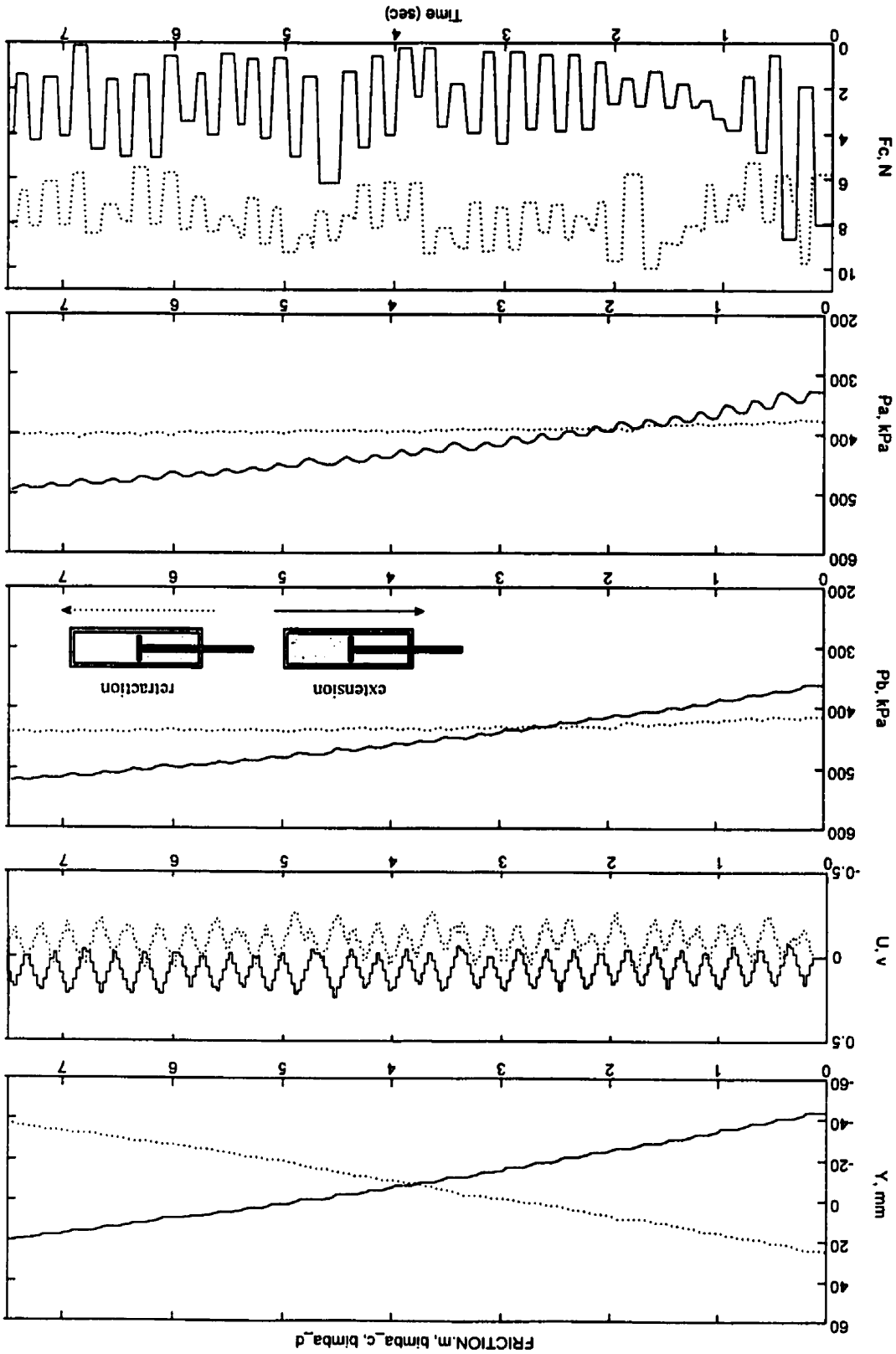
velocity and is about to stop, the pressure force is measured again to give an estimate of the coulomb dynamic friction. It is assumed that at low speed the contribution of viscous friction force is negligible. To investigate whether friction in an asymmetric cylinder is linear, the test was performed for both extension and retraction of the piston to determine the directional values of  $F_{CS}$  and  $F_{cd}$ .

Fig. 5.3 shows the response of the pneumatic system under the extension and retraction coulomb friction tests, in solid and dotted lines, respectively. From the top to the bottom of the figure, one has the position  $Y$ , the control signal  $U$ , the pressure in the small chamber  $P_b$ , the pressure in the large chamber  $P_a$  and most importantly, the coulomb friction response  $F_c$ . The latter is calculated by taking the difference of  $P_b$  and  $P_a$  at the instant motion is detected and accounting for different areas. The first observation is that friction appears to be direction dependent.

For extension, the calculated average static coulomb force  $F_{CS}$  was  $4.25\text{ N}$  with a standard deviation of  $0.85\text{ N}$ . The calculated average dynamic coulomb force  $F_{cd}$  was  $0.87\text{ N}$  with a standard deviation of  $0.53\text{ N}$ .

For retraction, the calculated average static coulomb force  $F_{CS}$  was  $8.62\text{ N}$  with a standard deviation of  $0.52\text{ N}$ . The calculated average dynamic coulomb force  $F_{cd}$  was  $6.97\text{ N}$  with a standard deviation of  $0.81\text{ N}$ .

Figure 5.3: Dynamic & Static Coulomb Force in Experiment - Extension and Retraction



### 5.3.2 Viscous Friction Coefficient ( $f_v$ ) and Effective Mass ( $M_e$ )

In Chapter 2, Eq. 2.29 presents the 3<sup>rd</sup> order model for the pneumatic positioner. The viscous friction coefficient is given as  $f_v$ . A number of techniques are available for experimental determination of the viscous friction coefficient. *Abou-Faissal (1997)* reports in his thesis a technique for determining the viscous force coefficient for a pneumatic actuator. The method is based on the fact that if the piston is forced to move at constant speed, then the acceleration becomes zero and the viscous force coefficient can be related to the differential pressure force, the dynamic coulomb force and the speed of the piston. The test requires a constant step input and when the piston reaches constant speed the viscous force coefficient can be calculated. *Abou-Faissal* implemented the technique on two *FESTO* pneumatic actuators of 700 mm and 400 mm strokes. Both actuators were long enough for constant speed to be reached and enabled the viscous force coefficient to be obtained. This is not the case for the *BIMBA* actuator which at a mere 120 mm of stroke is just too small for such a test to be performed.

A different technique for determining the viscous force coefficient was therefore used. Eq. 2.37 presents an ultimate gain formulation for a P-only controller in use with the 3<sup>rd</sup> order pneumatic model of Eq. 2.29. A relationship between the ultimate gain and the viscous friction coefficient can be seen. The same equation indicates that the ultimate gain also depends on the effective mass payload,  $M_e$ .

The method for determining both the viscous friction coefficient and the effective mass is as follows. A P-only controller is used for control. Initially the payload rests a small distance away from the setpoint. Once the test is initiated, the controller senses the error in the position and starts to move towards the setpoint. If  $K_p$  is considerably less than the ultimate gain, it will approach the setpoint with no overshoot and possibly a steady state error. If  $K_p$  is increased (but is still less than the ultimate gain), oscillations will occur about the setpoint but the system will eventually settle. If  $K_p$  is increased further, marginal stability will eventually be

reached which means that the system will enter a state of sustained oscillations. The amplitude and period of these oscillations can be related to the viscous friction coefficient and the effective mass.

In simulation, the same test was performed. In order to properly scale the ultimate gain for use in simulation, the following was considered:

- ♦ In the experiment, the control input to the servovalve ranges between  $-5\text{v}$  to  $5\text{v}$  and the position signal ranges between  $0\text{v}$  to  $10\text{v}$ . Therefore the input and output ranges are  $10 \{5\text{v}-(-5\text{v})\}$  and  $10 \{10\text{v}-0\text{v}\}$ , respectively. The ratio of the input over the output is  $1$ .
- ♦ In simulation, the control input to the servovalve ranges between  $-1\text{v}$  to  $1\text{v}$  (normalized) and the position signal ranges between  $-0.06\text{m}$  to  $0.06\text{m}$  ( $120\text{mm}$  stroke). Therefore the input and output ranges are  $2$  and  $0.12$ , respectively. The ratio of the input over the output is  $16.67$ .
- Therefore,  $K_P=1$  in the experiment corresponds to a  $K_P=16.67$  in simulation.

Fig. 5.4 presents the marginally stable position response of the pneumatic positioner, in the experiment with an unknown payload mass (large-dotted line). The ultimate gain used was  $3.2$ . The frequency and amplitude of the oscillations can be determined from the Figure as  $9.2\text{ Hz}$  and  $6.5\text{ mm}$  respectively. The sampling time was  $10\text{ ms}$ .

Fig. 5.4 also shows the simulated response of the pneumatic positioner (solid line) with the model as given in Chapter 2 and listed in Appendix B. The gain used was  $53.3$ , which was determined by considering the scaling factor of  $16.67$  required to convert from experiment to simulation and given the experimental ultimate gain of  $3.2$ . By adjusting the effective payload mass and the viscous friction coefficient entries in simulation, the amplitude and frequency of the oscillations of the marginally stable system can be changed. For an  $f_v$  of  $63\text{ Ns/m}$  and an  $M_e$  of  $2.2\text{ kg}$ , the amplitude and frequency match very closely the ones obtained in the experiment (large-dotted line response).

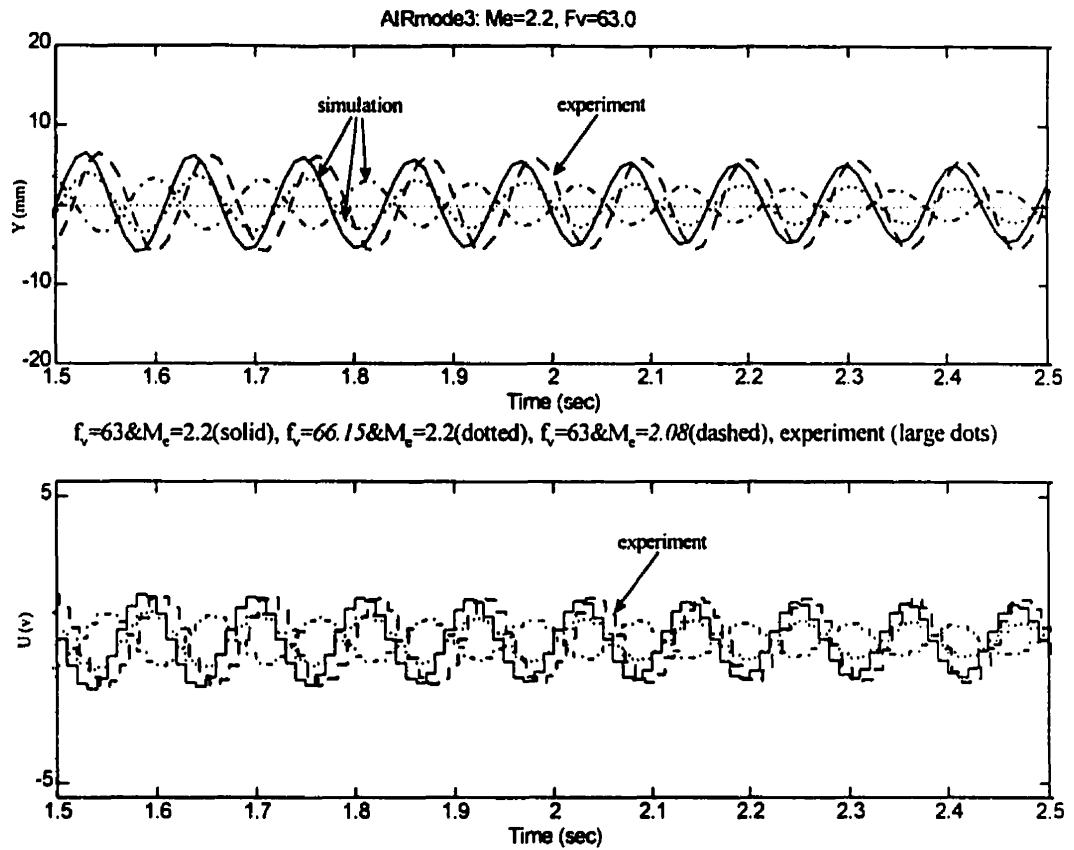


Figure 5.4: Viscous Friction Force and Effective Mass Payload - Experiment vs. Simulation

Two sensitivity tests were then performed that set out to evaluate the accuracy of the model: an intentional **5% increase** in the value of  $f_v$  (66.15 Ns/m) and a **5% decrease** in the value of  $M_e$  (2.08 kg). The responses are shown in dotted and dashed lines, in Fig. 5.4 respectively. One can realise that even a  $\pm 5\%$  error in the value of  $f_v$  or in the value of  $M_e$  result in approximately 50% decrease in the amplitude of oscillations and a phase shift on the order of  $180^\circ$ . Both are large deviations from the nominal response.

Note also that the phase shift in both the control signal and the position response of the experiment (large-dotted line) with respect to the control signal and the position of the nominal design in simulation (solid line) was intentional in order to better illustrate their individual performance.

In order to check whether the determined effective mass is realistic, the block the mass, the carriage and rollers, and the extension rod were weighed. The weights for each are  $1.12\text{ kg}$ ,  $0.19\text{ kg}$ , respectively and the total weight is  $2.05\text{ kg}$ . The small difference in the measured weight to the effective mass payload determined by the viscous friction method is only  $0.15\text{ kg}$ , which could be attributed to the inertia of the potentiometer belt. Therefore, the determined values for the viscous coefficient and the payload mass can be considered as good approximations for the physical system. The components are shown in Fig 5.5.

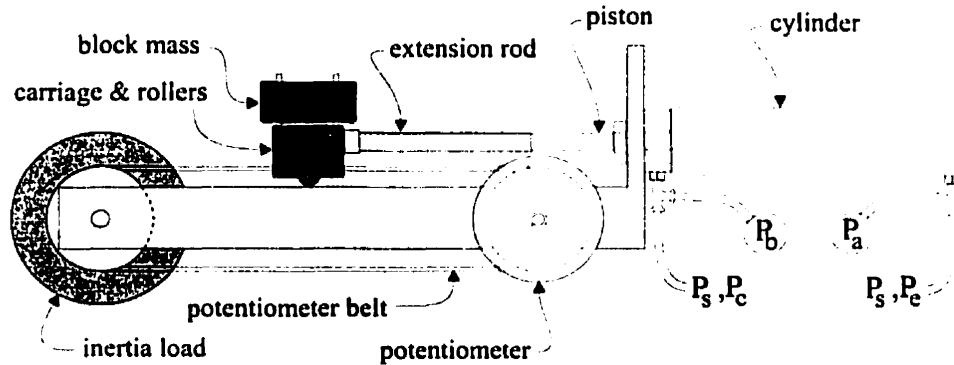


Figure 5.5: Effective Mass Components

Figure 5.6 shows a robustness test for the DSLM controller as designed in Chapter 4. The controller was designed for a settling time of  $0.2\text{ sec}$  and damping of  $1.0$ . Note that for this test the controller was designed for a payload of  $8.5\text{ kg}$ , which was experimentally done by adjusting an inertial load as shown in Figure 5.5. The effective payload was determined using the procedure outlined in Section 5.3.2.

The response of the nominal payload is shown as a solid line. The responses for the low payload ( $2.2\text{ kg}$ ) and the large payload ( $23\text{ kg}$ ) are shown in dotted and dashed lines, respectively. Note that the DSLM design requirements are roughly met in all cases, and the steady state errors were determined to be under  $0.2\text{ mm}$ , which is a very good result.

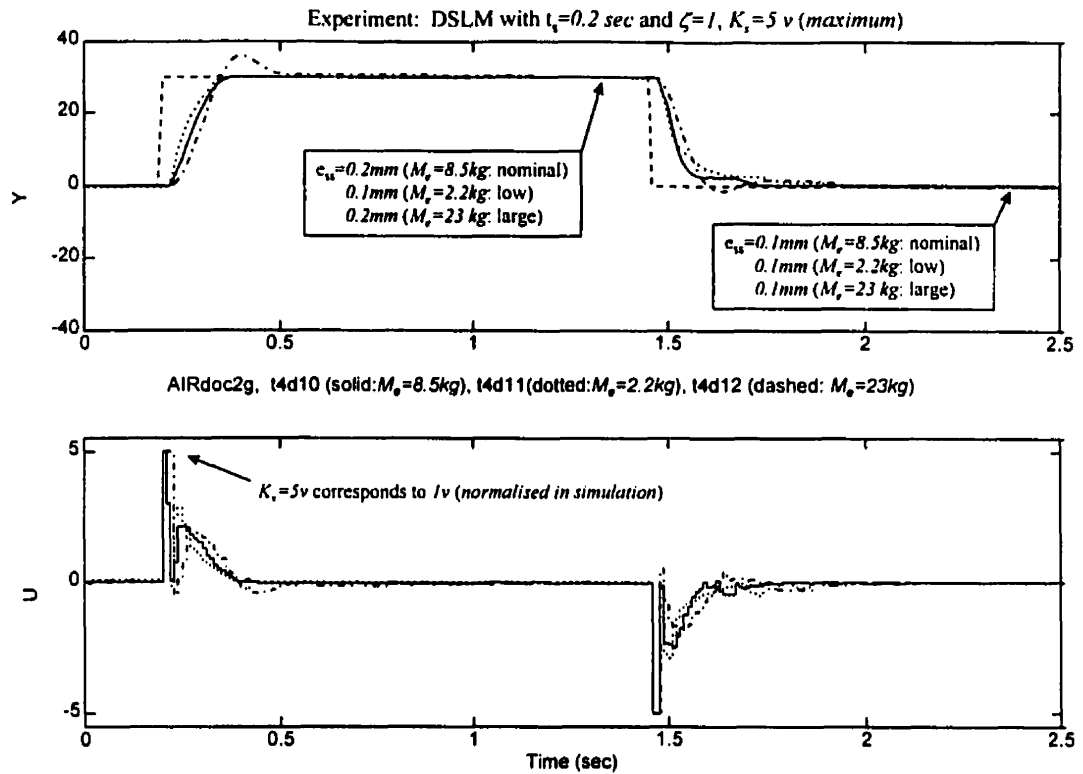


Figure 5.6: Robustness Test with DSLM, Experiment

#### 5.4 Choice of Setpoint change

Most pick-and-place applications start with the end effector at one location, then the end effector moves to another location and finally returns to the initial location. To mimic this typical industrial scenario, a 2-step setpoint change was chosen to be implemented in the experimental tests. There exist though an infinite number of different setpoint change scenarios. Chapter 2 demonstrated that the natural frequency and damping in pneumatic cylinders depend upon both the direction of the move (for rodded cylinders) and the location of the move (for rodless and rodded cylinders). For example, Fig. 2.9 showed that for a symmetric cylinder, the minimum natural frequency occurs at the center of the stroke and the maximum at the ends of the stroke. In order to test the controllers under these nonlinear conditions, 2 distinct locations were initially chosen, the center and the end of the stroke. The 4-step step change shown in Fig. 5.7 was used to test these pick-and-place scenarios.



The total stroke length for the *BIMBA* cylinder is *127 mm*. Thus it has *63.5 mm* of travel on either side of the center position. To prevent the piston from hitting the ends of the cylinder, the setpoints are selected to be a safe distance away from the endstops. In this case, *40 mm* of travel is considered appropriate. In Fig. 5.7, one can see four distinct setpoint change scenarios: *0 to 40 mm*, *40 to 0 mm*, *0 to -40 mm* and *-40 to 0 mm*. These are denoted as scenarios *1* to *4*, respectively.

The controller used in the test shown as Fig. 5.7 was a PVA controller. This linear controller was chosen because of its low robustness relative to CSLM and DSLM. It could therefore better demonstrate the relative performance of the four scenarios. For this asymmetric cylinder, retraction of the piston causes appreciable steady state error; *1.7 mm* and *1.5 mm* during setpoint scenarios 2 and 3 respectively. Setpoint scenario 4 indicates a significant steady state error of *0.3 mm* but also overshoots of 5%.

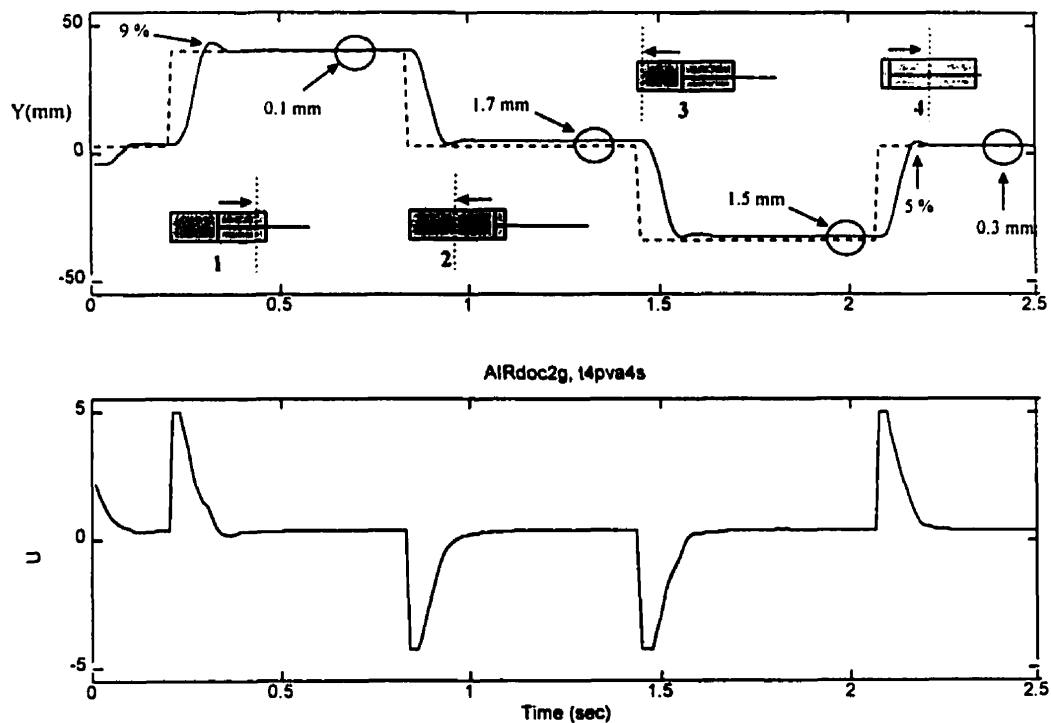


Figure 5.7: 4-Step Setpoint-change Scenario with PVA, Experiment

Since setpoint scenarios 3 and 4 appear to be the areas of increased control difficulty and lower performance, it was decided to use them as the benchmark setpoint change, with one slight modification. During experimental robustness tests, the possibility of large overshoots is increased. For this reason, to avoid hitting the ends of the cylinder, the setpoint change was modified slightly: the piston starts at  $-32\text{ mm}$ , moves to the center and then back to  $-32\text{ mm}$ . In the case of the nominal *BIMBA* cylinder, the  $-32\text{ mm}$  location corresponds to the quarter length of the stroke.

#### 5.4.1 Closed Loop Experiment and Model Validation

Once the friction forces and coefficients are calculated, a model validation test in the closed loop is performed. In the open loop, the typical control input step-sequence failed to provide a good result, because of the fact that an asymmetric cylinder behaves differently in extension than in retraction. Due to the unequal cylinder chamber areas, the piston moves faster in extension than in retraction. As a result, the piston moved closer and closer to the end of the stroke at each step change. This drift meant that a test of adequate duration could not be realised.

Fig. 5.8 shows the simulated result for the step change described in Section 5.3. A payload with an effective mass of  $2.2\text{ kg}$  was moved from the quarter length position of an asymmetric cylinder ( $-32\text{ mm}$ ) to the center and back. The nominal *BIMBA* cylinder was used. A viscous force coefficient of  $63\text{ Ns/m}$ , a dynamic coulomb force of  $3.9\text{ N}$  (average of extension and retraction dynamic coulomb forces) and a static coulomb force of  $6.4\text{ N}$  was used (average of extension and retraction static coulomb forces). Finally, a linear servovalve (*HR-Textron*) is modelled with a valve opening of  $2.13\text{ mm}^2$  capable of producing  $1.88\text{ l/sec}$  ( $4\text{ scfm}$ ) of maximum flow at a supply pressure of  $689.5\text{ kPa}$  ( $100\text{ psi}$ ). A sampling time of  $10\text{ msec}$  is used that matches the speed of the microcomputer / data acquisition system. A DSLM controller is applied which has been designed for a sliding settling time of  $0.2\text{ sec}$  and a damping of  $1.0$ . The state weights used were  $W_1=22$ ,  $W_2=2.5$  and  $W_3=0.35$ , which for a normalized  $K_S$  of  $1.0$  correspond to  $K_p=22$ ,  $K_v=2.5$  and  $K_a=0.35$ , respectively.

Figure 5.8 shows the response of the experiment under the same setpoint change scenario. One can see a good match between experiment and simulation. This leads to the conclusion that the model can be used to predict performance with different controllers for this particular setpoint scenario. This is not claimed to be proof that the model is valid for different setpoint scenarios. Therefore, testing the robustness of the controllers under consideration can be performed in simulation for a series of different cylinders for the adopted setpoint scenario.

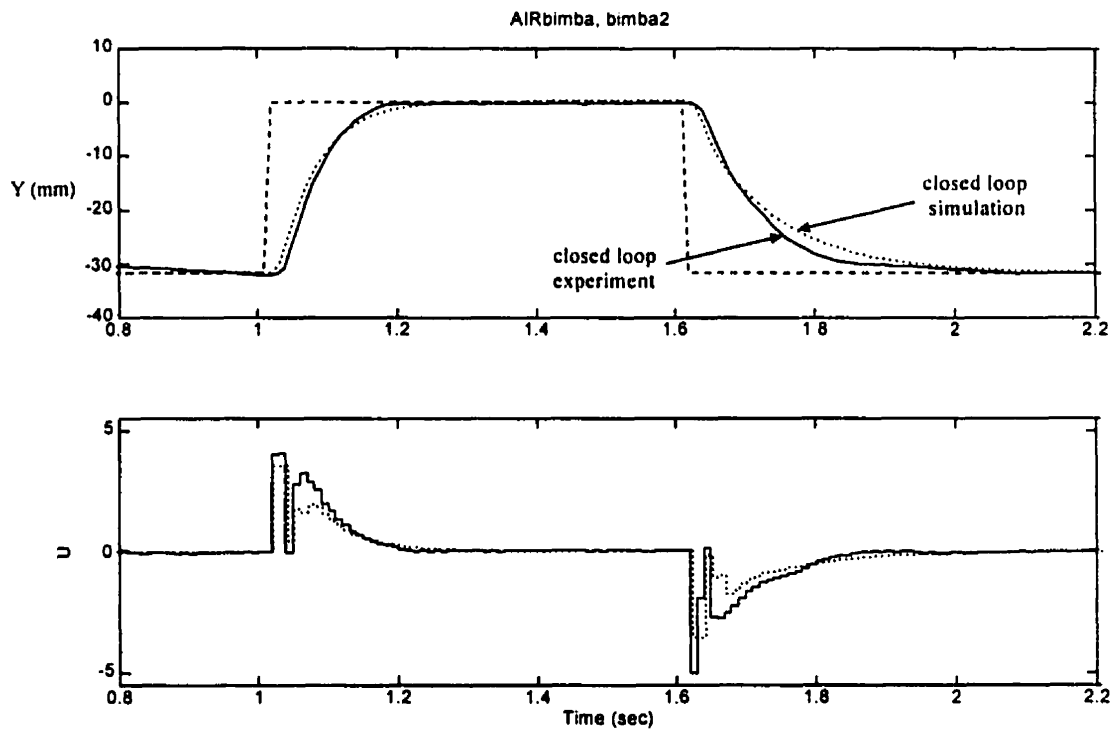


**Figure 5.8** Closed Loop Pneumatic Positioner Response, Simulation and Experiment

## 5.5 Robustness Results of PVA, CSLM and DSLM with Different Cylinders

Earlier sections in this chapter demonstrated how the unknown model parameters were determined for the nominal pneumatic positioner (servovalve: *4 scfm HR- Textron*, actuator: *BIMBA 095-DX*). The positioning performance and overall robustness of the conventional linear PVA and the nonlinear CSLM and DSLM controllers will now be compared under a series of simulation tests. These tests included a double bore and a double stroke scenario for which the controller and all other simulated hardware, such as the servovalve remained unaltered.

For the double *bore* scenario, the bore diameter was doubled while the stroke was left the same. A *BIMBA* cylinder that matches the double bore characteristic was selected from the manufacturer's catalog and its technical specifications were modeled in simulation. The double bore cylinder (*part # 315-DXP*) has a bore diameter of *50.8 mm*, a stroke of *127 mm* and a piston rod diameter of *15.8 mm*. The enclosed air volume of the double bore asymmetric cylinder is approximately 4 times greater than the volume of the nominal *BIMBA* cylinder (*part # 095-DX*).

Similarly, for the double *stroke* scenario the stroke was doubled while the bore diameter was left the same. A *BIMBA* cylinder that matches the double stroke characteristic was found from the manufacturer's catalog and its technical specifications were modeled in simulation. The double stroke cylinder (*part # 0910-DX*) has a stroke of *254 mm*, a bore diameter of *26.9 mm* and a piston rod diameter of *7.9 mm*. The enclosed air volume of the double stroke asymmetric cylinder is approximately 2 times greater than the volume of the nominal *BIMBA*. The technical specifications for both the double bore and the double stroke cylinders are included in Appendix A.

Of the two tests outlined above, the more demanding is the double bore test. The controllers were implemented in simulation for a setpoint scenario as outlined in Section 5.4 and were designed for a critically damped settling time of *0.2 sec*. The

controllers were tuned for an effective payload mass of  $2.2\text{ kg}$ . In the figures that follow, the position of the piston is shown as a percentage of the stroke so that the responses obtained under the double stroke test could be presented alongside the ones obtained with the nominal and double bore cylinders. This also implies that the setpoint scenario for all 3 cylinders (nominal, double bore and double stroke) was to move the piston from the quarter length position, to the center and back. In a cylinder that is linearized about the center position, the quarter length position is denoted as  $-25\%\text{ stroke}$  and the center as  $0\%\text{ stroke}$ , with the two ends of the cylinder denoted as  $-50\%\text{ stroke}$  and  $50\%\text{ stroke}$ .

In most cases, one can rate the responses in a qualitative manner by observing whether the trajectory requirements are met (settling time and overshoot), whether stiction is present in the position response, whether chatter appears in the control signal and whether there is considerable steady state error. In addition to qualitative observations, one can look at quantitative performance measures such as the integrated absolute error (*IAE*) and the integrated control effort (*ICE*). In order to obtain the *IAC* and *ICE*, the positioning error and control effort at every sampling interval are summed over the duration of the test. The *IAE* and *ICE* generated with the nominal cylinder can be used as the benchmark. It is expected that both quantities will increase for the double bore and double stroke tests. For the double bore test, the *IAE* and *ICE* can be compared directly to the benchmark measures obtained when using the nominal cylinder because the stroke is the same. However, for the double stroke test, the double distance that the piston travels, results in twice the positioning error at each sampling interval. To compensate for this inconsistency, the *IAE* generated under the double stroke test has to be divided by a factor of  $2.0$ . For a linear servovalve, such as the *HR-Textron*, one can say that the control input is proportional to the air flow. Due to air compressibility though, the motion of the piston is nonlinear to the air flow. Therefore, the *ICE* obtained from the double stroke scenario should not be compared to the benchmark *ICE*. Instead, the *ICE*

obtained from the 3 controllers for the double stroke test will be compared among themselves.

Fig. 5.9 shows the responses generated with the conventional *PVA* controller as applied to the pneumatic positioner. The responses for the nominal, double bore and double stroke cylinders are shown as solid, dotted and dashed lines, respectively. The top plot shows the position response as a percentage of stroke and the bottom plot shows the control input to the servovalve.

The solid line response (nominal cylinder) clearly shows the static coulomb friction effects. The positioner slows down as it approaches the setpoint. When its speed becomes low enough, stiction grabs hold of the piston. The resulting steady state error is sensed by the controller which compensates by increasing the control signal to free the cylinder. This corresponds to the sudden jump in the position. This stick-slip phenomenon occurs a few more times before the piston finally reaches the setpoint and results in a very jerky motion.

For the double bore scenario, the dotted lines indicate a considerably slower response. For the double stroke scenario, the dashed lines show an improved speed of response and the setpoint is reached at about the same time as it was reached by the nominal cylinder. The *IAE* and *ICE* for the 3 cylinders and *PVA* are shown in Table 5.2. In the same table, the *IAE* and *ICE* for the 3 cylinders and the 2 nonlinear controllers (*CSLM* and *DSLM*) are also given. The same table also tabulates the % increase in *IAE* for the double stroke and for the double bore cylinders, as compared to the benchmark *IAE* (nominal cylinder). Furthermore, the % increase in *ICE* for the double bore cylinder only as compared to the benchmark *ICE* is also shown.

Fig. 5.10 shows the responses generated with the *CSLM* controller ( $h=10\text{ ms}$ ) as applied to the pneumatic positioner. The responses for the nominal, double bore and double stroke cylinders are shown as solid, dotted and dashed lines, respectively. The

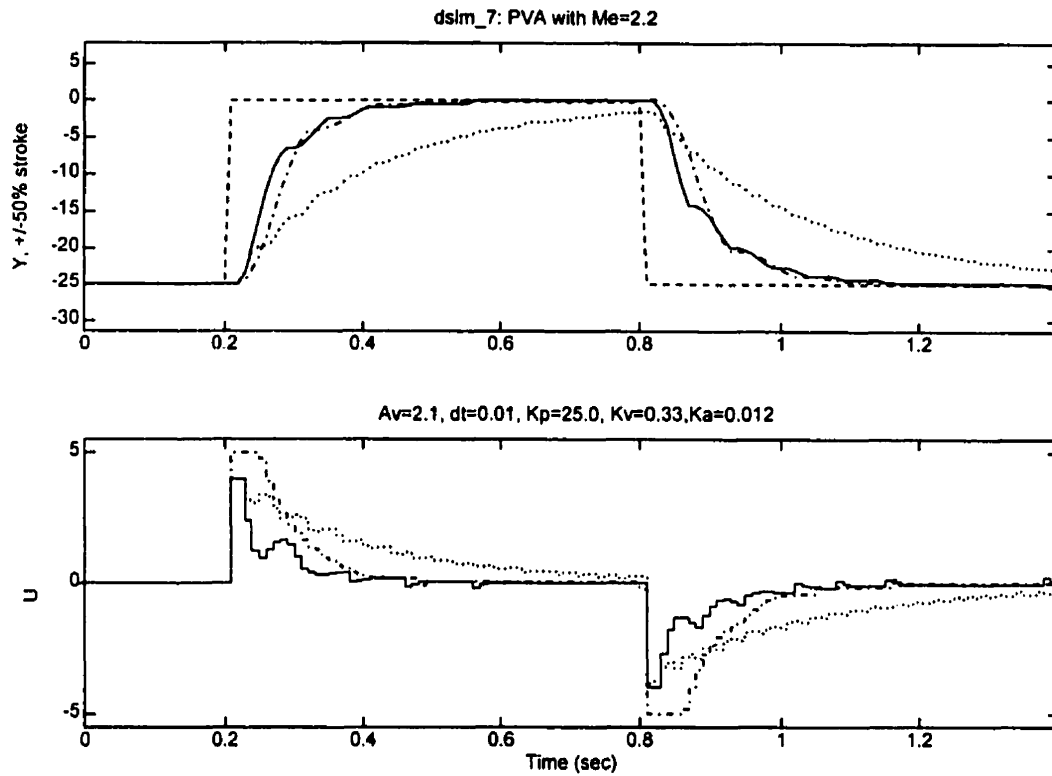
top figure shows the position response as a percentage of stroke, the middle figure shows the sliding function behavior and the bottom figure shows the control input to the servovalve.

The response of the nominal cylinder with CSLM can be described as slightly jerky and is marginally similar to the response with the PVA controller, as shown in Fig. 5.9. For the payload at hand, the boundary layer used was  $65.0$ . If a smaller boundary layer was used, excessive chatter would result which would cause greater steady state errors and increased oscillations. The inability of CSLM to adequately control a small payload boils down to sampling time intolerance. A small system time constant (due, to a small payload of  $2.2\text{ kg}$ ) combined with a relatively large sampling time, will degrade the overall performance of CSLM.

In the case of the double bore cylinder (dotted lines), one can see a much slower position response. The control signal appears more chattery and the sliding function diverges, contrary to the conditions of the sliding law. The extreme conditions of this test (incorrect cylinder model, small payload, high sampling time) have degraded the performance of CSLM to the point of instability.

In the case of the double stroke cylinder (dashed lines), one can see a much improved response. Despite a slightly greater settling time the sliding function converges and the control signal is smooth.

Fig. 5.11 shows the responses obtained with the DSLM controller. The responses for the nominal, double bore and double stroke cylinders are shown as solid, dotted and dashed lines, respectively. As before, the top figure shows the position response as a percentage of stroke, the middle figure shows the sliding function behavior and the bottom figure shows the control input to the servovalve.



*nominal (solid), double bore (dotted), double stroke (dashed)*

Figure 5.9: Robustness Tests with PVA - Simulation

Table 5.2: Summary of Quantitative Performance Measures for Robustness Tests

<b><u>PVA</u></b>	<b>Nominal-Benchmark</b>	<b>Double <math>\phi</math></b>	<b>% Increase for double <math>\phi</math></b>	<b>Double <math>L_c</math></b>	<b>% Increase for double <math>L_c</math></b>
<b>IAE</b>	481	1248	159%	542.5	13%
<b>ICE</b>	106	313	195%	214	-----
<b><u>CSLM</u></b>	<b>Nominal-Benchmark</b>	<b>Double <math>\phi</math></b>	<b>% Increase for double <math>\phi</math></b>	<b>Double <math>L_c</math></b>	<b>% Increase for double <math>L_c</math></b>
<b>IAE</b>	817	1759	115%	1266	55%
<b>ICE</b>	110	438	298%	201	-----
<b><u>DSLM</u></b>	<b>Nominal-Benchmark</b>	<b>Double <math>\phi</math></b>	<b>% Increase for double <math>\phi</math></b>	<b>Double <math>L_c</math></b>	<b>% Increase for double <math>L_c</math></b>
<b>IAE</b>	589	884	50%	722	23%
<b>ICE</b>	101	349	246%	210	-----



The response of the nominal cylinder with DSLM is smooth. The stiction effects seen with PVA and the control chatter seen with CSLM are no longer as visible. The sliding function converges to zero and the sliding conditions are met.

In the case of the double bore cylinder (dotted lines), the response shows a small delay. When compared to the delay that resulted with PVA and CSLM, it becomes clear that DSLM is the most robust of the 3 controllers, when the sampling time is large. In the case of the double stroke (dashed lines), the response improves further and is comparable to the one with the nominal cylinder.

Table 5.2 summarizes the *IAE* and *ICE* taken from Fig. 5.9, 5.10 and 5.11. If one compares the nominal *IAE* for PVA with the corresponding *IAE* for DSLM might prompt one to make the assumption that PVA behaves better than DSLM, in the absence of qualitative observations. The contrary, though is true. DSLM produces a smooth response, whereas PVA exhibits high stiction effects which are undesirable. Comparing the % *increase* in *IAE* for the three controllers at both robustness scenarios, one can see that DSLM has the lowest overall increase. This confirms the result of the qualitative observations. If one looks at the *ICE* for the 3 controllers, can realize that all exhibit roughly the same increase from the nominal values.

The performance of CSLM improves considerably with either the use of a sampling time in the order of *1.0 ms*, or the use of a larger payload. It has been seen in simulation that the performance and the robustness of CSLM can surpass those of DSLM provided the sampling time is sufficiently small, relative to the time constant of the system. Empirically, when selecting a suitable sampling time for CSLM, one needs to sample at least 20 times per time constant of the fastest component of the controlled system.

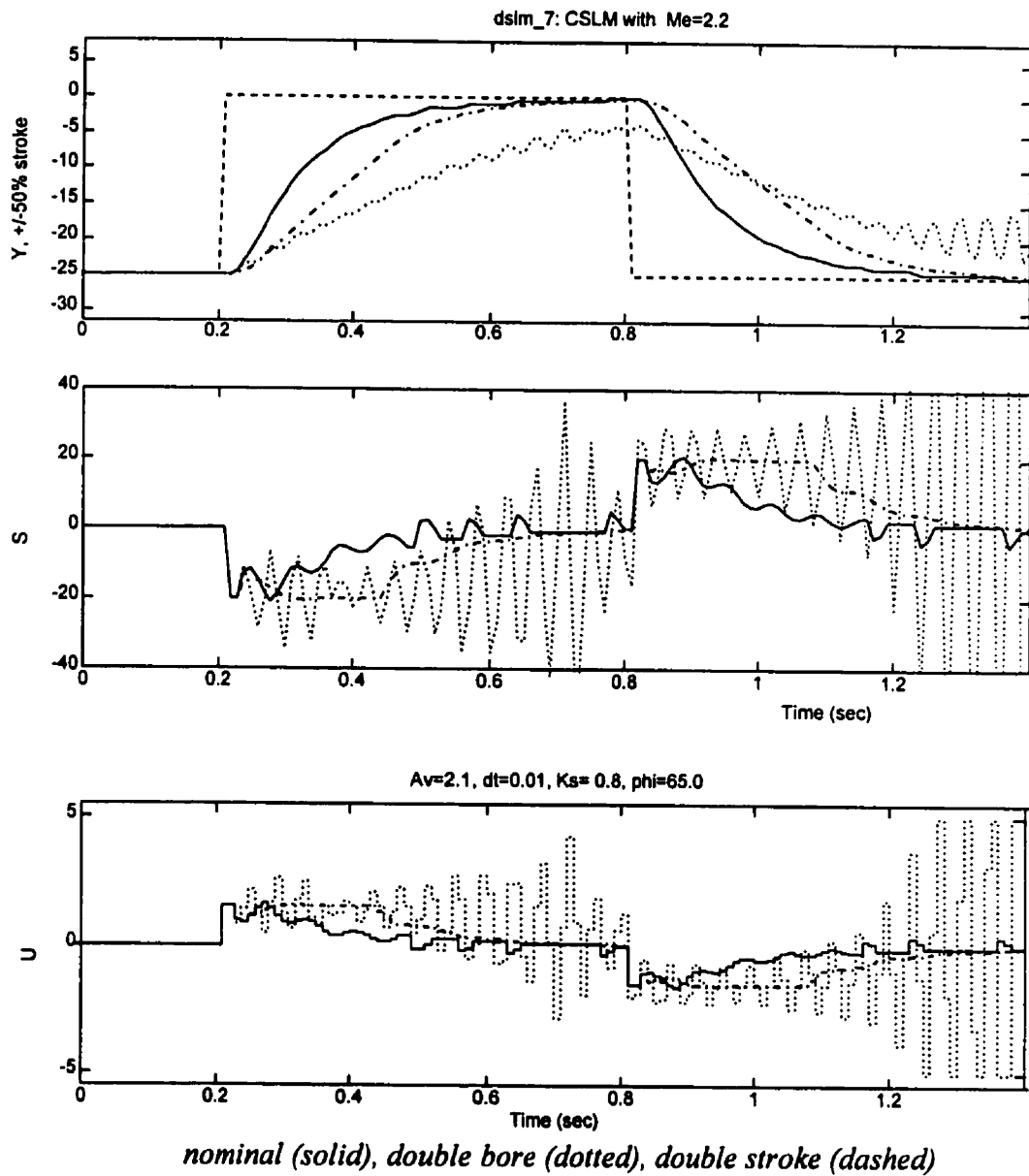


Figure 5.10: Robustness Tests with CSLM - Simulation

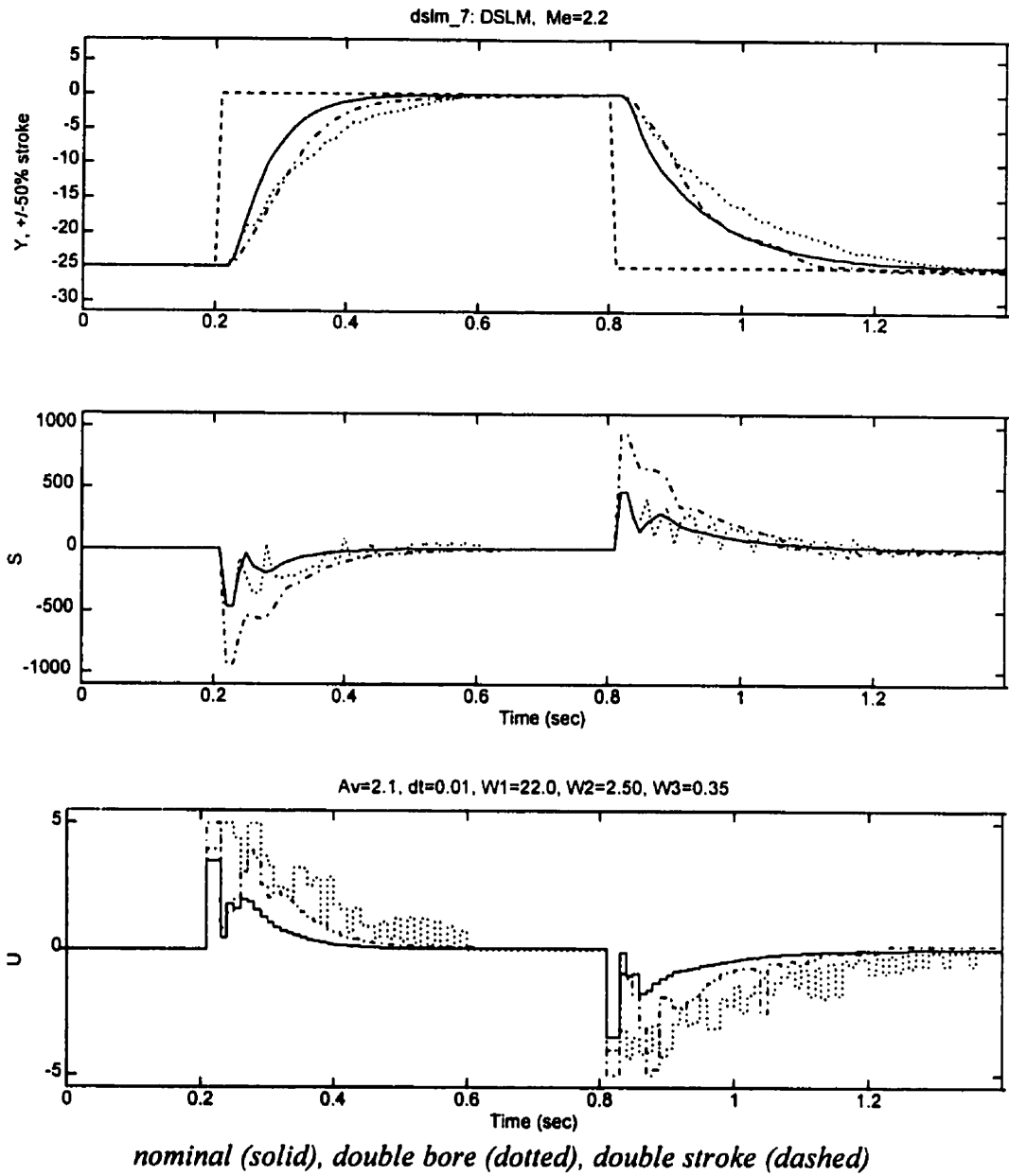


Figure 5.11: Robustness Tests with DSLM - Simulation

## 5.6 Summary

Following a set of experimental tests to validate the model coefficients, a series of robustness tests were performed in simulation. These tests were designed to verify the performance of the linear PVA and the nonlinear CSLM and DSLM controllers in the presence of significant model errors. The controllers were tuned to meet certain setpoint change scenarios for a particular pneumatic positioning system. They were then applied to a pneumatic system that had twice the cylinder bore diameter and twice the cylinder stroke. Qualitative observations such as smoothness of response, and quantitative measures such as the *IAE* and *ICE*, were used to evaluate the performance of the controllers.

For the simulated pneumatic systems and the implemented sampling time, DSLM was shown to be the more robust of the three controllers tested. Its greatest advantage is the ability to tolerate large sampling times. CSLM, on the other hand fails in the presence of large sampling times, which is the reason behind its poor performance in the tests presented in this chapter.

## CHAPTER 6

### CONCLUSIONS AND RECOMMENDATIONS

#### 6.1 Conclusions

The two main aspects of the design of pneumatic positioning systems, namely the sizing of the valve and cylinder and the design of an appropriate controller, were investigated in this thesis. The main objective was to improve the performance of pneumatic systems and generate a set of guidelines for better system design. The adopted nonlinear controller was Sliding Mode (SLM) control, in both continuous (CSLM) and discrete (DSLM) implementations.

##### 6.1.1 Pneumatic Positioning System

In Chapter 2, a linear and a nonlinear model of a pneumatic positioning system was developed. Models for system components were determined from first principles using *compressible* flow, *energy* conservation, *mass* balance and *force* balance equations. Conditions such as *choked* versus *subsonic* flow, static and dynamic coulomb friction, and air compressibility were combined to generate a 3<sup>rd</sup> order nonlinear model. Simulation tests with the nonlinear model indicated that in pneumatic positioning systems the dynamic performance (natural frequency and damping) depends on the position of the piston (rodded and rodless cylinders) and on the direction of the motion (rodded cylinders). The presence of these nonlinearities limits the performance of linear controllers since their design is based on a linear model of the system and do not compensate for large parameter variations.

The performance of the pneumatic positioning system was then tested in simulation. A linear PVA controller was used, for which the gains were determined from a linearised model of the pneumatic system for a set of time-domain performance parameters, namely settling time and overshoot. The application of a fixed gain linear controller to a system that was considered nonlinear was intentional in order to highlight how different parameters affected system performance. The following

conclusions resulted from the investigation of the pneumatic positioning system under PVA control:

- ♦ **Ultimate Gain - Cylinder Type:** When one needs to determine the ultimate gain that can be used for a *rodless* cylinder, then Eq. 2.37 can be used. If a *rodded* cylinder is used, the dynamic performance depends on the direction of motion (extension or retraction) which implies that the ultimate gain is different in either direction. In fact, the ultimate gain is lower if the piston is in extension than in retraction. Therefore, in order to predict the ultimate gain for a rodded cylinder, one should use the smaller of the two chamber areas in Eq. 2.37.
- ♦ **Sampling Time - Size Ratio:** Pneumatic systems exhibit localised dynamics, which could be a cause for control instability. If, for example, one works with a cylinder that has a high size ratio, then the natural frequency is higher than one that would result when a cylinder with the same capacity and a moderate size ratio is used. If the sampling time is not adjusted to account for the higher natural frequency, then the performance of the system degrades and instability could occur. The link between natural frequency and size ratio has been generally ignored in the literature.
- ♦ **Valve Center Configuration - Valve Port Ratio:** In the design of pneumatic systems, one should also consider the effects of the valve center configuration. For position control tasks, the servovalve should have a closed-center configuration since higher operating pressures are needed. Open center valves should be used only when free positioning of the payload is required.
- ♦ **Supply and Steady State Pressures:** A number of physical measurements of the servovalve and the actuator have been shown to affect the steady state pressures. Typically, higher operating pressures improve performance by

decreasing the effects of air compressibility. The only restriction is the maximum operating pressure that the pneumatic equipment can withstand.

- **Friction:** Low friction cylinders or valves that are insensitive to the lack of natural lubrication should be used to avoid stiction effects.

The nonlinear nature of a pneumatic positioning system requires a controller that is able to maintain a high level of performance despite variations in:

- Position of the setpoint,
- Direction of motion,
- Friction and,
- Noise.

Furthermore, the controller should also be able to provide reasonable performance despite:

- Improper sizing of pneumatic components and,
- Payload variations.

In the pneumatic system presented in this thesis, the natural frequency and damping were shown to vary by as much as a factor of 2.5 from the center to the ends of stroke. For this range of parameter variations, the PVA controller performed poorly. This is due to the fact that nonlinearities in the system are not compensated for. Hence, the interest in the nonlinear Sliding Mode Controllers which can handle these nonlinearities.

### **6.1.2 Continuous Sliding Mode Control**

In Chapter 3, the design procedure for the sliding surface of CSLM was presented and illustrated as Fig. 3.13. A continuous canonical system state space model is determined using a transformation matrix  $T$ . Time domain performance parameters of a 2<sup>nd</sup> order system are then used to generate the coefficients of the canonical sliding

surface. Finally, the canonical sliding surface is changed to its original state space variables by use of matrix  $T$ .

Basic issues for the design of a CSLM controller as applied to the control of a pneumatic positioning system were examined by means of simulation. These issues include the effect of the tuning parameters of CSLM, namely:

- ♦ The sliding gain, and
- ♦ The boundary layer thickness,

as well as the design parameters for the sliding surface, namely:

- ♦ The sliding settling time, and
- ♦ The damping factor,

and finally the effect of:

- ♦ The sampling time.

In summary, CSLM is a highly robust controller under the following conditions:

- ♦ **Sampling Time:** The sampling time needs to be sufficiently small, so that the continuous structure of the controller is not negated by large discrete sampling times and yet large enough to be achievable with a modest control computer. Empirically, one needs to use a sampling time at least 20 times smaller than the open loop time constant of the system. For example, if the open loop time constant for a particular pneumatic system is *0.1 sec*, the sampling time should be in the order of *0.005 sec*.
- ♦ **Boundary Layer:** The boundary layer needs to be sufficiently large so that chatter is eliminated and yet sufficiently small so that positioning accuracy is not compromised.

In general, CSLM is a fairly easy controller to design and use. Its performance is very good if the sampling time is sufficiently small. This thesis does not set out to



investigate the sampling time limitations of the CSLM controller in theory. Instead, the discrete (DSL<sub>M</sub>) implementation of CSLM was investigated, which compensates explicitly for the sampling time and was shown to be able to maintain stability even at high sampling times, while CSL<sub>M</sub> failed.

### 6.1.3 Discrete Sliding Mode Control

In Chapter 4, techniques for improving the basic DSL<sub>M</sub> control algorithm were reviewed. These techniques included state estimators, varying sliding gains, state weights and filters. The best features were then selected. A novel pole-placement approach for the determination of the sliding surface coefficients was then presented. The sliding surface was based on a dominant set of desired closed loop poles and can match the more conventional sliding surface design characteristic where the sliding surface has one order less than the system. A novel approach to the assignment of the switching gains for DSL<sub>M</sub> was also presented.

The following summarises the adopted design procedure for the sliding surface of a DSL<sub>M</sub> controller, and some of the modifications that were made on the switching law.

- ♦ **Sliding Surface Design:** A novel pole-placement technique for designing the sliding surface of a general  $n^{th}$  order system, which then focused on a typical  $3^{rd}$  order pneumatic system, was developed. The technique enables the designer to select sliding surface coefficients according to traditional time performance parameters, namely settling time and maximum overshoot (or damping).

To facilitate analysis, the closed loop dynamics of the system under pure sliding were modified to a canonical form. Techniques for generating the canonical state space matrices were presented. The coefficients of the characteristic equation of the closed loop canonical state space matrix were

then linked to desired poles in the discrete domain. Finally, the sliding surface coefficients were calculated to match a set of poles that generate a dominant 2<sup>nd</sup> order subsystem of the general 3<sup>rd</sup> order pneumatic system. The simulation responses with the pole placement technique for sliding surface design showed good trajectory tracking and design flexibility.

- **Varying Sliding Gain:** The switching laws of DSLM were modified to implement a varying sliding gain within the boundary layer which decreased in magnitude upon approach to the sliding surface. Therefore limit cycles, high chatter and large steady state errors could be eliminated.
- **State Weights:** To further optimize the responses, control or state weights were assigned to the individual states. A direct and novel comparison of the control structure of the DSLM controller to the control structure of the PVA controller indicated a direct relationship between the size of the switching elements (per state) to the linear PVA gains. The implementation of PVA gains as state weights for the DSLM controller resulted in very good setpoint tracking, decreased oscillations, good sliding function convergence and decreased control action.
- **Sliding Gain Bounds:** Bounds for the sliding gain for convergence stability were then determined in terms of the coefficients of the sliding surface, the desired reaching time, the sampling time and the control gain matrix.

The performance of DSLM indicated better behavior than CSLM in the presence of high static friction. CSLM and DSLM perform equally well in the presence of noise.

#### 6.1.4 Robustness Tests

Experimental open loop results for the pneumatic system were presented in Chapter 5. These tests were used to determine the model parameters for the pneumatic system. Then a series of tests were performed to confirm the robustness of the three controllers: the PVA, the CSLM and the DSLM. These tests evaluated the controllers under different scenarios: *double bore - same stroke* and *double stroke - same bore*. Qualitative observations such as smoothness of response and quantitative measures such as the *IAE* and *ICE*, were used to evaluate the performance of each controller for each of the robustness tests performed.

For the simulated pneumatic system and the implemented sampling time, DSLM was shown to be the more robust of the three controllers tested. Its greatest advantage over CSLM is the ability to tolerate large sampling times. An additional series of tests were performed to confirm the robustness of the three controllers in terms of incorrect payloads. The tests were implemented with sampling times of *1 ms* and *10 ms*. The conclusion was that at *10 ms*, DSLM was the more robust of the three controllers tested which confirms the result from Chapter 4. When a sufficiently small sampling time was used, which was the case with a sampling time of *1 ms*, CSLM was shown to be just as robust as DSLM. In all robustness tests performed, the SLM controllers were superior to the PVA controller.

#### 6.2 Design Recommendations

For both CSLM and DSLM the sliding gain needs to be sufficiently large without exceeding stability limits, so that model errors do not compromise robustness and yet small enough to be achievable in practice. In practice, the size of the control input that fully opens the selected valve (which meets steady state speed of response requirements of the pneumatic system), should be used for the size of the sliding gain.

For DSLM, the state weights for the switching laws of DSLM should match the gains of a PVA controller. The gains of the PVA should be designed for a critically

damped response and a settling time similar to the one used in the design of the sliding surface of DSLM. Furthermore, a varying sliding gain should be used within the boundary layer.

Generally, the control structure of DSLM is more complex than the control structure of CSLM. For this reason, CSLM with its simplicity of implementation and design has been more popular than DSLM. But with better design guidelines for both the sliding surface design and the switching laws, DSLM is becoming more attractive.

When implementing a CSLM controller, one should use the smallest sampling time available, since it enables the controller to reach its full capability. This is becoming easier with the ever increasing speed of microcomputers for control applications.

### **6.3 Recommendations for Future Work**

A theoretical investigation on the stability limits of CSLM should be performed, since DSLM surpasses the performance of CSLM only with large sampling times.

Recently, relatively inexpensive proportional valves by *ASCO* have come on the market (*price* < \$100). Although of lower bandwidth than the *HR-Textron* valve used in this thesis (25 Hz versus 200 Hz for latter), the performance of the pneumatic positioning system with these relatively inexpensive valves should be investigated.

An experimental verification of the effects of sizing ratio should also be performed that would investigate the robustness of CSLM and DSLM in the context of changes in cylinder bore and cylinder stroke, recognizing that *Iordanou and Surgenor (1997b)* only verified CSLM and DSLM in the context of changing payload mass.

Finally, a Kalman Filter can be used to provide optimal estimate for the output states if noise is present. Furthermore, the use of such a filter could further reduce noise problems associated with digital differentiation of the measured output.

## REFERENCES

- [1] **Abou-Fayssal, H** (1997), "Design, Analysis and Control of a Pneumatic Cartesian Robot", Master's Thesis, Department of Mechanical Engineering, Queen's University, Kingston April 1997.
- [2] **Abou-Fayssal, H and Surgenor, B. W.** (1997), "Experience with a Pneumatic Cartesian Robot and the Need for a Practical Friction Compensator", Tenth Bath International Fluid Power Workshop, Bath 97, UK, Sept 10-12th.
- [3] **Andersen, B.W** (1967), "The Analysis and Control of Pneumatic Systems ", John Wiley, New York.
- [4] **Åström, K.J and Wittenmark, B.** (1984), " Computer Controlled Systems", Prentice-Hall, Englewood Cliffs, New Jersey, Ch.11.
- [5] **Backe, W. and Eschmann, R.** (1993), "SSP-A Simulation Program for Pneumatics", 6<sup>th</sup> Bath International Fluid Power Workshop, Sept 23-24.
- [6] **Barnett, S.** (1990) "Matrices, Metrods and Applications", Oxford University Press.
- [7] **Beercheck R.C** (1985), "Controlling Air with Electronics", Machine Design, Vol. 57, No.16, pp.77-80.
- [8] **Bloch, A. and Drakunov, S.** (1995), "Tracking in Nonholonomic Dynamic Systems via Sliding Modes", Proc 34th IEEE Conference on Decision and Control, Dec 13-15, New Orleans, Louisiana, Vol.3, pp. 2103-2106.
- [9] **Blom A. and de Jager A. G.** (1991), " Robustness of a Second Order Sliding Mode Controller", ASME 93-WA/DSC, Advances in Robust and Non-Linear Control Systems, WAM '93, New Orleans, Nov 28-Dec 3, DSC-Vol. 53, pp 71-77.
- [10] **Bouri, M., Thomasset, D. and Scavarda, S.** (1994), "Non-Linear Sliding Mode Control of an Electropneumatic Servodrive", Proc of 7<sup>th</sup> Bath Int. Fluid Power Workshop, Sept. 21-23 1994.
- [11] **Burrows, C.R.** (1969), "Effect of Position on the Stability of Pneumatic Servosystems", IMechE Jrnl Mechanical Eng. Science, Vol. 11, No. 6, pp. 615-616.
- [12] **Burrows, C.R.** (1972) ,"Fluid Power Servomechanisms", Van Nostrand Reinhold Company.
- [13] **Burrows, C.R. and Webb, C. R.** (1969), "Further study of a low pressure on-off pneumatic servomechanism", Proc. Instn. Mech. Engineers, 184,849, Pt 1.
- [14] **Butler H., Honderd G. and VanAmerongen J.** (1991), " Model Reference Adaptive Control of a Gantry Crane Scale Model", IEEE Control Systems, Vol.11, No.1, pp 57-62.
- [15] **Deif, A.S.** (1982), "Advanced Matrix Theory", Abacus Press, England, Ch. 4.
- [16] **De-León, J. , Alvarez, Jm. and Castro, R.** (1995), "Sliding Mode Control and State Estimation for Nonlinear Singularly Perturbed Systems. Application to an Induction Machine", Proc 4th IEEE Conference on Control Applications, Sept 28-29, Albany, New York, pp. 998-1003.

- [17] **DeSantis, R.M.** (1989), "An Adaptive PI/Sliding Mode Controller for a Speed Drive", ASME Jnl DSMC, Vol. 111, pp 409-415.
- [18] **Drakunov, S. and Utkin, V.** (1995a), "Discrete-Event Sliding Mode Observers for Continuous-Time Systems", Proc 34th IEEE Conference on Decision and Control, Dec 13-15, New Orleans, Louisiana, Vol.3, pp. 3403-3405.
- [19] **Drakunov, S. and Utkin, V.** (1995b), "A Semigroup Approach to Discrete-Time Sliding Modes", Proc Amer Control Conf, June 21-23, Seattle, Washington, Vol.2, pp. 1314-1317.
- [20] **FESTO Pneumatic Tips** (1995), No.88.
- [21] **Fortel, H.** (1995), "A Generalised Normal Form and Its Application to Sliding Mode Control ", Proc 34th IEEE Conference on Decision and Control, Dec 13-15, New Orleans, Louisiana, Vol.1, pp. 13-18.
- [22] **Franklin, G.F., Powell, J.D. and Emami-Naeini, A.** (1991), "Feedback Control of Dynamic Systems ", 2nd Edition, Addison-Wesley Publishing Company, Reading Massachussets, Ch.8.
- [23] **Furuta, K.** (1990), "Sliding Mode Control of a Discrete System", Systems & Control Letters, Vol. 14, pp 145-152.
- [24] **Furuta, K., and Pan, Y.** (1995), "A New Approach to Design a Sliding Sector for VSS Controller", Proc Amer Control Conf, June 1995, Seattle, Washington, vol.2, pp. 1304-1308.
- [25] **Gamble, J.B and Vaughan, N.D.** (1994), "Comparison of Sliding Mode Control with state feedback and PID Control applied to a Proportional Solenoid Valve", WAM' 94, November 6-11, Chicago, FPST-Vol.1, pp. 51-58.
- [26] **Habibi, S.R.** (1995), "Sliding Mode Control of a Hydraulic Industrial Robot", Proc Amer Control Conf, June 1995, Seattle, Washington, vol.2, pp. 1523-1527.
- [27] **Hadi, S. A.** (1996), "Matrix Algebra as a Tool", Belmont: Duxbury Press, Ch. 2-9.
- [28] **Halme, J.S. and Handroos, H.M.** (1994), "Genetic Algorithm based on Self-Learning Control of Pneumatic Servos", Proc of 7<sup>th</sup> Bath International Fluid Power Workshop, 21-23 Sept. 1994.
- [29] **Harashima, F. Hashimoto, H. and Kondo S.** (1985), "MOSFET Converter-Fed Position Servo System with Sliding Mode Control", IEEE Transactions on Industrial Electronics, Vol. IE-32, No. 3, Aug 1985, pp. 238-244.
- [30] **Harashima, F. Hashimoto, H. and Maruyama, K.** (1986), "Sliding Mode Control of Manipulator with Time-Varying Switching Surfaces", Trans. of the Society of Instrument and Control Engineers, Vol. 22, No. 3, Mar 1986, pp. 335-342.
- [31] **Hitchcox, A. L.** (1996), "Understanding Proportional Pneumatics", Hydraulics & Pneumatics, Mar 1996, pp. 105-106, pp. 182-186.
- [32] **Hostetter, G.H.** (1988), "Digital Control System Design", Saunders College Publ., New York.
- [33] **Hwang, C.L.** (1992), "Design of Servocontroller via the Sliding Mode Technique", IEE Proceeding-D, Vol.139, No.5, pp 439-446.

- [34] **Hwang C.L., Lan C.H. and Jieng W.J.** (1993), "The Trajectory Tracking of an Electrohydraulic Servo-mechanism via a Sliding Mode Controller", Proc Instn Mech Engrs, Part I, Jnl Systems and Control Engineering, Vol.207, pp 135-142.
- [35] **Iordanou, H.N.** (1994), "An Experimental Study on the Robustness of Sliding Mode Control", Master's Thesis, Department of Mechanical Engineering, Queen's University, Kingston, May 1994.
- [36] **Iordanou, H.N, Surgenor, B.W. and Pieper, J.K.** (1995), "A Study on the Performance Improvement of DSLM", Proc American Control Conf, Seattle, June 21-23, Vol.2, pp.1533-1537.
- [37] **Iordanou H.N and Surgenor B.W.** (1996), "Discrete Versus Continuous Sliding Mode Control of a Pneumatic Positioning System", Ninth Bath International Fluid Power Workshop, Bath 96, UK, Sept 9-11th.
- [38] **Iordanou H.N and Surgenor B.W.** (1997a): "Experimantal Evaluation of the Robustness of Discrete Sliding Mode Control", IEEE Transactions on Control Systems Technology, March 1997, Vol.5, No.2, pp.254-260.
- [39] **Iordanou H.N and Surgenor B.W.** (1997b), "Sliding Surface Design for Discrete Sliding Mode Control and Application to a Pneumatic Positioning System", Tenth Bath International Fluid Power Workshop, Bath 97, UK, Sept 10-12th.
- [40] **Jian, S.** (1995), "Sliding Mode Control for Servo System with Varying Sliding Line", Proc 4th IEEE Conference on Control Applications, Sept 28-29, Albany, New York, pp. 1073-1077.
- [41] **Lai, J.Y., Menq, C.H. and Singh, R.** (1990), "Accurate Position Control of a Pneumatic Actuator" ASME Jnl Dynamic Systems, Measurements and Control, Vol. 112, pp.734-739.
- [42] **Lansky, Z.J and Schrader L.F.** (1986), "Industrial Pneumatic Control", Fluid Power and Control/6, New York and Basel.
- [43] **Luo, N. and Rodellar, J.** (1995), "Sliding Mode Control of a Class of Uncertain Coupled Systems: Application to Base Isolation Structures", Proc 34th IEEE Conference on Decision and Control, Dec 13-15, New Orleans, Louisiana, Vol.3, pp. 2127-2132.
- [44] **McCloy, D. and Martin, H.R.** (1980), "Control of Fluid Power: Analysis and Design", John Wiley, New York.
- [45] **Misawa, E.** (1995), "Observer-based Discrete-Time Sliding Mode Control with Computational Time Delay: The Linear Case", Proc Amer Control Conf, June 21-23, Seattle, Washington, Vol.2, pp. 1323-1327.
- [46] **Moore, P.R., Pu, J. and Harrison, R.** (1992), "Progression of Servo Pneumatics Towards Advanced Applications", 5<sup>th</sup> Bath International Fluid Power Workshop, Sept 16-18.
- [47] **Ogata, K.** (1990), "Modern Control Engineering", 2<sup>nd</sup> Edition, Prentice Hall, New Jersey, Ch.2.
- [48] **Paden, R. and Tomizuka, M.** (1995), "On the Analysis of Robust Discrete Time Feedback Control for Nonlinear Systems with Parametric Uncertainties",

- Proc Amer Control Conf, June 21-23, Seattle, Washington, Vol.2, pp. 1299-1303.
- [49] **Palm, W.** (1986), "Control Systems Engineering", John Wiley Inc. New York, Ch.2,3,4.
  - [50] **Paul, A.K, Mishra, J.K. and Radke, M.G.** (1994), "Reduced Order Sliding Mode Control for Pneumatic Actuator", IEEE Transactions on Control Systems Technology, Vol. 2, No.3, pg. 271-276.
  - [51] **Pieper, J.** (1992), "Discrete Sliding Mode Control", PhD Thesis, Department of Mechanical Engineering, Queen's University, Kingston, April 1992.
  - [52] **Pieper, J.K. and Surgenor, B.W.** (1992), "Optimal Discrete Sliding Mode Control with Application", Proceedings 1st IEEE Conference on Control Applications, Dayton, Ohio, Sept 13-16, Vol. 2, pp.916-921.
  - [53] **Pieper, J.K. and Surgenor, B.W.** (1993), "Discrete Sliding Control of a Coupled-Drives Apparatus with Optimal Sliding Surface and Switching Gain", IEE Proceedings-D, Vol.140, No.2, pp.70-78.
  - [54] **Pu, J. and Weston, R.H.** (1990), "Steady State Analysis of Pneumatic Servo Valves", Journal of Mechanical Engineering Science, Proc Instn Mech Engrs, Vol 204, pp. 377-387.
  - [55] **Pu, J. , Wong, C.B and Moore, P.R..** (1995), "Acceleration Characteristics of Servo-Controlled Pneumatic Cylinders", Fluid Power Systems Technology Symposia, ASME Winter Annual Meeting, Anaheim, California, Nov. 12-17.
  - [56] **Sarpturk, S.Z., Istefanopoulos Y. and Kaynak, O.** (1987), "On the Stability of Discrete-Time Sliding Mode Control Systems", IEEE Transactions on Automatic Control, Vol. AC-32, No. 10, Oct 1987, pp. 930-932.
  - [57] **Sira-Ramirez, H.** (1993) "On the dynamical Sliding Mode Control of Nonlinear Systems", Int. Jnl. Control, Vol.57, No.5, pp.1039-1061.
  - [58] **Shih, M.-C. and Tseng S.-I.** (1994), "Pneumatic Servo-Cylinder Position Control by PID-Self-Tuning Controller", JSME International Journal, Series C, Vol. 37, No.3, pp.565-572.
  - [59] **Slotine, J.J.E and Coetsee, J.A** (1986), "Adaptive Sliding Controller Synthesis for Non-Linear Systems", Int. Jnl. Control, Vol.43, No.6, pp.1631-1651.
  - [60] **Slotine, J.E. and Li, W.** (1991), "Applied Nonlinear Control", Prentice Hall, New Jersey, ch.7.
  - [61] **Soussi R. and Koivo A.J.** (1992), "Modelling and Control of a Rotary Crane for Swing-free Transport of Payloads", Proceedings 1st IEEE Conference on Control Applications, Dayton, Ohio, Sept 13-16, Vol. 2, pp.782-787.
  - [62] **Surgenor, B.W. and Iordanou, H.** (1993), "Electric versus Pneumatic Servo Control: A Case Study with a Gantry Crane Apparatus", ASME 93-WA/FPST-2, WAM '93, New Orleans, Nov 28-Dec 3.
  - [63] **Surgenor, B.W., and Vaughan N.D.** (1997), "Continuous Sliding Mode Control of a Pneumatic Actuator ", ASME Transactions on Dynamic Systems, Measurements and Control, September 1997, Vol.119, pp.578-581.

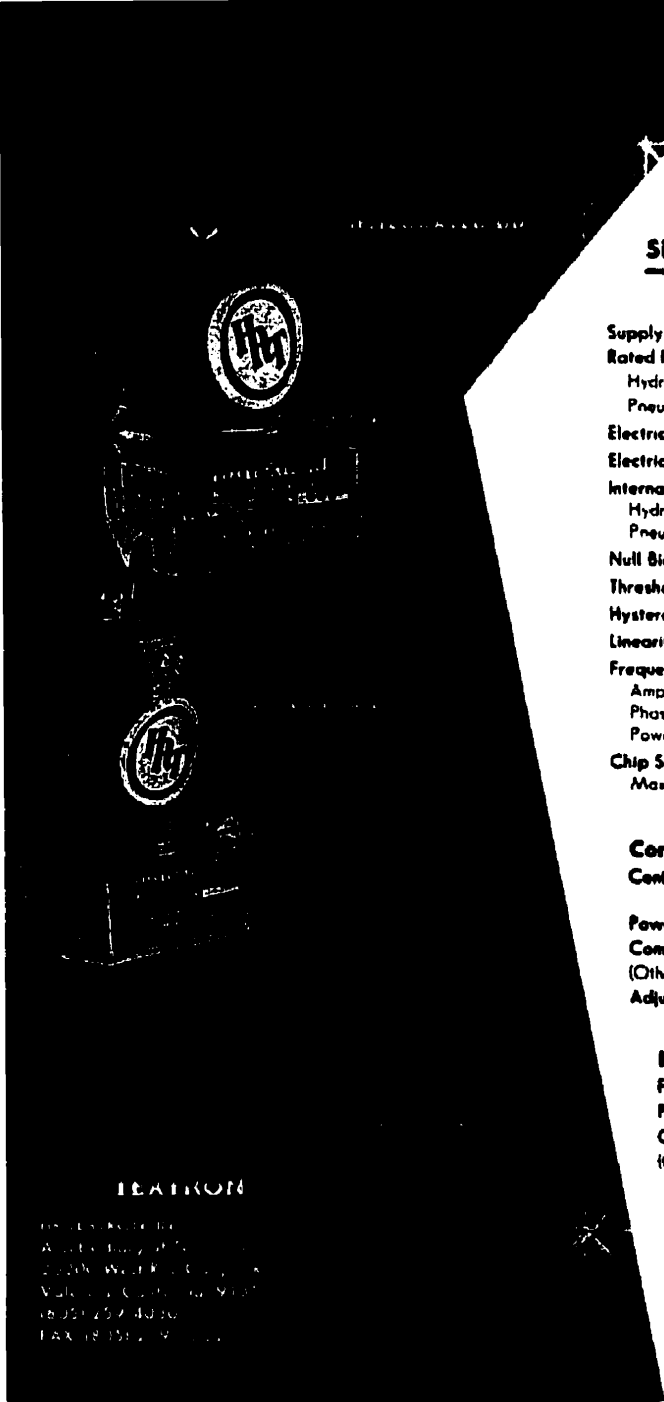


- [64] **Tang, J. and Walker, G** (1995), "Variable Structure Control of a Pneumatic Cylinder", ASME Jnl Dynamic Systems, Measurements and Control, Vol. 117, pp. 88-92.
- [65] **Thompson, S.** (1989), "Control Systems Engineering and Design", First Edition, Longman Scientific and Technical, John Wiley and Sons, New York, Ch.4 and 10.
- [66] **Tso, S.K., Lai, M.L. and Law, P.L.** (1993), "Variable-Structure Linear-Model-Following Control of Manipulators", Journal of Systems and Control Engineering, Proc Instn Mech Engs, Vol. 207, pp. 35-45.
- [67] **Uebing, M., Vaughan, N.D. and Surgenor, B.W.** (1997), "On Linear Dynamic Modelling of a Pneumatic Servo System", Proc of the Fifth Scandinavian International Conference on Fluid Power, May 28-30, Linköping, Sweden, pp. 363-378.
- [68] **Utkin, V.** (1977), "Variable Structure Systems with Sliding Modes", IEEE Trans. Auto. Control, Vol. AC-22, No.2, pp.212-222.
- [69] **Van de Vegte, J.** (1990), "Feedback Control Systems, Second Edition", Prentice Hall, New York, Ch.5.
- [70] **Wang, Sheng-G. and Lin, S. B.** (1995), "Robust Stability and Eigenvectors of Uncertain Matrices", Proc Amer Control Conf, June 21-23, Seattle, Washington, Vol.3, pp. 2399-2403.
- [71] **Woodham, C.A and Zinober, A.S.I** (1993) "Eigenvalue Placement in a Specified Sector for Variable Structure Control Systems ", Int. Jnl. Control, Vol.57, No.5, pp.1021-1037.
- [72] **Wright, P.** (1996) "Drive-by-Wire", Racecar, Vol.6, No.6, pp.16-19.
- [73] **Ye, N., Scavarda, S., Betemps, M. and Jutard A.** (1992), "Models of a Pneumatic PWM Solenoid Valve for Engineering Applications", Journal of Dynamic Systems, Measurement and Control, Vol. 114, pp. 680-687.
- [74] **Zhou, F and Fischer, D.G.** (1992), "MIMO Sliding Mode Control: A Lyapunov Approach" , Proc Amer Control Conf, June 26-28, Boston, Vol.2, pp. 1796-1799.
- [75] **Zhou, F and Fischer, D.G.** (1992), "Continuous Sliding Mode Control", Int Jnl Control, Vol. 55, No. 2, pp. 313-327.
- [76] **Zohdy, M.A., Fadali, M.S. and Liu, J.** (1995), "Variable Structure Dynamic Output Feedback", Proc Amer Control Conf, June 21-23, Seattle, Washington, Vol.2, pp. 1518-1522.

## APPENDIX A

### Technical Specifications

#### HR-Texttron Valve Specifications:



### HR-TEXTTRON MODEL 27A<sup>2</sup>

**For Low Pressure Hydraulic  
And Pneumatic Applications**

#### SERVOVALVE CHARACTERISTICS

*modular or integrated DDV*

<b>Supply Pressure</b>	to 1000 PSI
<b>Rated Flow</b>	
Hydraulic (GPM @ 1000 PSI)	0.4 0.9 1.8 3.5
Pneumatic (SCFM @ 100 PSI)	1.0 2.0 4.0 8.0
<b>Electrical Power - Full Hydraulic Flow</b>	1.2 Watts Max
<b>Electrical Power - Full Pneumatic Flow</b>	0.1 Watts Max
<b>Internal Leakage</b>	
Hydraulic	0.01 GPM Max @ 1000 PSI/D
Pneumatic	Negligible
<b>Null Bias</b>	± 1% of Rated Command
<b>Threshold</b>	0.5% of Rated Command Max
<b>Hysteresis</b>	1.0% of Rated Command Max
<b>Linearity</b>	5.0% of Rated Command Max
<b>Frequency Response</b>	(25% Command)
Amplitude Ratio	3dB @ 200Hz
Phase Angle	90 Degrees @ 150Hz
Power @ 150Hz	23 Watts (RMS)
<b>Chip Shear Force</b>	14.3 to 19 lb
<b>Max Power</b>	38 Watts

#### Control Module Characteristics

**Control Module Interface** 20 Pin Module - Consult HR for connection information

**Power Supply Required** 23 to 25 VDC 40 Watts Peak

**Command Input Signal** -5 to +5 VDC  
(Other Command Inputs Optional)

**Adjustable Upper Flow Limit** to 10% of Rated Flow

#### Integrated Electronics Characteristics

**Four Wire Interface** 2 Power and 2 Command

**Power Supply Required** 23 to 25 VDC 40 Watts Peak

**Command Input Signal** -5 to +5 VDC  
(Other Command Inputs Optional)

#### Related Products

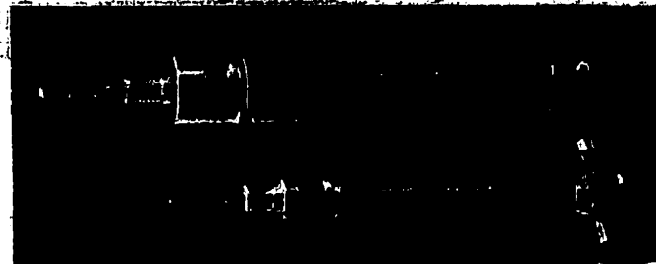
- High Pressure Version - Model 27A5
- Wide selection of mounting adaptors and manifolds
- Matching Two Channel Analog/Digital Control Card (Model EC27A)

**HR-TEXTTRON**  
 10000 KENNEDY BLVD.  
 WILSONVILLE, OR 97154  
 503/257-4030  
 FAX 503/257-4030

173

### BIMBA Cylinder Specifications:

## ***Bimba Original Line Stainless Steel Body Air Cylinders***



### Nominal Cylinder - Double Stroke Cylinder

09□-DX

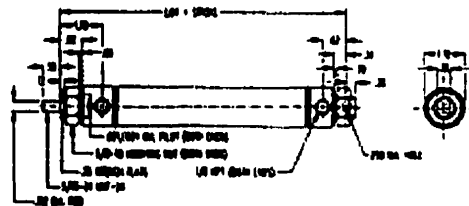


**\$21.35**

**BASE PRICE**

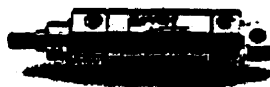
**Add \$1.25 per inch of stroke**

**Double Acting - Universal  
Mounting Pivot, or Double End  
Mounting - Air Return  
Standard Stroke Lengths:  
X", 1", 1½", 2", 2½", 3", 4", 5", 6", 7",  
8", 9", 10", 11", 12"  
Maximum Stroke - 32"  
Stainless Steel Rod Standard  
Rod Wiper \$2.35 Additional  
Optional Accessories:  
D-13498-A Pivot Bracket  
D-129 Mounting Bracket  
D-166-1 Piston Rod Clevis  
Base Weight: .33  
Adder Per Inch of Stroke: .05**



### Double Diameter Cylinder

## 31□-DXP



**\$51.85**

**BASE PRICE**

**Add \$2.30 per inch of stroke**

**Double Acting - Universal  
Mounting Type - Pivot or Double  
End - Air Return - Bronze Pivot  
Bushings**

**Standard Stroke Lengths:**  
1", 1 1/2", 2", 2 1/2", 3", 4", 5", 6", 7",  
8", 9", 10", 11", 12", 13", 14", 15",  
16", 17", 18", 19", 20", 21", 22",  
23", 24"

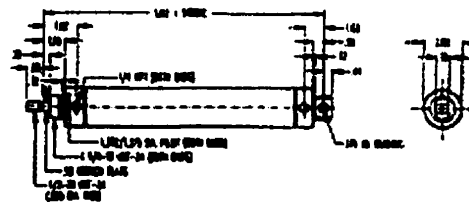
**Maximum Stroke - 32"**

**Stainless Steel Rod Standard**

**Optional Accessories:**  
D-231-3 Piston Rod Clevis  
D-815 Mounting Bracket  
D-620 Pivot Brackets  
D-505 Mounting Nut

**Base Weight: 1.62**

**Adder Per Inch of Stroke: .15**



**Data Acquisition Board:**

Model: LABMASTER  
Sampling Time: 10 ms  
Input Channels: 8 analog, set for 0 to 10 volts  
Output Channels: 2 analog, set for 0 to 10 volts  
A/D Resolution: 12 bit

**Potentiometer:**

Model: MIDORI  
Model number: CPP-45B  
Resistance: 500 ~ 20 K  
Standard Tolerance:  $\pm 15\%$   
Standard Linearity:  $\pm 0.5\%$   
Max. Power Rating: 3W / 70°C  
Mechanical Travel: 360°  
Maximum Torque: 18g-cm  
Maximum Weight: 60 g  
Mounting: Servo & Screw  
Bearing: Ball  
Operating Temp. Range: -40°C ~ +125°C

**Construction and Source of Data Acquisition Code:**

The original apparatus was built by Dr. Brian Surgenor while on sabbatical leave at Bath University, England in 1995. The original data acquisition code was written by Dr. Brian Surgenor. Subsequent modifications of a minor nature to both the apparatus and the code were made by the author for this study.

## APPENDIX B

### Simulation Source Code - Model Parameters

The following source code is a listing of the routines used in PC-MATLAB for simulation purposes. The component parameters and initial conditions are first listed. Then, the hysteresis model and flow conditions model is presented. The nonlinear valve model is used in the thesis, as well as a nonlinear static kinetic friction model. Finally, the cylinder volume and pressure model is presented along with the limits on position, velocity and control.

#### COMPONENT SETTINGS

$M_c$  = payload mass = 2.2 or 8.5 kg  
 $d_i$  = piston diameter = 25 or 26.99 mm  
 $A_1$  = chamber area =  $\pi \cdot (d_i^2)/4 \cdot 1e-06 \text{ m}^2$   
 $A_2$  = piston area =  $\pi \cdot (10^2)/4 \cdot 1e-06 \text{ m}^2$   
 $L_c$  = stroke length = 0.120 of 0.127 m  
 $C_d$  = discharge coefficient = 0.72  
 $A_v$  = valve supply opening = 2.13 or 3.4 mm<sup>2</sup>  
 $A_e$  = valve exhaust opening = ratio \*  $A_v$   
 $R_u$  = universal gas constant = 0.287 kJ/kgK  
 $C_L$  = leakage factor = 0 or 10  
Hys = valve deadband = 0.025  
 $V_{min}$  = end volume =  $10 \cdot 1e-6 \text{ m}^3$   
 $T_o$  = operating temperature = 293 K  
 $f_v$  = viscous coefficient = 70 (MARTONAIR), or  
63 (BIMBA) Ns/m  
 $F_c$  = static coulomb friction = 0, 10 (MARTONAIR)  
6.4 (BIMBA) N  
 $n_s$  = ideal or polytropic = 1 or 1.4  
 $P_o$  = atmospheric pressure = 101 kPa  
 $P_i$  = initial pressure = 400 kPa  
 $P_s$  = supply pressure = 653 kPa  
h = sampling and control interval = 0.01 sec

#### MARTONAIR [Ch.2-3-4]

Stroke Length = 120mm  
Chamber diameter = 25 mm  
Piston diameter = 10 mm  
 $f_v = 70 \text{ Ns/m}$ ,  $F_{cs} = 10 \text{ N}$ ,  $F_{cd} = 5 \text{ N}$

#### BIMBA 095-DX [Ch.5]

Stroke = 127mm  
Chamber diameter = 26.9mm  
Piston diameter = 7.9 mm  
 $f_v = 63 \text{ Ns/m}$ ,  $F_{cs} = 6.4 \text{ N}$ ,  $F_{cd} = 3.9 \text{ N}$

#### BIMBA 0910-DX [Ch.5]

Stroke = 254mm  
Chamber diameter = 26.9mm  
Piston diameter = 7.9 mm

#### BIMBA 315-DXP [Ch.5]

Stroke = 127mm  
Chamber diameter = 50.8mm  
Piston diameter = 15.8 mm

#### INITIAL CONDITIONS

$P_a = P_i$ ;  $P_b = P_s \cdot A_v / A_b$ ;  $dydt = 0$ ;  $y = 0$ ;  $u = 0$ ;  $V_{max} = 0$ ;  
 $d^2ydt^2 = 0$ ;  $m_a = 0$ ;  $m_b = 0$ ;  $P_r = 0$ ;  $F_p = 0$ ;

## HYSTERESIS MODEL

```
if u > Hys
    Pra = Ps/Ps; Prb = Po/Pb;
elseif u < -Hys
    Pra = Po/Pa; Prb = Pv/Ps;
else
    if flagN==0;
        Pra = 1; Prb = 1; % --- Closed Center
    Valve
    else
        Pra = Po/Pa; Prb = Po/Pb; % --- Open Center Valve
    end
end
```

## FLOW CONDITIONS

```
if Pra/b >= 1;
    Cma/b = 0;
elseif Pra/b >= 0.528;
    dy = (Pra/b^(2/1.4) - Pra/b^((1.4+1)/1.4));
    Cma/b = sqrt(2*1.4*dy/(1000*Ru*(1.4-1))); % --- Subsonic Flow
else
    Cma/b = 0.0405; % --- Choked Flow
end
```

## LINEAR VALVE MODEL

```
ma = Cd*0.0405*Av*1000*Ps/sqrt(To)* u;
mb = -ma;
```

## NONLINEAR VALVE MODEL

```
if u > Hys
    ma = Cd*Cma*u*Av*1000*Ps/sqrt(To);
    mb = -Cd*Cmb*u*Ae*1000*Pb/sqrt(To);
elseif u < -Hys
    ma = Cd*Cma*u*Ae*1000*Ps/sqrt(To);
    mb = -Cd*Cmb*u*Av*1000*Ps/sqrt(To);
else
    if flagN==0;
        ma = 0; mb = 0; % --- Closed Centre Valve
    else
        ma = -Cd*Cma*1.0*Ae*1000*Ps/sqrt(To); % --- Open Center Valve
        mb = -Cd*Cmb*1.0*Ae*1000*Pb/sqrt(To);
    end
end
```

## CYLINDER PROFILE

$$A_a = A_1; A_b = A_a;$$

*% --- Symmetric Actuator*

$$A_a = A_1; A_b = A_1 - A_2;$$

*% --- Asymmetric Actuator*

## CYLINDER MODEL

$$F_p = 1000 * (A_a * P_a - A_b * P_b);$$

$$\text{if } mlogic == 0 \ \& \ abs(F_p) > F_c;$$

*% --- Static-Kinetic Friction Model*

$$mlogic = 1;$$

$$\text{elseif } mlogic == 1 \ \& \ abs(F_p) < (F_c/2);$$

$$mlogic = 0;$$

end

$$\text{if } F_c == 0; mlogic = 1; \text{end}$$

$$\text{if } mlogic == 1;$$

$$d^2ydt^2 = (F_p - \text{sign}(dydt) * F_c/2 - F_v * dydt) / M_c;$$

$$dydt = dydt + h * d^2ydt^2;$$

else

$$dydt = 0; d^2ydt^2 = 0;$$

end

## STATE UPDATES

$$y = y + h * dydt;$$

$$\text{if } dydt > V_{max}; V_{max} = dydt; \text{end}$$

*% --- Velocity Limits*

$$\text{if } y < -L_c/2; y = -L_c/2; dydt = 0; \text{end}$$

*% --- Position Limits*

$$\text{if } y > L_c/2; y = L_c/2; dydt = 0; \text{end}$$

$$\text{if } u > u_{max}; u = u_{max}; \text{end}$$

*% --- Control Limits*

$$\text{if } u < -u_{max}; u = -u_{max}; \text{end}$$

## CYLINDER VOLUME MODEL

$$V_{a\_old} = V_a$$

*% --- Charging*

$$V_{b\_old} = V_b$$

*% --- Discharging*

$$V_a = A_a * (L_c/2 + y) + V_{min}$$

$$V_b = A_b * (L_c/2 - y) + V_{min}$$

$$dV_a dt = (V_a - V_{a\_old}) / h$$

$$dV_b dt = (V_b - V_{b\_old}) / h$$

## PRESSURE MODEL

$$dP_a dt = n_s * (R_u * T_o * m_a - P_a * dV_a dt) / V_a$$

$$P_a = P_a + h * dP_a dt$$

$$dP_b dt = n_s * (R_u * T_o * m_b - P_b * dV_b dt - C_L * P_b) / V_b$$

$$P_b = P_b + h * dP_b dt$$

$$\text{if } P_a < P_o; P_a = P_o; dP_a dt = 0; \text{end}$$

*% --- Pressure Limits*

$$\text{if } P_a > P_s; P_a = P_s; dP_a dt = 0; \text{end}$$

$$\text{if } P_b < P_o; P_b = P_o; dP_b dt = 0; \text{end}$$

$$\text{if } P_b > P_s; P_b = P_s; dP_b dt = 0; \text{end}$$

## SIMULATION SAMPLING TIME:

Examination of the program listing in the previous pages highlights that Euler's 1<sup>st</sup> order numerical method was used to solve the differential equations of the nonlinear model. For example, the difference equation for a chamber pressure (see Pressure Model in listing) is given as:

$$P_{k+1} = P_k + \dot{P}_k h$$

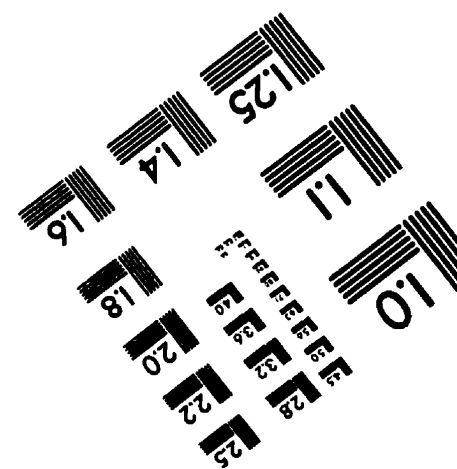
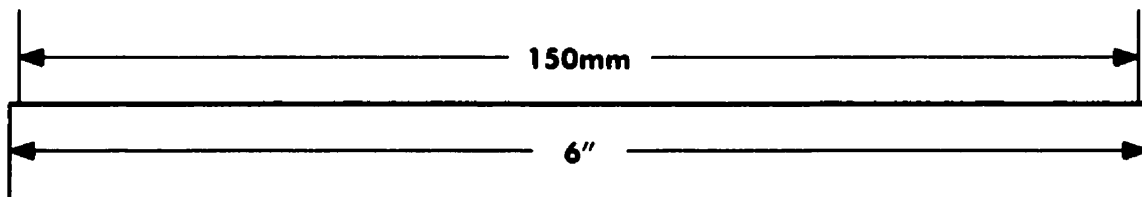
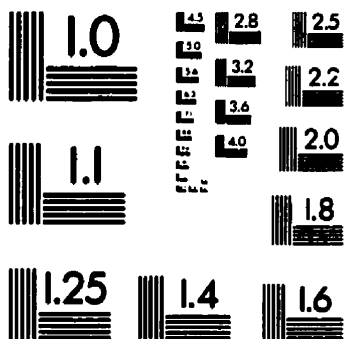
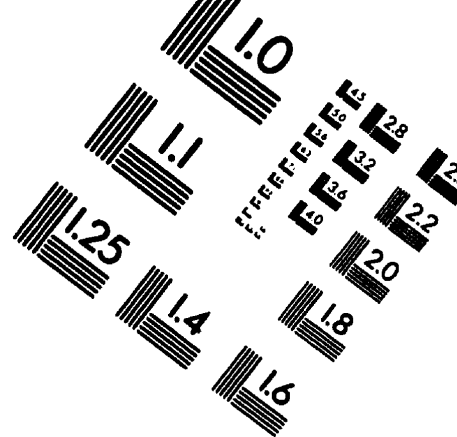
where  $k$  is the " $k^{\text{th}}$ " time step.

The simulation sampling time used was set to  $10\text{ ms}$ , to match the sampling time available to the experimental setup by the microcomputer in use. Using a sampling time of  $10\text{ ms}$  on a linear system with a  $\tau$  of  $100\text{ ms}$  ( $\tau/h=10$ ), results in a maximum numerical error of 18% (if one compares the *Euler* approximation to the exact solution step by step). But relative to the final steady state (unit step change), the error is less than 0.33%. Using a sampling time of  $10\text{ ms}$  on a linear system with a  $\tau$  of  $1000\text{ ms}$  ( $\tau/h=100$ ), results in a numerical error of 0.5%. As the  $\tau/h$  ratio increases the truncation error decreases, but the round-off error increases.

A sampling time of  $1\text{ ms}$  is not normally viewed as a "difficult" sampling time to achieve, but many industrial PLC based controllers can only sample at  $100\text{ ms}$ , although the actual microprocessor clock speed is considerably higher.



## TEST TARGET (QA=J)



**APPLIED IMAGE, Inc**  
1653 East Main Street  
Rochester, NY 14609 USA  
Phone: 716/482-0300  
Fax: 716/288-5989

© 1993, Applied Image, Inc., All Rights Reserved